Toxicology and Applied Pharmacology 253 (2011) 203–234

Contents lists available at ScienceDirect

Toxicology and Applied Pharmacology

journal homepage: www.elsevier.com/locate/ytaap

Development and evaluation of a harmonized physiologically based pharmacokinetic (PBPK) model for perchloroethylene toxicokinetics in mice, rats, and humans☆

Weihsueh A. Chiu [a,□], Gary L. Ginsberg [b]

[a] National Center for Environmental Assessment, U.S. Environmental Protection Agency, Washington, DC 20460, USA
[b] Connecticut Department of Public Health, Hartford, CT 06106, USA

article info

Article history:
Received 4 January 2011
Revised 9 March 2011
Accepted 27 March 2011
Available online 3 April 2011

Keywords:
Glutathione conjugation
Metabolism
Oxidation
Physiologically based pharmacokinetic (PBPK) model
Risk assessment
Tetrachloroethylene
Trichloroethylene
Uncertainty
Variability

abstract

This article reports on the development of a "harmonized" PBPK model for the toxicokinetics of perchloroethylene (tetrachloroethylene or perc) in mice, rats, and humans that includes both oxidation and glutathione (GSH) conjugation of perc, the internal kinetics of the oxidative metabolite trichloroacetic acid (TCA), and the urinary excretion kinetics of the GSH conjugation metabolites N-Acetylated trichlorovinyl cysteine and dichloroacetic acid. The model utilizes a wider range of in vitro and in vivo data than any previous analysis alone, with in vitro data used for initial, or "baseline," parameter estimates, and in vivo datasets separated into those used for "calibration" and those used for "evaluation." Parameter calibration utilizes a limited Bayesian analysis involving flat priors and making inferences only using posterior modes obtained via Markov chain Monte Carlo (MCMC). As expected, the major route of elimination of absorbed perc is predicted to be exhalation as parent compound, with metabolism accounting for less than 20% of intake except in the case of mice exposed orally, in which metabolism is predicted to be slightly over 50% at lower exposures. In all three species, the concentration of perc in blood, the extent of perc oxidation, and the amount of TCA production is well-estimated, with residual uncertainties of ~2-fold. However, the resulting range of estimates for the amount of GSH conjugation is quite wide in humans (~3000-fold) and mice (~60-fold). While even high-end estimates of GSH conjugation in mice are lower than estimates of oxidation, in humans the estimated rates range from much lower to much higher than rates for perc oxidation. It is unclear to what extent this range reflects uncertainty, variability, or a combination. Importantly, by separating total perc metabolism into separate oxidative and conjugative pathways, an approach also recommended in a recent National Research Council review, this analysis reconciles the disparity between those previously published PBPK models that concluded low perc metabolism in humans and those that predicted high perc metabolism in humans. In essence, both conclusions are consistent with the data if augmented with some additional qualifications: in humans, oxidative metabolism is low, while GSH conjugation metabolism may be high or low, with uncertainty and/or interindividual variability spanning three orders of magnitude. More direct data on the internal kinetics of perc GSH conjugation, such as trichlorovinyl glutathione or tricholorvinyl cysteine in blood and/or tissues, would be needed to better characterize the uncertainty and variability in GSH conjugation in humans.

Published by Elsevier Inc.

Introduction

Perchloroethylene (tetrachloroethylene or perc) is a volatile organic solvent that has had widespread commercial and industrial use, particularly for commercial dry cleaning, and to a lesser extent in degreasing of metal parts and as a chemical intermediate. Perc is also a common environmental contaminant at hazardous waste sites, in groundwater, and in ambient and indoor air. Like the related solvent trichloroethylene (TCE), perc is a dense nonaqueous-phase liquid and is particularly difficult to remediate once it has entered groundwater.

Understanding perc toxicokinetics is critical to both the qualitative and quantitative assessment of human health risks from environmental exposures and continues to be the subject of active research (Chiu et al., 2007; Sweeney et al., 2009; Boyes et al., 2009). A number of the neurotoxic effects of perc appear well correlated with parent compound concentrations at the target site (Bushnell et al., 2005), so characterizing perc blood or tissue concentrations can aid in

☆ This manuscript has been reviewed by the U.S. Environmental Protection Agency and approved for publication. The views expressed in this manuscript are those of the author(s) and do not necessarily reflect the views or policies of the U.S. Environmental Protection Agency or the Connecticut Department of Public Health.

□ Corresponding author at: Express Delivery Address: U.S. Environmental Protection Agency — 8623P, Two Potomac Yard (North Building), 2733 South Crystal Drive, Arlington, VA 22202, USA. Fax: +1 703 347 8692.
E-mail addresses: chiu.weihsueh@epa.gov (W.A. Chiu), gary.ginsberg@ct.gov (G.L. Ginsberg).

0041-008X/$ – see front matter. Published by Elsevier Inc.
doi:10.1016/j.taap.2011.03.020

performing risk assessment-related extrapolations, such as between rodents and humans or between exposure routes. In addition, understanding perc metabolism is especially important toxicologically because specific metabolites or metabolic pathways are associated with a number of observed toxic endpoints.

Perc and its metabolites trichloroacetic acid (TCA) and dichloroacetic acid (DCA) cause a number of similar effects in the liver of laboratory animals, including hepatomegaly in rats and mice and hepatocarcinogenicity in multiple strains and both sexes of mice but not in rats (NCI, 1977; NTP, 1986; JISA, 1993; DeAngelo et al., 1999, 2008; Pereira, 1996). As with TCE (Evans et al., 2009; Buben and O'Flaherty, 1985), it has been noted that perc-induced hepatomegaly in mice is better correlated with oxidative metabolism than with the parent compound (Buben and O'Flaherty, 1985). Thus, it has been hypothesized that hepatotoxicity from perc exposure is a result of oxidative metabolism. Under this hypothesis, the lack of apparent hepatocarcinogenicity in rats as compared to the clear hepatocarcinogenicity in mice may partially be explained by differences in perc oxidative metabolism and/or internal doses of TCA, which seem to correlate with sensitivity. However, TCA itself appears to be a more potent hepatocarcinogen in mice than rats, a difference which is as yet not fully explained.

In the kidney, perc causes tubular toxicity in both mice and rats, and is associated in one study with small increases in the incidences of kidney tumors rats (NTP, 1986; JISA, 1993). These effects are thought to be associated with the perc metabolism by glutathione (GSH) conjugation, based on the production in the kidney of nephrotoxic and genotoxic metabolites from this pathway (Lash and Parker, 2001). It has been hypothesized that quantifying differences in the extent of GSH conjugation across species can help to explain the observed species differences in carcinogenicity. However, attempts to make such inferences based on in vitro data have been inconsistent (e.g., Green et al., 1990; Dekant et al., 1998; Lash et al., 1998), and no attempt as yet has been made to incorporate GSH conjugation in a PBPK model.

It is less clear to what extent other effects of perc in rodents, such as brain gliomas (NTP, 1986) or mononuclear cell leukemias (JISA, 1993) in rats, are a result of perc itself and/or one or more metabolites. In terms of epidemiologic data, some studies suggest that the kidney and liver may be targets of perc toxicity in humans (Gennari et al., 1992; Mutti et al., 1992; Brodkin et al., 1995), but the available data are too limited to make any definitive conclusions. A recently updated occupational cohort study reported a new finding of increased incidence of end-stage renal disease among dry cleaning workers, further supporting a role for perc in kidney toxicity (Calvert et al., 2010). However, the strongest and most consistent epidemiologic evidence remains that for neurotoxic effects (Altmann et al., 1995; Echeverria et al., 1995; Ferroni et al., 1992; Schreiber et al., 2002; Seeber, 1989).

A simplified metabolism scheme for perc is shown in Fig. 1. Briefly, as reviewed by Lash and Parker (2001), metabolism of perc occurs through two main irreversible pathways: oxidation via the microsomal mixed-function oxidase system (i.e., cytochrome P450s) and conjugation with GSH by glutathione S-transferases. The primary

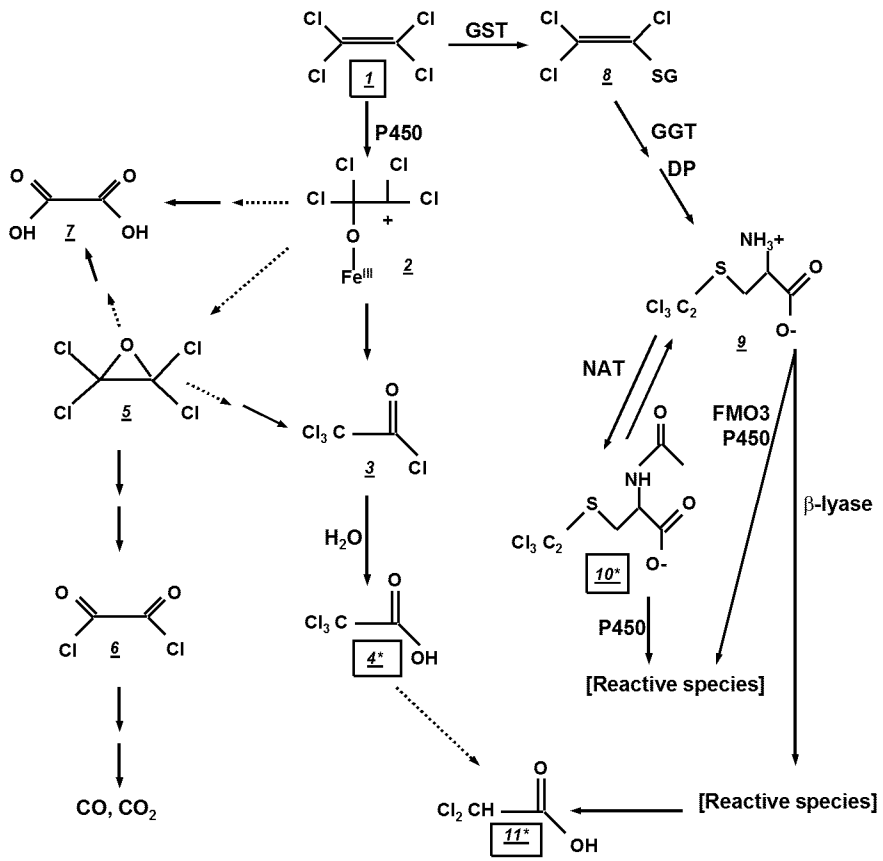

Fig. 1. Simplified perchloroethylene (perc) metabolism scheme. 1, tetrachloroethylene; 2, tetrachloroethylene-Fe–O intermediate; 3, trichloroacetyl chloride; 4, trichloroacetic acid; 5, tetrachloroethylene oxide; 6, ethandioyl dichloride; 7, oxalic acid; 8, S-(1,2,2-trichlorovinyl) glutathione (TCVG); 9 S-(1,2,2-trichlorovinyl)-L-cysteine (TCVC); 10, N-acetyl trichlorovinyl cysteine (NAcTCVC); 11, dichloroacetic acid. Enzymes: cytochrome P450 (P450), glutathione-S transferase (GST), gamma-glutamyltransferase (GGT), dipeptidase (DP), beta-lyase (β-lyase), flavin mono-oxygenase-3 (FMO3), N-Acetyl transferase (NAT). Metabolites marked with asterisk (*) are known urinary metabolites. Dotted lines indicate hypothesized or quantitatively minor pathways. Boxes indicate chemicals/metabolites included explicitly in the PBPK model (see Fig. 3).

stable metabolite is TCA, a product of perc oxidation, with the remaining hypothesized intermediates from either pathway being short-lived. The P450 isoform CYP2E1 is thought to be most important for perc oxidation based on analogy to other volatile organic compounds, but based on in vitro data using different inducers and inhibitors, other P450 isoforms likely play a role (Lash and Parker, 2001; Doherty et al., 1996; Costa and Ivanetich, 1980). Perc is first oxidized to a Fe–O intermediate, the primary fate of which is thought to be trichloroacetyl chloride (metabolite 2), which then hydrolyses to yield TCA (metabolite 4). It was initially hypothesized that the epoxide (perc oxide [metabolite 5]) rearranged to form trichloroacetyl chloride. However, subsequent experiments (Yoshioka et al., 2002) suggest that this does not occur, and the epoxide decomposes to ethandioyl dichloride (metabolite 6) and then to CO and CO_2. Moreover, given the pattern of in vivo and in vitro metabolites, the epoxide pathway is likely to be small. It had also been hypothesized that the epoxide can rearrange to form chloral (metabolite 5), but Lash and Parker (2001) suggest that this pathway is either absent or minor. Finally, oxalic acid has been reported as both an in vivo and in vitro product of perc oxidation (Pegg et al., 1979; Yoshioka et al., 2002), and may either be derived from the epoxide or directly from the Fe–O intermediate.

With respect to the conjugative pathway, trichlorovinylglutathione (TCVG) (metabolite 8) is further processed to form the cysteine conjugate S-trichlorovinyl-L-cysteine (TCVC) (metabolite 9), which can undergo bioactivation by beta-lyase or flavin-containing monooxygenases (FMO) to reactive species (Anders et al., 1988; Krause et al., 2003) or (reversible) N-acetylation to the mercapturate N-acetyl trichlorovinyl cysteine (NAcTCVC) (metabolite 10). NAcTCVC, in turn, can be excreted in urine or sulfoxidated by CYP3A to reactive species (Werner et al., 1996). Dichloroacetic acid (DCA), excreted in urine, is thought to be an end product of beta-lyase-mediated bioactivation (Lash and Parker, 2001). It has also been suggested that DCA is a result of dechlorination of TCA, derived from the oxidative pathway. Data from the related compound TCE suggest that in that case, DCA formation is likely dominated by hydrolysis of dichloroacetyl chloride, rather than dechlorination of TCA. As compared to perc exposure, trichloroethylene exposure leads to higher amounts of TCA, in conjunction with the lower amounts of DCA detectable in blood or urine. This is inconsistent with the DCA detected in urine after perc exposure being produced via dechlorination of TCA, and supports the hypothesis that DCA is derived predominantly from GSH conjugation of perc.

A number of PBPK models have been developed for perc toxicokinetics in both rodents and humans, though there are markedly fewer in vivo pharmacokinetic data, particularly for mice and humans, than is the case for TCE. Among the multi-species PBPK models, those developed by Chen and Blancato (1987) and Rao and Brown (1993) were fit to previously published total metabolism data in mice and rats and perc and TCA data in humans. Gearhart et al. (1993) performed in vivo experiments in mice to support their PBPK model for perc and TCA, and fit their model to previously published human data to support the human version of their model. Reitz et al. (1996) performed in vitro and in vivo experiments to support their PBPK model in mice and rats, and used a "parallelogram approach" to estimate metabolic parameters in humans. Clewell et al. (2005) updated the Gearhart et al. (1993) model, including consideration of human toxicokinetic data published by Volkel et al. (1998). In addition, a number of PBPK models were developed only in humans, primarily to characterize uncertainty and/or human variability. Bois et al. (1996), which was updated by Chiu and Bois (2006), used a Bayesian analysis in conjunction with a PBPK model that was structurally similar to that used by Reitz et al. (1996), and was only calibrated to the parent compound data. Covington et al. (2007) applied the same methodology to the Clewell et al. (2005) human PBPK model, using additional data on the parent compound perc and its metabolite TCA. Finally, Qiu et al. (2010) performed an update to the Covington et al. (2007) analysis, adding additional human data from Chiu et al. (2007) and Chien (1997). A key controversy surrounding the application of PBPK models to perc toxicokinetics is the question of how much perc is metabolized in humans at low doses, with estimates across the various models spanning a range of an order of magnitude or more, as shown in Fig. 2 (Chiu, 2007).

These analyses have a number of key limitations. First, in no case has all the available data in mice, rats, and humans, been considered together in a single analysis. Thus, the extent to which different results reflect use of different datasets and model structures is unclear. Moreover, while all the models estimate total metabolism, those estimates are based on different types of data. In particular, one set of available models generally calibrate metabolism to disappearance of the parent compound, while another (overlapping) set assume that total metabolism is proportional to production of TCA. However, none of the models address GSH conjugation, which may be an important contributor to total metabolism, especially since perc is known to be a poorer substrate for oxidation than many other related volatile organic compounds. These limitations were also noted in the National Research Council (NRC) report Review of the Environmental Protection Agency's Draft IRIS Assessment of Tetrachloroethylene (NRC, 2010). In particular, they concluded that, while a number of PBPK models have been developed for perc, they all have some key limitations that limit the confidence with which they can be used for risk assessment. NRC (2010) recommended the development of a "harmonized" PBPK model integrating previous models and data. They pointed to the availability of in vitro and in vivo data relevant to the GSH conjugation pathway, and recommended exploring the possibility of adding the GSH pathway to a harmonized PBPK model.

In order to inform the dose metric options available for use in risk assessment, the present analysis addresses these limitations in existing PBPK models by better characterizing the metabolism of perc, the relative contributions of oxidation and conjugation to perc metabolism, and their uncertainties given the available data. In particular, first, a comprehensive literature search was made of relevant toxicokinetic studies and the available toxicokinetic data digitized. These data were further separated into "calibration" and "evaluation" datasets. Sorting of data into calibration and evaluation

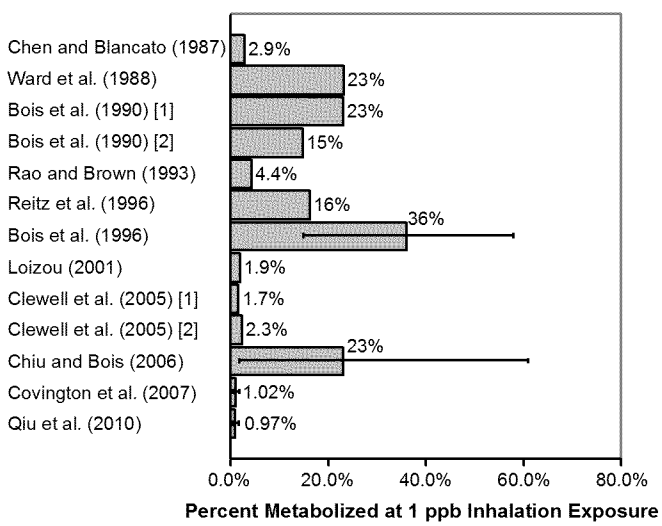

Fig. 2. Previously published estimates for the total amount of perc metabolized at 0.001 ppm (1 ppb) continuous inhalation exposure. All estimates are point estimates except for Bois et al. (1996) and Chiu and Bois (2006), which are estimates of combined uncertainty and population variability (95% confidence intervals), and Covington et al. (2007) and Qiu et al. (2010), which are estimates of uncertainty in the population mean (90% confidence intervals).

subsets, as described in Materials and methods, aimed to ensure ample independent data were available for both phases of model development. Second, a harmonized PBPK model structure was developed that separately tracked perc oxidation and GSH conjugation. Because the related chlorinated solvent TCE both shares a metabolite (TCA) and has many qualitative toxicokinetic similarities (e.g., metabolism through both oxidation by P450 and conjugation with GSH), the basic structure of the "harmonized" perc PBPK model is based on the previously published "harmonized" TCE model (Hack et al., 2006; Chiu et al., 2009), with modifications motivated by the extant perc PBPK models. Part of the motivation for using the TCE model as a starting point is the fact that a comprehensive analysis of TCA dosimetry was performed as part of the TCE analysis, and those results can be directly carried over to the present analysis for perc.

Therefore, this paper (1) describes the updated model structure, (2) documents the development of baseline parameter estimates from the scientific literature, (3) obtains optimized estimates for key model parameters fit to in vivo calibration data, (4) compares model predictions with evaluation data, (5) calculates predictions for key internal dose metrics of relevance to risk assessment, (6) performs a local sensitivity analysis, and (7) characterizes the overall confidence in the PBPK model predictions. Finally, the discussion provides a number of insights from this harmonization, including reconciling the different results on perc metabolism at low doses in humans, comments on the use of MCMC-based methods in a limited Bayesian analysis, and potential next steps to improve the quantitative characterization of perc toxicokinetics.

Materials and methods

Updated PBPK model structure

Perc-specific modifications of Chiu et al. (2009) TCE model

The updated perc PBPK model is illustrated in Fig. 3, and is based on the TCE PBPK model reported by Chiu et al. (2009) with changes based solely on differences in metabolites or metabolism pathways (model equations contained in Appendix A). Because only TCA has been consistently detected as an oxidative metabolite of perc, the submodels involving trichloroethanol (TCOH) and its glucuronide are removed. Some changes from the TCE model are made in the treatment of extrahepatic oxidation to reflect the fact that the formation of TCA (the only tracked oxidative metabolite) occurs spontaneously from decomposition of trichloroacetyl chloride. In the liver, a second saturable pathway was added, given available evidence that P450s in addition to CYP2E1 are involved in perc metabolism (Lash and Parker, 2001). In addition, perc oxidation in the kidney is added, with a fraction of the TCA produced assumed to be directly excreted in urine, as was hypothesized by Clewell et al. (2005) and Covington et al. (2007) in their human perc PBPK model. TCA formed

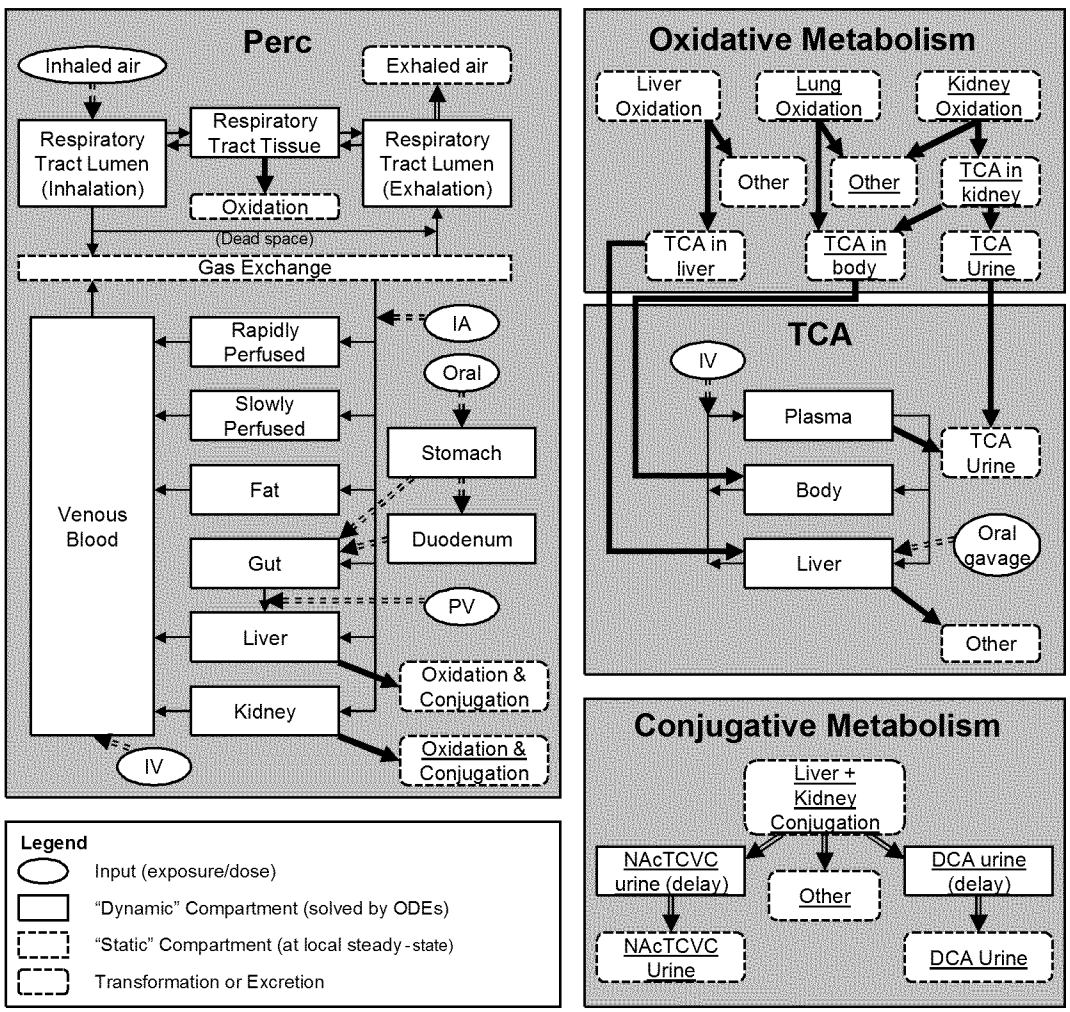

Fig. 3. Overall structure of updated PBPK model for TCE and metabolites. Boxes with underlined labels are additions or modifications of the Chiu et al. (2009) model, discussed in text.

from this pathway that is not immediately excreted is placed in the TCA body compartment.

Conjugative metabolism in the kidney is retained, motivated by the in vitro data (discussed below) showing perc conjugation in freshly isolated cells and subcellular fractions of the kidney. Because of the availability of urinary data on DCA (Volkel et al., 1998) – an end product of beta-lyase-mediated bioactivation of TCVC – the TCVC bioactivation pathway is separated into beta-lyase-dependent and beta-lyase-independent pathways. Unlike with TCE, no in vivo data on the glutathione conjugate (TCVG in the case of perc) are available, so processing of perc GSH conjugates is simplified. In particular, the fractional yield of urinary DCA and urinary NAcTCVC are estimated, with the residual fraction consisting of a lumping of all other possible fates of GSH conjugates, including non-beta-lyase-dependent bioactivation pathways and end-products of beta-lyase metabolism other than urinary DCA. In order to better fit the time-course of urinary excretion, an empirical "delay" parameter (a "fitted" value) is added for urinary excretion of DCA and NAcTCVC, and constitutes a lumping the processes of formation, urinary excretion, and other clearance pathways.

PBPK model parameters and baseline values

Baseline (i.e., point estimate) values for PBPK model parameters (Table A1) are developed using standard methodologies to ensure biological plausibility, using an approach similar to that reported by Chiu et al. (2009). In keeping with standard practice, many of the PBPK model parameters are "scaled" by body weight, cardiac output, etc. In addition, because of the expected correlation between VMax and KM during optimization, one of these is always reparameterized to a clearance (VMax/KM) term. So as to ensure a consistent model structure across species, as well as to improve the performance of the Markov chain Monte Carlo (MCMC) algorithm, parameters are further scaled to the baseline point-estimates where available, as was done by Chiu et al. (2009). For example, to obtain the actual liver volume in liters, a point estimate is first obtained by multiplying the fixed, species-specific baseline point estimate for the fractional liver volume by a fixed body weight (measured or species-specific default), with density of 1 kg/L assumed to convert from kg to liters. Any deviation from this point estimate is represented by multiplying by a separate "scaling" parameter VLivC that has a value of 1 if there is no deviation from the point estimate.

As was emphasized by Chiu et al. (2009), it is important that baseline parameter estimates be independent of the in vivo toxicokinetic data that is to be used later for formal calibration, lest the same data be used twice. Therefore, the data considered in developing baseline parameters are restricted to physiological measurements (e.g., volumes and flows) and measurements from in vitro studies (e.g., partition coefficients, binding coefficients, and metabolism and clearance rates).

Baseline values for physiological parameters

Baseline physiological parameters are the same as those in Chiu et al. (2009) and are largely estimated based on the standard references ICRP (2002) and Brown et al. (1997). For a few of these parameters, such as hematocrit and respiratory tract volumes in rodents, additional published sources are used as available (Hejtmancik et al., 2002; Sarangapani et al. 2003), but no attempt is made to compile a comprehensive review of available measurements. In addition, a few parameters, such as the slowly perfused volume, are calculated by imposing total mass or flow balances.

Baseline values for chemical-specific absorption parameters

No in vitro data are available to estimate perc oral (gavage) absorption parameters. Absorption rates were determined separately (by optimization) for aqueous gavage and oil gavage since the lipophilicity of perc would be expected to result in different absorption rates depending on the vehicle.

Baseline values for chemical-specific distribution parameters

For chemical-specific distribution parameters, primarily in vitro data from available sources are used. Six studies are identified with in vitro partition coefficient data for perc (Gargas et al., 1989; Gearhart et al., 1993; Koizumi, 1989; Mahle et al., 2007; Mattie et al., 1994; Reitz et al., 1996). For parameters for which more than one reported value is available, the data are pooled to obtain baseline partition coefficient estimates. Pooling is considered reasonable because the variability among estimates is relatively low, with coefficients of variation of less than 30%. For TCA partitioning and protein binding, the posterior means from Chiu et al. (2009) for the population mean parameters are used.

Conversions of in vitro data to inform baseline metabolism parameters

In vitro metabolism data are typically reported in terms of activity (nmol/min) per mg protein (for data from microsomes or cytosol) or per million cells (for data from cell preparations). A two-step process is employed for conversion of in vitro measures to PBPK model parameters. First, in order to have a common basis for comparison, the reported data are converted to an activity per g tissue (see Table 1, discussed below). Second, activities and concentrations are converted to VMax, Km, and/or VMax/Km values in units typically used in PBPK models (see Supplementary Materials, Table S2).

For the first step, conversion from reported activity to activity per g tissue, the published data are fairly limited. A summary of data from a literature search is provided in Supplementary Materials (Table S1), with the selected values summarized in Table 1. For the liver, rat and human data are the most numerous. For rats, the geometric means of the results from Table S1 are used. For human liver, the central estimates reported in the review by Barter et al. (2007) are used for microsomal protein content and hepatocellularity. For hepatic cytosolic protein content, it is assumed that the cytosolic protein per cell is the same in rats and humans, based on the observation that the microsomal protein per cell is similar in rats and humans. For mouse liver, both the cytosolic protein per cell and microsomal protein per cell is assumed to be the same as for rats, using the mouse hepatocellularity reported in Sohlenius-Sternbeck (2006). For the kidney, significantly less data are available, with only the single study in rats by Bong et al. (1985) reporting total and microsomal protein content. Thus, the microsomal protein content in rats is based on Bong et al. (1985). As an approximation, the difference between total and microsomal protein content is used for cytosolic protein content in the rat. For nephrocellularity, the value reported by Nyengaard et al.

Table 1
Conversion factors used for in vitro metabolism data.

Tissue	Liver			Kidney		
Species	Mouse	Rat	Human	Mouse	Rat	Human
Fraction						
Microsomal (mg protein/g tissue)	43[a]	38[b]	32[c]	16[f]	16[f]	16[f]
Cytosolic (mg protein/g tissue)	99[a]	87[b]	72[d]	86[f]	86[f]	86[f]
Cellularity (10^6 cells/g tissue)	135[e]	119[b]	99[c]	126[g]	126[g]	126[g]

[a] Cellularity multiplied by rat values for microsomal or cytosolic protein per cell.
[b] Geometric mean of available values (see Supplementary Materials, Table S1).
[c] Central estimate from Barter et al. (2007).
[d] Cellularity multiplied by rat value for cytosolic protein per cell.
[e] Value reported by Sohlenius-Sternbeck (2006).
[f] Value reported by Bong et al. (1985) for rats, with cytosolic protein assumed to be the difference between total and microsomal protein.
[g] Value reported by Nyengaard et al. (1993) for rats.

(1993) for total tubular cells per g of kidney in rats is used for all species. Note that these conversions are only used to scale the in vitro metabolism data to a common basis in g of tissue within the same species. Differences in the complement of metabolizing enzymes between species would presumably be accounted for in the in vitro metabolism data themselves.

For the second conversion (see Supplementary Materials, Table S2), in addition to standard unit conversions (e.g., nmol to mg and min to h), it is assumed that the measured concentrations in vitro are equivalent to tissue concentrations in vivo. Therefore, because Km values in the PBPK model are given in terms of venous blood concentrations, a conversion is performed using the tissue:blood partition coefficient. Clearance (VMax/Km) values are converted similarly.

Baseline values for rates of perc oxidation

For perc oxidation, four in vitro studies were identified, consisting of data from microsomes or cells from the liver and microsomes from the kidney (Costa and Ivanetich, 1980, 1984; Lash et al., 2007; Reitz et al., 1996). For clearance (VMax/Km), the baseline estimate is derived from the geometric mean of Costa and Ivanetich (1980, 1984) (1.42 ± 1.04 and 1.77 ± 1.02, respectively) and pooling of Reitz et al. (1996) and Lash et al. (2007) (2.20), giving VMax/Km = 1.8 nmol/min/g liver/mM. Uncertainty is dominated by uncertainty in Km for Costa and Ivanetich (1980, 1984), with CV = 0.73 and 0.56 for the two estimates (1.1 ± 0.80 and 0.64 ± 0.37, respectively), with a third, higher, estimate (3.92) based on pooling of Reitz et al. (1996) and Lash et al. (2007). For Km in the rat, the geometric mean of the three Km values is used, weighted equally under the assumption that between-study systematic errors dominate over within-study experimental errors, and giving a result of 1.4 mM.

For mouse and human liver oxidation estimates, the VMax/Km ratios from Reitz et al. (1996) are used to scale the rat central estimate to the other species, leading for the mouse to VMax/Km = 10 nmol/min/g liver/mM (5.6-fold greater than rat) and for the human to VMax/Km = 0.81 nmol/min/gliver/mM (2.22-fold less than rat). For Km, the baseline estimate is the same central estimate as the rat, Km = 1.4 mM, based on expectation of similar Km values across species.

For extra-hepatic metabolism, in vitro ratios to the liver are used to derive metabolism estimates. The only perc-specific data for kidney oxidation are in the rat at 2 mM (Lash et al., 2007), with the clearance ratio between kidney and liver (on a per g tissue basis) of 0.013. This ratio for clearance is used for all species. The ratio of the renal to hepatic Km in tissue concentration units is assumed to be 1 (converted to Km in venous blood by using the liver–blood and kidney–blood partition coefficients). There are no available data on lung oxidation of perc, so the ratio of lung to liver oxidation for TCE from Green et al. (1997) is used. The ratio of the lung to hepatic Km in tissue concentration units (i.e., adjusted using liver–blood and lung–blood partition coefficients) is assumed to be 1, which is then converted to Km in air (in the lumen) by using the blood–air partition coefficients. These conversions are all documented in Supplementary Materials (Table S2).

Baseline values for the yield of TCA, and for TCA distribution, metabolism, and excretion

A minor fraction of perc oxidation is assumed to form compounds other than TCA. Biochemical and in vitro data all suggest that TCA, derived from trichloracetyl chloride, is the predominant metabolite of perc oxidation. Based on the metabolism scheme shown in Fig. 1, the three possible fates of the perc-Fe–O intermediate are trichloroacetyl chloride, the epoxide, and oxalic acid. Trichloroacetylchloride can either bind covalently to cellular constituents or undergo hydrolysis to form TCA. In vitro, Costa and Ivanetich (1980, 1984) reported that in microsomal and isolated hepatocyte preparations of rat liver, TCA was the only chlorinated metabolite found. In addition, the implied low-concentration clearance rate of TCA production from rat liver microsomes reported by Costa and Ivanetich (1980) [VMax/KM = 0.04 (CI: 0.02–0.13) nmol/min/mg protein/mM] is consistent with the production of all water-soluble metabolites from rat liver microsomes at a low concentration (0.068 mM) reported by Reitz et al. (1996) (clearance rate of 0.06 nmol/min/mg protein/mM). More recently, Yoshioka et al. (2002) reported only TCA and oxalic acid produced from phenobarbitol-induced rat liver microsomes preparations, with TCA accounting for 81% of the total. In addition, they reported that the pattern of products of epoxide hydrolysis – which results almost exclusively in CO and CO_2 – differs markedly from the products of perc oxidation in vivo or in vitro. Therefore, they concluded that the data are inconsistent with significant formation of the epoxide following perc oxidation, and therefore support the conclusion that the trichloroacetyl chloride pathway being predominant.

Overall, given the available data, it appears unlikely that the fraction of oxidation producing products other than TCA is greater than 50%, and the fraction is likely to be much less. In preliminary analyses, including this parameter in the optimization runs leads to estimates ranging 0.1%–1.4% in mice and 0.11%–6.3% in rats, indicating that mass balance substantially constrains the amount of oxidation to compounds other than TCA. In humans, the parameter was not separately identifiable from estimates of GSH conjugation flux, with estimates ranging 0.2%–92%. Therefore, by analogy to available rodent data, which indicates that between 80% and 100% of oxidation forms TCA, leaving only 0–20% forming other compounds, the human baseline value of the fraction of oxidation assumed to form compounds other than TCA is set to 10%. Unless the actual fraction forming other compounds is greater than 50% (e.g., a much larger amount of trichloroacetyl chloride is covalently bound in humans than in rodents), the uncertainty in the total flux of perc oxidation due to this assumption is not more than 2-fold.

TCA absorption, distribution, protein binding, and metabolism parameters are derived from the posterior population means from the Chiu et al. (2009) TCE model analysis, which included a number of TCA dosing studies.

Table 2
Comparisons of activities in liver subcellular fractions across species and studies[a].

Study	Activity (pmol/min/mg protein)		
	Lash et al. (1998)	Dekant et al. (1998)	Green et al. (1990)
Substrate concentration	2 mM	3 mM	10 mM
Rat liver			
Males			
Cytosol	177	84.5	18.2
Microsomes	140	□1	6.4
Females			
Cytosol	104	19.5	n.m.
Microsomes	62	□1	n.m.
Mouse liver			
Males			
Cytosol	345	27.9	3.4
Microsomes	272	□1	□1
Females			
Cytosol	408	26	n.m.
Microsomes	260	□1	n.m.
Human liver			
Males			
Cytosol	n.m.	□1	□1
Microsomes	n.m.	□1	□1
Females			
Cytosol	n.m.	□1	n.m.
Microsomes	n.m.	□1	n.m.

n.m. = not measured.

[a] Lash et al. (1998) and Green et al. (1990) used B6C3F1 mice and F44 rats. Dekant et al. (1998) did not specify the strain of mice or rats used.

Table 3
Comparisons of activities in kidney subcellular fractions across species and studies[a].

Study	Activity (pmol/min/mg protein)	
	Lash et al. (1998)	Dekant et al. (1998)
Substrate concentration	2 mM	3 mM
Rat kidney		
Males		
Cytosol	10.8	□1
Microsomes	17.8	□1
Females		
Cytosol	3.7	□1
Microsomes	8.2	□1
Mouse kidney		
Males		
Cytosol	72.5	11.6
Microsomes	121.3	□1
Females		
Cytosol	49.8	12.2
Microsomes	57.7	□1

[a] Lash et al. (1998) used B6C3F1 mice and F44 rats. Dekant et al. (1998) did not specify the strain of mice or rats used.

Baseline values for rates of GSH conjugation

Four studies were located that measured perc GSH conjugation in vitro (Green et al., 1990; Dekant et al., 1998; Lash et al., 1998, 2007). Green et al. (1990) and Dekant et al. (1998) measured GSH conjugation in cytosol and microsomes of mice, rats, and humans, and could only detect activity at the highest substrate concentration used (10 mM and 3 mM, respectively). Lash et al. (1998) measured GSH conjugation in cytosol and microsomes in mice and rats at 1 and 2 mM. Lash et al. (1998, 2007) both measured GSH conjugation in freshly isolated rat liver or kidney cells, with Lash et al. (1998) reporting measurements at 0.5, 1, and 2 mM and Lash et al. (2007) only reporting measurements at 2 mM. Whereas for oxidation, metabolism estimates from different studies and preparations (subcellular fractions versus whole cells) appear to be relatively consistent, for GSH conjugation, the results appear far less consistent. As shown in Tables 2 and 3, the differences among data at single concentrations of 210 mM (presumed to be near-maximal rates) from Green et al. (1990), Dekant et al. (1998), and Lash et al. (1998) spread over about a 100-fold or more range even within the same species and type of experimental preparation (e.g., male rat cytosol). The fact that the ordering is generally (though not exclusively) Green b Dekant b Lash suggests contribution from a systematic difference, possibly due to the different analytical methods employed. In addition, after accounting for protein content, estimates based on whole cells differed from those based on subcellular fractions, sometimes by an order of magnitude.

Only rat data from Lash et al. (1998) are at multiple concentrations so that both VMax and KM can be estimated. Therefore, initially, VMax and Km are fitted to GSH conjugation data from rat hepatocytes from Lash et al. (1998). Thereafter, the in vitro Km is fixed — i.e., for each species, the same in vitro Km is used for both the liver and the kidney. Alternative rat VMax values are obtained by refitting to either Dekant et al. (1998) or Green et al. (1990). Because the fit to Dekant et al. (1998) is intermediate between the fit t oLash et al. (1998) and the fit to Green et al. (1990) (see Fig. 4, panel A for a summary), it was selected as a baseline value, though a high degree of uncertainty is acknowledged. Similarly, for mouse liver, in vitro VMax is obtained by refitting (using the rat Km) to the more limited data from Dekant et al. (1998) and Green et al. (1990) (see Fig. 4, panel B). For consistency, the Dekant et al. (1998) value is selected for the mouse baseline value, though the value derived from Green et al. (1990) was 10-fold less. In humans, there are only data from Dekant et al. (1998), which were reported as non-detects. Therefore, the in vitro VMax is obtained by refitting (using the rat Km) to half the nominal detection limit. Given the wide variation in measures of GSH conjugation in rats, it is expected that these estimates in mice and human are equally or even more uncertain. For instance, in vitro data reported by Lash et al. (1998b, 1999) and Green et al. (1997) on hepatic GSH conjugation of

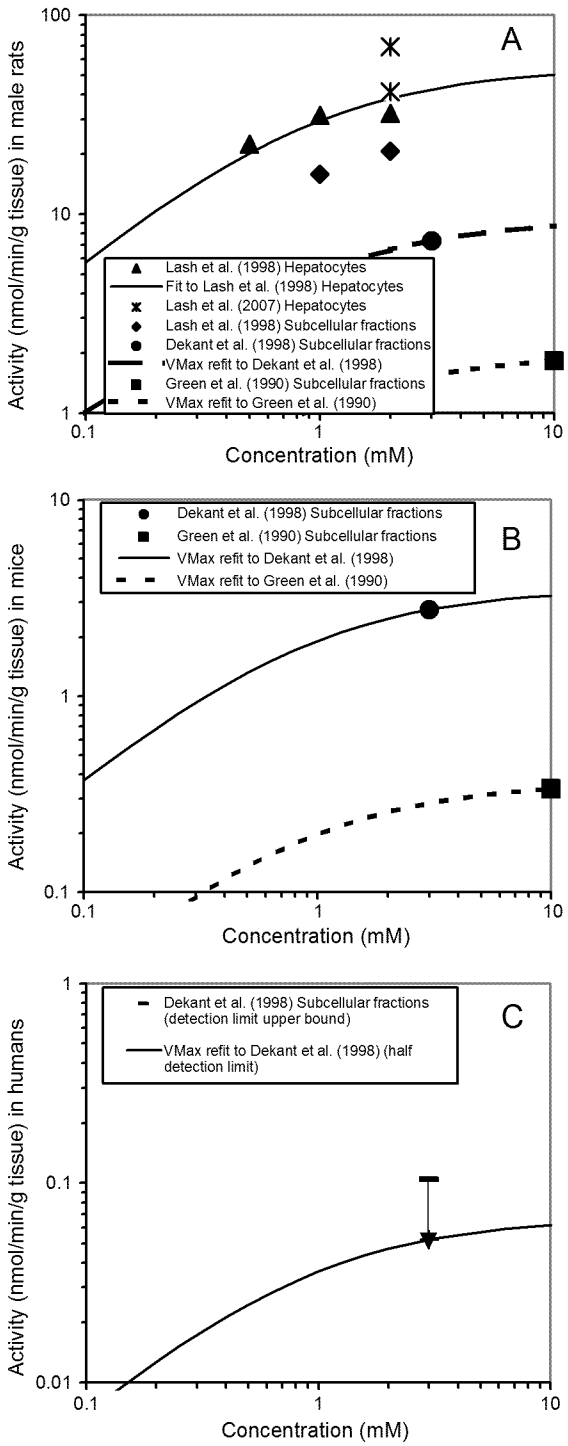

Fig. 4. Fits of VMax and Km to in vitro GSH conjugation data (A = Rats, B = Mice, and C = Humans). The value of Km from the fit to rat hepatocyte data of Lash et al. (1998) was used for all other fits. Baseline values for VMax were based on the Dekant et al. (1998) fits for each species, but a high degree of uncertainty is acknowledged given the consistently lower values suggested by Green et al. (1990) and the consistently higher values suggested by Lash et al. (1998, 2007).

TCE in mice, rats, and humans span a range of three to five orders of magnitude (Lash et al., 2000).

For kidney GSH conjugation, each in vitro VMax is scaled by using in vitro measures of the activity ratio between the kidney and the liver, with a preference for whole cell measurements because of the differences in cytosolic and microsomal protein content. In male rats, Dekant et al. (1998) reported no detectable activity in the kidney, whereas Lash et al. (1998, 2007) reported a ratio of 0.13 to 0.67 in kidney cells/hepatocytes and 0.06 to 0.08 in subcellular fractions. In male mice, where only subcellular data are available, Dekant et al. (1998) reported a ratio of 0.36 in males, whereas Lash et al. (1998) reported a ratio of 0.14 to 0.16. In humans, no data on perc are available, but Lash et al. (1999) reported a ratio of about 0.13 for VMax and 0.16 for VMax/Km for TCE using subcellular fractions. Therefore, a baseline in vitro ratio of 0.15 is selected for all species, which is within about 4-fold of all the available data.

Baseline values for subsequent metabolism and excretion of GSH conjugation products

Green et al. (1990) report kinetic parameters for bioactivation of TCVC by renal beta-lyase, based on cytosolic fractions. However, no data are available either on the other pathways of TCVC metabolism or on total clearance of TCVC. Thus, these data are not informative as to PBPK model parameters for either the relative fractional yields of urinary DCA and NAcTCVC or the shape of the time-course of urinary excretion. Unlike the case of the yield of TCA from oxidation, available data provide very limited support for urinary excretion products being an accurate quantitative measure of GSH conjugation flux. First, for TCA, the internal kinetics of TCA after it is produced are well calibrated from the Chiu et al. (2009) TCE model, so there is no need to rely on urinary excretion alone to estimate flux. Second, TCA results from spontaneous reactions occurring after oxidation to the perc-Fe–O intermediate, where as NAcTCVC and DCA are the result of multi-enzyme, multi-organ processing of the initial GSH conjugate, with little quantitative data as to the fractional yields of alternative pathways. Finally, Volkel et al. (1998) reported a species differences in the pattern of urinary excretion products, with rat urine containing predominantly DCA and human urine containing predominantly NAcTCVC. Therefore, there is little reason to assume that the relationship between urinary products and total flux is constant across species.

Therefore, no baseline values are assigned to the PBPK model parameters for the fractional yield of urinary DCA and NAcTCVC from GSH conjugation, and these parameters need to be optimized.

In vivo toxicokinetic data for calibration and evaluation

A literature search was made for in vivo data not previously considered in the PBPK modeling of perc and metabolites. At a minimum, data needed to include the exposure level, duration, and time of sample collection. Dermal exposure studies are not included because the current model does not include that exposure pathway. In addition, urinary excretion data that consisted only of concentrations are excluded since the PBPK model predicts the rate and/or cumulative amount of excretion (converting concentrations to amounts requires additional assumptions as to urinary volume and time between voids). These criteria led to omissions of a number of datasets such as human data from Ohtsuki et al. (1983) and Ikeda et al. (1972), particularly given the availability of numerous higher quality datasets that provide cumulative excretion data.

The studies with in vivo data considered for analysis are listed in Tables 4–6 and are separated into a "calibration" dataset and "evaluation" dataset. The following procedure is used to identify the "calibration" dataset. First, to be considered for "calibration," studies need to have (1) data at more than one time point and either (2a) data on one more metabolite, such as TCA, (2b) data on total metabolism, such as closed chamber or mass balance, or (2c) data on perc in one organ in addition to blood or breath. Additionally, in sets of similar data that include shorter and longer dosing periods, only the shorter period is used for "calibration." Data on TCA dosing previously incorporated in the TCE PBPK model are not considered here because the TCE PBPK model's TCA sub-model, along with its posterior distributions for the TCA sub-model parameters, are used as inputs to the present perc PBPK model. Evaluation of toxicokinetic data in mice administered TCA in drinking water is reported separately (Chiu, in press).

Model evaluation

Verification

The TCE model upon which the perc model is based had been previously verified by coding in MCSim and MatLab, as reported by Chiu et al. (2009). The current model is verified by coding in both MCSim and ACSLXtreme and comparing model predictions. In addition, mass balances are checked for each dosing regime and were found to be within the error tolerances of the ODE solver.

Baseline comparison with in vivo data

A comparison between model predictions using baseline parameters and a subset of the in vivo calibration data is used to determine whether

Table 4
Mouse in vivo toxicokinetic data used in PBPK model calibration and evaluation.

Reference	Strain	Sex	Exposures (dose range)	Measurements (time range)	Calibration	Evaluation
Buben and O'Flaherty (1985)	Swiss-Cox	M	Oil gavage (20–2000 mg/kg/day)	TCA urine (n.s.)		✓
Gargas, 1988, reported in Reitz et al. (1996)	B3C3F1	M	Closed chamber (1.5–400 ppm)	Chamber concentration (0–6 h)	✓	
Gearhart et al. (1993)	B6C3F1	M	Closed chamber (200–3500 ppm) Oil gavage (536–1072 mg/kg)	Chamber concentration (0–8 h) Venous blood TCA blood (1–48 h)	✓	
Green (2003)	B6C3F1	M + F	Inhalation (10–200 ppm)	TCA blood (102 h)		✓
Ikeda and Ohtsuji (1972)	DD	M + F	Inhalation (200 ppm)	TCA urine		✓
Odum et al. (1988)	B6C3F1	M + F	Inhalation (400 ppm)	TCA blood (1–54 h)		✓
Philip et al. (2007)	Swiss-Webster	M	Aqueous gavage (150–1000 mg/kg/day)	Venous blood Tissues: Liver, kidney TCA blood TCA liver (0–24 h and 696–720 h)	✓ (single dose)	✓ (repeated dose)
Reitz et al. (1996)	B6C3F1	M	Inhalation (11–1201 ppm)	Exhaled as perc (6–21 h) Retained dose (6 h) Fraction metabolized (54–71 h)	✓	
Schumann et al. (1980)	B6C3F1	M	Inhalation (10.6 ppm) Oil gavage (500 mg/kg)	Retained dose (6 h) Fraction metabolized (78 h)		✓

Table 5
Rat in vivo toxicokinetic data used in PBPK model calibration and evaluation.

Reference	Strain	Sex	Exposures (dose range)	Measurements (time range)	Calibration	Evaluation
Boyes et al. (2009)	Long–Evans	M	Inhalation (250–4000 ppm)	Arterial blood Tissues: brain (1–7 h)	✓	
Dallas et al. (1994a, 1994c)	Sprague–Dawley	M	Intra-arterial (10 mg/kg) Inhalation (500 ppm) Aqueous gavage (10 mg/kg)	Arterial blood Tissues: Liver, kidney, brain, muscle, fat, lung, heart (0–72 h)	✓	
Dallas et al. (1994b)	Sprague–Dawley	M	Inhalation (50–500 ppm)	Arterial blood Exhaled breath (2–600 h)		✓
Dallas et al. (1995)	Sprague–Dawley	M	Intra-arterial (1–10 mg/kg) Aqueous gavage (1–10 mg/kg)	Venous blood (0–30 h)		✓
Franz and Watanabe (1983)	Sprague–Dawley	M	Drinking water (8.09 mg/kg)	Amount exhaled (12–84 h)		✓
Gargas, 1988, reported in Reitz et al. (1996)	Sprague–Dawley	M	Closed chamber (1–1020 ppm)	Chamber concentration (0–5 h)	✓	
Ikeda and Ohtsuji (1972)	Wistar	M + F	Inhalation (200 ppm)	TCA urine (48 h)		✓
Ikeda et al. (1972)	Wistar	F	Inhalation (2–400 ppm)	TCA urine (48 h)		✓
Odum et al. (1988)	F344	M + F	Inhalation (400 ppm)	TCA blood (1–54 h)	✓	
Pegg et al. (1979)	Sprague–Dawley	M	Oil gavage (1–500 mg/kg) Inhalation (9.12–573 ppm)	Venous blood (1–36 h) Amount or fraction exhaled (72 h) Retained dose, inhalation exposures only (6 h)	✓	
Reitz et al. (1996)	F344	M	Inhalation (11.9–1146 ppm)	Exhaled as perc (6–27 h) Retained dose (6 h) Fraction metabolized (54–72 h)	✓	
Savolainen et al. (1977)	Sprague–Dawley	M	Inhalation (200 ppm)	Venous blood Tissues: Liver, brain, fat, lung (120–126 h)		✓
Volkel et al. (1998)	Wistar	M + F	Inhalation (10–400 ppm)	TCA blood (6–30 h) TCA urine (0–78 h) NAc-TCVC urine (0–66 h)	✓	
Warren et al. (1996)	Sprague–Dawley	M	Aqueous gavage (160–480 mg/kg)	Arterial blood (0–95 h) Tissues: Liver, brain, muscle, fat (0–1.5 h)	✓	

in vitro-derived metabolism parameters were consistent with in vivo data. This initial comparison is performed "a priori" — without fitting or adjusting any parameters. This "baseline subset" includes only studies by inhalation exposure (so absorption parameters would not need to be fitted) and only data related to either the parent compound (e.g., blood, tissue, air, or chamber concentrations), mass balance (e.g., total recovered radioactivity), or TCA.

Estimation of metabolism parameters

Selection of parameters for optimization. Because the purpose of this analysis is partly to determine the feasibility of including the GSH pathway, a full Bayesian uncertainty/variability analysis is not performed at this stage. Based on the results of the "baseline comparison," the values for a limited number of parameters (see Appendix Table A1 and Table 7) were replaced by optimized values obtained by fitting to in vivo data. This includes all perc metabolism parameters, so that in the optimization results, the original in vitro-based baseline parameter estimates are not given any weight in the parameter estimation, as bounded log-uniform prior distributions are assigned to them (see below). However, the baseline parameters are considered in the evaluation of the optimization results (discussed below). All other parameters, including most physiological parameters and partition coefficients, remain fixed at their baseline values.

For perc oxidation, preliminary analyses revealed that only a subset of the parameters is identifiable. In particular, in mice, only a single saturable (VMax and KM) and single linear pathway (VMax2/KM2 ratio) could be estimated. Similar to what was found by Gearhart

Table 6
Human in vivo toxicokinetic data used in PBPK model calibration and evaluation.

Reference	Individual data? (n)	Sex	Exposure dose range	Measurements (time range)	Calibration	Evaluation
Chien (1997)	Yes (1)	M	0.06–5 ppm	Alveolar breath (0–13 h)		✓
Chiu et al. (2007)	Yes (6)	M	1 ppm	Alveolar breath Venous blood TCA blood TCA urine (0–166 h)	✓	
Fernandez et al. (1976)	Some (7)	M + F	100–200 ppm	Alveolar breath (0–12 h) TCA urine, for 2 individuals (0–72 h)	✓ (TCA [n = 2])	✓ (others)
Hake and Stewart (1977)	Some (1)			Alveolar breath (0–2.5 h)		✓
Monster et al. (1979)	Yes (6)	M	72–144 ppm	Alveolar breath Venous blood TCA blood TCA urine (0–167 h)	✓	
Stewart et al. (1961)	No			Alveolar breath (0–150 h)		✓
Stewart et al. (1970)	No			Alveolar breath (0–440 h)		✓
Volkel et al. (1998)	Yes (6)	M + F	10–40 ppm	TCA plasma (6–30 h) TCA urine (0–78 h) NAc-TCVC urine (0–35 h)	✓	

Table 7
Log-likelihood and parameters after calibration.

Parameter	Baseline	Post-calibration (posterior mode)	GSD of posterior modes across chains	Range of posterior modes across chains
Mouse				
Ln(Likelihood)	–	−1780	–	−1808 to −1780
QP (L/h)	2.09	2.89	1.03	2.86–3.22
VMax (mg/h) (saturable oxidation pathway)	0.23	0.026	1.16	0.022–0.0369
KM (L/h) (saturable oxidation pathway)	88.6	0.417	1.28	0.338–0.892
VMax2/KM2 (L/h) (linear oxidation pathway)	–	0.0188	1.05	0.0165–0.0207
VMaxTCVG/KMTCVG (L/h) (linear conjugation pathway)	0.656	6.83E−05	3.83	3.05E−05–0.00179
kMetTCA (/h)	1.48	0.638	1.05	0.56–0.695
kUrnTCA (/h)	2.93	1.26	1.05	1.11–1.38
Rat				
Ln(Likelihood)	–	−1314	–	−1321 to −1314
QP (L/h)	10.2	6.31	1.02	6.28–6.68
VMax (mg/h) (saturable oxidation pathway)	0.256	0.87	1.37	0.415–1.93
KM (L/h) (saturable oxidation pathway)	69.7	31.1	1.39	14.8–71.9
VMaxTCVG/KMTCVG (L/h) (linear conjugation pathway)	2.22	0.00204	1.27	0.00131–0.00355
kDCA (/h)	–	0.129	1.65	0.0758–0.451
FracNATUrn	–	0.0143	1.29	0.00919–0.0253
FracDCAUrn	–	0.702	1.26	0.43–0.98
Human				
Ln(Likelihood)	–	1828	–	1790–1828
QP (L/h)	372	476	1.1	450–640
VMax/KM (L/h) (linear oxidation pathway)	0.353	0.454	1.08	0.346–0.468
VMaxKid/KMKid (L/h) (linear oxidation pathway)	0.00076	0.0947	1.09	0.0702–0.105
VMaxTCVG/KMTCVG (L/h) (linear conjugation pathway)	0.0196	5.26	17.1	0.00194–5.48
kNAT (/h)	–	0.28	1.07	0.228–0.293
FracNATUrn	–	0.000482	15.8	0.000472–1
FracDCAUrn	–	0.00022	18.5	1.12E−05–0.442

et al. (1993), restricting oxidation further to a single saturable pathway led to a significantly poorer fit. In rats and humans, on the other hand, a second pathway could not be identified. Thus, rats were modeled using a single saturable pathway (VMax and KM). Furthermore, in humans, only the linear rate of oxidation could be identified (VMax/KM ratio), as the available data was not adequate to estimate the degree of saturation. As discussed by Clewell et al. (2005), the time course of urinary excretion of TCA in humans is better fit by allowing direct excretion of TCA following oxidation in the kidney (see also earlier discussion under model structure). Therefore, for humans, the linear rate of kidney oxidation is also estimated to improve the fit over that from using "baseline" parameters. Furthermore, in mice, preliminary analyses showed that the time-course of TCA in blood decayed too rapidly, even after correcting the overall metabolism of perc to TCA. Therefore, the clearance parameters for TCA are further optimized. This is not altogether unreasonable, since the posterior distribution for the population means of these parameters had 95% confidence intervals spanning 5- to 6-fold. In order to maintain the appropriate ratio between urinary excretion and "other" metabolism that was predicted by Evans et al. (2009) and Chiu et al. (2009), the ratio between the two clearance parameter was fixed.

For GSH conjugation, preliminary analyses revealed that only the linear rate of perc conjugation could be estimated (VMaxTCVG/KMTCVG ratio). In addition, fractional yields of urinary NAcTCVC and DCA and the empirical delay parameters for urinary excretion are also estimated, given the lack of any in vitro data from which to estimate a baseline value. In rats, preliminary analyses found the NAcTCVC delay parameter to be poorly identified, so its rate is fixed to an arbitrarily high value (i.e., no delay). In humans, DCA data consisted of non-detects, so the empirical delay parameter for DCA could not estimated and its rate is fixed to an arbitrarily high value.

Finally, the ventilation–perfusion ratio is optimized because initial analyses suggest best fit values different from the standard baseline values. This is to be expected, as inter-individual and study-to-study differences in alveolar ventilation rate have been previously documented in the literature on the toxicokinetics of inhaled compounds (e.g., Johanson and Filser, 1992; Monster et al., 1979). To ensure that values have biological basis, physiological bounds are set to restrict the range of permitted optimized values.

Optimization approach. A "traditional" optimization approach using algorithms such as Nelder–Mead was considered. However, one of the difficulties with the usual optimization routines found in standard software packages is that they are best suited for situations where (1) there is a good guess as to the initial starting point; (2) the number of parameters optimized at a time is quite small (less than 5, usually); (3) all the parameters need to be identifiable; (4) there is a single mode near to the "initial guess" for the parameters; and (5) the sampling distribution of the parameters is close to being asymptotically normal. These limitations lead to a number of somewhat ad hoc "workarounds," including use of "visual" fitting to obtain initial parameter estimates and subdividing the data and parameters so that only a few data and parameters are estimated at a time. To avoid such ad hoc approaches, limited Bayesian analysis is utilized involving flat priors and making inferences only using posterior modes obtained via MCMC. This approach is more flexible for a number of reasons. First, it uses starting points randomly selected over a wide range, so requires only some bounds (that can be quite wide) rather than a good "initial guess" for the parameters, (addressing point 1, above). The wide range of starting points also may better locate multiple modes (addressing point 4, above). Second, it is computationally efficient even when simultaneously optimizing a larger set of parameters and when some parameters are not (or only weakly) identifiable (addressing points 2 and 3, above). Third, it directly samples from the parameter sampling distribution, rather than relying on its being close to asymptotically normal (addressing point 5, above). Fourth, if an extension to full hierarchical population analysis is performed, then the same software can be used with minimal recoding. It is acknowledged that alternative optimization techniques could be used, such as simulated annealing (Belisle, 1992), and it would be interesting to compare results in future work.

Specifically, for each species, let the data have a "type" label i (e.g., i = 1, closed chamber; i = 2, venous blood; etc.) and an index j, so each data point is denoted y_{ij}. For a given set of parameters θ, the natural logarithm of each data point is assumed to be normally distributed, with variance σ_i^2, about the natural logarithm of the PBPK model predictions $f_{ij}(\theta)$. The log-likelihood (LL) function is therefore:

$$LL\left(\theta;\sigma^2\right) = -\Sigma_{ij}\left[\ln\left(2\pi\sigma_i^2\right)/2 + \left(\ln y_{ij} - \ln f_{ij}(\theta)\right)^2/2\sigma_i^2\right] \quad (1)$$

Therefore, all data points for a given data type (all closed chamber data) are assumed to have their own variance. The parameters θ are the "scaling parameters" shown in Table A1, whereas the parameters σ^2 represent the "residual error." Data from each species are grouped together, so this "residual error" that is represented by the variance parameters σ_i^2 includes experimental error and model error, as well as inter-strain (for rodents), inter-study, inter-group, and inter-individual variability. Importantly, the variance parameters are estimated as part of the parameter calibration, and so contain information about the degree of "residual error" between the model predictions and the data. Bounded log-uniform distributions (or uniform distributions on the log-transformed parameters) are used as priors for all parameters, spanning either biological bounds (such as for the ventilation-perfusion ratio) or a sufficiently wide range so as to be inconsequential to the results (all other parameters, including variance parameters). With these choices for priors, the posterior mode and MLE estimate over the log-transformed parameters will coincide numerically, though there is a conceptual difference in the treatment of parameters in the two approaches.

To account for sampling variation as well as to access multiple local maxima, if they exist, multiple independent MCMC chains, each of length 5000 (retaining only every 10 samples to reduce storage requirements), are used, each with different random starting points and random number seeds. In mice and rats, 24 independent chains were used. Because of preliminary analyses revealed multiple maxima, in humans 48 independent chains were used to better cover each maximum. The parameter set with highest overall posterior probability out of the (24 or 48) × 500 = (12,000 or 24,000) recorded samples is selected as the posterior mode. The parameter sets with the highest posterior probability in each chain ("chain-specific posterior mode") are used to assess the sampling uncertainty in the posterior mode as well as the presence or absence of multiple local maxima. From here forward, the "optimized values" refer to the collection of chain-specific posterior modes.

Model parameter and model fit evaluation

Optimized values of model parameters, particular for metabolism, are evaluated with respect to values obtained from the literature for perc or related compounds. For hepatic metabolism, comparison is made with the in vitro measurements used to derive the baseline values (see above), as well as data from related compounds TCE, CH_2I_2, and CH_2Cl_2. In particular, comparison is made to TCE oxidation as reported by Lipscomb et al. (1998) for in vitro VMax and KM in mouse, rat, and human liver microsomes. Comparison is made to TCE GSH conjugation as reported by Green et al. (1997a) in mouse, rat, and human liver cytosol, and by Lash et al. (1998b, 1999) in mouse and rat liver subcellular fractions and in human hepatocytes. Comparison is made to CH_2I_2 and CH_2Cl_2 GSH conjugation as reported by Wheeler et al. (2001) in bacteria that were transfected with human GSTT1. These two substrates represent the minimum and maximum reported activities among the 5 halomethanes for which HCHO formation could be detected. For these data, the conversion required use of the molecular weight of GSTT1 (29 kDa), assuming its responsible for at least of a portion of the cytosolic activity, and the amount of GSTT1 in liver cytosol, estimated to be about 0.02% (Juronen et al., 1996).

In terms of model fit, first a qualitative, visual comparison is made between model predictions using posterior mode parameters and both the "calibration" data and the "evaluation" data. Then, more quantitatively, the residual error estimates are evaluated, along with the geometric mean and standard deviations of the ratio between predicted and observed data, for both the "calibration" and "evaluation" datasets.

Dose metric and mass balance predictions based on posterior mode parameter estimates

The following dose metrics are assessed for continuous exposures (10 weeks for rodents, 100 weeks for humans) at 0.01–1000 ppm in air or 0.01–1000 mg/kg/day by oral intake (e.g., drinking water):

- Daily area-under-the-curve of perc in blood,
- Amount metabolized by oxidation (as fraction of intake),
- Amount metabolized by GSH conjugation (as fraction of intake), and
- Equivalent daily production of TCA per kg body weight.

With respect to the last dose metric, TCA produced in the kidney and excreted directly to urine is not included, since it does not reach any target organ (i.e., the liver) or enter systemic circulation.

Dose metrics are evaluated using the overall posterior mode as well as using each chain-specific posterior modes. From these dose metrics, the overall mass balance can be inferred.

Local sensitivity analyses to inform dose metric uncertainty

The sampling distribution of posterior modes only provides a sense of the uncertainty with respect to the optimized parameters, not with respect to the fixed parameters. Assessing the degree of uncertainty that may result from fixing these parameters requires three pieces of information on each parameter:

1. The extent to which dose metric predictions are sensitive to the parameter,
2. How much a priori data supports the parameter's value, and
3. The extent to which predictions (fits) to the empirical data are sensitive to the parameter (as a partial indicator of identifiability).

For considerations (1) and (3), local sensitivity analysis is performed with respect to the predicted dose metrics and calibration data points, respectively. For simplicity, the dose metrics were only evaluated at "moderate" rodent exposures (10 ppm and 100 mg/kg/day) and "low" human exposures (0.01 ppm and 0.01 mg/kg/day), since these are of primary interest to environmental risk assessment. To perform local sensitivity analysis, each parameter is centered either on its baseline value or on its posterior mode, and then increased and decreased by 5%. The relative change in the model output f(θ) is used to estimate a local sensitivity coefficient (SC) as follows:

$$SC = 10 \times \left[f\left(\theta_b^-\right) - f(\theta_b^+)\right] \Big/ \left[f\left(\theta_b^-\right) + f(\theta_b^+)\right] \quad (2)$$

Here, $\theta_\pm$ is the posterior mode or baseline value of ±5%. For log-transformed parameters, 0.05 was added or subtracted from the baseline value, whereas for untransformed parameters, the baseline value was multiplied by 1.05 or 0.95. For (1), f(θ) is one of the dose metrics described above, and for (3), f(θ) is one of the model predictions of the calibration data used to derive the posterior mode. The resulting values of SC are binned into five categories according to their sensitivity coefficient: none (|SC| = 0) very low (0b|SC|≤ 0.1), low (0.1b |SC| ≤ 0.5), medium (0.5b|SC| ≤ 1.0), and high (|SC|N1.0).

For consideration (2), a judgment is made based on the sources of the baseline parameter values. For parameters estimated by optimization, consideration (3) is also informed by the sampling distribution of posterior modes.

Note that local sensitivity analyses as typically performed in deterministic PBPK modeling can only inform the "primary" effects of parameter uncertainties — i.e., the direct change on the quantity of interest due to change in a parameter. They cannot address the propagation of uncertainties through an analysis, such as those that can arise due to parameter correlations in the parameter fitting process. Those can only be addressed in a global sensitivity analysis or more comprehensive Bayesian approach, which is left for future work.

Results

Model parameter evaluation

Statistical uncertainty

Table 7 summarizes the statistical characteristics of the optimized parameters, comparing the baseline value, overall posterior mode, the GSD of the chain-specific posterior modes, and the range of the chain-specific posterior modes. A large (e.g., N10-fold) GSD or range of chain-specific posterior mode is indicative of either multiple local maxima and/or poor identifiability. For ease of interpretation, all parameters have been converted to physical units using the scaling relations from Table A1. For pathways modeled with a linear rate only, the ratio VMax/KM is shown.

In mice, as shown in Table 7, the alveolar ventilation QP and the parameters for perc oxidation and TCA clearance are consistently estimated, with GSDs across chains of 1.3 or less and range of estimates spanning 3-fold or less. This suggests that the data are highly informative as to these parameters, without multiple modes or degeneracies. The linear rate of GSH conjugation, however, has somewhat more uncertainty, with estimates range spanning almost two orders of magnitude.

In rats, QP, VMax and KM for oxidation, linear rate for GSH conjugation, and the fraction of GSH conjugation appearing as NAcTCVC and DCA in urine are all consistently estimated, with GSDs across chains of 1.3-fold or less and range of estimates spanning 3-fold or less. This suggests that the data are highly informative as to these parameters, without multiple modes or degeneracies. Much more uncertain is the urinary delay constant for DCA, with estimates spanning two orders of magnitude.

In humans, QP, the linear rate for hepatic and kidney oxidation, and the urinary delay constant for NAcTCVC are consistently estimated, with GSDs across chains of 1.1-fold or less, and estimates spanning a range of 2-fold or less. This suggests that the data are highly informative as to these parameters, without multiple modes or degeneracies. Parameters directly related to the GSH conjugation – the linear rate of conjugation and the fractional yields of urinary NAcTCVC and DCA – appear much more uncertain, with the overall posterior mode and alternative posterior modes spanning about 3 and a half-orders of magnitude. In particular, they appear to show two distinct modes — one with "high" GSH conjugation (the overall posterior mode) and one with "low" GSH conjugation (a number of the alternative posterior modes).

Biological plausibility

Model parameters are evaluated with respect to values obtained from the literature for perc and related compounds. As shown in Table 7, the posterior mode estimates of the alveolar ventilation rate are higher than baseline values in mice and humans, and lower than baseline values in rats. However, they remain reasonable physiological values (e.g., compared with Brown et al., 1997). In mice, the optimized values for TCA clearance were about two-fold lower than the baseline values obtained from the posterior population mean of the Evans et al. (2009) TCE PBPK model, though they remain with the 95% confidence interval.

In terms of perc metabolism parameters, Fig. 5 compares the in vivo predictions for hepatic metabolism with available in vitro data. For oxidation, in mice and rats, the optimized values are about an order of magnitude higher than baseline values, whereas in humans, the optimized values are quite similar to baseline values. However, they do not appear unreasonable compared to other compounds. For example, as shown in Fig. 5, the linear rates are lower than those for TCE, which is known to be more extensively oxidized by P450s than perc. At higher substrate concentrations the predicted rate of oxidation of perc in mice and humans is greater than that for TCE, but this is an artifact of the assumption of a linear rate necessitated by KM being unidentifiable. In humans, the optimized rate of kidney oxidation is much higher than the baseline value (see Table 7), consistent with the finding of Clewell et al. (2005). However, the overall contribution of renal oxidation is only about 20% of that of hepatic oxidation. This finding is consistent with data suggesting that perc is oxidized by P450 isoforms in addition to CYP2E1, which appears to be not expressed (or expressed to a very low extent) in the kidney (Lash and Parker, 2001).

For GSH conjugation, the range of the in vitro data is quite wide, especially when also taking into considering data from other compounds (see Fig. 5). In mice and rats, the in vitro data on perc GSH conjugation (filled symbols in Fig. 5) spans the range of estimates from optimization to in vivo data. For humans, the in vitro data only consist of non-detects from Dekant et al. (1998), which, if assumed to be half the detection limit, are more consistent with the alternative posterior modes. Data from TCE (open symbols in Fig. 5) show the long-standing discrepancy between TCE GSH conjugation measurements by Lash et al. (1998b, 1999) and Green et al. (1997a), and span the range of estimates from optimization to in vivo data. Data from halomethanes show a range of activities, with the largest and smallest reported in Wheeler et al. (2001) shown in Fig. 5. Note, however, that the lower rate from Wheeler et al. (2001) shown is only slightly above what could be detected, so values below that are not unreasonable. Therefore, the ranges of predicted rates for perc are consistent with the range inferred from halomethanes. In addition, somewhat higher rates are also reasonably plausible if GSTT1 only accounts for a portion of the overall GSH conjugation of perc. Overall, the in vivo optimized values do not appear to be substantially outside the bounds suggested by available in vitro data.

Model fit evaluation

The fits between model predictions and in vivo data for the baseline and optimized model are summarized in Table 8 (residual error estimates and prediction/observation residuals), Fig. 6 (residual plots for selected measurements), and Supplementary Materials (individual time-courses). The discussion here focuses on summary results from Table 8 and Fig. 6, with the Supplementary Materials containing discussion of individual time-courses.

Mouse model

In mice, the largest discrepancy in baseline predictions is for TCA in blood and liver, which are under-predicted by about a 20-fold difference on average (see Table 8 baseline residuals, and Fig. 6A). Closed chamber concentrations and other measurements of perc itself, however, are relatively well predicted at baseline, with ratios of predicted/observed of about 2-fold on average (see Table 8 baseline residuals). These results suggest that while baseline predictions of total metabolism in mice are fairly accurate, the prediction for the relative proportion of oxidation to conjugation is much too low or TCA elimination is much slower that predicted by previous modeling of TCE and TCA.

As expected, the optimized parameters had increased oxidation, decreased conjugation, and decreased values for TCA clearance (see Table 7), resulting in substantially better fits to TCA (Table 8 calibration data residuals). For mice calibration data, the poorest fits (residual error GSDN3.0) are to the rate of perc exhalation (from Reitz

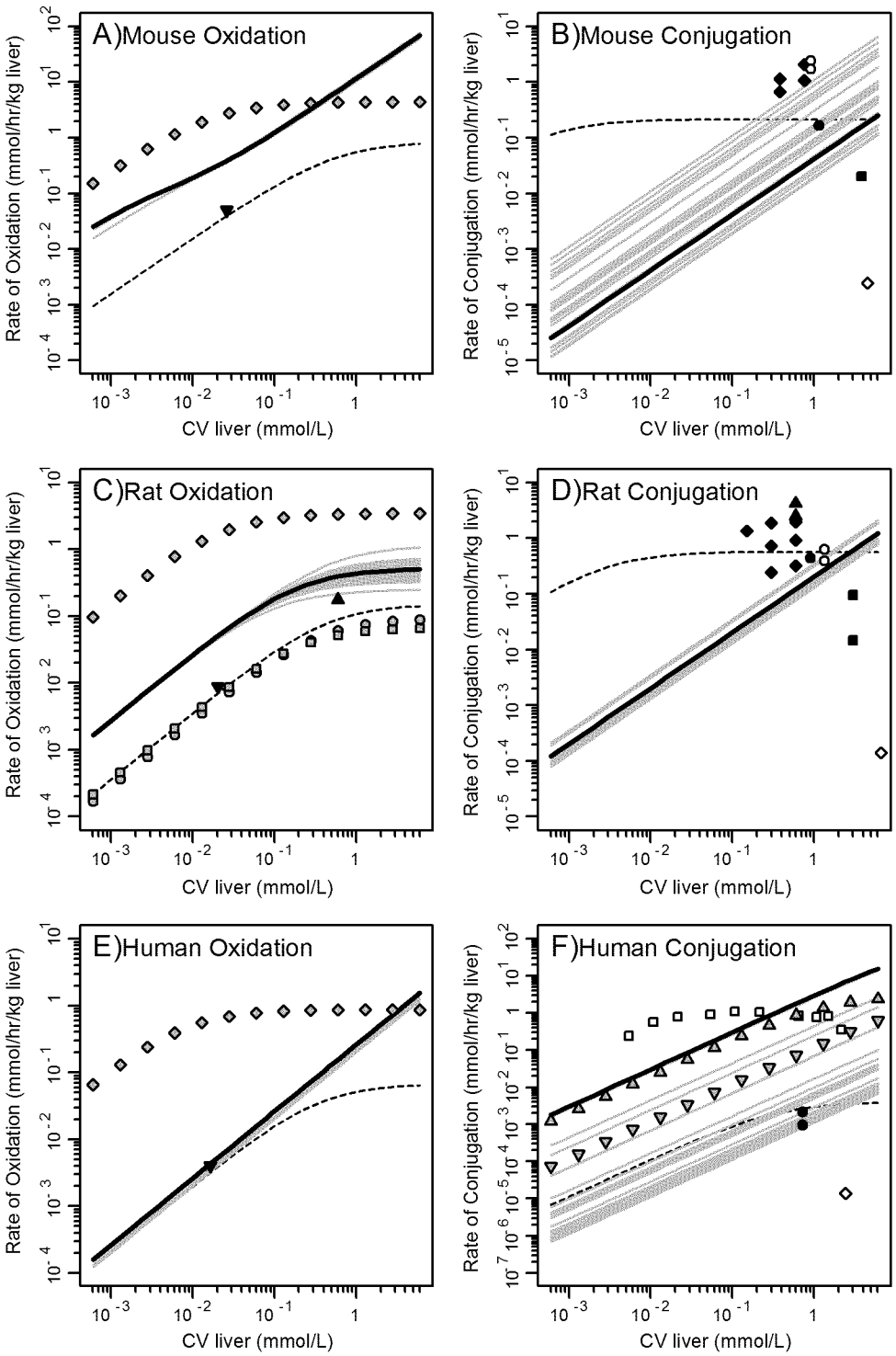

Fig. 5. Comparison of mouse (A–B), rat (C–D), and human (E–F) rates of hepatic oxidation (A, C, and E) or conjugation (B, D, and F) measured in vitro (symbols) and predicted by the model (lines). Data shown consist of measurements of perc in vitro oxidation and conjugation [solid circle: Dekant et al. (1998), solid square: Green et al. (1990); solid diamond: Lash et al. (1998); solid triangle: Lash et al. (2007); solid upside-down triangle: Reitz et al. (1996)], reported fits of in vitro perc VMax and Km for oxidation [gray-filled circle: Costa and Ivanetich (1980); gray-filled square: Costa and Ivanetich (1984); gray-filled diamond: Lipscomb et al. (1998); gray-filled triangle: Wheeler et al. (2001) CH_2I_2; gray-filled upside-down triangle: Wheeler et al. (2001) CH_2Cl_2], and measurements of TCE in vitro conjugation [open circle: Lash et al. (1998b); open square: Lash et al. (1999); open diamond: Green et al. (1997)]. Model predictions are using baseline parameters (dotted line), overall posterior mode parameters (solid thick line), and alternative posterior mode parameters (gray lines).

et al., 1996). It is unclear how to completely reconcile the extremely well-fit closed chamber data with the more poorly fit C-14 data from Reitz et al. (1996), but inter-study variation cannot be ruled out. All the remaining calibration data had more modest (b2-fold) residual errors. For mice evaluation data, the poorest fits are to the fraction of retained perc exhaled and the liver concentration of TCA, with the predictions and observations differing by 3-fold or more on average. Part of the difficulty in fitting the TCA data stems from the different degree of dose-proportionality between tissues (liver and blood) and the observed differences between single and repeated dosing

Table 8
Posterior modes for residual calibration error and statistics of residuals for calibration and evaluation data.

Measurement	Baseline residuals (predicted/observed)		Calibration data: residuals (predicted/observed)		Evaluation data residuals (predicted/observed)		Estimated calibration error (GSD = exp(σ))	
	GM	GSD	GM using posterior mode	GSD using posterior mode	GM using posterior mode	GSD using posterior mode	GSD using posterior mode	Range across chains
Mouse								
Closed chamber concentration	1.08	1.50	1.02	1.22	–	–	1.21	1.21–1.24
Perc venous blood concentration	0.98	2.00	0.78	1.85	0.66	1.65	2.01	1.77–2.30
TCA blood concentration	0.048	4.65	1.05	1.88	1.24	1.67	1.90	1.82–2.04
Retained dose	1.16	1.16	1.34	1.35	0.82	–	1.81	1.36–3.03
Fraction of retained dose metabolized	0.49	1.80	0.77	1.38	0.66	–	1.49	1.28–4.65
Fraction of retained dose exhaled	–	–	–	–	3.48	–	–	–
Total amount metabolized	–	–	–	–	1.46	–	–	–
Total amount of perc exhaled	–	–	–	–	0.98	–	–	–
Rate of perc exhalation	2.27	1.83	3.24	1.54	–	–	4.26	3.05–5.28
Perc liver concentration	0.91	5.04	0.98	1.75	0.60	2.40	1.61	1.54–2.13
Perc kidney concentration	1.30	3.08	1.01	1.57	0.93	1.75	1.56	1.47–1.79
TCA liver concentration	0.056	2.76	0.82	1.61	3.20	1.70	1.59	1.53–1.89
Cumulative urinary excretion of TCA	–	–	–	–	1.18	1.55	–	–
Rat								
Perc venous blood concentration	1.07	2.27	1.36	1.60	0.94	2.17	1.75	1.69–1.99
Perc brain concentration	0.56	3.94	1.03	1.78	1.90	1.35	1.78	1.72–2.11
Perc liver concentration	0.24	5.59	1.11	2.25	1.42	1.51	2.34	1.96–2.72
Perc kidney concentration	0.10	1.98	0.59	2.22	–	–	2.49	2.22–3.19
Perc muscle concentration	0.26	4.79	0.80	2.49	–	–	2.71	2.23–3.21
Perc fat concentration	0.23	3.76	0.70	1.80	2.81	1.26	2.04	1.88–2.3
Perc arterial blood concentration	0.26	3.49	1.00	1.77	0.54	1.83	1.73	1.64–1.84
TCA blood concentration	0.092	3.02	0.87	1.77	–	–	1.94	1.62–2.14
Retained dose	1.07	1.33	0.70	1.19	–	–	1.41	1.37–2.79
Fraction of retained dose exhaled	0.38	2.71	1.11	1.16	–	–	1.33	1.11–3.39
Amount of perc exhaled	0.41	3.34	1.13	1.14	1.01	–	1.16	1.12–2.71
Closed chamber concentration	0.29	2.42	0.95	1.29	–	–	1.32	1.28–1.33
Perc exhaled breath concentration			–	–	0.33	1.80		
Fraction of retained dose metabolized	2.04	1.47	0.56	1.46	–	–	2.14	1.52–9.05
Rate of perc exhalation	1.01	1.87	1.20	1.58	–	–	1.67	1.49–1.95
Cumulative urinary excretion of TCA	0.03	1.57	1.01	1.10	0.50	2.54	1.16	1.11–1.16
Cumulative urinary excretion of NAc-TCVC	3850	1.86	0.91	1.37	–	–	1.45	1.31–1.51
Cumulative urinary excretion of DCA	45	1.36	0.97	1.26	–	–	1.32	1.22–1.39
Human								
Perc alveolar breath concentration	1.06	1.82	0.93	1.73	0.83	3.11	1.75	1.73–1.77
TCA blood or plasma concentration	0.80	1.85	1.02	1.81	–	–	1.81	1.73–1.87
Perc venous blood concentration	1.36	1.65	1.07	1.71	2.16	1.15	1.71	1.71–1.88
Cumulative urinary excretion of TCA	0.45	2.25	1.00	1.96	–	–	1.92	1.91–1.99
Cumulative urinary excretion of NAc-TCVC	4.02	1.41	1.01	1.41	–	–	1.42	1.37–1.43

GM = geometric mean; GSD = geometric standard deviation.

experiments. Both of these results suggest that additional non-linearities, such as tissue-specific protein binding, inhibition of metabolism, and/or the effects of hepatic injury (Philip et al., 2007), need to be included to more accurately predict TCA time-courses following perc exposure. All the remaining evaluation data was predicted to within about 2-fold on average.

Rat model

In rats, the largest discrepancies in baseline predictions are for perc in tissues, closed chamber concentrations, and TCA in blood and urine, which are underpredicted by 3- to 300-fold (see Table 8 baseline residuals, and Fig. 6B). These results suggest that baseline predictions of total metabolism are too high in rats, while baseline predictions of oxidative metabolism are too low.

As expected, the optimized parameters had increased oxidation and decreased conjugation, resulting in a clear improvement in model fit across all the data (see Fig. 6B, and Table 8 calibration data residuals). For rat calibration data, the poorest fits are to the fraction of retained perc metabolized and rate of perc exhalation (both from Reitz et al., 1996) and perc in various tissues (from Dallas et al., 1994a, 1994c; and Warren et al., 1996), with residual errors of 2- to 3-fold. As with mice, it is unclear how to completely reconcile the extremely well-fit closed chamber data with the more poorly fit C-14 data from Reitz et al. (1996), but inter-study variation cannot be ruled out. All the remaining data have more modest (b2-fold) residual errors. For rat evaluation data, the poorest fits are to perc in fat (Savolainen et al., 1977) and exhaled breath (Dallas et al., 1994b) with the predictions and observations differing by more than 2-fold on average. The remaining evaluation data had less than 2-fold residuals on average, though there is some degree of variability between studies.

Human model

In humans, the baseline predictions were better than those in rodents. The greatest discrepancies were with respect to TCA urinary excretion, but in some cases the baseline estimates were overestimates while in others they were underestimates. The results in humans suggest that baseline predictions for oxidation are fairly accurate on average, but that there is significant inter-individual variability. In addition, baseline predictions for total metabolism in humans do not appear inconsistent with the parent compound data.

Optimization of human parameter leads to a decrease in the overall deviation between observations and predictions, but not as dramatically as with mice and rats. For human calibration data, all the fits have calibration residuals centered on 1 with scatter of about

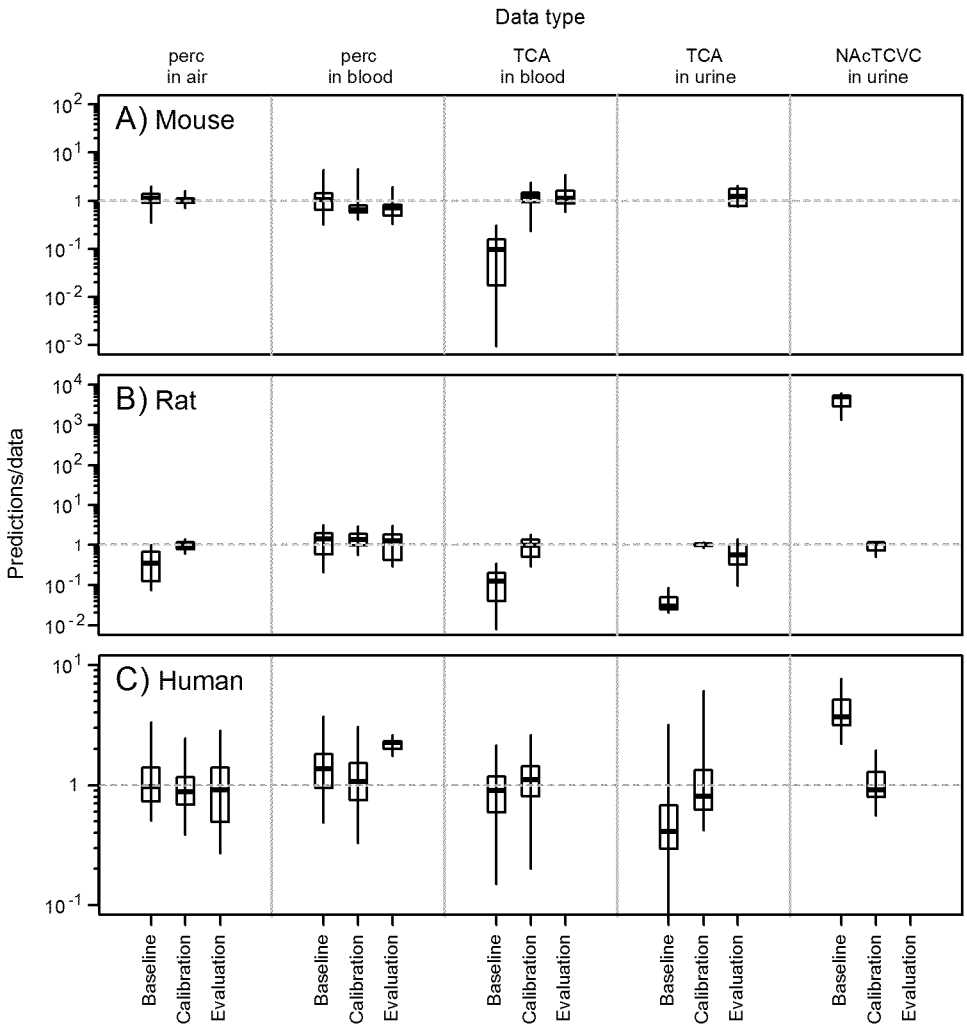

Fig. 6. Comparison of residuals (model predictions/in vivo data) in mice (A), rats (B), and humans (C). Each boxplot consists of the median (thick line), interquartile region (box), and 95% quantile region (error bars). For the selected data types, residuals are shown for baseline data and baseline predictions (using baseline parameters), calibration data and calibration predictions (using the posterior mode parameters), and evaluation data and evaluation predictions (also using the posterior mode parameters). The dashed horizontal gray line in each panel represents predictions = data.

2-fold (see Table 8, calibration data residuals), and corresponding residual errors less than 2-fold (see Table 8, estimate residual error). For human evaluation data, the poorest fits are to perc in blood (from Stewart et al., 1961), with the predictions and observations differing by more than 2-fold on average. The remaining evaluation data had less than 2-fold residuals on average.

As discussed above under "model parameter evaluation," the parameter optimization procedure revealed two distinct modes in the rate of GSH conjugation — one with "high" GSH conjugation (the overall posterior mode) and one with "low" GSH conjugation (a number of the alternative posterior modes). The log-likelihood for the overall posterior mode with high GSH conjugation is 38 units higher than the alternative posterior modes with low GSH conjugation, which would be significant by any classical statistical test. This reflects the collective improvement in fit over many time-courses, but it is difficult to discern a qualitatively significant improvement in model fit in individual time courses. Specific examples are shown in Figs. 7–10, in which time-courses using the overall posterior mode (with "high" predictions for GSH conjugation) are compared those using the alternative posterior modes (which include both "high" and "low" predictions for GSH conjugation). In particular, these Figures show the calibration predictions for the individual in each study with the greatest difference in log-likelihood between the overall posterior mode and the lowest alternative posterior mode. Clearly, the degree of deviation is far less than the intra- and inter-individual variability evident in the data. Intra-individual variability (partially related to experimental variance) is particularly prominent in the perc and TCA blood data in subject B from Chiu et al. (2007) (Fig. 7). Inter-individual variability is evident when comparing TCA in urine across all four figures (Figs. 7, panel D, 8, panels C and D, 9, panel D, and 10, panels A and B) — some data were higher than the predictions and some lower. Similarly, between Subjects C and E from Volkel et al. (1998), the amount of NAcTCVC in urine also showed substantial variability well in excess of the difference among the predictions.

Finally, it is interesting to note that there is inter-study and inter-individual variability in whether the overall posterior mode parameters lead to a better fit than a "low" GSH conjugation alternative posterior mode parameter. In particular, comparing partial log-likelihoods for each individual (i.e., the likelihood for the data for that individual) between overall posterior mode with the lowest alternative posterior mode (which predicted "low" GSH conjugation), 15 individuals had higher partial log-likelihoods using the overall posterior mode, while 5 individuals had higher partial log-likelihoods using the lowest alternative posterior mode. This raises the possibility

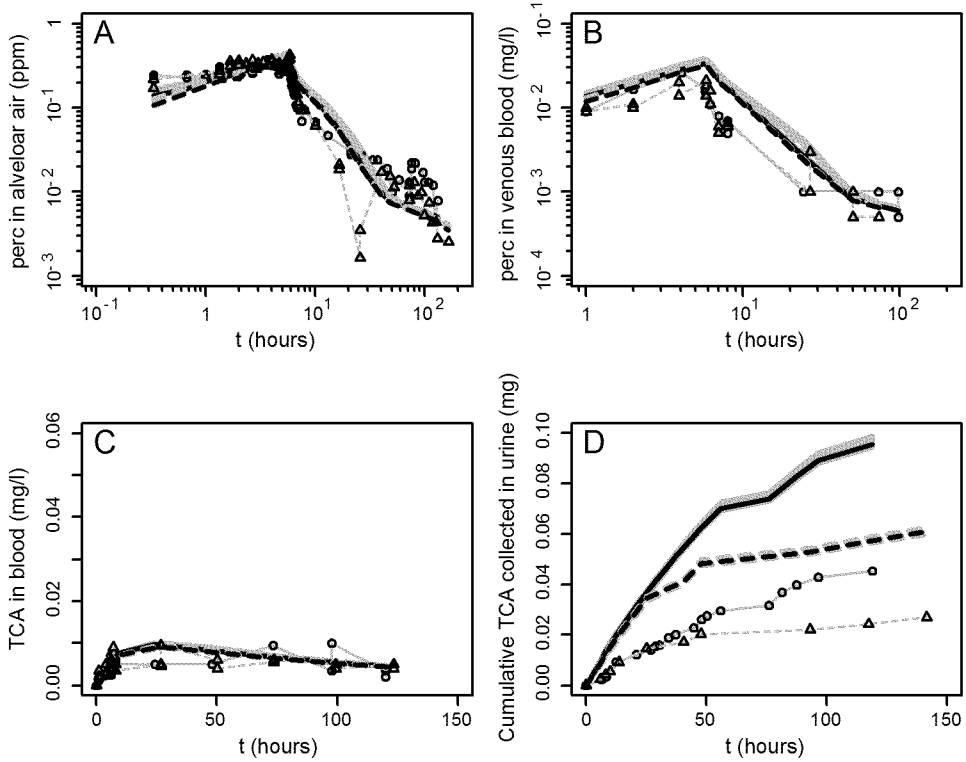

Fig. 7. Comparison of data and model predictions for perc in alveolar air (A) and blood (B) and TCA in blood (C) and urine (D) for human subject B from Chiu et al. (2007) exposed to 1 ppm for 6 h. Within this study, this individual has the greatest difference in log-likelihood between the overall posterior mode and the lowest chain-specific posterior mode. Circles are data (connected by thin lines for clarity), the thick solid line is the overall posterior mode, and the gray lines show chain-specific posterior modes.

that inter-individual variability may play a role in the range of estimated responses, though this inference is limited in part by there being only 20 subjects in the calibration dataset.

Summary evaluation of model fit

Overall, across all three species, the fitted model predictions were generally within about 3-fold of the observed data, with a few cases,

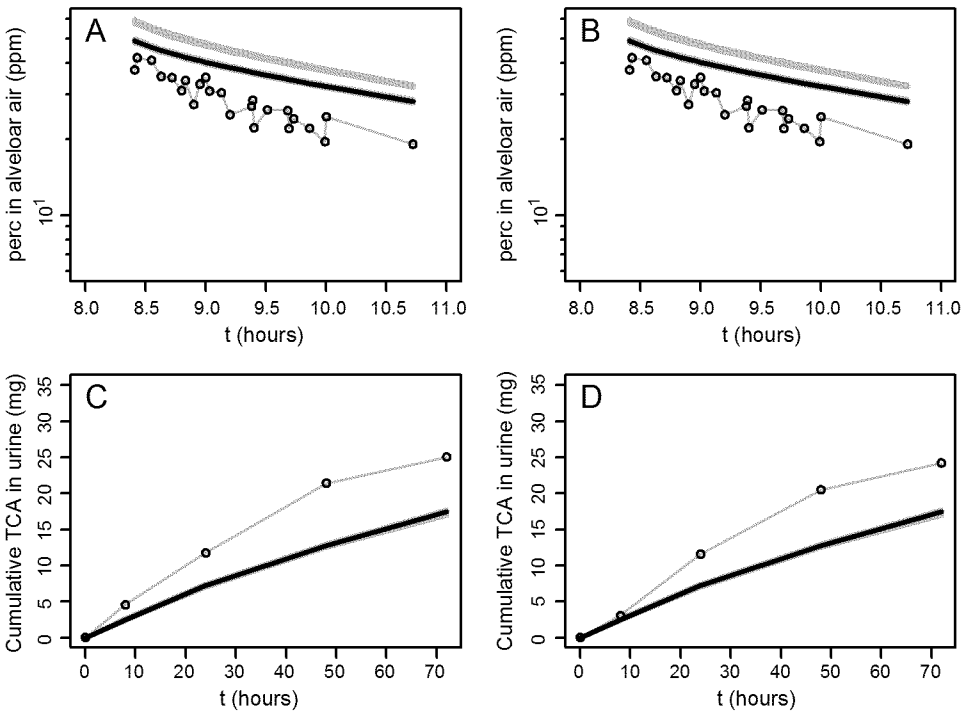

Fig. 8. Comparison of data and model predictions for perc in alveolar air (A–B) and TCA in urine (C–D) for subjects from Fernandez et al. (1976) exposed to 150 ppm for 8 h. Circles are data (connected by thin lines for clarity), the thick solid line is the overall posterior mode, and the gray lines show chain-specific posterior modes.

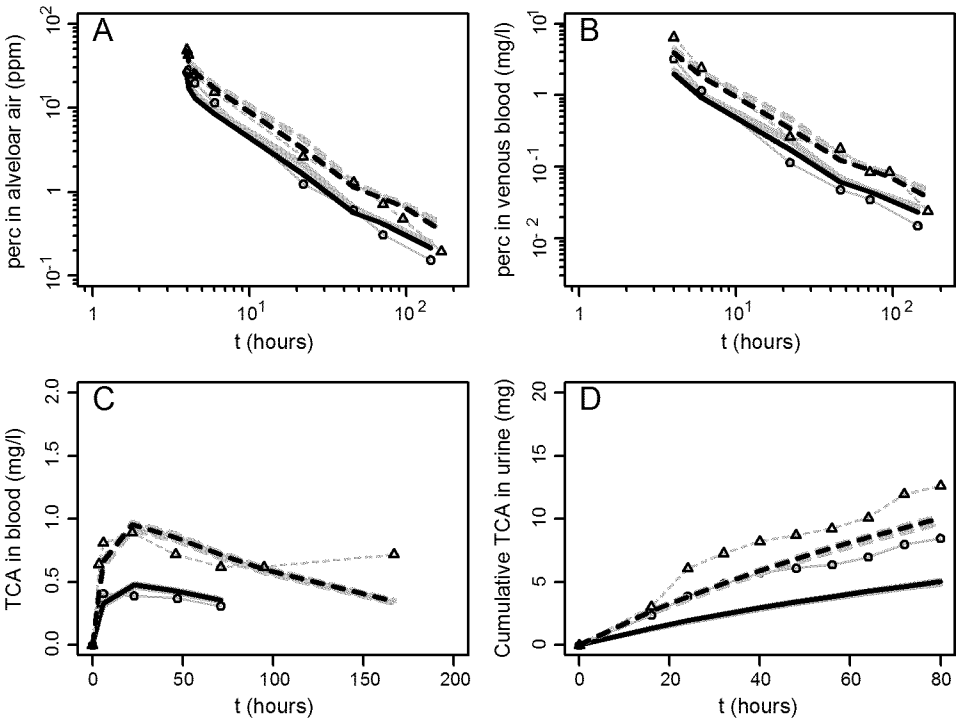

Fig. 9. Comparison of model predictions for perc in alveolar air (A) and blood (B) and TCA in blood (C) and urine (D) for human subject C from Monster et al. (1979) exposed to 72 (data: circles, predictions: thick lines) and 144 ppm for 4 h (data: triangles, predictions: thick dashed lines). Within this study, this individual has the greatest difference in log-likelihood between the overall posterior mode and the lowest chain-specific posterior mode. The solid lines are the overall posterior mode, and the gray lines show chain-specific posterior modes.

noted above, in which the discrepancies were larger but within about an order of magnitude. Only in the case of TCA in mice after high exposures is there evidence that additional pharmaceokinetic or pharmacodynamic mechanisms affecting disposition may be useful to evaluate. In most other cases, when comparing the same or similar measurements following the same routes of exposure, the model

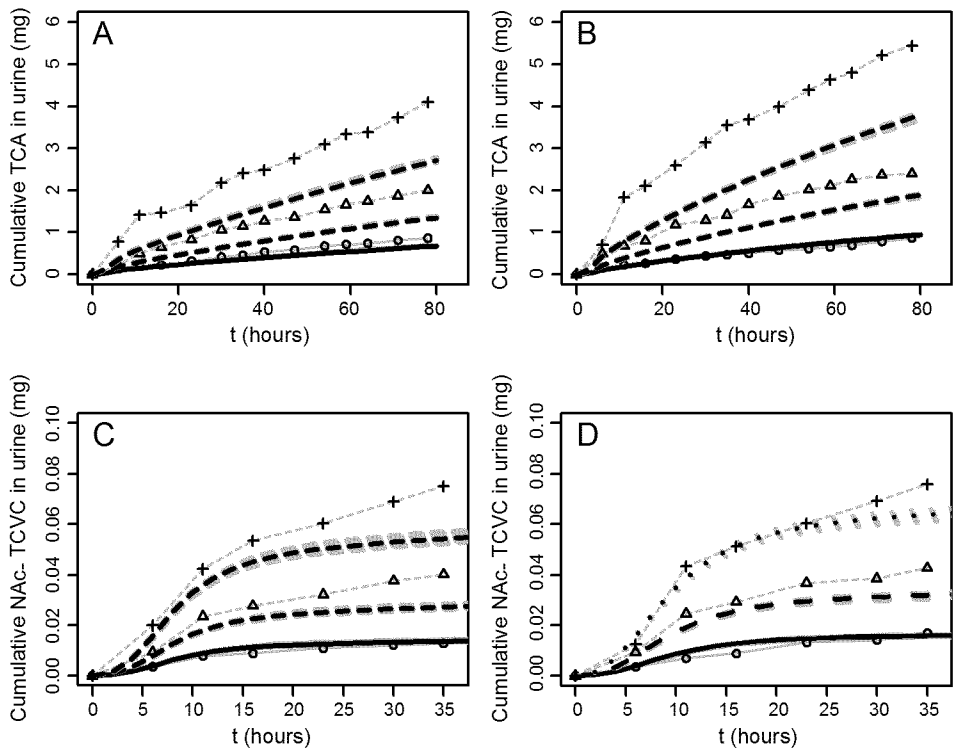

Fig. 10. Comparison of model predictions for TCA (A–B) and NAcTCVC (C–D) in urine for human subjects C (a female, panels A and C) and E (a male, panels B and D) from Volkel et al. (1998) exposed to 10 (data: circles, predictions: thick lines), 20 ppm (data: triangles, predictions: dashed lines), and 40 ppm (data: crosses, predictions: dotted lines) for 6 h. Within this study, for each sex, these individuals have the greatest difference in log-likelihood between the overall posterior mode and the lowest chain-specific posterior mode. The solid lines are the overall posterior mode, and the gray lines show chain-specific posterior modes.

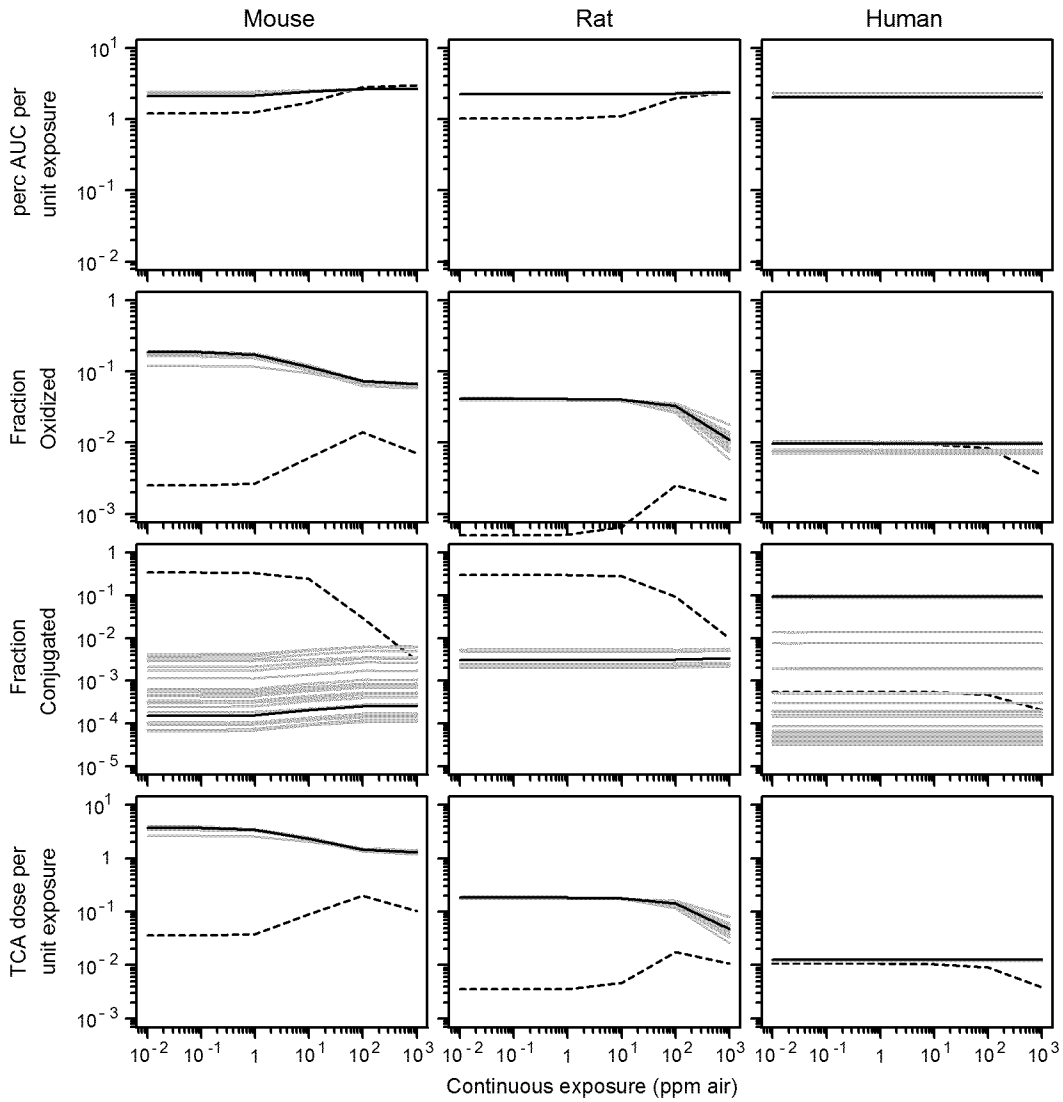

Fig. 11. Dose metric predictions for continuous inhalation exposure in mice, rats, and humans. Units are as follows: perc AUC in blood, mg h/L/day per ppm in air; fraction oxidized, mg/kg/day oxidized per mg/kg/day intake; fraction conjugated, mg/kg/day conjugated per mg/kg/day intake; TCA dose, mg/kg/day systemic TCA per ppm in air, where TCA directly excreted from the kidney is not included. The dotted lines show the baseline predictions, the solid lines show the overall posterior mode, and the gray lines show chain-specific posterior modes (24 separate runs for mice and rats, and 48 separate runs for humans). In some cases, the gray lines are not visible because the chain-specific runs all coincide.

predictions were usually not consistently in one direction greater or less than the observations. In addition, in humans, the observations themselves show substantial variability between individuals, and in some cases among the data for a single individual. Thus, overall, these suggest that the discrepancies in model fits reflect mostly variability, with some experiments under-predicted and others over-predicted.

Dose metric and mass balance predictions based on posterior modes

Figs. 11 and 12 summarize the PBPK model dose metric predictions based on the baseline, overall posterior mode, and chain-specific posterior mode parameters (see Supplementary Materials, Tables S6–S9, for tabular representation). For ease of comparison, the perc AUC and TCA dose metrics have been scaled by the exposure unit and the same ordinate scale for each dose metric is used across all three species.

The uncertainty due to the distribution of chain-specific posterior modes contributes to the overall uncertainty in the predicted dose metric. As shown in Figs. 11 and 12, in some cases, this source of uncertainty is minimal (when the chain-specific predictions overlap), and in others, there is a substantial amount of uncertainty remaining in the dose metric predictions, even after calibration (when there is a large spread in chain-specific predictions, shown in gray).

The blood perc dose metric has by far the least amount of this chain-to-chain uncertainty. This is true across all species, routes of exposure, and exposure levels. The dose metrics with the next lower amount of chain-to-chain uncertainty are perc oxidation and TCA formation. As discussed above, there are some discrepancies between predictions and observations for blood perc and TCA in blood and urine. The predictions for GSH conjugation are more uncertain. In the rat model, the ranges of chain-specific posterior modes span 1.3-fold or less, but the range in the mouse and human models are higher. For the mouse model, the range is about 60-fold and in the human model, the range is about 3000-fold.

From these dose metrics, the total mass balance of perc can be inferred. In particular, in mice, the model predicts total metabolism to be less than 20% of intake by inhalation, though up to almost 60% of intake by ingestion. Of this, the vast majority is predicted to be oxidation, with the fraction attributable to conjugation being less than 1% for inhalation and less than 2% for ingestion. Thus, while there is substantial uncertainty in the amount of GSH conjugation in mice, it

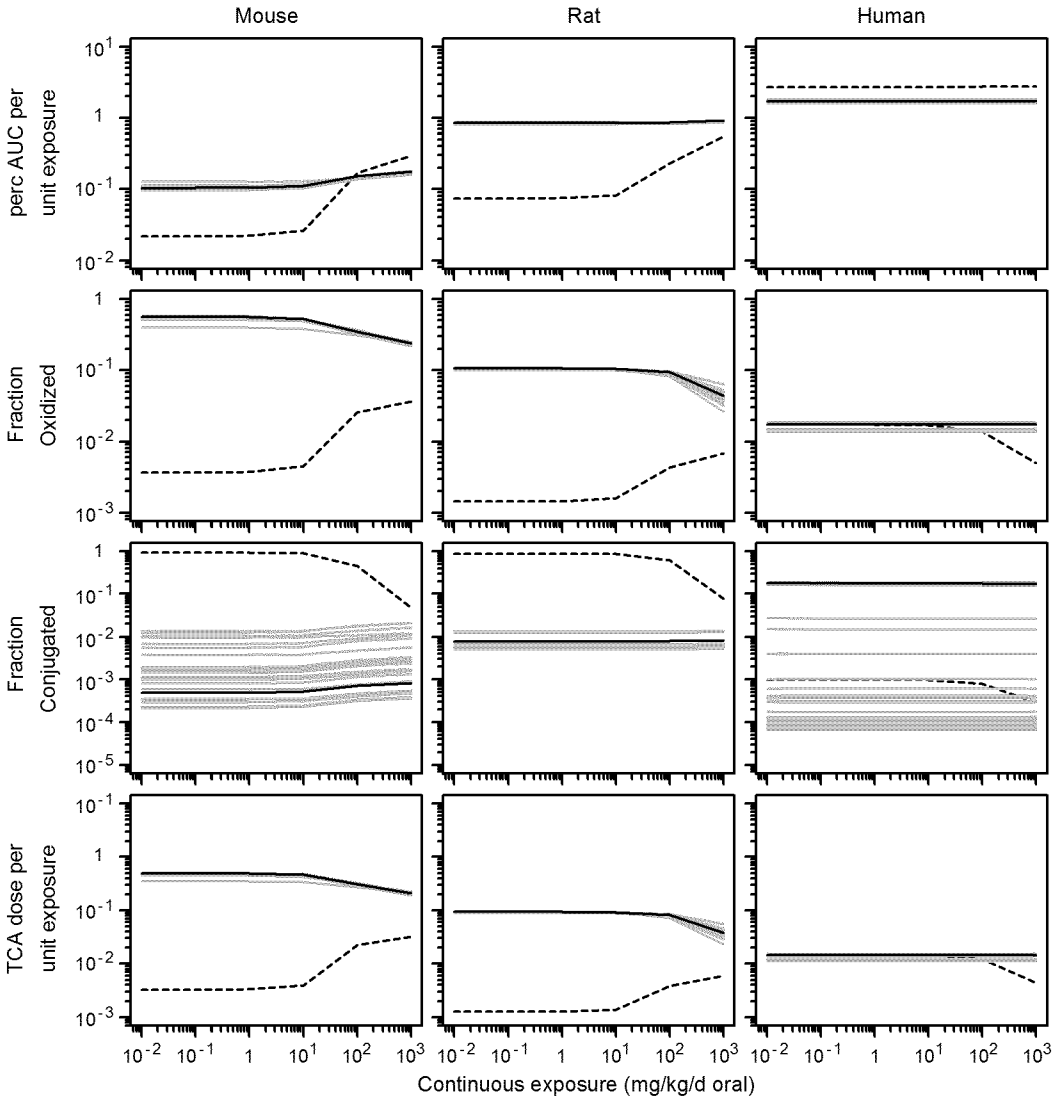

Fig. 12. Dose metric predictions for continuous oral exposure in mice, rats, and humans. Units are as follows: perc AUC in blood, mg h/L/day per oral mg/kg/day; fraction oxidized, mg/kg/day oxidized per mg/kg/day intake; fraction conjugated, mg/kg/day conjugated per mg/kg/day intake; TCA dose, mg/kg/day systemic TCA per oral mg/kg/day, where TCA directly excreted from the kidney is not included. The dotted lines show the baseline predictions, the solid lines show the overall posterior mode, and the gray lines show chain-specific posterior modes (24 separate runs for mice and rats, and 48 separate runs for humans). In some cases, the gray lines are not visible because the chain-specific runs all coincide.

nonetheless is predicted to account for only a small fraction of the overall disposition of perc in mice. Moreover, the estimates of total metabolism are unaffected by this uncertainty. Overall, the disposition of perc is predominantly by exhaled breath for inhalation, and by metabolism for ingestion.

In rats, the model predicts total metabolism to be about 4% by inhalation and 10% by ingestion (with a decrease at high exposures due to saturation). Again, the vast majority is predicted to be oxidation, with GSH conjugation accounting for 0.3% or less for inhalation and 0.6% or less for ingestion. Thus, total metabolism, oxidation, and conjugation are all relatively tightly estimated, and the disposition of perc is dominated by exhaled breath.

In humans, the model predicts total metabolism to be about 10% or less by inhalation and about 20% or less by ingestion. While the amount attributable to oxidation is fairly tightly estimated at about 1% from inhalation and 2% by ingestion, the amount attributable to GSH conjugation ranges from less than 0.003% to 10% by inhalation, and 0.006% to 19% by ingestion. For GSH conjugation, the available in vivo data are inadequate to constrain the flux through this pathway, either extreme providing plausible fits to the data. Moreover, as discussed above in Model parameter evaluation, in vitro data are also highly uncertain, as there is a wide range of in vitro estimates of perc GSH conjugation. Nonetheless, the range of total metabolism is narrower, from 1% to 10% for inhalation and 2% to 20% by ingestion, with the lower estimate reflecting the prediction that oxidation dominates total metabolism, and the higher estimate reflecting the prediction that GSH conjugation dominates total metabolism. Thus, in any case, the disposition of perc is predominantly by exhaled breath.

Results of local sensitivity analyses

The results of local sensitivity analyses, centered on the overall posterior mode, are shown in Table 9 (most sensitive parameters only) and Supplementary Materials (complete results, Tables S10–S12). In each table, the parameter sensitivity coefficients are given for

Table 9
Selected local parameter sensitivity analyses results.

Species	AUCCBld (|SC|)		FracOx (|SC|)		FracGSH (|SC|)		TCASys (|SC|)		Calibration data (# of data points)			
Scaling parameter	Inh	Oral	Inh	Oral	Inh	Oral	Inh	Oral	VL	L	M	H
Mouse												
InQCC	0.18	0.74	0.72	0.49	0.58	0.74	0.28	0.49	61	173	229	29
InVPRC	0.21	0.87	0.86	0.25	0.77	0.4	0.14	0.25	121	260	94	17
QGutC	0.03	0.11	0.12	0.2	0.17	0.3	0.12	0.2	340	136	12	0
InDRespC	0.03	0.11	0.02	0.03	0.03	0.05	0.02	0.03	467	25	0	0
VLivC	0.18	0.39	0.72	0.74	0.51	0.43	0.72	0.74	118	263	105	2
PBC	0.85	0.87	0.58	0.25	0.92	0.4	0.58	0.25	39	337	114	2
InKMC	0.06	0.13	0.27	0.26	0.15	0.13	0.27	0.26	408	79	0	0
InClC	0.18	0.39	0.72	0.74	0.42	0.39	0.72	0.74	94	237	156	0
InCl2OxC	0.08	0.21	0.31	0.39	0.19	0.21	0.31	0.39	122	268	95	0
InFracOtherC	0	0	0	0	0	0	0.1	0.1	84	22	0	0
InClTCVGC	b0.01	b0.01	b0.01	b0.01	1	1	b0.01	b0.01	461	0	0	0
Rat												
InQCC	0.08	0.91	0.89	0.79	0.89	0.91	0.11	0.79	43	210	300	112
InVPRC	0.08	0.93	0.92	0.59	0.91	0.69	0.08	0.59	86	308	165	106
QGutC	b0.01	0.02	0.02	0.17	0.02	0.2	0.02	0.17	610	35	10	10
InDRespC	0.01	0.12	0.01	0.08	0.01	0.09	0.01	0.08	514	149	1	0
VLivC	0.08	0.09	0.9	0.92	0.12	0.11	0.9	0.92	419	184	62	0
PBC	0.92	0.93	0.89	0.59	0.92	0.69	0.89	0.59	54	248	292	71
InKMC	b0.01	0.01	0.03	0.12	b0.01	0.01	0.03	0.12	602	35	0	0
InClC	0.08	0.09	0.9	0.92	0.1	0.09	0.9	0.92	473	134	58	0
InFracOtherC	0	0	0	0	0	0	0.1	0.1	38	19	0	0
InClTCVGC	b0.01	b0.01	b0.01	b0.01	0.99	0.99	b0.01	b0.01	621	2	35	0
Human												
InQCC	0.14	0.8	0.81	0.8	0.8	0.8	0.19	0.8	2	438	0	0
InVPRC	0.15	0.85	0.85	0.64	0.85	0.61	0.15	0.62	307	1097	387	24
QGutC	b0.01	0.03	0.03	0.12	0.03	0.15	0.03	0.14	1787	28	0	0
VLivC	b0.01	0.01	0.81	0.85	0.04	0.03	0.89	0.92	1117	106	592	0
VKidC	b0.01	b0.01	0.17	0.13	0.02	0.01	0.09	0.07	1354	367	94	0
PBC	0.85	0.85	0.85	0.64	0.85	0.61	0.85	0.62	55	577	1109	74
InClC	0.01	0.02	0.98	0.98	0.02	0.02	0.98	0.98	1117	0	698	0
InFracOtherC	0	0	0	0	0	0	0.1	0.1	208	601	0	0
InClKidLivC	b0.01	b0.01	0.17	0.13	b0.01	b0.01	0.09	0.07	1354	364	97	0
InClTCVGC	0.13	0.18	0.17	0.18	0.82	0.82	0.17	0.18	615	1074	126	0

Column 1: scaling parameter; columns 2–9: absolute value of sensitivity coefficient for continuous exposures at 10 ppm in air or 100 mg/kg/day oral intake, with values ≥ 0.1 in bold (only parameters with at least one bolded value are included—see Supplementary Materials Tables S10–S12 for full results); columns 10–13: number of calibration data points with absolute value of sensitivity coefficient that is very low (VL: 0b|SC| ≤ 0.1), low (L: 0.1b|SC| ≤ 0.5), medium (M: 0.5b|SC| ≤ 1.0), and high (H: |SC|N1.0).

each dose metric for each route of exposure. For each parameter, the right four columns give the number of data points (out of the entire calibration set) which have sensitivity coefficients in the various categories from very low to high. There are two criteria for a dose metric to be confidently estimated: the most sensitive parameters for a given dose metric should either (1) have strong a priori information as to their value, or (2) have substantial data to which they are sensitive in model fitting.

For perc in blood, by far the most sensitive parameters are the blood–air partition coefficient, the cardiac output and alveolar ventilation rates, parameters for which there is substantial a priori information and for which the data are highly informative (significant number of data points with medium or high sensitivity). Only in the mouse and human models do perc in blood have some sensitivity to metabolism scaling parameters (mouse: InKMC, InClC, and InCl2OxC, for the KM, and clearances for oxidation; humans: InClTCVGC, for the clearance for GSH conjugation). This differential sensitivity is because disposition is vastly dominated by exhaled breath in rats, whereas in mice and humans, oxidative and GSH conjugation metabolism, respectively, play a larger role.

For oxidation, additional sensitive parameters are oxidative clearance and KM and the volume of the liver (because it is used to scale oxidative metabolism). There is moderate sensitivity to blood flow to the gut (portal vein), as it determines the delivery of perc to the liver for metabolism. In humans, there is some additional sensitivity of oxidation to kidney oxidative metabolism as well as GSH conjugation (due to competition for substrate). While there are little a priori data on these parameters, there are informative calibration data. For TCA production, the sensitivity is similar to that for oxidation, with some additional sensitivity to the fraction of oxidation that produces something other than TCA.

For GSH conjugation, in addition to the parameters sensitive for perc in blood, the blood flow to the gut (which determines delivery of perc to the liver for metabolism) and the clearance for GSH conjugation are sensitive parameters. In mice, there are no data of more than very low sensitivity for estimating GSH conjugation, whereas there are more data in rats and humans. In addition, there is a large amount of data in humans with low sensitivity, which collectively contribute to the weight that informs the value of the GSH clearance parameter.

Summary evaluation of PBPK model predictions

Table 10 summarizes the PBPK model predictions and the various measures that may contribute to the overall uncertainty in the PBPK model predictions. Clearly, the highest confidence dose metric is the AUC of perc in blood. As shown in Figs. 11 and 12, there is little spread in chain-specific predictions for this dose metric. The main source of uncertainty in this case is the residual difference between the model predictions and the calibration and evaluation data—a factor of about 2-fold for each species. Therefore, this dose metric can be considered reliably estimated for use in dose response analyses with the

Table 10
Summary and evaluation of the reliability of perc dose metrics.

Dose metric species	Inhalation prediction (posterior mode)[a]	Ingestion prediction (posterior mode) [a]	% or fold prediction range[a]	Calibration error (GSD)[a]	Evaluation error (GSD)[a]	Additional potential concerns
AUCCBld	mg-l/h/day/ppm	mg-l/h/day/(mg/kg/day)				
Mouse	2.4	0.15	b10%	~2-fold	~2-fold	None
Rat	2.3	0.83	b10%	~2-fold	~2-fold	None
Human	2.0	1.7	b20%	~2-fold	~2-fold	None
FracOx	% of intake	% of intake				
Mouse	12	35	b40%	~2-fold	~2-fold	Some sensitivity to lung metabolism
Rat	3.9	8.9	b20%	~2-fold	~2-fold	None
Human	0.98	1.8	b1.5-fold	~2-fold	~3-fold	Some sensitivity to fraction of oxidation to TCA
FracGSH	% of intake	% of intake				
Mouse	0.02	0.07	~60-fold	NA	NA	None
Rat	0.2	0.6	b30%	~2-fold	NA	None
Human	9.4	18	~3000-fold	~2-fold	NA	Calibration data cannot distinguish between modes
TCASys	mg/kg/day/ppm	mg/kg/day/mg/kg/day				
Mouse	2.3	0.31	b30%	~2-fold	~2-fold	Some sensitivity to fraction of oxidation to TCA
Rat	0.18	0.079	b20%	~2-fold	~2-fold	Some sensitivity to fraction of oxidation to TCA
Human	0.013	0.015	b40%	~2-fold	~3-fold	Some sensitivity to fraction of oxidation to TCA

[a] Evaluated in rodents at 10 ppm in air by inhalation and 100 mg/kg/day orally, and in humans at 0.01 ppm in air by inhalation and 0.01 mg/kg/day orally.

acknowledgement of a possible 2-fold residual error. The majority of perc absorbed is generally exhaled rather than metabolized, with the exception of exposure via ingestion in mice in which metabolism is slightly more than half of the total disposition. Therefore, these predictions are not especially sensitive to metabolism parameters, and depend mostly on physiological characteristics (such as alveolar ventilation) and biochemical parameters (such as partition coefficients).

Interestingly, the AUC predictions are generally consistent with the default assumption of equivalent ppm in air leading to equivalent internal doses, as the estimates of AUC of perc in blood are within 2-fold of each other across species. In addition, at the higher oral doses (e.g., 100 mg/kg/day), re-scaling the AUC in blood by body weight to the ¾ power leads to estimates across species within 3-fold of each other. These can be explained by the sensitivity analysis, which showed AUC in blood to be most sensitive to cardiac output, alveolar ventilation, and the partition coefficient, all of which either are similar across species or scale approximately allometrically by body weight to the ¾ power across species. This is also because the majority of perc elimination is generally via exhalation of unchanged parent compound, so parameters governing metabolism, which are more variable across species, are also less influential in determining perc AUC in blood.

The next highest confidence is in the estimates of perc oxidation and TCA formation (see Table 10). As was the case for AUC of perc in blood, there is little spread in chain-specific predictions for this dose metric (shown in Figs. 11 and 12). Here, the uncertainty in the estimates of perc oxidation in mice and rats is predominantly from the 2-fold residual difference between model predictions and the calibration and evaluation data. Metabolic parameters for the oxidative pathway are also reliably estimated in the mouse and rat. The range in estimates of perc oxidation in humans is largely dominated by inter-individual variability — i.e., the differences in urinary excretion of TCA across individuals. Thus, the central tendencies for the population are well estimated, even if particular individuals may vary to a fair degree. In addition, there is some sensitivity in humans to the assumptions as to the fraction of oxidation not producing TCA (fixed at 10%), this is not likely to be more than 2-fold unless a much larger amount of trichloroacetyl chloride is covalently bound in humans than in rodents. However, as discussed in the Introduction and Materials and methods, it is felt that the available data supports the model description of oxidative metabolism resulting primarily in TCA. Thus, at the population level, these dose metrics should be considered reliable for use in risk assessment with the acknowledgement of a residual error of about 2-fold or less.

In terms of predicted inter-species differences, the PBPK model generally predicts the greatest oxidative metabolism in mice, followed by rats, and then humans. Thus, humans would be predicted to receive a smaller internal dose of oxidative metabolites for the same applied dose, whether scaled by body weight or allometrically by body weight to the ¾ power. From an overall mass balance perspective, the predicted fraction oxidized for inhalation exposures declines from ~12% in mice, to ~4% in rats, to ~1% in humans (see Table 10). By ingestion, the predicted progression for oxidation is ~35% in mice, to ~9% in rats, to 2% in humans (see Table 10). The difference between rats and humans is similar to what would be expected from allometric scaling (factor of ~4). On the other hand, the difference between mice and humans is greater that the allometric expectation, consistent with the general characteristic of mice having greater relative oxidative capacity than humans.

Estimates of GSH conjugation appear more uncertain, especially in humans, as shown dramatically by the large spread in predictions across chains displayed in Figs. 11 and 12. In rats, the calibration data suggests about a 2-fold uncertainty, with the range of different optimizations being much smaller (see Table 10). In mice, there are no data on this pathway other than as a "mass balance" from total metabolism (e.g., closed chamber studies), so the uncertainty is greater, about 60-fold (see Table 10). In humans, the predicted range of estimates is extraordinarily large. In particular, there are evidently two local maxima, each of which gives similar model fits, but for which model predictions differ by 3000-fold.

In terms of overall disposition in the context of inter-species differences, in mice and rats the evidence appears to support a low flux of GSH conjugation, with the overall posterior mode in mice being about 10-fold smaller than that in rats (see Table 10). However, the uncertainty range in the mouse estimates overlaps with the rat estimates, so the data are also consistent with mice having either equal or greater GSH conjugation. The overall posterior mode in humans predicts around 40-fold greater GSH conjugation as compared to rats. However, the uncertainty range in humans overlaps with the rat estimates, so the data are also consistent with humans having either equal or greater GSH conjugation.

Discussion

Harmonization has simultaneously "reduced" and "revealed" uncertainty!

Prior to this analysis, there seemed to be an unresolvable conflict between PBPK model-based analyses that predicted high versus low amounts of perc metabolized in humans. There were strong opinions and analyses on either side of the debate, without a clear means of resolution. It was the key insight of the NRC (2010) review to recommend separation of total metabolism into the oxidative and GSH conjugation pathways that has simultaneously "reduced" and "revealed" uncertainty in perc toxicokinetics. It has "reduced" uncertainty in the sense that there is now fairly high confidence in the predictions of oxidative metabolism across species. It has "revealed" uncertainty in the sense that it has been made clear that the previously debated uncertainties in total metabolism can be essentially attributed to uncertainty in GSH conjugation, which is substantial.

In this context, it is now clear why previous analyses came up with such different conclusions. Those analyses that concluded low total perc metabolism all restricted the fraction of total (not oxidative) metabolism that was TCA to a fairly significant percentage — 30 to 100% (e.g., Chen and Blancato, 1987; Clewell et al., 2005; Covington et al., 2007; Qiu et al., 2010). Thus, as was noted by the NRC (2010), total metabolism constrained in this manner essentially only measures oxidative metabolism. On the other hand, those analyses that concluded high total perc metabolism essentially lumped oxidative and GSH conjugation metabolism together without restrictions as to the fraction producing TCA and/or made inferences based on disappearance of the parent compound (e.g., Ward et al., 1988; Bois et al., 1990, 1996; Reitz et al., 1996; Chiu and Bois, 2006). Therefore, these two groups of analyses are not actually comparable.

Reflecting on these previous analyses also provides insight into why the current analyses revealed two divergent estimates in humans. In essence, the analysis suggests that once total metabolism is decoupled from oxidation by allowing for a separate independent pathway, the in vivo data cannot distinguish between widely different estimates of GSH conjugation flux. First, because even in the case of "high" GSH conjugation predictions, less than 20% is metabolized, available parent compound data (alveolar breath and venous blood) cannot discriminate between 20% and essentially 0% metabolism, given the inter- and intra-individual variability in the data. Interestingly, this same uncertainty range of 0–20% total metabolism was noted in purely empirical analyses of alveolar breath data by Chiu et al. (2007). Second, the only other in vivo data informative of this pathway – urinary excretion NAcTCVC – only provides an indirect measure of the GSH conjugation flux due to its being a product of multiple subsequent steps after perc GSH conjugation. Thus, an additional assumption needs to be made as to the yield of NAcTCVC (as opposed to other end products — see Fig. 1), a parameter which, when estimated statistically, is found to be highly uncertain.

Given the uncertainties associated with the in vivo data on perc as to the flux of GSH conjugation, another approach would be to examine the biological plausibility of different estimates based on in vitro data either on perc or other related compounds. Unfortunately, such data are also found to have high uncertainties, even in rodents (see Fig. 5, and section "Model parameter evaluation"). Moreover, in humans, the only perc-specific datum is a non-detect, with the rest of the comparison data based on related halogenated compounds. Thus, the best that can be concluded is that the wide range of estimates from in vitro data is consistent with the range of estimates determined statistically from in vivo data, and that none of estimates is necessarily implausible biologically. Additional, more speculative, approaches to evaluate the different estimates are discussed below in the section on potential risk assessment implications.

Is it uncertainty or variability?

A further consideration is whether the existence of two distinct "modes" is a reflection of true variability in the form of a bimodal distribution for human GSH conjugation. When the true distribution is multi-modal, fitting a unimodal distribution may only pick out one mode. Some weak evidence for this possibility is the fact that some individuals' data appear to be fit better using the overall posterior mode, while others' appear to be fit better using an alternative posterior mode with "low" GSH conjugation. Certainly, there are numerous well-known polymorphisms in the enzyme families that metabolize perc (Ginsberg et al., 2009a, 2009b), some of which are also known to be multi-modal. For instance, GST-M1 and GST-T1 are known to have a substantial fraction of the population that is homozygous-null (Walker et al., 2009). In addition, NAT2 is known from drug metabolism studies to have a population distribution that is a mixture of slow and fast metabolizers (Walker et al., 2009). These enzymes belong to families that are critical for the GSH conjugation pathway of perc, and it is therefore certainly biologically plausible that a multi-modal distribution for GSH conjugation exists. Unfortunately, it is not known which particular GST(s) or NAT(s) isozyme(s) is(are) involved in the GSH conjugation pathway of perc, so whether a multi-modal distribution is consistent with known polymorphisms cannot be determined. In addition, in vitro data on TCE conjugation reported only 3- to 8-fold variation in GSH conjugation, without evidence of a non-conjugating phenotype (Lash et al., 1999), suggesting that uncertainty may be a greater contribution to the overall distribution. Overall, at this point, it is not possible to disentangle uncertainty and variability in the extent of perc GSH conjugation in humans. However, this suggests an additional "qualification" to the overall conclusions as to human perc metabolism — that GSH conjugation may be highly uncertain and/or highly variable.

Potential implications for current and future risk assessments

The results of this analysis can support the choice(s) of internal dose metrics that may be used when conducting dose–response analyses of perc toxicity in current and future risk assessments, both of perc and other chemicals. Such analyses may include route-to-route or inter-species extrapolation of toxicologically equivalent doses, comparison of parent and metabolite toxicity based on a common internal dose metric, and investigation of the shape of the dose–response curve.

With respect to current efforts to assess human health risks to perc, it appears that the harmonized PBPK model can be reliably used to analyze dose–response data on effects related to either the parent compound or oxidative metabolism. Thus, model performance appears adequate, and the overall uncertainties appear to be modest for predictions related to such dose metrics. However, any applications of estimates for the GSH conjugation pathway in dose response analyses may involve much greater uncertainty.

Assessors conducting dose response analyses for perc health endpoints that may be associated with GSH conjugation metabolites need to weigh the impact of uncertainties. In some cases, the impact may be minimal. For instance, for human route-to-route extrapolation, the estimates for the ppm inhalation exposure leading to an equivalent internal dose metric as a given oral exposure span a range of 1.3-fold or less for any of the dose metrics evaluated. Therefore, the sensitivity to the choice of "high" or "low" GSH conjugation estimates is quite limited, as expected from the analysis of Chiu and White (2006) for generic volatile organics.

For interspecies extrapolation, the impact of the GSH conjugation uncertainties is much greater, but some arguments could be made in favor of using the current model estimates of GSH metabolism. On the one hand, it could be argued that the overall posterior mode, which predicts high GSH conjugation in humans, may be a preferred estimate because it has an overall better fit than the alternative posterior modes that predict lower GSH conjugation. However, the extent to which the overall posterior mode reflects a better fit to the data is rather modest when viewed qualitatively. It could also be argued that the estimates of high GSH conjugation should be used because they are more "conservative" and thus ensures protection of public health, though this is more of a science policy decision than one based on the science alone. In addition, under the hypothesis that the "low" and "high" GSH conjugation predictions reflect human variability, rather than uncertainty, then an argument could be made for using the "high" GSH conjugation predictions because they may be an accurate reflection of at least a substantial portion of the human population. This hypothesis is biologically plausible based on what is known about other substrates for GSTs and NATs in the human population, though perc-specific data supporting it are lacking. In addition, recent human data provide support for tetrachloroethylene nephrotoxicity (Calvert et al., 2010), providing qualitative support for the importance of GSH conjugation pathway in humans. However, the overall epidemiologic database is mixed. On the other hand, in rats and mice, where GSH conjugation is better estimated, the oxidative pathway is predominant. Thus is could be argued by analogy that in humans, this should also be the case, lending support to the "low" estimate of GSH conjugation.

Given the very large uncertainty in the estimates of GSH metabolism, the statistical uncertainty in dose response analyses would be much less if using a less specific internal dose metric that is nonetheless still more proximate and relevant than administered dose. That is, analyses could utilize a more reliably estimated PBPK model-based internal dose metric in place of estimates of GSH conjugation. Such an "intermediate" choice in this case could be the AUC of perc in blood. From a biological perspective, because there is limited hepatic first-pass, perc in blood is more proximate to toxicity than administered dose, as it captures the concentration of perc delivered to tissues. While not capturing differences in local metabolic activation across species, this metric does account for differences in physiological parameters and blood–air partitioning. In addition, it is much more reliably estimated than the amount GSH conjugation itself, in part because there is a significant amount of empirical data on blood perc to support the model parameters.

It is useful to consider what additional data or analyses could help to better characterize the extent of GSH conjugation. In terms of analysis, an obvious question is whether a full population Bayesian analysis would be of benefit beyond its methodological research value and provide a better basis for dose–response analyses. On the one hand, it could potentially better quantify and disaggregate the contributions of uncertainty, variability and model misspecification to the range of estimates and residual errors estimated here. However, such an analysis needs to be done with care, especially if there are multiple local maxima. In addition, given the large potential uncertainties, the extent to which the model results depend on the choice of prior distributions would need to be assessed. While non-informative priors could be used, it was found by Chiu et al. (2009) that this led to too slow a rate of convergence given currently available computation resources, though this may be surmountable with either a combined multi-species approach (as was utilized by Chiu et al., 2009) or a more efficient modern MCMC algorithm, though probably not using MCSim. More importantly, however, it is by no means guaranteed that such an analysis will lead to a firm conclusion as to whether the presence of "high" and "low" GSH conjugation predictions reflect predominantly uncertainty or variability, nor whether one or the other set of predictions will be substantially more favored. The decision, then, rests on whether the uncertain value-added of such an analysis is considered worth the time and effort to attempt it. On balance, it does not appear that development of a full population Bayesian analysis of these data would either adequately repay the very substantial time and resource commitment that would be required, or, in the end, would substantially improve the scientific basis for perc dose–response analyses used in current risk assessment efforts.

A more fruitful line of inquiry may be whether additional data could be collected to substantially better characterize the GSH conjugation pathway. Human in vivo data would be ideal, but this may require development of reliable human kinetic biomarkers for this pathway. For TCE, there was one study that measured the primary GSH conjugate, DCVG, in blood (Lash et al., 1999), though some have questioned the reliability of those measurements (Dekant, 2010). Nonetheless, unequivocal measurement of TCVG in blood following perc exposure would provide highly informative data from which to estimate GSH conjugation. TCVC in blood could also be informative, though it is not clear how much would be expected to be systemically available because it is largely formed in the kidney, where it may be immediately processed to downstream metabolites. Also potentially informative would be better total mass balance data in humans, particularly if augmented by blood and urine measurements GSH conjugation products. Another possibility would be more reliable in vitro measurements of GSH conjugation metabolism, particularly at low concentrations where the clearance rate could be estimated. However, some calibration of the in vitro-to-in vivo extrapolation would be necessary. Identification of which GST isozymes are involved in perc GSH conjugation and with NAT isozymes are involved in N-acetylation of TCVC may also facilitate both in vitro and in vivo studies, and provide a basis for hypothesizing what extents of inter-species differences and human variability are biologically plausible. Overall, however, it is likely that data generation along any of these lines would involve significant experimental challenges and require several years; thus while such work might provide valuable input for future risk assessment efforts, it would not be available meet near-term needs.

A few comments are warranted on the approaches utilized in this analysis, and their potential utility in analyses supporting risk assessments other than perc. As was discussed in Chiu et al. (2009), it is important that analyses done for risk assessments – particularly ones using complex models and large datasets – be highly transparent and objective. To this end, this paper has attempted to fully document the PBPK model, its parameters, data, and assumptions. In addition, a clear separation was maintained between "baseline" parameter estimates derived from a priori information, and "calibrated" parameter estimates obtained by fitting to in vivo data. While this separation is technically important for Bayesian analysis so as to maintain its mathematical and statistical validity, it also has benefits in terms of transparency and objectivity for less involved analyses. Another approach which may merit broader application is the use of more limited Bayesian analysis using flat priors, which provides a useful and more flexible method for parameter optimization and assessing parameter uncertainty as compared to approaches that have been typically used. While the approach described here is somewhat more involved than "traditional" optimization, it requires a much lower level of effort than a full hierarchical population-based Bayesian analysis while at the same time retaining some of the benefits.

Summary conclusions

In sum, the paper reports on the development of a "harmonized" PBPK model for perc toxicokinetic in mice, rats, and humans that

includes both oxidation and GSH conjugation of perc, the internal kinetics of the metabolite TCA, and the urinary excretion kinetics of the metabolites NAcTCVC and DCA. The model is calibrated or evaluated against the available in vivo toxicokinetic data, utilizing a wider range of data than any previous analysis alone. Upon evaluation, dose metrics related to perc in blood, perc oxidation, and TCA production are considered reliable for dose–response analyses in all three species, while there are substantial uncertainties in the amount of GSH conjugation in humans and mice. In addition, the disposition of perc is largely by exhalation of the parent compound, with the exception of low (≤ 10 mg/kg day) oral doses in mice at which up to 56% is metabolized. This analysis appears to reconcile the disparity between those previously published analyses that concluded ~1% perc metabolism in humans and those that predicted N20% perc metabolism in humans. In essence, both conclusions are consistent with the data if augmented by some additional qualifications: oxidative metabolism is low in humans, while GSH conjugation metabolism may be high or low in humans, with high uncertainty and/or variability. Clearly, more direct data would be needed to better quantify GSH conjugation in humans.

Conflict of interest statement

The authors declare that there are no conflicts of interest.

Acknowledgments

Contract support for this work was provided by Battelle Memorial Institute (Contract EP-C-09-006, Eva McLanahan, Work Assignment Manager), which conducted the toxicokinetic data literature search and digitized and tabulated much of the available data. The authors would also like to thank Dr. Jeffrey Fisher and colleagues for providing the data used in their perc PBPK model; Drs. Eva McLanahan, Paul Schlosser, and Nina Wang for helpful suggestions as to PBPK model development; and Dr. Andrew Bray, Ms. Rebecca Brown Dzubow, Dr. Kathryn Guyton, Dr. Maureen Gwinn, Dr. Elaina Kenyon, Dr. Leonid Kopylev, Dr. Sheppard Martin, Dr. Paul Schlosser, Ms. Cheryl Siegel Scott, Dr. Ravi Subramaniam, and Mr. Paul White for helpful comments during the preparation of this manuscript. G. Ginsberg is partially supported by an Oak Ridge Institute for Science and Education academic fellowship to participate in risk assessment activities with the U.S. Environmental Protection Agency's National Center for Environmental Assessment. The authors would like to thank the anonymous reviewers for comments that significantly strengthened the analysis and presentation of results.

Appendix A. PBPK model equations and baseline parameters

The equations below, along with the parameters in Table A1, specify the PBPK model. The same equations are in the PBPK model code, with some additional provisions for unit conversions (e.g., ppm to mg/L) or numerical stability (e.g., truncating small values at 10^{-15}, so states are never negative).

Perc sub-model

Gas exchange, respiratory metabolism, arterial blood concentration, and closed chamber concentrations

The respiratory tract model is the same as that used by Evans et al. (2009) and Chiu et al. (2009). For an open chamber concentration of Conc and a closed chamber concentration of ACh/VCh, the rates of change for the amount in the respiratory lumen during inhalation (AInhResp, in mg), the amount in the respiratory tract tissue (AResp, in mg), and the respiratory lumen during exhalation (AExhResp, in mg), are given by:

$$d(AInhResp)/dt = (QM \times CInh) + (DResp \times (CResp - CInhResp)) - (QM \times CInhResp)$$
$$d(AResp)/dt = (DResp \times (CInhResp - CExhResp - 2 \times CResp)) - RAMetLng$$
$$d(AResp)/dt = (DResp \times (CInhResp - CExhResp - 2 \times CResp)) - RAMetLng$$
$$d(AExhResp)/dt = (QM \times (CInhResp - CExhResp)) + (QP \times (CArt\_tmp/PB - CInhResp)) + (DResp \times (Cresp - CExhResp))$$

where

CInh = inhaled concentration (mg/L) = ACh/VCh + Conc
QM = minute volume (L/h) = QP/0.7
CInhResp = concentration in respiratory lumen during inhalation (mg/L) = AInhResp/VRespLum
CResp = concentration in respiratory tract tissue (mg/L) = AResp/VRespEff
CExhResp = concentration in respiratory lumen during exhalation (mg/L) = AExhResp/VRespLum
RAMetLng = rate of metabolism in respiratory tract tissue = (VMaxClara × CResp)/(KMClara + CResp)
CArt_tmp = arterial blood concentration after gas exchange = (QC × CVen + QP × CInhResp)/(QC + (QP/PB))

Because alveolar breath concentrations may include desorption from the respiratory tract tissue, the concentration at the alveolae (CArt_tmp/PB) may not equal the measured concentration in end-exhaled breath. It is therefore assumed that the ratio of the measured end-exhaled breath concentration to the concentration in the absence of desorption is the same as the ratio of the rate of perc leaving the lumen to the rate of perc entering the lumen:

$$CAlv = (CArt\_tmp = PB) = (QM \times CMixExh) - ((QP \times CArt\_tmp/PB) + ((QM - QP) \times CInhResp))$$

That is, it is assumed that desorption occurs proportionally throughout the "breath." The concentration of arterial blood entering circulation needs to add the contribution from the intra-arterial dose (IADose in mg/kg, infused over a time period TChng):

$$CArt = CArt\_tmp + kIA = QC$$
$$kIA = (IADose \times BW) = TChng$$

For closed chamber experiments, the additional differential equation for the amount in the chamber (ACh, in mg) is

$$d(ACh)/dt = Rodents \times (QM \times CMixExh - QM \times ACh = VCh) - kLoss \times Ach$$

where Rodents is the number of animals in the chamber, and kLoss is the chamber loss rate (per h).

Oral absorption to gut compartment

For oil gavage, the dose PDose is defined in terms of units of mg/kg, entering the stomach during a time TChng, with rates of change in the stomach (AStom, in mg) and duodenum (ADuod, in mg):

$$d(AStom)/dt = kStom - (AStom \times (kAS + kTSD))$$
$$d(ADuod)/dt = (kTSD \times AStom) - (kAD \times ADoud)$$

where

kStom = rate of perc entering stomach (mg/h) = (PDose × BW)/TChng

Note that there is absorption to the gut from both the stomach and duodenal compartments, as was assumed for TCE (Evans et al., 2009;

Chiu et al., 2009). For aqueous gavage, the dose PDoseAq is similarly defined, with rates of change in the stomach (AStomAq, in mg) and duodenum (ADuodAq, in mg):

$$dðAStomAqÞ=dtp = AStomAq - AStomAq \cdot ðkASAq + kTSDAqÞ$$
$$dtðADoudAqÞ = ðkTSDAq \cdot AStomAqÞ - kADAq \cdot AdouAq$$

where

kStomAq = rate of perc entering stomachðmg=hÞ = ðPDoseAq · BWÞ=TChng

For drinking water, the rate Drink is defined in terms of mg/kg/day, and it is assumed that absorption is direct to the gut:

$$kDrink = ðDrink \cdot BWÞ=24:0$$

Therefore, the total rate of absorption to the gut via oral exposure (RAO, in mg/h) is:

$$RAO = kDrink + ðkAS \cdot AStomÞ + ðkAD \cdot ADoudÞ + ðkASAq \cdot AStomAqÞ + ðkADAq \cdot ADoudAqÞ$$

The differential equation for the gut compartment (AGut, in mg) is therefore given by

$$dðAGutÞ=dt = QGut \cdot ðCArt - CVGutÞ + RAO$$

where

CVGut = concentration in the gutðmg=LÞ = AGut=VGut=PGut

Non-metabolizing tissues

The differential equations for non-metabolizing tissues (rapidly perfused, ARap, in mg; slowly perfused, ASlw, in mg; and fat, AFat, in mg) follow the standard flow-limited form:

$$dðARapÞ=dt = Qrap \cdot ðCArt - CVRapÞ$$
$$dðASlwÞ=dt = QSlw \cdot ðCArt - CVSlwÞ$$
$$dðAFatÞ=dt = QFat \cdot ðCArt - CVFatÞ$$

where

CVRap = venous blood concentration leaving rapidly perfused issues = ARap/VRap/PRap

CVSlw = venous blood concentration leaving slowly perfused issues = ASlw/VSlw/PSlw

CVFat = venous blood concentration leaving fat = AFat/VFat/PFat

Liver compartment

The liver has two metabolizing pathways. The oxidative pathway is assumed to be described by two saturable pathways:

$$RAMetLiv1 = \text{Rate of PERC oxidation by P450 in liver}ðmg=hÞ = ðVMax \cdot CVLivÞ=ðKM + CVLivÞ + ðVMax2 \cdot CVLivÞ \cdot ðKM2 + CVLivÞ$$

The second pathway is identifiable in mice, so is omitted in rats and humans. Moreover, only the linear term is identifiable in mice, so only the ratio VMax2/KM2 is optimized.

$$RAMetLiv2 = \text{Rate of PERC metabolized to TCVG in liver}ðmg=hÞ = ðVMaxTCVG \cdot CVLivÞ=ðKMTCVG + CLivÞ$$

In all three species, only the linear term is identifiable, so only the ratio VMaxTCVG/KMTCVG is optimized.

The differential equation for perc in liver (ALiv, in mg) is thus:

$$dðALivÞ=dt = ðQLiv \cdot ðCArt - CVLivÞÞ + ðQGut \cdot ðCVGut - CVLivÞÞ - RAMetLiv1 - RAMetLiv2$$

where

CVLiv = venous blood concentration leaving liver = ALiv=VLiv=PLiv

Kidney compartment

The kidney also has two metabolizing pathways:

RAMetKid1 = Rate of PERC oxidized in kidney (mg/h)
= (VMaxKid · CVKid)/(KMKid + CVKid)

RAMetKid2 = Rate of PERC metabolized to TCVG in kidney (mg/h)
= (VMaxKidTCVG · CVKid)/(KMKidTCVG + CVKid)

The differential equation for perc in kidney (AKid, in mg) is thus:

$$dðAKidÞ=dt = ðQKid \cdot ðCArt - CVKidÞÞ - RAMetKid1 - RAMetKid2$$

where

CVKid = venous blood concentration leaving kidney = CKid=PKid

Venous blood compartment

The venous blood compartment (ABld, in mg) has inputs both from the venous blood exiting tissues as well as from an IV dose (IVDose in mg/kg infused during a time TChng), and output to the gas exchange region.

$$dðABldÞ=dt = ðQFat \cdot CVFat + QGutLiv \cdot CVLiv + QSlw \cdot CVSlw + QRap \cdot CVRap + QKid \cdot CVKidÞ + kIV - CVen \cdot QC$$

where

kIV = IV infusion rate = (IVDose · BW)/TChng

CVen = concentration in mixed venous blood = ABld/VBld

TCA sub-model

The TCA sub-model is the same as that in Hack et al. (2006), Evans et al. (2009), and Chiu et al. (2009). In brief, TCA in plasma is assumed to undergo saturable plasma protein binding. TCA in tissues is assumed to be flow-limited, but with the tissue partition coefficient reflecting equilibrium with the free concentration of TCA in plasma.

Plasma binding and concentrations

For an IV dose of TCA given by IVDoseTCA (mg/kg during an infusion period of TChng), the rate of the change of the amount of total TCA in plasma (APlasTCA, in mg) is

$$dðAPlasTCAÞ=dt = kIVTCA + ðQBodPlas \cdot CVBodTCAÞ + ðQG \cdot CVLivPlasÞ - ðQCPlas \cdot CPasTCAÞ - RUrnTCAplas$$

where

kIVTCA = rate of IV infusion of TCA = (IVDoseTCA · BW)/TChng

QBodPlas = plasma flow from body = QBod · FracPlas

QGutLivPlas = plasma flow from liver = (QGut + QLiv) · FracPlas

CVBodTCA = venous concentration leaving body
= CPlasTCABnd + CVBodTCAFree

CVBodTCAFree = free venous concentration leaving body
= (ABodTCA/VBod/PBodTCA)

CVLivTCA = venous concentration leaving liver
= CPlasTCABnd + CVLivTCAFree

CVLivTCAFree = free venous concentration leaving liver
= (ALivTCA/VLiv/PLivTCA)
QCPlas = total plasma flow = QC × FracPlas
RUrnTCAplas = rate of urinary excretion of TCA from plasma
= kUrnTCA × APlasTCAFree

The free (CPlasTCAFree) and bound (CPlasTCABnd) concentrations are calculated from the total concentration (CPlasTCA = APlasTCA/VPlas) by solving the equations:

$$CPlasTCABndMole = BMax \times CPlasTCAFreeMole / (kDissoc + CPlasTCAFreeMole)$$
$$CPlasTCABndMole = CPlasTCAMole - CPlasTCAFreeMole$$

Here the suffix "Mole" means that all concentrations are in micromole/L, because BMax and kDissoc in Table A1 are given in those units. These lead to explicit solutions of

$$CPlasTCAFreeMole = (sqrt(a \times a + b) - a) / 2$$

$$a = kDissoc + BMax - CPlasTCAMole$$
$$b = 4.0 \times kDissoc \times CPlasTCAMole$$

CPlasTCABndMole = bound concentration of TCA = CPlasTCAMole
− CPlasTCAFreeMole

These concentrations are converted to mg/L (CPlasTCABnd and CPlasTCAFree) by multiplying by the molecular weight in mg/μmol. The amount of free TCA in plasma is thus

$$APlasTCAFree = CPlasTCAFree \times VPlas$$

Body compartment

The rate of change for the amount of TCA in the body (ABodTCA, in mg) is given by

$$dABodTCA/dt = QBodPlas \times (CPlasTCAFree - CBodTCAFree) + StochTCAPERC \times (1 - FracOthel) \times RAMetLng + StochTCAPERC \times (1 - FracOthel) \times (1 - FracKidTCA) \times RAMetKid1$$

The first term reflects the free TCA in plasma flowing into and out of the body compartment, the second term reflects the production of TCA from lung metabolism, and the third term reflects production of TCA from kidney metabolism. Lung and kidney metabolism is adjusted for molecular weights and production of oxidative metabolites other than TCA. Kidney metabolism is further adjusted for direct excretion of TCA after production in the kidney, without entering systemic circulation.

Liver compartment

The rate of change for the amount of TCA in the liver (ALivTCA, in mg) is given by

$$dALivTCA/dt = QGutLivPlas \times (CPlasTCAfree - CVLivTCAFree) + (1 - FracOthel) \times StochTCAPERC \times RAMetLiv1 - RAMetTCA + kPOTCA$$

The first term reflects the free TCA in plasma flowing into and out of the liver compartment, the second term reflects production of TCA from liver metabolism of perc, the third term reflect other clearance of TCA from the liver, and the fourth term reflects absorption from the stomach of TCA. The contribution from liver metabolism of perc is adjusted for molecular weights and production of oxidative metabolites other than TCA. The rate of clearance of TCA is given by

$$RAMetTCA = kMetTCA \times ALivTCA$$

The oral intake rate of TCA (mg/h) includes a one compartment stomach. So for an oral dose of PODoseTCA (in mg/kg), occurring over a time TChng, the rate of change of TCA in the stomach (AStomTCA, in mg) is given by:

$$dAStomTCA/dt = KStomTCA - AStomTCA \times kASTCA$$
$$kStomTCA = \text{rate of input into stomach} = (PODoseTCA \times BW) / Tchng$$

The rate of absorption into the liver is thus

$$kPOTTCA = AStomTCA \times kASTCA$$

Total urinary excretion of TCA

Total urinary excretion of TCA includes both TCA cleared from plasma as well as "direct" excretion from TCA produced from kidney metabolism of perc. The rate of change of TCA in urine (AUrnTCA, in mg) is thus

$$dAUrnTCA/dt = RUrnTCA$$
$$RUrnTCA = RUrnTCAplas + StochTCAPERC \times (1 - FracOthel) \times FracKidTCA \times RametKid1$$

The first term was defined above in the plasma compartment. The second term is the contribution from kidney metabolism of perc.

For some human data (Chiu et al., 2007), urinary excretion was only collected during certain time periods, with data missing in other time periods. Thus, a switch UrnMissing was defined which equals 0 during times of urine collection, and 1 when urinary data are missing. The total amount of urinary TCA "collected" (AUrnTCA_collect, in mg) is thus given by

$$dAUrnTCA\_collect/dt = (1 - UrnMissing) \times RUrnTCA$$

GSH conjugation sub-model

The GSH conjugation sub-model only tracks the urinary excretion of NAcTCVC and DCA, with an intermediary delay compartment. The rate of change for NAcTCVC in the "delay compartment" (ANTCVC, in mg) is:

$$dANTCVC/dt = (RAMetLiv2 + RAMetKid2) \times FracNATUrn - StochTCVPERC \times StochN \times RUrnNTCVC$$

The first term is the contributions from liver and kidney GSH conjugation, adjusted for fraction of GSH conjugation producing NAcTCVC and for molecular weights, the second term is the urinary excretion of NAcTCVC:

$$RUrnNTCVC = \text{rate of urinary excretion of NAcTCVC (mg/h)} = ANTCVC \times kNAT$$

For the amount of NAcTCVC appearing in urine (AUrnNTCVC, in mg), the rate of change is

$$dAUrnNTCVC/dt = RUrnNTCVC$$

The rates of change for DCA in the delay compartment (ADCA, in mg) and appearing in urine (AUrnDCA, in mg) are similarly:

$$dADCA/dt = (RAMetLiv2 + RAMetKid2) \times FracDCAUrn \times StochTCVPERC \times StochDCATCVC - RUrnDCA \times dAUrnDCA/dt = RUrnDCA$$

RUrnDCA = rate of urinary excretion of DCA (mg/h) = ADCA × kDCA

Table A1
PBPK model baseline parameters.

Parameter	Description (units)	Formula	Baseline value or parameter	Description	Mouse	Rat	Human F/M	Scaling parameter	Sources(s)
QC	Cardiac output (L/h)	$QC = QCC_0 \times \exp(InQCC) \times BW^{0.75}$	QCC_0	Cardiac Output allometrically scaled	11.6	13.3	16/16	InQCC	a, b
QP	Alveolar ventilation (L/h)	$QP = QC \times VPR_0 \times \exp(InVPR)$	VPR_0	Ventilation-perfusion ratio	2.5	1.9	0.96/0.96	InVPRC	a, b, Optimized
QFat	Blood flow to fat (L/h)	$QFat = QC \times QFatC_0 \times QFatC$	$QFatC_0$	Fraction of blood flow to fat	0.07	0.07	0.085/0.05	QFatC	a, b
QGut	Blood flow to gut (L/h)	$QGut = QC \times QGutC_0 \times QGutC$	$QGutC_0$	Fraction of blood flow to gut	0.141	0.153	0.21/0.19	QGutC	a, b
QLiv	Hepatic artery blood flow (L/h)	$QLiv = QC \times QLivC_0 \times QLivC$	$QGutC_0$	Fraction of blood flow to hepatic artery	0.02	0.021	0.065/0.065	QLivC	a, b
QSlw	Blood flow to slowly perfused tissues (L/h)	$QSlw = QC \times QSlwC_0 \times QSlwC$	$QSlwC_0$	Fraction of blood flow to slowly perfused tissues	0.217	0.336	0.17/0.22	QSlwC	a, b
QKid	Blood flow to kidney (L/h)	$QKid = QC \times QKidC_0 \times QKidC$	$QKidC_0$	Fraction of blood flow to kidney	0.091	0.141	0.17/0.19	QKidC	a, b
QRap	Blood flow to rapidly perfused tissues (L/h)	$QRap = QC - (QFat + QGut + QLiv + QSlw + QKid)$	–	–	–	–	–	–	
DResp	Diffusion clearance rate (L/h)	$DResp = QP \times \exp(InDRespC)$	–	–	–	–	–	InDRespC	c
FracPlas	Fraction of blood that is plasma	$FracPlas = FracPlas_0 \times FracPlasC$	$FracPlas_0$	Fraction of blood that is plasma	0.52	0.53	0.615/0.567	FracPlasC	b, c, d
VFat	Volume of fat (L)	$VFat = BW \times VFatC_0 \times VFatC$	$VFatC_0$	Fraction of body weight that is fat	0.07	0.07	0.317/0.199	VFatC	a, b
VGut	Volume of gut (L)	$VGut = BW \times VGutC_0 \times VGutC$	$VGutC_0$	Fraction of body weight that is gut	0.049	0.032	0.022/0.02	VGutC	a, b
VLiv	Volume of liver (L)	$VLiv = BW \times VLivC_0 \times VLivC$	$VLivC_0$	Fraction of body weight that is liver	0.055	0.034	0.023/0.025	VLivC	a, b
VRap	Volume of rapidly perfused tissues (L)	$VRap = BW \times VRapC_0 \times VRapC$	$VRapC_0$	Fraction of body weight that is rapidly perfused	0.1	0.088	0.093/0.088	VRapC	a, b
VRespLum	Volume of respiratory tract lumen (L)	$VRespLum = BW \times VRespLumC_0 \times VRespLumC$	$VRespLumC_0$	Respiratory lumen volume as fraction body weight	0.004667	0.004667	0.002386/0.002386	VRespLumC	e
VResp	Volume of respiratory tract tissue (L)	$VResp = BW \times VRespC_0 \times VRespC$	$VRespC_0$	Fraction of body weight that is respiratory tract	0.0007	0.0005	0.00018/0.00018	VRespC	a, b, e
VKid	Volume of kidney (L)	$VKid = BW \times VKidC_0 \times VKidC$	$VKidC_0$	Fraction of body weight that is kidney	0.017	0.007	0.0046/0.0043	VKidC	a, b,
VBld	Volume of blood (L)	$VBld = BW \times VBldC_0 \times VBldC$	$VBldC_0$	Fraction of body weight that is blood	0.049	0.074	0.068/0.077	VBldC	a, b,
VSlw	Volume of slowly perfused tissue (L)	$VSlw = BW \times VperfC_0 - (VFat + VGut + VLiv + VRap + VResp + VKid + VBld)$	$VperfC_0$	Fraction of body weight that is blood perfused	0.8897	0.8995	0.85778/0.8560	–	
PB	Perc blood–air PC	$PB = PB_0 \times PBC$	PB_0	Perc blood–air PC	18.6	15.1	14.7	PBC	f
PFat	Perc fat–blood PC	$PFat = (PFatC_0/PB) \times PFatC$	$PFatC_0$	Perc fat–air PC	1510.8	1489.3	1450.0	PFatC	f
PGut	Perc gut–blood PC	$PGut = (PGutC_0/PB) \times \exp(InPGutC)$	$PGutC_0$	Perc gut–air PC	62.1	40.6	59.9	InPGutC	f
PLiv	Perc liver–blood PC	$PLiv = (PLivC_0/PB) \times \exp(InPLivC)$	$PLivC_0$	Perc liver–air PC	48.8	50.3	61.1	InPLivC	f
PRap	Perc rapidly perfused-blood PC	$PRap = (PRapC_0/PB) \times \exp(InPRapC)$	$PRapC_0$	Perc rapidly perfused-air PC	62.1	40.4	59.9	InPRapC	f
PResp	Perc respiratory tract tissue–blood PC	$PResp = (PrespC_0/PB) \times \exp(InPRespC)$	$PRespC_0$	Perc respiratory tract–air PC	79.1	32.7	58.6	InPRespC	f
PKid	Perc kidney–blood PC	$PKid = (PKidC_0/PB) \times \exp(InPKidC)$	$PKidC_0$	Perc kidney–air PC	79.1	32.7	58.6	InPKidC	f
PSlw	Perc slowly perfused-blood PC	$PSlw = (PSlwC_0/PB) \times \exp(InPSlwC)$	$PSlwC_0$	Perc slowly perfused-air PC	79.1	21.6	70.5	InPSlwC	f
TCAPlas	TCA blood–plasma concentration ratio	$TCAPlas = FracPlas + (1 - FracPlas) \times PRBCPlasTCA_0 \times \exp(InPRBCPlasTCAC)$	$PRBCPlasTCA_0$	TCA red blood cell–plasma partition coefficient	0.5	0.5	0.5/0.5	InPRBCPlasTCAC	c, g
PBodTCA	Free TCA body-plasma PC	$PBodTCA = TCAPlas \times PBodTCAC_0 \times \exp(InPBodTCAC)$	$PBodTCAC_0$	Free TCA body–blood PC	0.88	0.88	0.52	InPBodTCAC	c, h
PLivTCA	Free TCA liver–plasma PC	$PLivTCA = TCAPlas \times PLivTCAC_0 \times \exp(InPLivTCAC)$	$PLivTCAC_0$	Free TCA liver–blood PC	1.18	1.18	0.66	InPLivTCAC	c, h
kDissoc	Protein TCA dissociation constant (microM)	$kDissoc = kDissoc_0 \times \exp(InkDissocC)$	$kDissoc_0$	Protein TCA dissociation constant (microM)	107	275	182	InkDissocC	c, i
BMax	Protein concentration (microM)	$BMax = BMaxkD_0 \times kDissoc \times \exp(InBMaxkDC)$	$BMaxkD_0$	BMax/kDissoc ratio	0.88	1.22	4.62	InBMaxkDC	c, i

(continued on next page)

Table A1 (continued)

Parameter	Description (units)	Formula	Baseline value or parameter	Description	Mouse	Rat	Human F/M	Scaling parameter	Sources(s)
kTSD	Perc oil gavage stomach–duodenum transfer coefficient (/h)	kTSD = exp(lnkTSD)	1.4	–	–	–	–	lnkTSD	Optimized in mouse and rat
kAS	Perc oil gavage stomach-absorption coefficient (/h)	kAS = exp(lnkAS)	1.4	–	–	–	–	lnkAS	Optimized in mouse and rat
kAD	Perc oil gavage duodenum-absorption coefficient (/h)	kAD = exp(lnkAD)	0.75	–	–	–	–	lnkAD	Optimized in mouse and rat
kTSDAq	Perc aqueous gavage stomach-duodenum transfer coefficient (/h)	kTSDAq = exp(lnkTSDAq)	1.4	–	–	–	–	lnkTSDAq	Optimized in mouse and rat
kASAq	Perc aqueous gavage stomach-absorption coefficient (/h)	kASAq = exp(lnkASAq)	1.4	–	–	–	–	lnkASAq	Optimized in mouse and rat
kADAq	Perc aqueous gavage duodenum-absorption coefficient (/h)	kADAq = exp(lnkADAq)	0.75	–	–	–	–	lnkADAq	Optimized in mouse and rat
kASTCA	TCA stomach absorption coefficient (/h)	kASTCA = exp(lnkASTCA)	0.75	–	–	–	–	lnkASTCA	–
KM	KM for first perc hepatic oxidation pathway (mg/L blood)	KM = KM_0 × exp(lnKMC)	KM_0	KM for perc hepatic oxidation (mg/L blood)	88.6	69.7	55.8	lnKMC	See text; Optimized
VMax	VMax for first perc hepatic oxidation pathway (mg/h)	VMax = KM × ClC_0 × VLiv × exp(lnClC)	ClC_0	VMax/KM per kg liver for perc hepatic oxidation (L blood/h/kg liver)	1.57	0.36	0.202	lnClC	See text; Optimized
KM2	KM for second perc hepatic oxidation pathway (mg/L blood)	KM2 = KM × exp(lnKM2C)	–					lnKM2C (ln of ratio to first pathway KM)	See text; Optimized
VMax2	VMax for second perc hepatic oxidation pathway (mg/h)	VMax2 = KM2 × (VMax/KM)exp (lnCl2OxC)	–	Scaled to first pathway Clearance				lnClC2OxC (ln of ratio to first pathway clearance)	See text; Optimized
FracOther	Fraction of perc oxidation not to TCA	FracOther = exp(lnFracOtherC)/ (1 + exp(lnFracOtherC))	0.1	–	–	–	–	lnFracOtherC	See text
KMKid	KM for perc renal oxidation (mg/L blood)	KMKid = KM × $KMKidLiv_0$ × exp (lnKMKidLivC)	$KMKidLiv_0$	Ratio of kidney to liver oxidation KM in blood	0.616	1.53	1.04	lnKMKidLivC	See text; Optimized in humans
VMaxKid	VMax for perc renal oxidation (mg/h)	VMaxKid = (VMax/KM) × (VKid/ VLiv) × KMKid × $ClKidLiv_0$ × exp(lnClKidLivC)	$ClKidLiv_0$	Ratio of kidney to liver oxidation VMax/KM per kg tissue (mg/h/kg per mg/h/kg)	0.0211	0.0085	0.0125	lnClKidLivC	See text; Optimized in humans
FracKidTCA	Fraction of renal TCA production going directly to urine	FracKidTCA = exp(lnFracKidTCAC)/ (1 + exp(lnFracKidTCAC))	0.5	–	–	–	–	lnFracKidTCAC	See text

KMClara	KM for perc lung oxidation (mg/L air)	$KMClara = KM \times PLiv \times KMRespLiv_0 \times \exp(lnKMRespLivC)/(PB \times PResp)$	$KMRespLiv_0$	Ratio of lung to liver KM in tissue (mg/L per mg/L)	1	1	1	lnKMRespLivC	See text
VMaxClara	VMax for perc lung oxidation (mg/h)	$VMaxClara = VMax \times VMaxLungLiv_0 \times \exp(lnVMaxLungLivC)$	$VMaxLungLiv_0$	Ratio of lung to liver total VMax (mg/h per mg/h)	0.07	0.0144	0.0138/0.0128	lnVMaxLungLivC	See text
VMaxTCVG	VMax for perc hepatic GSH conjugation (mg/h)	$VMaxTCVG = VMaxTCVG_0 \times VLiv \times \exp(lnVMaxTCVGC)$	$VMaxTCVG_0$	VMax per kg liver for perc GSH conjugation (L blood/h/kg liver)	35.3	93.9	0.665	lnVMaxTCVGC	See text; Optimized
KMTCVG	KM for perc hepatic GSH conjugation (mg/L blood)	$KM = VMaxTCVG/(ClTCVG_0 \times \exp(lnClTCVGC)$	$ClTCVG_0$	VMax/KM for perc hepatic GSH conjugation (L blood/h)	0.656	2.218	0.0196	lnClTCVGC	See text; Optimized
VMaxKidTCVG	VMax for perc renal GSH conjugation (mg/h)	$VMaxKidTCVG = (VMaxTCVG/VLiv \times VKid \times VMaxKidLivTCVG_0 \times \exp(lnVMaxKidLivTCVGC)$	$VMaxKidLivTCVG_0$	Ratio of kidney to liver GSH conjugation VMax per kg tissue (mg/h/kg per mg/h/kg)	0.15	0.15	0.15	lnVMaxKidLivTCVGC	See text;
KMKidTCVG	KM for perc renal GSH conjugation (mg/L blood)	$KMKid = VMaxKidTCVG/(VMaxTCVG/KMTCVG/VLiv \times VKid \times ClKidLivTCVG_0 \times \exp(lnClKidLivTCVGC)$	$ClKidLivTCVG_0$	Ratio of kidney to liver GSH conjugation VMax/KM per kg tissue (L/h/kg per L/h/kg)	0.24	0.098	0.14	lnClKidLivTCVGC	See text;
kUrnTCA	Rate constant for TCA excretion to urine (/h)	$kUrnTCA = GFR\_BW \exp(lnkUrnTCAC) \times \exp(lnkTotTCAC) \times BW/VPlas$	GFR_BW	Glomerular filtration rate per kg body weight (L/h/kg)	0.6	0.522	0.108	lnkUrnTCAC	c, j
kMetTCA	Rate constant for other TCA clearance (/h)	$kMetTCA = BW^{-1/4} \times \exp(lnkMetTCAC) \times \exp(lnkTotTCAC)$	–	–	–	–	–	lnkMetTCAC	c
FracNATUrn	Fraction of GSH conjugation to urinary NAcTCVC	$FracNATUrn = \exp(lnFracNATUrnC)/(1 + \exp(lnFracNATUrnC))$	–	–	–	–	–	lnFracNATUrnC	Optimized in rat and human
FracDCAUrn	Fraction of GSH conjugation to urinary DCA	$FracDCAUrn = (1 - FracNATUrn) \times \exp(lnFracDCAUrnC)/(1 + \exp(lnFracDCAUrnC))$	–	–	–	–	–	lnFracDCAUrnC	Optimized in rat and human
kNAT	Rate constant for urinary excretion of DCA (/h)	$kNAT = BW^{-1/4} \times \exp(lnkNATC)$	–	–	–	–	–	lnkNATC	Optimized in rat and human
kDCA	Rate constant for urinary excretion of NAcTCVC (/h)	$kDCA = BW^{-1/4} \times \exp(lnkDCAC)$	–	–	–	–	–	lnkDCAC	Optimized in rat

a: Brown et al. (1997).
b: ICRP (2002).
c: Posterior mean from Chiu et al. (2009).
d: Measurements in control F344 rats and B6C3F1 mice at 19 weeks of age from Hejtmancik et al. (2002).
e: Sarangapani et al. (2003).
f: In mice, blood–air from Gargas et al. (1989), Reitz et al. (1996), Gearhart et al. (1993); liver, kidney, and muscle (slowly perfused) from Gearhart et al. (1993); gut, rapidly perfused used geometric mean of kidney and liver; respiratory tract used kidney. In rats, blood–air, fat, liver, muscle (slowly perfused) from Gargas et al. (1989), Koizumi (1989), and Mahle et al. (2007); kidney and brain (rapidly perfused) used Mahle et al. (2007); gut used geometric mean of kidney and liver; respiratory tract used kidney. In humans, blood–air from Gargas et al. (1989), Sato and Nakajima (1979), Koizumi (1989), Gearhart et al. (1993), Mahle et al. (2007), Mahle et al. (2007), and Fisher et al. (1997); kidney, liver, and muscle (slowly perfused) used Gearhart et al. (1993); gut and rapidly perfused used geometric mean of kidney and liver; and respiratory tract used kidney.
g: Baseline corresponds to Blood/Plasma concentration ratio of 0.76 measured in rats from Schultz et al. (1999).
h: Abbas and Fisher (1997); Fisher et al. (1998).
i: Geometric mean of Lumpkin et al. (2003), Schultz et al. (1999), Templin et al. (1993, 1995); and Yu et al. (2000).
j: Clearance based on glomerular filtration rates across species from Lin (1995).

The rate of production of "other" products of GSH conjugation (AGSHOther, in mg perc equivalents) is

$$d(AGSHOther)/dt = (RAMetLiv2 + RAMetKid2) \times (1 - FracNATUrn - FracDCAUrn)$$

Appendix B. Supplementary data

Supplementary data to this article can be found online at doi:10.1016/j.taap.2011.03.020.

References

Abbas, R., Fisher, J.W., 1997. A physiologically based pharmacokinetic model for trichloroethyleneandits metabolites,chloralhydrate,trichloroacetate,dichloroacetate, trichloroethanol, and trichloroethanol glucuronide in B6C3F1 mice. Toxicol. Appl. Pharmacol. 147, 15–30.

Altmann, L., Neuhann, H.F., Kramer, U., Witten, J., Jermann, E., 1995. Neurobehavioral and neurophysiological outcome of chronic low-level tetrachloroethene exposure measured in neighborhoods of dry cleaning shops. Environ. Res. 69, 83–89.

Anders, M.W., Lash, L., Dekant, W., Elfarra, A.A., Dohn, D., 1988. Biosynthesis and biotransformation of glutathione S-conjugates to toxic metabolites. Crit. Rev. Toxicol. 18, 311–341.

Barter, Z.E., Bayliss, M.K., Beaune, P.H., Boobis, A.R., Carlile, D.J., Edwards, R.J., Houston, J.B., Lake, B.G., Lipscomb, J.C., Pelkonen, O.R., Tucker, G.T., Rostami-Hodjegan, A., 2007. Scaling factors for the extrapolationof in vivo metabolic drug clearance from in vitro data: reaching a consensus on values of human microsomal protein and hepatocellularity per gram of liver. Curr. Drug Metab. 8 (1), 33–45.

Belisle, C.J.P., 1992. Convergence theorems for a class of simulated annealing algorithms on R^d. J. Appl. Prob. 29, 885–895.

Bois, F.Y., Zeise, L., Tozer, T.N., 1990. Precision and sensitivity of pharmacokinetic models for cancer risk assessment: tetrachloroethylene in mice, rats, and humans. Toxicol. Appl. Pharmacol. 102, 300–315.

Bois, F.Y., Gelman, A., Jiang, J., Maszle, D.R., Zeise, L., Alexeef, G., 1996. Population toxicokinetics of tetrachloroethylene. Arch. Toxicol. 70, 347–355.

Bong, M., Laskowska-Klita, T., Szymczyk, T., 1985. Effect of the benzene fraction of petroleum on protein content in rat liver and kidney. Bull. Environ. Contam. Toxicol. 34 (1), 45–54.

Boyes, W.K., Bercegeay, M., Oshiro, W.M., Krantz, Q.T., Kenyon, E.M., Bushnell, P.J., Benignus, V.A., 2009. Acute perchloroethylene exposure alters rat visual-evoked potentials in relation to brain concentrations. Toxicol. Sci. 108, 159–172.

Brodkin, C.A., Daniell, W., Checkoway, H., Echeverria, D., Johnson, J., Wang, K., Stomaey, R., Green, D., Redlich, C., Gretch, D., Rosenstock, L., 1995. Hepatic ultrasonic changes in workers exposed to perchloroethylene. Occup. Environ. Med. 52, 679–685.

Brown, R.P., Delp, M.D., Lindstedt, S.L., Rhomberg, L.R., Beliles, R.P., 1997. Physiological parameter values for physiologically based pharmacokinetic models. Toxicol. Ind. Health 13, 407–484.

Buben, J.A., O'Flaherty, E.J., 1985. Delineation of the role of metabolism in the hepatotoxicity of trichloroethylene and perchloroethylene: a dose–effect study. Toxicol. Appl. Pharmacol. 78, 105–122.

Bushnell, P.J., Shafer, T.J., Bale, A.S., Boyes, W.K., Simmons, J.E., Eklund, C., Jackson, T.L., 2005. Developing an exposure dose response model for organic solvents: overview and progress on in vitro models and dosimetry. Environ. Toxicol. Pharmacol. 19, 607–614.

Calvert, G.M., Ruder, A.M., Petersen, M.R., 2010. Mortality and end-stage renal disease incidence among dry leaning workers. Occup. Environ. Med. doi:10.1136/oem.2010.060665.

Chen, C., Blancato, J., 1987. Role of pharmacokinetic modeling in risk assessment: perchloroethylene as an example. Pharmacokinetics in Risk Assessment: Drinking Water and Health. National Academy Press, Washington, DC, pp. 369–390.

Chien, Y.C., 1997. The influences of exposure pattern and duration on elimination kinetics and exposure assessment of tetrachloroethylene in humans. PhD thesis, Rutgers University, New Brunswick, NJ.

Chiu, W.A., 2007. Statistical issues in physiologically based pharmacokinetic modeling. In: Lipscomb, J.C., Ohanian, E.V. (Eds.), Toxicokinetics and Risk Assessment. Informa Healthcare, New York.

Chiu, W.A., in press. Trichloroacetic acid: updated estimates of its bioavailability and its contribution to trichloroethylene-induced mouse hepatomegaly. Toxicology. doi:10.1016/j.tox.2011.04.009.

Chiu, W.A., Bois, F.Y., 2006. Revisiting the population toxicokinetics of tetrachloroethylene. Arch. Toxicol. 80, 382–385.

Chiu, W.A., White, P., 2006. Steady-state solutions to PBPK models and their applications to risk assessment I: route-to-route extrapolation of volatile chemicals. Risk Anal. 26 (3), 769–780.

Chiu, W.A., Micallef, S., Monster, A.C., Bois, F.Y., 2007. Toxicokinetics of inhaled trichloroethylene and tetrachloroethylene in humans at 1 ppm: empirical results and comparisons with previous studies. Toxicol. Sci. 95, 23–36.

Chiu, W.A., Okino, M.S., Evans, M.V., 2009. Characterizing uncertainty and population variability in the toxicokinetics of trichloroethylene and metabolites in mice, rats, and humans using an updated database, physiologically based pharmacokinetic (PBPK) model, and Bayesian approach. Toxicol. Appl. Pharmacol. 241, 36–60.

Clewell, H.J., Gentry, P.R., Kester, J.E., Andersen, M.E., 2005. Evaluation of physiologically based pharmacokinetic models in risk assessment: an example with perchloroethylene. Crit. Rev. Toxicol. 35, 413–433.

Costa, A.K., Ivanetich, K.M., 1980. Tetrachloroethylene metabolism by the hepatic microsomal cytochrome P-450 system. Biochem. Pharmacol. 29, 2863–2869.

Costa, A.K., Ivanetich, K.M., 1984. Chlorinated ethylenes: their metabolism and effect on DNA repair in rat hepatocytes. Carcinogenesis 5, 1629–1636.

Covington, T.R., Robinan Gentry, P., Van Landingham, C.B., Andersen, M.E., Kester, J.E., Clewell, H.J., 2007. The use of Markov chain Monte Carlo uncertainty analysis to support a Public Health Goal for perchloroethylene. Regul. Toxicol. Pharmacol. 47, 1–18.

Dallas, C.E., Chen, X.M., O'Barr, K., Muralidhara, S., Varkonyi, P., Bruckner, J.V., 1994a. Development of a physiologically based pharmacokinetic model for perchloroethylene using tissue concentration–time data. Toxicol. Appl. Pharmacol. 128, 50–59.

Dallas, C.E., Muralidhara, S., Chen, X.M., Ramanathan, R., Varkonyi, P., Gallo, J.M., Bruckner, J.V., 1994b. Use of a physiologically based model to predict systemic uptake and respiratory elimination of perchloroethylene. Toxicol. Appl. Pharmacol. 128, 60–68. doi:10.1006/taap.1994.1180.

Dallas, C.E., Chen, X.M., Muralidhara, S., Varkonyi, P., Tackett, R.L., Bruckner, J.V., 1994c. Use of tissue disposition data from rats and dogs to determine species differences in input parameters for a physiological model for perchloroethylene. Environ. Res. 67, 54–67.

Dallas, C.E., Chen, X.M., Muralidhara, S., Varkonyi, P., Tackett, R.L., Bruckner, J.V., 1995. Physiologically based pharmacokinetic model useful in prediction of the influence of species, dose, and exposure route on perchloroethylene pharmacokinetics. J. Toxicol. Environ. Health 44, 301–317.

DeAngelo, A.B., George, M.H., House, D.E., 1999. Hepatocarcinogenicity in the male B6C3F1 mouse following a lifetime exposure to dichloroacetic acid in the drinking water: dose–response determination and modes of action. J. Toxicol. Environ. Health A 58, 485–507.

DeAngelo, A.B., Daniel, F.B., Wong, D.M., George, M.H., 2008. The induction of hepatocellular neoplasia by trichloroacetic acid administered in the drinking water of the male B6C3F1 mouse. J. Toxicol. Environ. Health A 71, 1056–1068.

Dekant, W., 2010. Toxicological review of trichloroethylene in support of the IRIS database (Draft of October 2009): comments of Prof. W. Dekant, submitted as part of Comments of the Halogenated Solvents Industry Alliance, Inc. url: http://www.regulations.gov/search/Regs/home.html#documentDetail?R=0900006480a8dd76.

Dekant, W., Birner, G., Werner, M., Parker, J., 1998. Glutathione conjugation of perchloroethene in subcellular fractions from rodent and human liver and kidney. Chem. Biol. Interact. 116 (1–2), 31–43.

Doherty, A.T., Ellard, S., Parry, E.M., Parry, J.M., 1996. An investigation into the activation and deactivation of chlorinated hydrocarbons to genotoxins in metabolically competent human cells. Mutagenesis 11, 247–274.

Echeverria, D., White, R.F., Sampaio, C., 1995. A behavioral evaluation of PCE exposure in patients and dry cleaners: a possible relationship between clinical and preclinical effects. J. Occup. Environ. Med. 37, 667–680.

Evans, M.V., Chiu, W.A., Okino, M.S., Caldwell, J.C., 2009. Development of an updated PBPK model for trichloroethylene and metabolites in mice, and its application to discern the role of oxidative metabolism in TCE-induced hepatomegaly. Toxicol. Appl. Pharmacol. 236, 329–340.

Fernandez, J., Guberan, E., Caperos, J., 1976. Experimental human exposures to tetrachloroethylene vapor and elimination in breath after inhalation. Am. Ind. Hyg. Assoc. J. 37, 143–150.

Ferroni, C., Selis, L., Mutti, A., Folli, D., Bergamaschi, E., Franchini, I., 1992. Neurobehavioral and neuroendocrine effects of occupational exposure to perchloroethylene. Neurotoxicology 13, 243–247.

Fisher, J., Mahle, D., Bankston, L., Greene, R., Gearhart, J., 1997. Lactational transfer of volatile chemicals in breast milk. Am. Ind. Hyg. Assoc. J. 58 (6), 425–431.

Fisher, J.W., Mahle, D., Abbas, R., 1998. A human physiologically based pharmacokinetic model for trichloroethylene and its metabolites, trichloroacetic acid and free trichloroethanol. Toxicol. Appl. Pharmacol. 152, 339–359.

Franz, S.W., Watanabe, P.G., 1983. Tetrachloroethylene: balance and tissue distribution in male Sprague–Dawley rats by drinking-water administration. Toxicol. Appl. Pharmacol. 69, 66–72.

Gargas, M.L. (1988). Tissue Solubilities and Biotransformation Rates of Halocarbons: Experimental Determinations and Quantitative Modeling. A dissertation submitted to Wright State University, Dayton, OH.

Gargas, M.L., Burgess, R.J., Voisard, D.E., Cason, G.H., Andersen, M.E., 1989. Partition coefficients of low-molecular-weight volatile chemicals in various liquids and tissues. Toxicol. Appl. Pharmacol. 98, 87–99.

Gearhart, J.M., Mahle, D.A., Greene, R.J., Seckel, C.S., Flemming, C.D., Fisher, J.W., Clewell 3rd, H.J., 1993. Variability of physiologically based pharmacokinetic (PBPK) model parameters and their effects on PBPK model predictions in a risk assessment for perchloroethylene (PCE). Toxicol. Lett. 68, 131–144.

Gennari, P., Naldi, M., Motta, R., Nucci, M.C., Giacomini, C., Violante, F.S., Raffi, G.B., 1992. gamma-Glutamyltransferase isoenzyme pattern in workers exposed to tetrachloroethylene. Am. J. Ind. Med. 21, 661–671.

Ginsberg, G., Smolenski, S., Hattis, D., Guyton, K.Z., Johns, D.O., Sonawane, B., 2009a. Genetic polymorphism in glutathione transferases (GST): population distribution of GSTM1, T1, and P1 conjugating activity. J. Toxicol. Environ. Health B Crit. Rev. 12, 389–439.

Ginsberg, G., Smolenski, S., Neafsey, P., Hattis, D., Walker, K., Guyton, K.Z., Johns, D.O., Sonawane, B., 2009b. The influence of genetic polymorphisms on population

variability in six xenobiotic-metabolizing enzymes. J. Toxicol. Environ. Health B Crit. Rev. 12, 307–333.
Green, T., 2003. Perchloroethylene Induced Mouse Liver Tumours: Mode of Action Studies. Central Toxicology Laboratory, Alderley Park Macclesfield, Cheshire, UK. Document number CTL/024741/RES/REPT-001, August 6, 2003.
Green, T., Odum, J., Nash, J.A., Foster, J.R., 1990. Perchloroethylene-induced rat kidney tumors: an investigation of the mechanisms involved and their relevance to humans. Toxicol. Appl. Pharmacol. 103 (1), 77–89.
Green, T., Mainwaring, G.W., Foster, J.R., 1997. Trichloroethylene-induced mouse lung tumors: studies of the mode of action and comparisons between species. Fundam. Appl. Toxicol. 37, 125–130.
Hack, C.E., Chiu, W.A., Jay Zhao, Q., Clewell, H.J., 2006. Bayesian population analysis of a harmonized physiologically based pharmacokinetic model of trichloroethylene and its metabolites. Regul. Toxicol. Pharmacol. 46, 63–83.
Hake, C.L., Stewart, R.D., 1977. Human exposure to tetrachloroethylene: inhalation and skin contact. Environ. Health Perspect. 21, 231–238.
Hejtmancik, M.R., Trela, B.A., Kurtz, P.J., Persing, R.L., Ryan, M.J., Yarrington, J.T., Chhabra, R.S., 2002. Comparative gavage subchronic toxicity studies of o-chloroaniline and m-chloroaniline in F344 rats and B6C3F1 mice. Toxicol. Sci. 69, 234–243.
Ikeda, M., Ohtsuji, H., 1972. A comparative study of the excretion of Fujiwara reaction-positive substances in urine of humans and rodents given trichloro-or tetrachloro-derivatives of ethane and ethylene. Br. J. Ind. Med. 29, 99–104.
Ikeda, M., Ohtsuji, H., Imamura, T., Komoike, Y., 1972. Urinary excretion of total trichloro-compounds, trichloroethanol, and trichloroacetic acid as a measure of exposure to trichloroethylene and tetrachloroethylene. Br. J. Ind. Med. 29, 328–333.
International Commission on Radiological Protection (ICRP), 2002. Basic anatomical and physiological data for use in radiological protection:reference values. A Report of Age- and Gender-related Differences in the Anatomical and Physiological Characteristics of Reference Individuals. Ann ICRP, 32. ICRP Publication 89, pp. 5–265.
Japan Industrial Safety Association (JISA), 1993. Carcinogenicity Study of Tetrachloroethylene by Inhalation in Rats and Mice. Japan Industrial Safety Association, Hadano, Japan.
Johanson, G., Filser, J.G., 1992. Experimental data from closed chamber gas uptake studies in rodents suggest lower uptake rate of chemical than calculated from literature values on alveolar ventilation. Arch. Toxicol. 66, 291–295.
Juronen, E., Tasa, G., Uuskula, M., Pooga, M., Mikelaar, A.V., 1996. Purification, characterization and tissue distribution of human class theta glutathione S-transferase S-transferse T1–1. Biochem. Mol. Biol. Int. 39, 21–29.
Koizumi, A., 1989. Potential of physiologically based pharmacokinetics to amalgamate kinetic data of trichloroethylene and tetrachloroethylene obtained in rats and man. Br. J. Ind. Med. 46, 239–249.
Krause, R.J., Lash, L.H., Elfarra, A.A., 2003. Human kidney flavin-containing monooxygenases and their potential roles in cysteine s-conjugate metabolism and nephrotoxicity. J. Pharmacol. Exp. Ther. 304, 185–191.
Lash, L.H., Parker, J.C., 2001. Hepatic and renal toxicities associated with perchloroethylene. Pharmacol. Rev. 53, 177–208.
Lash, L.H., Qian, W., Putt, D.A., Desai, K., Elfarra, A.A., Sicuri, A.R., Parker, J.C., 1998. Glutathione conjugation of perchloroethylene in rats and mice in vitro: sex-, species-, and tissue-dependent differences. Toxicol. Appl. Pharmacol. 150, 49–57.
Lash, L.H., Lipscomb, J.C., Putt, D.C., Parker, J.C., 1999. Glutathione conjugation of trichloroethylene in human liver and kidney: kinetics and individual variation. Drug Metab. Dispos. 27, 351–359.
Lash, L.H., Fisher, J.W., Lipscomb, J.C., Parker, J.C., 2000. Metabolism of trichloroethylene. Environ. Health Perspect. 108 (Suppl. 2), 177–200.
Lash, L.H., Putt, D.A., Huang, P., Hueni, S.E., Parker, J.C., 2007. Modulation of hepatic and renal metabolism and toxicity of trichloroethylene and perchloroethylene by alterations in status of cytochrome P450 and glutathione. Toxicology 235, 11–26.
Lin, J.H., 1995. Species similarities and differences in pharmacokinetics. Drug Metab. Dispos. 23, 1008–1021.
Lipscomb, J.C., Fisher, J.W., Confer, P.D., Byczkowski, J.Z., 1998. In vitro to in vivo extrapolation for trichloroethylene metabolism in humans. Toxicol. Appl. Pharmacol. 152, 376–387.
Lumpkin, M.H., Bruckner, J.V., Campbell, J.L., Dallas, C.E., White, C.A., Fisher, J.W., 2003. Plasma binding of trichloroacetic acid in mice, rats, and humans under cancer bioassay and environmental exposure conditions. Drug Metab. Dispos. 31, 1203–1207.
Mahle, D.A., Gearhart, J.M., Grigsby, C.C., Mattie, D.R., Barton, H.A., Lipscomb, J.C., Cook, R.S., 2007. Age-dependent partition coefficients for a mixture of volatile organic solvents in Sprague–Dawley rats and humans. J. Toxicol. Environ. Health A 70 (20), 1745–1751.
Mattie, D.R., Bates, G.D., Jepson, G.W., Fisher, J.W., McDougal, J.N., 1994. Determinants of skin:air partition coefficients for volatile chemicals: experimental method and applications. Fundam. Appl. Toxicol. 22, 51–57.
Monster, A.C., Boersma, G., Steenweg, H., 1979. Kinetics of tetrachloroethylene in volunteers; influence of exposure concentration and work load. Int. Arch. Occup. Environ. Health 42, 303–309.
Mutti, A., Alinovi, R., Bergamaschi, E., Biagini, C., Cavazzini, S., Franchini, I., Lauwerys, R. R., Bernard, A.M., Roels, H., Gelpi, E., Rosello, J., Ramis, I., Price, R.G., Taylor, S.A., De Broe, M., Nuyts, G.D., Stolte, H., Fels, L.M., Herbort, C., 1992. Nephropathies and exposure to perchloroethylene in dry-cleaners. Lancet 340, 189–193.
National Cancer Institute (NCI), 1977. Bioassay of tetrachloroethylene for possible carcinogenicity. DHEW Pub. (NIH) 77-813. Tech Rep Ser. 13. National Toxicology Program, National Institutes of Health, Public Health Service, U.S. Department of Health and Human Services, Atlanta, GA.
National Research Council (NRC), 2010. Review of the Environmental Protection Agency's Draft IRIS Assessment of Tetrachloroethylene. National Academy Press, Washington, DC.
National Toxicology Program (NTP), 1986. NTP toxicology and carcinogenesis studies of tetrachloroethylene (perchloroethylene) (CAS No.127-18-4). 344/N rats and B6C3F1 mice. Tech Rep Ser 311. National Toxicology Program, National Institutes of Health, Public Health Service, U.S. Department of Health and Human Services, Atlanta, GA.
Nyengaard, J.R., Flyvbjerg, A., Rasch, R., 1993. The impact of renal growth, regression and regrowth in experimental diabetes mellitus on number and size of proximal and distal tubular cells in the rat kidney. Diabetologia 36, 1126–1131.
Odum, J., Green, T., Foster, J.R., Hext, P.M., 1988. The role of trichloracetic acid and peroxisome proliferation in the differences in carcinogenicity of perchloroethylene in the mouse and rat. Toxicol. Appl. Pharmacol. 92, 103–112.
Ohtsuki, T., Sato, K., Koizumi, A., Kumai, M., Ikeda, M., 1983. Limited capacity of humans to metabolize tetrachloroethylene. Int. Arch. Occup. Environ. Health 51, 381–390.
Pegg, D.G., Zempel, J.A., Braun, W.H., Watanabe, P.G., 1979. Disposition of tetrachloro (^{14}C)ethylene following oral and inhalation exposure in rats. Toxicol. Appl. Pharmacol. 51, 465–474.
Pereira, M.A., 1996. Carcinogenic activity of dichloroacetic acid and trichloroacetic acid in the liver of female B6C3F1 mice. Fundam. Appl. Toxicol. 31, 192–199.
Philip, B.K., Mumtaz, M.M., Latendresse, J.R., Mehendale, H.M., 2007. Impact of repeated exposure on toxicity of perchloroethylene in Swiss Webster mice. Toxicology 232, 1–14.
Qiu, J., Chien, Y.C., Bruckner, J.V., Fisher, J.W., 2010. Bayesian analysis of a physiologically based pharmacokinetic model for perchloroethylene in humans. J. Toxicol. Environ. Health A 73 (1), 74–91.
Rao, H.V., Brown, D.R., 1993. A physiologically based pharmacokinetic assessment of tetrachloroethylene in groundwater for a bathing and showering determination. Risk Anal. 13, 37–49.
Reitz, R.H., Gargas, M.L., Mendrala, A.L., Schumann, A.M., 1996. In vivo and in vitro studies of perchloroethylene metabolism for physiologically based pharmacokinetic modeling in rats, mice, and humans. Toxicol. Appl. Pharmacol. 136, 289–306.
Sarangapani, R., Gentry, P.R., Covington, T.R., Teeguarden, J.G., Clewell 3rd., H.J., 2003. Evaluation of the potential impact of age- and gender-specific lung morphology and ventilation rate on the dosimetry of vapors. Inhal. Toxicol. 15, 987–1016.
Sato, A., Nakajima, T., 1979. Partition coefficients of some aromatic hydrocarbons and ketones in water, blood and oil. Br. J. Ind. Med. 36, 231–234.
Savolainen, H., Pfaffli, P., Tengen, M., Vainio, H., 1977. Biochemical and behavioural effects of inhalation exposure to tetrachlorethylene and dichlormethane. J. Neuropathol. Exp. Neurol. 36, 941–949.
Schreiber, J.S., Hudnell, H.K., Geller, A.M., House, D.E., Aldous, K.M., Force, M.S., Langguth, K., Prohonic, E.J., Parker, J.C., 2002. Apartment residents' and day care workers' exposures to tetrachloroethylene and deficits in visual contrast sensitivity. Environ. Health Perspect. 110, 655–664.
Schultz, I.R., Merdink, J.L., Gonzalez-Leon, A., Bull, R.J., 1999. Comparative toxicokinetics of chlorinated and brominated haloacetates in F344 rats. Toxicol. Appl. Pharmacol. 158, 103–114.
Schumann, A.M., Quast, J.F., Watanabe, P.G., 1980. The pharmacokinetics and macromolecular interactions of perchloroethylene in mice and rats. Toxicol. Appl. Pharmacol. 55, 207–219.
Seeber, A., 1989. Neurobehavioral toxicity of long-term exposure to tetrachloroethylene. Neurotoxicol. Teratol. 11, 579–583.
Sohlenius-Sternbeck, A.K., 2006. Determination of the hepatocellularity number for human, dog, rabbit, rat and mouse livers from protein concentration measurements. Toxicol. In Vitro 20 (8), 1582–1586.
Stewart, R.D., Gay, H.H., Erley, D.S., Hake, C.L., Schaffer, A.W., 1961. Human exposure to tetrachloroethylene vapor. Arch. Environ. Health 2, 516–522.
Stewart, R.D., Baretta, E.D., Dodd, H.C., Torkelson, T.R., 1970. Experimental human exposure to tetrachloroethylene. Arch. Environ. Health 20 (2), 225–229.
Sweeney, L.M., Kirman, C.R., Gargas, M.L., Dugard, P.H., 2009. Contribution of trichloroacetic acid to liver tumors observed in perchloroethylene (perc)-exposed mice. Toxicology 260, 77–83.
Templin, M.V., Parker, J.C., Bull, R.J., 1993. Relative formation of dichloroacetate and trichloroacetate from trichloroethylene in male B6C3F1 mice. Toxicol. Appl. Pharmacol. 123, 1–8.
Templin, M.V., Stevens, D.K., Stenner, R.D., Bonate, P.L., Tuman, D., Bull, R.J., 1995. Factors affecting species differences in the kinetics of metabolites of trichloroethylene. J. Toxicol. Environ. Health 44, 435–447.
Volkel, W., Friedewald, M., Lederer, E., Pahler, A., Parker, J., Dekant, W., 1998. Biotransformation of perchloroethene: dose-dependent excretion of trichloroacetic acid, dichloroacetic acid, and N-acetyl-S-(trichlorovinyl)-L-cysteine in rats and humans after inhalation. Toxicol. Appl. Pharmacol. 153, 20–27.
Walker, K., Ginsberg, G., Hattis, D., Johns, D.O., Guyton, K.Z., Sonawane, B., 2009. Genetic polymorphism in N-Acetyltransferase (NAT): population distribution of NAT1 and NAT2 activity. J. Toxicol. Environ. Health B Crit. Rev. 12, 440–472.
Ward, R.C., Travis, C.C., Hetrick, D.M., Andersen, M.E., Gargas, M.L., 1988. Pharmacokinetics of tetrachloroethylene. Toxicol. Appl. Pharmacol. 93, 108–117.
Warren, D.A., Reigle, T.G., Muralidhara, S., Dallas, C.E., 1996. Schedule-controlled operant behavior of rats following oral administration of perchloroethylene: time course and relationship to blood and brain solvent levels. J. Toxicol. Environ. Health 47, 345–362.

Werner, M., Birner, G., Dekant, W., 1996. Sulfoxidation of mercapturic acids derived from tri- and tetrachloroethene by cytochromes P450 3A: a bioactivation reaction in addition to deacetylation and cysteine conjugate beta-lyase mediated cleavage. Chem. Res. Toxicol. 9, 41–49.

Wheeler, J.B., Stourman, N.V., Their, R., Dommermuth, A., Vuilleumier, S., Rose, J.A., Armstrong, R.N., Guengerich, F.P., 2001. Conjugation of haloalkanes by bacterial and mammalian glutathione transferases: mono- and dihalomethanes. Chem. Res. Toxicol. 14, 1118–11127.

Yoshioka, T., Krauser, J.A., Guengerich, F.P., 2002. Tetrachloroethyleneoxide: hydrolytic productsand reactionswith phosphateand lysine.Chem.Res. Toxicol. 15, 1096–1105.

Yu, K.O., Barton, H.A., Mahle, D.A., Frazier, J.M., 2000. In vivo kinetics of trichloroacetate in male Fischer 344 rats. Toxicol. Sci. 54, 302–311.

Development and evaluation of a harmonized physiologically based pharmacokinetic (PBPK) model for perchloroethylene toxicokinetics in mice, rats, and humans – Supplementary Materials

Weihsueh A. Chiu* and Gary L. Ginsberg†

* National Center for Environmental Assessment, U.S. Environmental Protection Agency, Washington DC, USA, 20460; E-mail: chiu.weihsueh@epa.gov

† Connecticut Department of Public Health, Hartford, Connecticut, 06106, USA; E-mail: gary.ginsberg@ct.gov

Corresponding Author (Express Delivery Address):
Weihsueh A. Chiu, Ph.D.
U.S. Environmental Protection Agency – 8623P
Two Potomac Yard (North Building)
2733 South Crystal Drive
Arlington, VA 22202
Phone: 703-347-8607; Fax: (703) 347-8692; E-mail: chiu.weihsueh@epa.gov

Section: Regular Articles
Short title: Harmonized PBPK model of perc

Disclaimer:
This manuscript has been reviewed by the U.S. Environmental Protection Agency and approved for publication. The views expressed in this manuscript are those of the author(s) and do not necessarily reflect the views or policies of the U.S. Environmental Protection Agency or the Connecticut Department of Public Health.

Conflict of Interest statement: The authors declare that there are no conflicts of interest.

Table S-1. Reported conversion factors for in vitro data.

Reference	Species	Tissue	TP (mg/g)	MSP (mg/g)	CSP (mg/g)	Cell (10^6/g)
Barter et al. (2007) weighted mean	**Human**	**Liver**		**32**		**99**
Knaak et al. (1993)	Human	Liver	131	9		
Sohlenius-Sternbeck (2006)	Human	Liver	90			139
Barter et al. (2007) review	Rat	Liver				
Pelkonen et al. (1973)				40		–
Selgen (1973)				–		128
Zahlten & Stratman (1974)				–		98, 120
Joly et al. (1975)				45		–
Baarnhielm et al. (1986)				54		–
Chiba et al. (1990)				36		–
Carlile et al. (1999)				60		97
Griffiths et al. (2005)*				62		167
Prasanna et al. (1989)	Rat	Liver	203	22	78	
van Bree et al. (1990)	Rat	Liver		34.7		
Brown et al. (1996)	Rat	Liver		30	95	
Sohlenius-Sternbeck (2006)	Rat	Liver	112			117
Ekins et al. (1995)	Rat	Liver				117
Kedderis et al. (1995)	Rat	Liver		15.4	87.5	
Knaak et al. (1993)	Rat	Liver	164	59		
Bong et al. (1985)	Rat	Liver	161	34		
Rat Geometric Mean			**157**	**38**	**87**	**119**
Sohlenius-Sternbeck (2006)	Mouse	Liver	115			135
Bong et al. (1985)	Rat	Kidney	102	16		
Nyengaard et al. (1993)	Rat	Kidney				126

Notes:
Rows in **bold** are summaries statistics (as indicated) across multiple studies.
TP = total protein content (mg/g tissue)
MSP = microsomal protein content (mg/g tissue)
CSP = cytosolic protein content (mg/g tissue)
Cell = cellularity (10^6 cells/g tissue)
* Griffiths et al. (2005) as cited in Barter et al. (2007) could not be located.

Table S-2. Baseline perc metabolism PBPK parameter values derived from in vitro data

		In vitro baseline values				PBPK model baseline values[a]			
Metabolism parameter (abbreviation)	**Abbreviation**	**M**	**R**	**H**	**Units (see text)**	**M**	**R**	**H**	**Units**
K_M for hepatic Perc oxidation	**K_MC**	1.4	**1.4**	1.4	mM liver	88.6	**69.7**	55.8	mg/L blood[a]
V_{MAX}/K_M for hepatic Perc oxidation	**ClC**	**10**	**1.8**	**0.81**	nmol/min/g liver/mM	**1.57**	**0.360**	**0.202**	L blood/hr/kg liver[b,c]
Ratio of renal to hepatic K_M for Perc oxidation	**K_MKidLivC**	1	1	1	(mM kidney)/(mM liver)	0.616	1.53	1.04	(mg/L blood kidney)/ (mg/L blood liver)[d]
Ratio of renal to hepatic V_{MAX}/K_M for Perc oxidation	**ClKidLivC**	0.013	**0.013**	0.013	(nmol/min/g kidney/mM)/ (nmol/min/g liver/mM)	0.0211	**0.0085**	0.0125	(L/hr/kg kidney)/ (L/hr/kg liver) [c,e]
Ratio of lung to hepatic V_{MAX} for Perc oxidation	**V_{MAX}LungLivC**	**0.55**	**0.098**	**0.046**	(nmol/min/g lung)/ (nmol/min/g liver)	**0.55**	**0.098**	**0.046**	(mg/hr/kg lung)/ (mg/hr/kg liver) [c]
Ratio of lung to hepatic K_M for Perc oxidation	**KMRespLivC**	1	1	1	(mM respiratory tract tissue)/(mM liver)	1	1	1	(mM respiratory tract tissue)/(mM liver)
V_{MAX} for hepatic Perc GSH conjugation	**V_{MAX}TCVGC**	**3.55**	**9.44**	**0.0668**	nmol/min/g liver	**35.3**	**93.9**	**0.665**	mg/hr/kg liver[c,f]
V_{MAX}/K_M for hepatic Perc GSH conjugation	**ClTCVGC**	**4.17**	**11.1**	**0.0784**	nmol/min/g liver/mM	**0.656**	**2.218**	**0.0196**	L blood/hr/kg liver[b,c]
Ratio of renal to hepatic V_{MAX} for Perc GSH conjugation	**V_{MAX}KidLivTCVGC**	**0.15**	**0.15**	**0.15**	(nmol/min/g kidney)/ (nmol/min/g liver)	**0.15**	**0.15**	**0.15**	(mg/hr/kg kidney)/ (mg/hr/kg liver) [c,g]
Ratio of renal to hepatic V_{MAX}/K_M for Perc GSH conjugation	**ClKidLivTCVGC**	**0.15**	**0.15**	**0.15**	(nmol/min/g kidney/mM)/ (nmol/min/g liver/mM)	**0.24**	**0.098**	**0.14**	(L/hr/kg kidney)/ (L/hr/kg liver) [c,e]

[a] mM liver = 165.83 mg/L liver = (165.83/PCliv) mg/L blood, where PCliv = 2.62 (mouse), 3.33 (rat), 4.16 (human).
[b] nmol/min/g liver/mM = 1e-6 L liver/min/g liver = 0.06 L liver/hr/kg liver = (0.06 × PCliv) L blood/hr/kg liver.
[c] Additional scaling by tissue volume(s) to derive whole organ Vmax, Km, or Vmax/Km parameter (see Table 1).
[d] (mM kidney/mM liver) = (PCliv/PCkid) ((mg/L blood kidney)/(mg/L blood liver)), where PCkid = 4.25 (mouse), 2.17 (rat), 3.99 (human).
[e] (nmol/min/g kidney/mM)/(nmol/min/g liver/mM) = (PCkid/PCliv) (L/hr/kg kidney)/(L/hr/kg liver).
[f] nmol/min/g liver = 1e-6 mmol/min/g liver = 0.06 mmol/hr/kg liver = 9.95 mg/hr/kg liver.
[g] (nmol/min/g kidney)/(nmol/min/g liver) = (PCkid/PCliv) (mg/hr/kg kidney)/(mg/hr/kg liver).

Detailed comparison of optimized predictions and data

Mouse

Time-course plots of the mouse PBPK model predictions as compared to calibration or evaluation data, using baseline and maximum likelihood estimate (MLE) parameters, are shown on the pages indicated in Table S-1. Data are denoted by symbols, connected by thin grey lines for clarity. Symbols for increasing dose groups are in the following order: circle, triangle, plus, X, diamond. For baseline plots, predictions are thick black lines. For MLE plots, the overall MLE predictions are thick black lines, with alternative MLE predictions as thick grey lines. For predictions, line types for increasing dose groups are in the following order: solid, dash, dot, dash-dot, long dash. A discussion of the mouse calibration and evaluation results follows.

For the calibration data in mice, the model has some difficulty simultaneously fitting closed chamber data (Gearhart et al., 1993, and Gargas, 1988, reported in Reitz et al., 1996 and Sweeney et al., 2009) and the C-14 mass balance data on total metabolism (Reitz et al., 1996). The maximum likelihood approach preferred the excellent fits to the closed chamber data (due to there being much more data), and so the mass balance data of Reitz et al. (1996) was more poorly fit as a consequence. Perc in blood and tissues are somewhat underpredicted (Gearhart et al., 1993; Philip et al., 2007). Further, the model can not simultaneously account for the proportional dose-response for TCA in liver and lack of dose-response for TCA in blood following single gavage perc exposure reported by Philip et al. (2007).

In terms of evaluation data, perc in blood and kidney from repeated gavage perc exposure (Philip et al., 2007) were well-predicted at the lower doses, but the model did not account for the greater than proportional increase in perc in liver at higher doses in that study. The amount of urinary excretion of TCA was predicted to within 2-fold (Buben and O'Flaherty, 1985; Ikeda and Ohtsuji, 1972), suggesting good mass balance. TCA in blood from Green et al. (2003) and at the lower two exposures in Philip et al. (2007) were fairly well predicted, but the model could not account for the lack of proportional increase between the middle and high dose in Philip et al. (2007). Similarly, for TCA in liver, the lack of dose-response reported in Philip et al. (2007) after repeated dosing (in contrast to the proportional increase reported in the same study after a

single dose) was not predicted. Finally, total metabolism reported by Schumann et al. (1980) was somewhat under-predicted following inhalation exposure but somewhat over-predicted following oral exposure, but with errors of less than 2-fold.

Table S-3. Mouse data and predictions (pages 1-7)

Reference	Strain	Sex	Exposures (dose range)	Measurements (time range)	Page number	
					Baseline	MLE
Calibration					***1***	***2-4***
Gearhart et al. (1993)	B6C3F1	M	Closed chamber (200-3500 ppm) Oil gavage (536-1072 mg/kg)	Chamber concentration (0-8 hr) Venous blood TCA blood (1-48 hr)	1	2
Odum et al. (1998)	B6C3F1	M+F	Inhalation (400 ppm)	TCA blood (1-54 hr)	1	2
Gargas et al., reported in Reitz et al. (1996)	B3C3F1	M	Closed chamber (1.5-400 ppm)	Chamber concentration (0-6 hr)	1	2
Reitz et al. (1996)	B6C3F1	M	Inhalation (11-1201 ppm)	Exhaled as perc (6-21 hr) Retained dose (6 hr) Fraction metabolized (54-71 hr)	1	2-3
Philip et al. (2007) (single dose)	Swiss-Webster	M	Aqueous gavage (150-1000 mg/kg/d)	Venous blood Tissues: Liver, kidney TCA blood TCA liver (0-24 hr)		3-4
Evaluation						***5-7***
Buben and O'Flaherty (1985)	Swiss-Cox	M	Oil gavage (20-2000 mg/kg/d)	TCA urine (n.s.)		5
Green et al. (2003c)	B6C3F1	M+F	Inhalation (10-200 ppm)	TCA blood (102 hr)		5
Ikeda and Ohtsuji (1972)	DD	M+F	Inhalation (200 ppm)	TCA urine		5
Philip et al. (2007) (repeated dose)	Swiss-Webster	M	Aqueous gavage (150-1000 mg/kg/d)	Venous blood Tissues: Liver, kidney TCA blood TCA liver (696-720 hr)		5-6
Schumann et al. (1980)	B6C3F1	M	Inhalation (10.6 ppm) Oil gavage (oral) (500 mg/kg)	Retained dose (6 hr) Fraction metabolized (78 hr)		6-7

Rat

Time-course plots of the rat PBPK model predictions as compared to calibration or evaluation data, using baseline and maximum likelihood estimate (MLE) parameters, are shown on the pages indicated in Table S-2. Data are denoted by symbols, connected by thin grey lines for clarity. Symbols for increasing dose groups are in the following order: circle, triangle, plus, X, diamond. For baseline plots, predictions are thick black lines. For MLE plots, the overall MLE predictions are thick black lines, with alternative MLE predictions as thick grey lines. For predictions, line types for increasing dose groups are in the following order: solid, dash, dot, dash-dot, long dash. A discussion of the rat calibration and evaluation results follows.

In the rat calibration data, perc in blood and tissues were generally well simulated, although inter- and intra-study variability is evident as some data were either over- or under-predicted (Boyes et al., 2009; Dallas et al. 1994a, 1994c; Pegg et al., 1979; Warren et al. 1996). Some of this variability may be due to strain differences, which were not separately evaluated here. Closed chamber and total metabolism measures were also well simulated, although there is some under-prediction of total metabolism, particularly at lower doses (Pegg et al., 1979; Reitz et al., 1996). TCA in blood is well predicted for Odum et al. (1988) but somewhat under-estimated for Volkel et al. (1998). TCA in urine from Volkel et al. (1998) is well predicted. With respect to the GSH conjugation urinary metabolite data from Volkel et al. (1998), the model can not simultaneously account for the nearly proportional change in DCA in urine from 10 ppm to 400 ppm perc exposures, and the non-proportional increase in NAcTCVC at 400 ppm. However, the effect of this discrepancy on the predicted overall flux of GSH conjugation is minimal, since the DCA excretion is about 10-fold higher than NAcTCVC excretion.

In terms of rat evaluation data, there is consistent under-prediction of perc in blood and exhaled air following inhalation and ia exposures reported by Dallas et al. (1994b, 1995), but over-prediction for oral exposures (Dallas et al., 1995). In addition, perc in blood and tissues are over-predicted as compared to data reported by Savolainen et al. (1977) following inhalation exposures. The amount of perc exhaled as reported by Franz and Watanabe (1983) is well predicted, as are the amounts of TCA in urine reported by Ikeda and Ohtsuji (1972) and Ikeda et al. (1972).

Table S-4. Rat data and predictions (pages 8-21)

Reference	Strain	Sex	Exposures (dose range)	Measurements (time range)	Page number(s)	
					Baseline	MLE
Calibration					***8-12***	***13-19***
Boyes et al. (2009)	Long-Evans	M	Inhalation (250-4000 ppm)	Arterial blood Tissues: brain (1-7 hr)	8	13
Dallas et al. (1994a, 1994c)	Sprague-Dawley	M	Intra-arterial (ia) (10 mg/kg) Inhalation (inh) (500 ppm) Aqueous gavage (aq gav) (10 mg/kg)	Arterial blood Tissues: Liver, kidney, brain, muscle, fat, lung, heart (0-72 hr)	8-10	13-16
Odum et al. (1998)	F344	M+F	Inhalation (400 ppm)	TCA blood (1-54 hr)	10	16
Pegg et al. (1979)	Sprague-Dawley	M	Oil gavage (1-500 mg/kg) Inhalation (9.12-573 ppm)	Venous blood (1-36 hr) Amount or fraction exhaled (72 hr) Retained dose, inhalation exposures only (6 hr)	10	16-17
Gargas et al., reported in Reitz et al. (1996)	Sprague-Dawley	M	Closed chamber (1-1020 ppm)	Chamber concentration (0-5 hr)	11	17
Reitz et al. (1996)	F344	M	Inhalation (11.9-1146 ppm)	Exhaled as perc (6-27 hr) Retained dose (6 hr) Fraction metabolized (54-72 hr)	11	17
Volkel et al. (1998)	Wistar	M+F	Inhalation (10-400 ppm)	TCA blood (6-30 hr) TCA urine (0-78 hr) NAc-TCVC urine (0-66 hr)	11-12	17-18
Warren et al. (1996)	Sprague-Dawley	M	Aqueous gavage (160-480 mg/kg)	Arterial blood (0-95 hr) Tissues: Liver, brain, muscle, fat (0-1.5 hr)		19
Evaluation						***20***
Dallas et al. (1994b)	Sprague-Dawley	M	Inhalation (50-500 ppm)	Arterial blood Exhaled breath (2-600 hr)		20
Dallas et al. (1995)	Sprague-Dawley	M	Intra-arterial (ia) (1-10 mg/kg) Aqueous gavage (po) (1-10 mg/kg)	Venous blood (0-30 hr)		20
Franz and Watanabe (1983)	Sprague-Dawley	M	Drinking water (8.09 mg/kg)	Amount exhaled (12-84 hr)		20
Ikeda and Ohtsuji (1972)	Wistar	M+F	Inhalation (200 ppm)	TCA urine (48 hr)		20
Ikeda et al. (1972)	Wistar	F	Inhalation (2-400 ppm)	TCA urine (48 hr)		21
Savolainen et al. (1977)	Sprague-Dawley	M	Inhalation (200 ppm)	Venous blood Tissues: Liver, brain, fat, lung (120-126 hr)		21

Human

Time-course plots of the human PBPK model predictions as compared to calibration or evaluation data, using baseline and maximum likelihood estimate (MLE) parameters, are shown on the pages indicated in Table S-3. Data are denoted by symbols, connected by thin grey lines for clarity. Symbols for increasing dose groups are in the following order: circle, triangle, plus, X, diamond. For baseline plots, predictions are thick black lines. For MLE plots, the overall MLE predictions are thick black lines, with alternative MLE predictions as thick grey lines. For predictions, line types for increasing dose groups are in the following order: solid, dash, dot, dash-dot, long dash. A discussion of the human calibration and evaluation results follows.

In the human calibration data, predictions for perc in alveolar air and blood were generally quite accurate, although some inter- and intra-individual variability is evident (Chiu et al., 2007; Monster et al., 1979). Alveolar breath concentrations for Fernandez et al. (1976) were over-predicted, though by less than 2-fold. TCA blood concentrations were also fairly consistent across studies and individuals, again with some inter-individual variability. Much more inter-individual or inter-study variability is evident for measurements of TCA and NAcTCVC in urine. For instance, for Chiu et al. (2007), predictions for urinary TCA were quite accurate for Individual F, but were an order of magnitude too high for Individual C. Variation in TCA urinary excretion among the subjects in Monster et al. (1979) and Volkel et al. (1998) was less, but still clearly visible. The model under-predicted TCA in urine reported by Fernandez et al. (1976), but by an amount smaller than the variability observed in the other studies. For urinary excretion of NAcTCVC reported by Volkel et al. (1998), the accuracy of the results was best at the lower two exposures. At the highest exposure, some subjects exhibited saturation of NAcTCVC excretion while others did not, whereas the model assumed a linear rate and thus fit the non-saturating individuals the best. Overall, inter-individual variability substantially contributes to the errors in model fitting – a demonstration of the difficulty in teasing apart uncertainty and variability in the absence of a hierarchical population model.

In terms of human evaluation data, there was generally quite good agreement with the alveolar breath concentrations reported by Chien (1997) following multiple controlled and environmental exposure experiments, though some intra-individual variation was evident. The

model generally over-predicted post-exposure alveolar breath concentrations reported by Fernandez et al. (1976) by a similar amount to that observed with respect to the calibration data. However, data during exposure and post-exposure data for a couple of the experiments were well predicted. Alveolar breath concentrations were generally well simulated in comparison to data reported by Hake and Stewart (1977), Stewart et al. (1961), and Stewart et al. (1970), although perc blood concentrations during exposure were over-predicted as compared to data from Stewart et al. (1961).

Table S-5. Human data and predictions (pages 22-52)

Reference	Individual data? (n)	Sex	Exposures (dose range)	Measurements (time range)	Page number(s)	
					Baseline	MLE
Calibration					***22-31***	***32-43***
Chiu et al. (2007)	Yes (6)	M	1 ppm	Alveolar breath Venous blood TCA blood TCA urine (0-166 hr)	22-25	32-35
Fernandez et al. (1976) (n=2, with TCA urine)	Some (7)	M+F	100-200 ppm	Alveolar breath (0-12 hr) TCA urine, for 2 individuals (0-72 hr)	25-26	35-36
Monster et al. (1979)	Yes (6)	M	72-144 ppm	Alveolar breath Venous blood TCA blood TCA urine (0-167 hr)	26-30	36-40
Volkel et al. (1998)	Yes (6)	M+F	10-40 ppm	TCA plasma (6-30 hr) TCA urine (0-78 hr) NAc-TCVC urine (0-35 hr)	30-31	40-43
Evaluation						***44-52***
Chien (1997)	Yes (1)	M	0.06-5 ppm	Alveolar breath (0-13 hr)		44-49
Fernandez et al. (1976) (other individuals)	Some (7)	M+F	100-200 ppm	Alveolar breath (0-12 hr)		49-50
Hake and Stewart (1977)	Some (1)	M	150 ppm	Alveolar breath (0-2.5 hr)		51
Stewart et al. (1961)	No	M	100-200 ppm	Alveolar breath Venous blood (0-150 hr)		51
Stewart et al. (1970)	No	M	100 ppm (single and repeated)	Alveolar breath (0-440 hr)		51-52

Table S-6. Predictions for Area Under the Curve of perc in blood (mg-hr/l/d per ppm in air or mg-hr/l/d per mg/kg/d oral intake) using posterior mode parameters.

Species Continuous exposure	Baseline	posterior mode	GSD of posterior modes across chains	Range of posterior modes across chains
Mouse				
0.01 ppm	1.2	2.13	1.03	2.11-2.42
0.1 ppm	1.2	2.13	1.03	2.12-2.42
1 ppm	1.26	2.18	1.02	2.16-2.44
10 ppm	1.73	2.43	1.01	2.39-2.53
100 ppm	2.8	2.64	1	2.64-2.68
1000 ppm	2.98	2.68	1	2.67-2.72
0.01 mg/kg/d	0.0217	0.104	1.06	0.0957-0.126
0.1 mg/kg/d	0.0218	0.104	1.06	0.0958-0.126
1 mg/kg/d	0.0221	0.105	1.06	0.0965-0.127
10 mg/kg/d	0.0265	0.112	1.05	0.103-0.129
100 mg/kg/d	0.168	0.152	1.03	0.138-0.152
1000 mg/kg/d	0.296	0.178	1.03	0.159-0.18
Rat				
0.01 ppm	1.03	2.25	1	2.25-2.27
0.1 ppm	1.03	2.25	1	2.25-2.27
1 ppm	1.04	2.25	1	2.25-2.27
10 ppm	1.11	2.25	1	2.25-2.27
100 ppm	2	2.29	1	2.28-2.32
1000 ppm	2.4	2.39	1.01	2.36-2.42
0.01 mg/kg/d	0.0737	0.852	1.02	0.807-0.86
0.1 mg/kg/d	0.0738	0.852	1.02	0.807-0.86
1 mg/kg/d	0.0744	0.852	1.02	0.807-0.86
10 mg/kg/d	0.0816	0.854	1.02	0.809-0.861
100 mg/kg/d	0.23	0.864	1.02	0.821-0.869
1000 mg/kg/d	0.543	0.912	1.02	0.869-0.919
Human				
0.01 ppm	2.35	2.03	1.05	2.01-2.36
0.1 ppm	2.35	2.03	1.05	2.01-2.36
1 ppm	2.35	2.03	1.05	2.01-2.36
10 ppm	2.35	2.03	1.05	2.01-2.36
100 ppm	2.35	2.03	1.05	2.01-2.36
1000 ppm	2.37	2.04	1.05	2.01-2.36
0.01 mg/kg/d	2.71	1.74	1.03	1.58-1.82
0.1 mg/kg/d	2.71	1.74	1.03	1.58-1.82
1 mg/kg/d	2.71	1.74	1.03	1.58-1.82
10 mg/kg/d	2.71	1.74	1.03	1.58-1.82
100 mg/kg/d	2.72	1.74	1.03	1.58-1.82
1000 mg/kg/d	2.75	1.74	1.03	1.58-1.83

Table S-7. Predictions for fraction of perc in oxidized by P450s (mg/kg/d oxidized per mg/kg/d intake) using posterior mode parameters.

Species Continuous exposure	Baseline	Post-calibration (posterior mode)	GSD of posterior modes across chains	Range of posterior modes across chains
Mouse				
0.01 ppm	0.00252	0.188	1.1	0.12-0.192
0.1 ppm	0.00254	0.187	1.09	0.12-0.191
1 ppm	0.00269	0.174	1.08	0.115-0.179
10 ppm	0.0062	0.118	1.06	0.0934-0.124
100 ppm	0.0141	0.0732	1.04	0.0632-0.075
1000 ppm	0.00716	0.0664	1.05	0.0574-0.0688
0.01 mg/kg/d	0.00367	0.561	1.08	0.395-0.574
0.1 mg/kg/d	0.00368	0.561	1.08	0.395-0.574
1 mg/kg/d	0.00374	0.557	1.07	0.394-0.57
10 mg/kg/d	0.00445	0.524	1.07	0.38-0.535
100 mg/kg/d	0.0253	0.35	1.04	0.308-0.367
1000 mg/kg/d	0.0361	0.239	1.03	0.216-0.25
Rat				
0.01 ppm	0.000501	0.0419	1.02	0.0387-0.042
0.1 ppm	0.000502	0.0419	1.02	0.0387-0.042
1 ppm	0.000514	0.0418	1.02	0.0386-0.0419
10 ppm	0.000662	0.0409	1.02	0.0379-0.0409
100 ppm	0.0025	0.0331	1.07	0.0263-0.0358
1000 ppm	0.00153	0.011	1.27	0.00587-0.0181
0.01 mg/kg/d	0.00143	0.106	1.02	0.0988-0.107
0.1 mg/kg/d	0.00144	0.106	1.02	0.0988-0.107
1 mg/kg/d	0.00145	0.106	1.02	0.0987-0.107
10 mg/kg/d	0.00158	0.105	1.02	0.0977-0.105
100 mg/kg/d	0.00431	0.0934	1.04	0.0817-0.096
1000 mg/kg/d	0.00686	0.0434	1.2	0.026-0.0631
Human				
0.01 ppm	0.00971	0.0098	1.12	0.00694-0.0104
0.1 ppm	0.00971	0.0098	1.12	0.00694-0.0104
1 ppm	0.00969	0.0098	1.12	0.00694-0.0104
10 ppm	0.00955	0.0098	1.12	0.00694-0.0104
100 ppm	0.00828	0.0098	1.12	0.00694-0.0104
1000 ppm	0.00355	0.0098	1.12	0.00693-0.0104
0.01 mg/kg/d	0.0173	0.0175	1.09	0.0134-0.0184
0.1 mg/kg/d	0.0173	0.0175	1.09	0.0134-0.0184
1 mg/kg/d	0.0173	0.0175	1.09	0.0134-0.0184
10 mg/kg/d	0.0169	0.0175	1.09	0.0134-0.0184
100 mg/kg/d	0.0138	0.0175	1.09	0.0134-0.0184
1000 mg/kg/d	0.00492	0.0175	1.09	0.0133-0.0184

Table S-8. Predictions for fraction of perc in conjugated with GSH (mg/kg/d conjugated per mg/kg/d intake) using posterior mode parameters.

Species Continuous exposure	Baseline	Post-calibration (posterior mode)	GSD of posterior modes across chains	Range of posterior modes across chains
Mouse				
0.01 ppm	0.348	0.000151	3.87	6.39e-05-0.00415
0.1 ppm	0.347	0.000152	3.87	6.43e-05-0.00417
1 ppm	0.337	0.000159	3.86	6.83e-05-0.0043
10 ppm	0.244	0.000207	3.81	8.95e-05-0.00523
100 ppm	0.0299	0.000251	3.79	0.000109-0.00642
1000 ppm	0.00301	0.000258	3.79	0.000111-0.00663
0.01 mg/kg/d	0.929	0.000481	3.89	0.000208-0.0134
0.1 mg/kg/d	0.929	0.000481	3.89	0.000208-0.0134
1 mg/kg/d	0.928	0.000485	3.89	0.00021-0.0135
10 mg/kg/d	0.914	0.000521	3.87	0.000229-0.0141
100 mg/kg/d	0.454	0.000706	3.82	0.00031-0.0181
1000 mg/kg/d	0.0485	0.000821	3.81	0.000362-0.0212
Rat				
0.01 ppm	0.303	0.00308	1.27	0.00195-0.00519
0.1 ppm	0.303	0.00308	1.27	0.00195-0.00519
1 ppm	0.301	0.00309	1.27	0.00195-0.0052
10 ppm	0.286	0.00309	1.27	0.00196-0.00521
100 ppm	0.0939	0.00316	1.27	0.002-0.00529
1000 ppm	0.0099	0.00335	1.27	0.00213-0.00559
0.01 mg/kg/d	0.874	0.00783	1.27	0.00498-0.0133
0.1 mg/kg/d	0.874	0.00783	1.27	0.00498-0.0133
1 mg/kg/d	0.873	0.00783	1.27	0.00498-0.0133
10 mg/kg/d	0.861	0.00785	1.27	0.00499-0.0133
100 mg/kg/d	0.608	0.00795	1.27	0.00506-0.0134
1000 mg/kg/d	0.078	0.00838	1.27	0.00535-0.0141
Human				
0.01 ppm	0.000544	0.0936	17.5	3.16e-05-0.1
0.1 ppm	0.000543	0.0936	17.5	3.16e-05-0.1
1 ppm	0.000543	0.0936	17.5	3.16e-05-0.1
10 ppm	0.000535	0.0936	17.5	3.16e-05-0.1
100 ppm	0.000468	0.0935	17.5	3.16e-05-0.1
1000 ppm	0.000207	0.0926	17.4	3.16e-05-0.0991
0.01 mg/kg/d	0.000972	0.177	17.1	6.47e-05-0.188
0.1 mg/kg/d	0.000972	0.177	17.1	6.47e-05-0.188
1 mg/kg/d	0.00097	0.177	17.1	6.47e-05-0.188
10 mg/kg/d	0.00095	0.177	17.1	6.47e-05-0.188
100 mg/kg/d	0.000788	0.177	17.1	6.47e-05-0.187
1000 mg/kg/d	0.000289	0.175	17	6.47e-05-0.185

Table S-9. Predictions for TCA produced systemically (mg/kg/d systemic TCA per ppm in air or mg/kg/d systemic TCA per mg/kg/d oral intake) using posterior mode parameters.

Species Continuous exposure	Baseline	Post-calibration (posterior mode)	GSD of posterior modes across chains	Range of posterior modes across chains
Mouse				
0.01 ppm	0.0361	3.74	1.08	2.63-3.94
0.1 ppm	0.0363	3.71	1.08	2.62-3.9
1 ppm	0.0384	3.45	1.07	2.53-3.59
10 ppm	0.0886	2.34	1.04	2.05-2.47
100 ppm	0.202	1.46	1.03	1.36-1.55
1000 ppm	0.103	1.32	1.04	1.18-1.43
0.01 mg/kg/d	0.00325	0.497	1.08	0.35-0.509
0.1 mg/kg/d	0.00326	0.496	1.08	0.35-0.508
1 mg/kg/d	0.00331	0.493	1.07	0.349-0.505
10 mg/kg/d	0.00394	0.464	1.07	0.337-0.473
100 mg/kg/d	0.0224	0.31	1.04	0.273-0.325
1000 mg/kg/d	0.032	0.212	1.03	0.191-0.222
Rat				
0.01 ppm	0.00352	0.182	1.02	0.173-0.189
0.1 ppm	0.00353	0.182	1.02	0.173-0.189
1 ppm	0.00361	0.181	1.02	0.173-0.189
10 ppm	0.00465	0.177	1.02	0.169-0.183
100 ppm	0.0176	0.144	1.07	0.117-0.158
1000 ppm	0.0108	0.0476	1.26	0.0261-0.0798
0.01 mg/kg/d	0.00127	0.0941	1.02	0.0875-0.0952
0.1 mg/kg/d	0.00127	0.0941	1.02	0.0875-0.0951
1 mg/kg/d	0.00128	0.094	1.02	0.0874-0.095
10 mg/kg/d	0.0014	0.0929	1.02	0.0866-0.0934
100 mg/kg/d	0.00382	0.0828	1.04	0.0724-0.0851
1000 mg/kg/d	0.00607	0.0385	1.2	0.023-0.0559
Human				
0.01 ppm	0.0106	0.0125	1.02	0.0117-0.0128
0.1 ppm	0.0106	0.0125	1.02	0.0117-0.0128
1 ppm	0.0106	0.0125	1.02	0.0117-0.0128
10 ppm	0.0104	0.0125	1.02	0.0117-0.0128
100 ppm	0.00906	0.0125	1.02	0.0117-0.0128
1000 ppm	0.00388	0.0125	1.02	0.0117-0.0128
0.01 mg/kg/d	0.0153	0.0145	1.09	0.0111-0.0152
0.1 mg/kg/d	0.0153	0.0145	1.09	0.0111-0.0152
1 mg/kg/d	0.0153	0.0145	1.09	0.0111-0.0152
10 mg/kg/d	0.015	0.0145	1.09	0.0111-0.0152
100 mg/kg/d	0.0123	0.0145	1.09	0.0111-0.0152
1000 mg/kg/d	0.00436	0.0145	1.09	0.011-0.0152

Table S-10. Mouse local parameter sensitivity analyses.

	AUCCBld (|SC|)		FracOx (|SC|)		FracGSH (|SC|)		TCASys (|SC|)		Calibration data (# of data points)			
Scaling parameter	**Inh**	**Oral**	**Inh**	**Oral**	**Inh**	**Oral**	**Inh**	**Oral**	**VL**	**L**	**M**	**H**
lnQCC	**0.18**	**0.74**	**0.72**	**0.49**	**0.58**	**0.74**	**0.28**	**0.49**	61	173	229	29
lnVPRC	**0.21**	**0.87**	**0.86**	**0.25**	**0.77**	**0.4**	**0.14**	**0.25**	121	260	94	17
QFatC	0	0	0	0	0	0	0	0	238	244	5	1
QGutC	0.03	**0.11**	**0.12**	**0.2**	**0.17**	**0.3**	**0.12**	**0.2**	340	136	12	0
QLivC	<0.01	0.02	0.02	0.03	0.02	0.04	0.02	0.03	482	6	0	0
QSlwC	0	0	0	0	0	0	0	0	452	35	0	0
QKidC	0	0	0	0	<0.01	<0.01	0	0	200	0	0	0
lnDRespC	0.03	**0.11**	0.02	0.03	0.03	0.05	0.02	0.03	467	25	0	0
FracPlasC	0	0	0	0	0	0	0	0	92	9	5	0
VFatC	<0.01	<0.01	<0.01	<0.01	<0.01	<0.01	<0.01	<0.01	270	199	12	4
VGutC	<0.01	0	0	0	0	0	0	0	474	12	0	0
VLivC	**0.18**	**0.39**	**0.72**	**0.74**	**0.51**	**0.43**	**0.72**	**0.74**	118	263	105	2
VRapC	<0.01	0	0	0	0	0	0	0	482	3	0	0
VRespLumC	0	0	0	0	0	0	0	0	201	0	0	0
VRespEffC	0	0	0	0	0	0	0	0	448	0	0	0
VKidC	<0.01	<0.01	<0.01	<0.01	0.09	0.04	<0.01	<0.01	476	3	0	0
VBldC	<0.01	0	0	0	0	0	0	0	488	0	0	0
PBC	**0.85**	**0.87**	**0.58**	**0.25**	**0.92**	**0.4**	**0.58**	**0.25**	39	337	114	2
PFatC	<0.01	<0.01	<0.01	<0.01	<0.01	<0.01	<0.01	<0.01	253	214	13	4
lnPGutC	<0.01	0	0	0	0	0	0	0	476	12	0	0
lnPLivC	<0.01	<0.01	<0.01	<0.01	<0.01	<0.01	<0.01	<0.01	457	9	3	19
lnPRapC	<0.01	0	0	0	0	0	0	0	485	3	0	0
lnPRespC	<0.01	<0.01	<0.01	<0.01	<0.01	<0.01	<0.01	<0.01	435	0	0	0
lnPKidC	<0.01	0	0	0	0	0	0	0	465	0	3	20
lnPSlwC	<0.01	<0.01	<0.01	0	<0.01	<0.01	<0.01	0	278	210	0	0
lnPRBCPlasTCAC	0	0	0	0	0	0	0	0	12	83	12	0
lnPBodTCAC	0	0	0	0	0	0	0	0	6	39	54	8
lnPLivTCAC	0	0	0	0	0	0	0	0	2	53	42	9
lnkDissocC	0	0	0	0	0	0	0	0	28	76	0	0
lnBMaxkDC	0	0	0	0	0	0	0	0	25	78	2	0
lnkTSD	0	0	0	0	0	0	0	0	2	26	7	1
lnkAS	0	0	0	0	0	0	0	0	36	0	0	0
lnkAD	0	0	0	0	0	0	0	0	6	30	0	0
lnkTSDAq	0	0	0	0	0	0	0	0	26	88	0	0
lnkASAq	0	0	0	0	0	0	0	0	16	60	38	0
lnkADAq	0	0	0	0	0	0	0	0	33	74	2	5
lnKMC	0.06	**0.13**	**0.27**	**0.26**	**0.15**	**0.13**	**0.27**	**0.26**	408	79	0	0
lnClC	**0.18**	**0.39**	**0.72**	**0.74**	**0.42**	**0.39**	**0.72**	**0.74**	94	237	156	0
lnCl2OxC	0.08	**0.21**	**0.31**	**0.39**	**0.19**	**0.21**	**0.31**	**0.39**	122	268	95	0
lnFracOtherC	0	0	0	0	0	0	**0.1**	**0.1**	84	22	0	0
lnKMKidLivC	<0.01	<0.01	<0.01	<0.01	<0.01	<0.01	<0.01	<0.01	397	0	0	0
lnClKidLivC	<0.01	<0.01	<0.01	<0.01	<0.01	<0.01	<0.01	<0.01	399	0	0	0
lnFracKidTCAC	0	0	0	0	0	0	<0.01	<0.01	90	0	0	0
lnKMRespLivC	<0.01	<0.01	<0.01	<0.01	<0.01	<0.01	<0.01	<0.01	342	0	0	0
lnVMaxLungLivC	<0.01	<0.01	0.04	0.02	<0.01	<0.01	0.04	0.02	468	11	0	0
lnClTCVGC	<0.01	<0.01	<0.01	<0.01	**1**	**1**	<0.01	<0.01	461	0	0	0
lnVMaxKidLivTCVGC	0	0	0	0	0	0	0	0	5	0	0	0
lnClKidLivTCVGC	<0.01	<0.01	<0.01	0	0.09	0.04	<0.01	0	335	0	0	0
lnkUrnTCAC	0	0	0	0	0	0	0	0	47	33	20	6
lnkMetTCAC	0	0	0	0	0	0	0	0	35	38	24	9
lnkTotTCAC	0	0	0	0	0	0	0	0	21	38	14	31

Column 1: scaling parameter; columns 2-9: absolute value of sensitivity coefficient for continuous exposures at 10 ppm in air or 100 mg/kg/d oral intake, with values ≥0.1 in **bold**; columns 10-13: number of calibration data points with absolute value of sensitivity coefficient that is very low (VL: 0<|SC|≤ 0.1), low (L: 0.1<|SC|≤0.5), medium (M: 0.5<|SC|≤ 1.0), and high (H: |SC|>1.0).

Table S-11. Rat local parameter sensitivity analyses.

	AUCCBld (|SC|)		FracOx (|SC|)		FracGSH (|SC|)		TCASys (|SC|)		Calibration data (# of data points)			
Scaling parameter	**Inh**	**Oral**	**Inh**	**Oral**	**Inh**	**Oral**	**Inh**	**Oral**	**VL**	**L**	**M**	**H**
lnQCC	0.08	**0.91**	**0.89**	**0.79**	**0.89**	**0.91**	**0.11**	**0.79**	43	210	300	112
lnVPRC	0.08	**0.93**	**0.92**	**0.59**	**0.91**	**0.69**	0.08	**0.59**	86	308	165	106
QFatC	0	0	0	0	0	0	0	0	149	421	85	9
QGutC	<0.01	0.02	0.02	**0.17**	0.02	**0.2**	0.02	**0.17**	610	35	10	10
QLivC	<0.01	<0.01	<0.01	0.02	<0.01	0.03	<0.01	0.02	640	6	0	0
QSlwC	0	0	0	0	0	0	0	0	584	56	6	2
QKidC	0	0	0	0	0	0	0	0	559	4	0	0
lnDRespC	0.01	**0.12**	0.01	0.08	0.01	0.09	0.01	0.08	514	149	1	0
FracPlasC	0	0	0	0	0	0	0	0	14	38	4	0
VFatC	<0.01	<0.01	<0.01	<0.01	<0.01	<0.01	<0.01	<0.01	245	254	122	42
VGutC	0	0	0	0	0	0	0	0	632	20	12	0
VLivC	0.08	0.09	**0.9**	**0.92**	**0.12**	**0.11**	**0.9**	**0.92**	419	184	62	0
VRapC	0	0	0	0	0	0	0	0	634	24	4	0
VRespLumC	0	0	0	0	0	0	0	0	443	0	0	0
VRespEffC	0	0	0	0	0	0	0	0	549	0	0	0
VKidC	<0.01	<0.01	<0.01	<0.01	0.02	0.01	<0.01	<0.01	642	0	0	0
VBldC	0	0	0	0	0	0	0	0	644	12	2	0
PBC	**0.92**	**0.93**	**0.89**	**0.59**	**0.92**	**0.69**	**0.89**	**0.59**	54	248	292	71
PFatC	<0.01	<0.01	<0.01	<0.01	<0.01	<0.01	<0.01	<0.01	259	258	93	47
lnPGutC	0	0	0	0	0	0	0	0	629	22	12	0
lnPLivC	<0.01	<0.01	<0.01	<0.01	<0.01	<0.01	<0.01	<0.01	582	22	29	29
lnPRapC	0	<0.01	0	0	0	<0.01	<0.01	0	546	36	31	49
lnPRespC	<0.01	<0.01	<0.01	<0.01	<0.01	<0.01	<0.01	<0.01	650	0	0	0
lnPKidC	0	0	0	0	0	0	0	0	625	0	1	25
lnPSlwC	0	<0.01	<0.01	<0.01	<0.01	<0.01	<0.01	<0.01	387	242	12	23
lnPRBCPlasTCAC	0	0	0	0	0	0	0	0	18	40	0	0
lnPBodTCAC	0	0	0	0	0	0	0	0	13	29	15	1
lnPLivTCAC	0	0	0	0	0	0	0	0	6	47	5	0
lnkDissocC	0	0	0	0	0	0	0	0	53	0	0	0
lnBMaxkDC	0	0	0	0	0	0	0	0	23	20	16	0
lnkTSD	0	0	0	0	0	0	0	0	7	4	1	0
lnkAS	0	0	0	0	0	0	0	0	10	0	0	0
lnkAD	0	0	0	0	0	0	0	0	3	5	4	0
lnkTSDAq	0	0	0	0	0	0	0	0	102	38	34	0
lnkASAq	0	0	0	0	0	0	0	0	102	38	34	0
lnkADAq	0	0	0	0	0	0	0	0	21	106	47	0
lnKMC	<0.01	0.01	0.03	**0.12**	<0.01	0.01	0.03	**0.12**	602	35	0	0
lnClC	0.08	0.09	**0.9**	**0.92**	**0.1**	0.09	**0.9**	**0.92**	473	134	58	0
lnFracOtherC	0	0	0	0	0	0	**0.1**	**0.1**	38	19	0	0
lnKMKidLivC	0	0	<0.01	<0.01	0	0	<0.01	<0.01	245	0	0	0
lnClKidLivC	<0.01	<0.01	<0.01	<0.01	<0.01	<0.01	<0.01	<0.01	576	0	0	0
lnFracKidTCAC	0	0	0	0	0	0	<0.01	<0.01	58	0	0	0
lnKMRespLivC	<0.01	<0.01	<0.01	<0.01	<0.01	<0.01	<0.01	<0.01	605	0	0	0
lnVMaxLungLivC	<0.01	<0.01	<0.01	<0.01	<0.01	<0.01	<0.01	<0.01	622	0	0	0
lnClTCVGC	<0.01	<0.01	<0.01	<0.01	**0.99**	**0.99**	<0.01	<0.01	621	2	35	0
lnVMaxKidLivTCVGC	0	0	0	0	0	0	0	0	1	0	0	0
lnClKidLivTCVGC	<0.01	<0.01	<0.01	<0.01	0.02	0.01	<0.01	<0.01	584	0	0	0
lnkUrnTCAC	0	0	0	0	0	0	0	0	5	29	17	5
lnkMetTCAC	0	0	0	0	0	0	0	0	13	40	6	0
lnFracNATUrnC	0	0	0	0	0	0	0	0	21	0	16	0
lnFracDCAUrnC	0	0	0	0	0	0	0	0	3	19	0	0
lnkDCAC	0	0	0	0	0	0	0	0	14	6	0	0

Column 1: scaling parameter; columns 2-9: absolute value of sensitivity coefficient for continuous exposures at 10 ppm in air or 100 mg/kg/d oral intake, with values ≥0.1 in **bold**; columns 10-13: number of calibration data points with absolute value of sensitivity coefficient that is very low (VL: 0<|SC|≤ 0.1), low (L: 0.1<|SC|≤0.5), medium (M: 0.5<|SC|≤ 1.0), and high (H: |SC|>1.0).

Table S-12. Human local parameter sensitivity analyses.

	AUCCBld (|SC|)		FracOx (|SC|)		FracGSH (|SC|)		TCASys (|SC|)		Calibration data (# of data points)			
Scaling parameter	**Inh**	**Oral**	**Inh**	**Oral**	**Inh**	**Oral**	**Inh**	**Oral**	**VL**	**L**	**M**	**H**
lnQCC	**0.14**	**0.8**	**0.81**	**0.8**	**0.8**	**0.8**	**0.19**	**0.8**	2	438	0	0
lnVPRC	**0.15**	**0.85**	**0.85**	**0.64**	**0.85**	**0.61**	**0.15**	**0.62**	307	1097	387	24
QFatC	0	0	0	0	0	0	0	0	176	1410	176	53
QGutC	<0.01	0.03	0.03	**0.12**	0.03	**0.15**	0.03	**0.14**	1787	28	0	0
QLivC	<0.01	0.01	<0.01	0.04	0.01	0.05	0.01	0.05	1802	10	0	0
QSlwC	0	0	0	0	0	0	0	0	1101	695	1	0
QKidC	0	<0.01	<0.01	<0.01	<0.01	<0.01	<0.01	<0.01	1778	0	0	0
lnDRespC	<0.01	<0.01	<0.01	<0.01	<0.01	<0.01	<0.01	<0.01	1812	0	0	0
FracPlasC	0	0	0	0	0	0	0	0	268	252	338	0
VFatC	<0.01	<0.01	<0.01	<0.01	<0.01	<0.01	<0.01	<0.01	329	111	0	0
VGutC	0	0	0	0	0	0	0	0	1789	11	0	0
VLivC	<0.01	0.01	**0.81**	**0.85**	0.04	0.03	**0.89**	**0.92**	1117	106	592	0
VRapC	0	0	<0.01	0	<0.01	0	0	0	1548	267	0	0
VRespLumC	0	0	0	0	0	0	0	0	1185	0	0	0
VRespEffC	0	0	0	0	0	0	0	0	1567	0	0	0
VKidC	<0.01	<0.01	**0.17**	**0.13**	0.02	0.01	0.09	0.07	1354	367	94	0
VBldC	0	<0.01	<0.01	0	<0.01	<0.01	<0.01	<0.01	1167	648	0	0
PBC	**0.85**	**0.85**	**0.85**	**0.64**	**0.85**	**0.61**	**0.85**	**0.62**	55	577	1109	74
PFatC	<0.01	<0.01	<0.01	<0.01	<0.01	<0.01	<0.01	<0.01	1278	407	126	4
lnPGutC	0	<0.01	<0.01	0	<0.01	<0.01	<0.01	0	1804	11	0	0
lnPLivC	0	0	0.01	<0.01	<0.01	0	0.01	<0.01	1798	17	0	0
lnPRapC	0	<0.01	<0.01	0	<0.01	<0.01	<0.01	<0.01	1611	201	0	0
lnPRespC	<0.01	<0.01	0.01	<0.01	<0.01	<0.01	0.01	<0.01	1766	0	0	0
lnPKidC	0	0	0	0	0	0	0	0	1809	0	0	0
lnPSlwC	<0.01	<0.01	<0.01	<0.01	<0.01	<0.01	<0.01	<0.01	696	1035	76	8
lnPRBCPlasTCAC	0	0	0	0	0	0	0	0	842	0	0	0
lnPBodTCAC	0	0	0	0	0	0	0	0	237	543	88	0
lnPLivTCAC	0	0	0	0	0	0	0	0	782	78	0	0
lnkDissocC	0	0	0	0	0	0	0	0	785	0	0	0
lnBMaxkDC	0	0	0	0	0	0	0	0	169	532	136	0
lnClC	0.01	0.02	**0.98**	**0.98**	0.02	0.02	**0.98**	**0.98**	1117	0	698	0
lnFracOtherC	0	0	0	0	0	0	**0.1**	**0.1**	208	601	0	0
lnKMKidLivC	0	0	0	0	0	0	0	0	204	0	0	0
lnClKidLivC	<0.01	<0.01	**0.17**	**0.13**	<0.01	<0.01	0.09	0.07	1354	364	97	0
lnFracKidTCAC	0	0	0	0	0	0	0.05	0.04	553	254	0	0
lnKMRespLivC	<0.01	<0.01	0.01	<0.01	<0.01	<0.01	0.01	<0.01	1797	0	0	0
lnVMaxLungLivC	<0.01	<0.01	0.01	<0.01	<0.01	<0.01	0.01	<0.01	1796	0	0	0
lnClTCVGC	**0.13**	**0.18**	**0.17**	**0.18**	**0.82**	**0.82**	**0.17**	**0.18**	615	1074	126	0
lnVMaxKidLivTCVGC	0	0	0	0	0	0	0	0	154	0	0	0
lnClKidLivTCVGC	<0.01	<0.01	<0.01	<0.01	0.02	0.02	<0.01	<0.01	1815	0	0	0
lnkUrnTCAC	0	0	0	0	0	0	0	0	266	152	429	4
lnkMetTCAC	0	0	0	0	0	0	0	0	761	77	0	0
lnFracNATUrnC	0	0	0	0	0	0	0	0	140	0	108	0
lnFracDCAUrnC	0	0	0	0	0	0	0	0	156	0	18	0
lnkNATC	0	0	0	0	0	0	0	0	197	36	18	0

Column 1: scaling parameter; columns 2-9: absolute value of sensitivity coefficient for continuous exposures at 0.01 ppm in air or 0.01 mg/kg/d oral intake, with values ≥0.1 in **bold**; columns 10-13: number of calibration data points with absolute value of sensitivity coefficient that is very low (VL: 0<|SC|≤ 0.1), low (L: 0.1<|SC|≤0.5), medium (M: 0.5<|SC|≤ 1.0), and high (H: |SC|>1.0).

References not cited in main manuscript text

Baarnhielm C, Dahlback H and Skanberg I. 1986. In-vivo pharmacokinetics offelodipine predicted from in-vitro studies in rat, dog and man. Acta Pharmacol. et toxicol. 59: 113-122.

Brown CD, Wong BA, Fennell TR. 1996. In vivo and in vitro kinetics of ethylene oxide metabolism in rats and mice. Toxicol Appl Pharmacol. 136(1):8-19.

Carlile DJ, Hakooz N, Bayliss MK, Houston JB. 1999. Microsomal prediction of in vivo clearance of CYP2C9 substrates in humans. Br J Clin Pharmacol. Jun;47(6):625-35.

Chiba M, Fujita S, Suzuki T. 1990. Pharmacokinetic correlation between in vitro hepatic microsomal enzyme kinetics and in vivo metabolism of imipramine and desipramine in rats. J Pharm Sci. 79(4):281-7.

Ekins S, Murray GI, Burke MD, Williams JA, Marchant NC, Hawksworth GM. 1995. Quantitative differences in phase I and II metabolism between rat precision-cut liver slices and isolated hepatocytes. Drug Metab Dispos. 23(11):1274-9.

Joly JG, Doyon C, Peasant Y. 1975 Cytochrome P-450 measurement in rat liver homogenate and microsomes. Its use for correction of microsomal losses incurred by differential centrifugation. Drug Metab Dispos. 3(6):577-86.

Kedderis GL, Batra R, Turner MJ Jr. 1995. Conjugation of acrylonitrile and 2-cyanoethylene oxide with hepatic glutathione. Toxicol Appl Pharmacol. 135(1):9-17.

Knaak JB, al-Bayati MA, Raabe OG, Blancato JN. 1993. Development of in vitro Vmax and Km values for the metabolism of isofenphos by P-450 liver enzymes in animals and human.Toxicol Appl Pharmacol. 120(1):106-13.

Pelkonen O, Kaltiala EH, Larmi TK, Kärki NT. 1973. Comparison of activities of drug-metabolizing enzymes in human fetal and adult livers. Clin Pharmacol Ther.14(5):840-6.

Prasanna HR, Hart RW, Magee PN. 1989. Effect of dehydroepiandrosterone (DHEA) on the metabolism of 7,12-dimethylbenz[a]anthracene (DMBA) in rats. Carcinogenesis. 10(5):953-5.

Selgen, PO. (1973) Preparation of rat liver cells. 3. Enzymatic requirements for tissue dispersion. Exp Cell Res. 82(2):391-8.

van Bree, L. Commandeur, J. Lamberts, B. Cornelissen, M. van Roon, M. Laterveer, H. de Vries, J., 1990. Induction of drug metabolism enzymes by dihalogenated biphenyls. J. Biochem. Toxicol. 5, 57−63.

Zahlten RN, Stratman FW. 1974. The isolation of hormone-sensitive rat hepatocytes by a modified enzymatic technique. Arch Biochem Biophys. 163(2):600-8.

Gearhart et al. (1993) [Mouse]

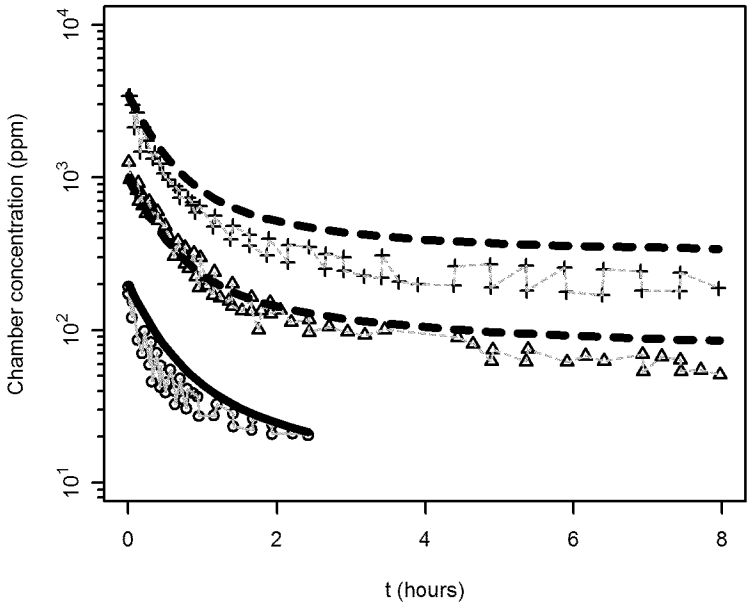

Reitz et al. (1996) [Mouse]

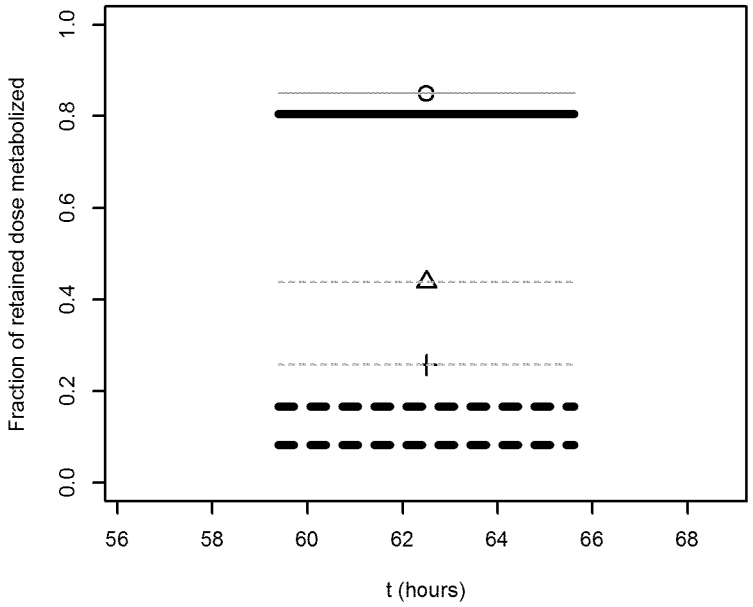

Odum et al. (1998) [Mouse]

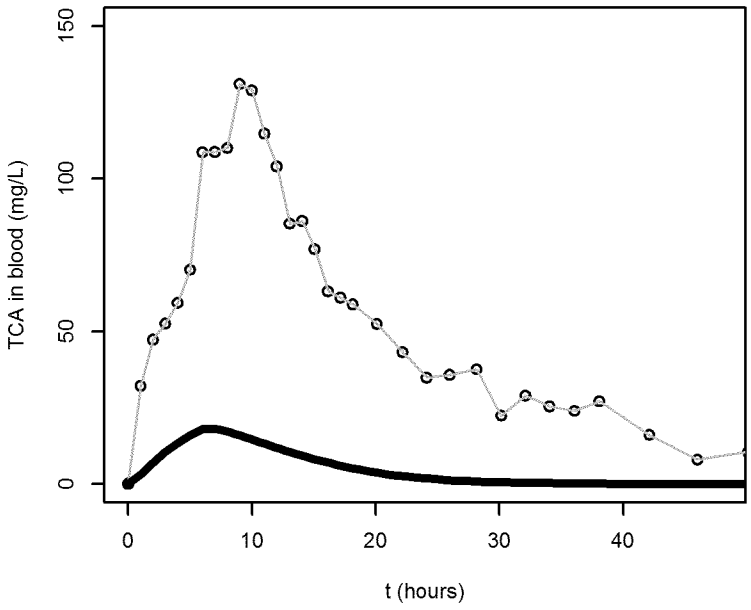

Reitz et al. (1996) [Mouse]

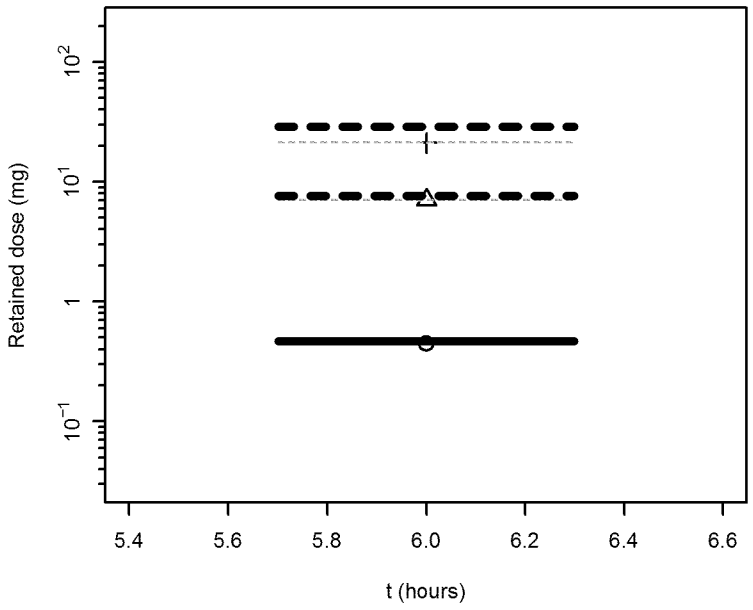

Gargas et al. (reported in Reitz et al., 1996) [Mouse]

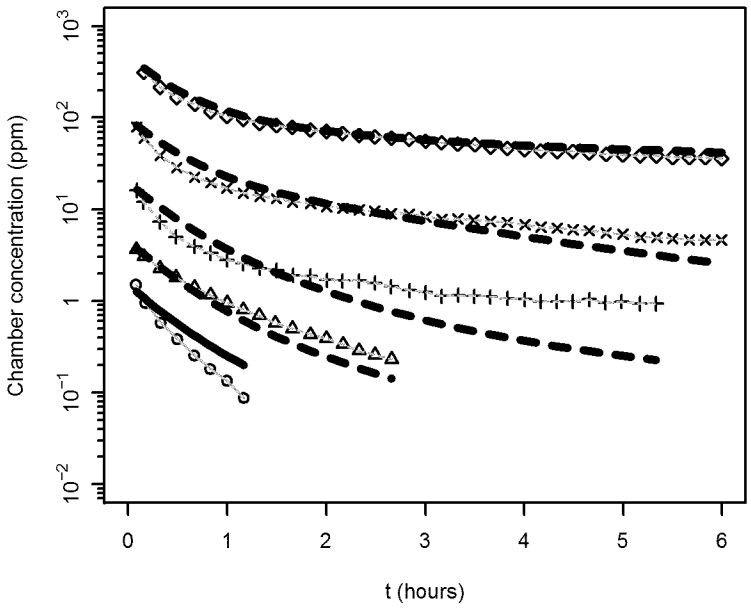

Reitz et al. (1996) [Mouse]

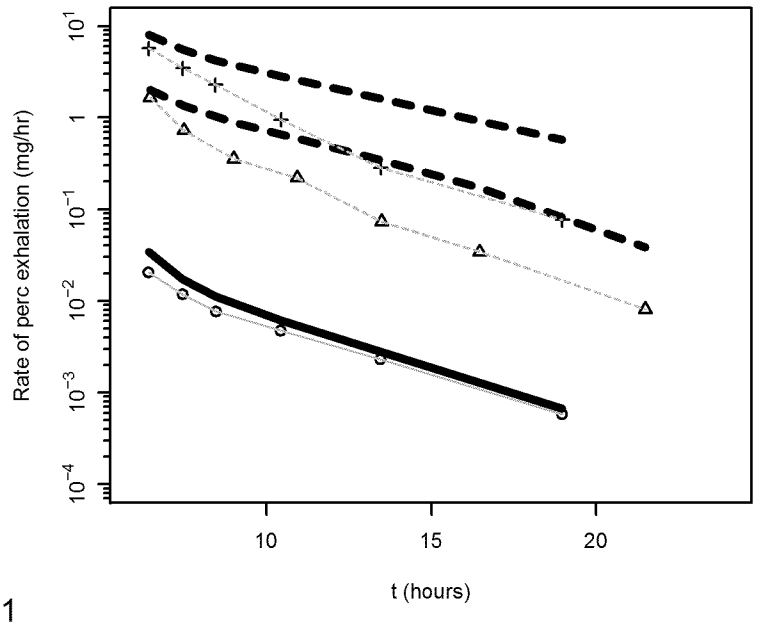

Gearhart et al. (1993) [Mouse]

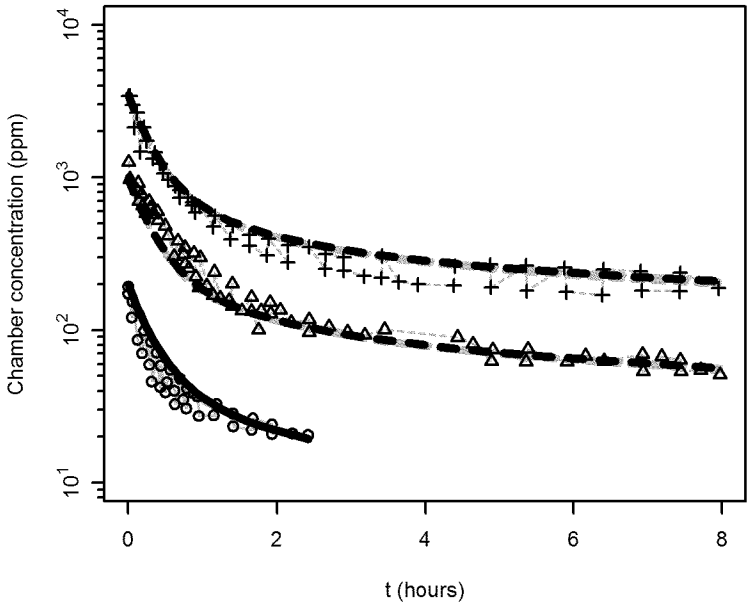

Odum et al. (1998) [Mouse]

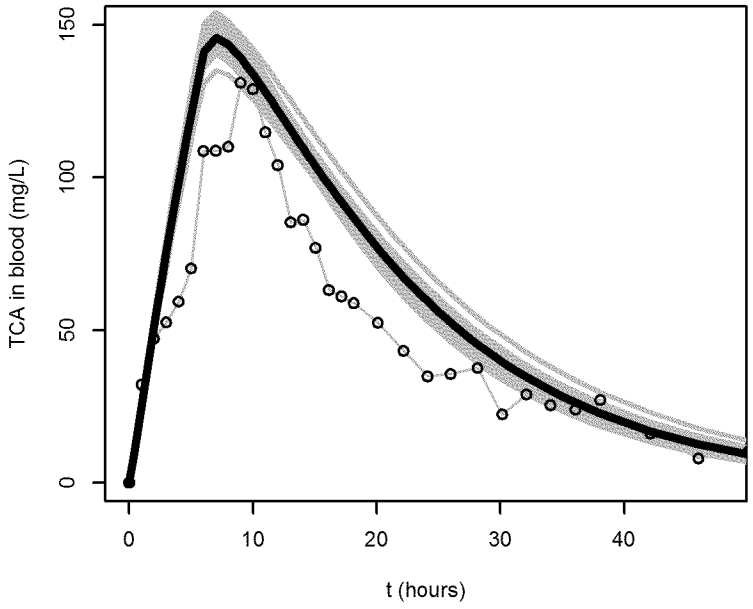

Gearhart et al. (1993) [Mouse]

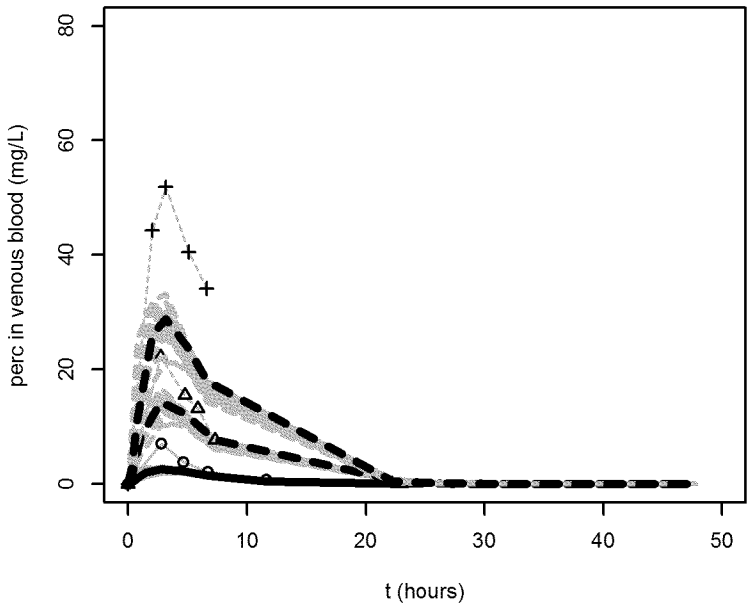

Gargas et al. (reported in Reitz et al., 1996) [Mouse]

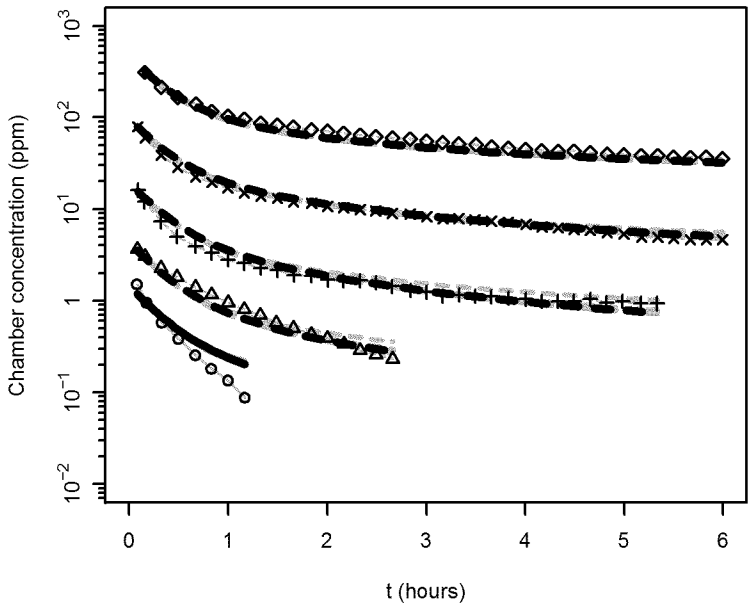

Gearhart et al. (1993) [Mouse]

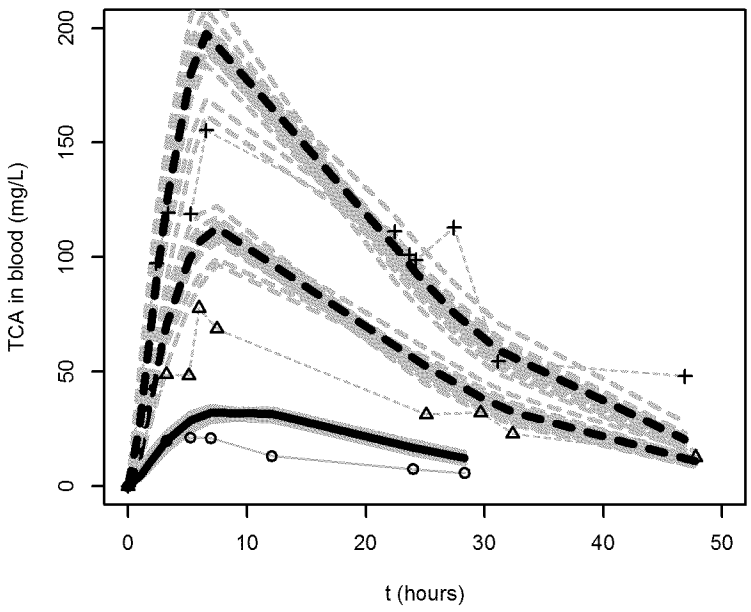

Reitz et al. (1996) [Mouse]

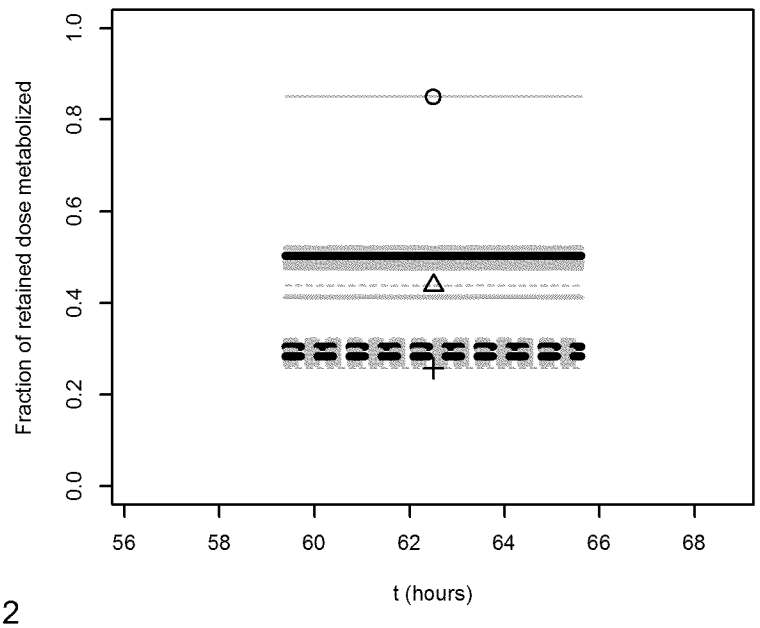

Reitz et al. (1996) [Mouse]

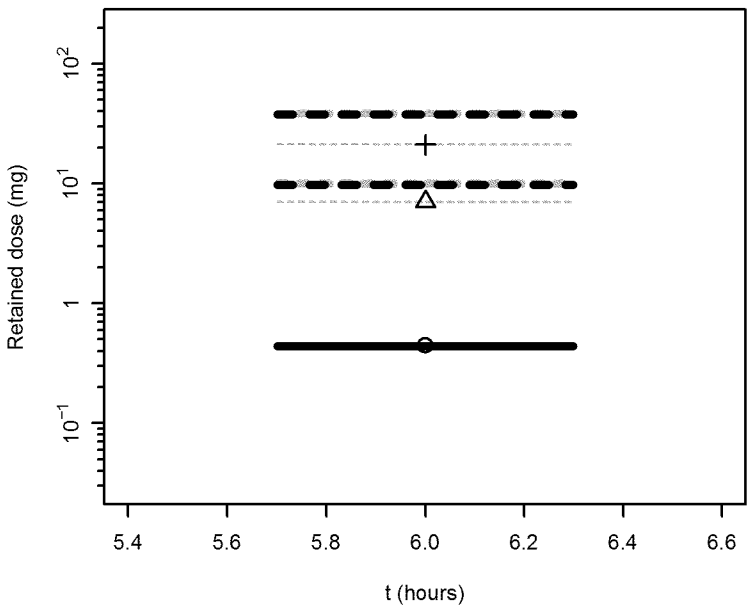

Philip et al. (2007) [Mouse]

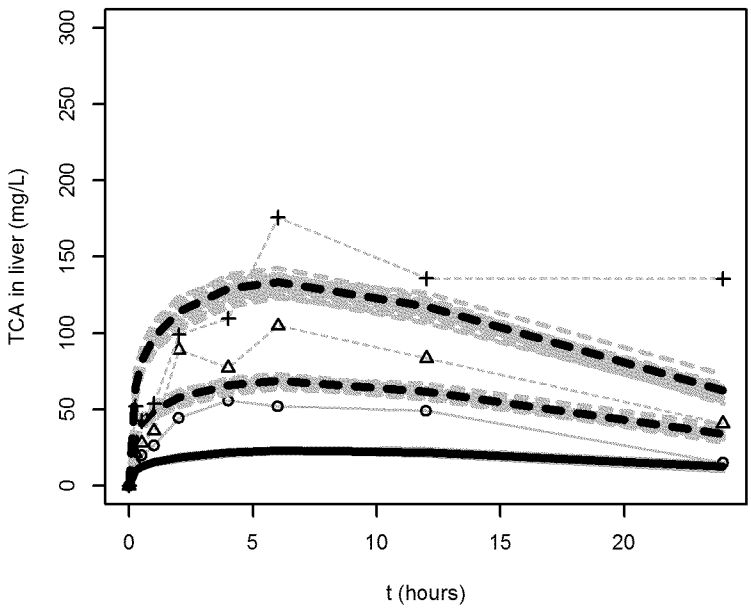

Reitz et al. (1996) [Mouse]

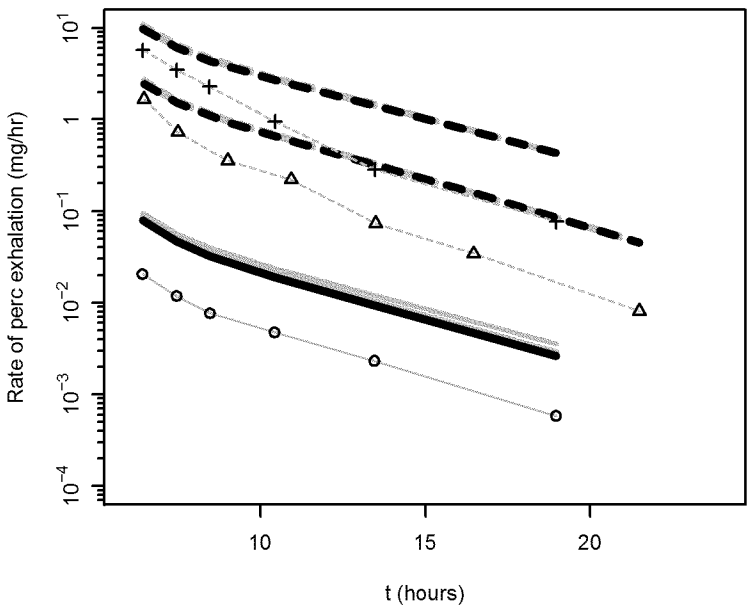

Philip et al. (2007) [Mouse]

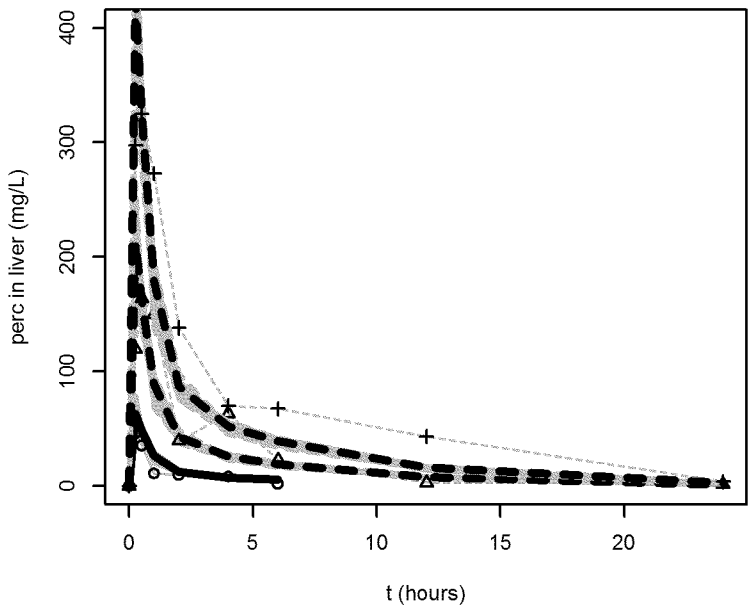

Philip et al. (2007) [Mouse]

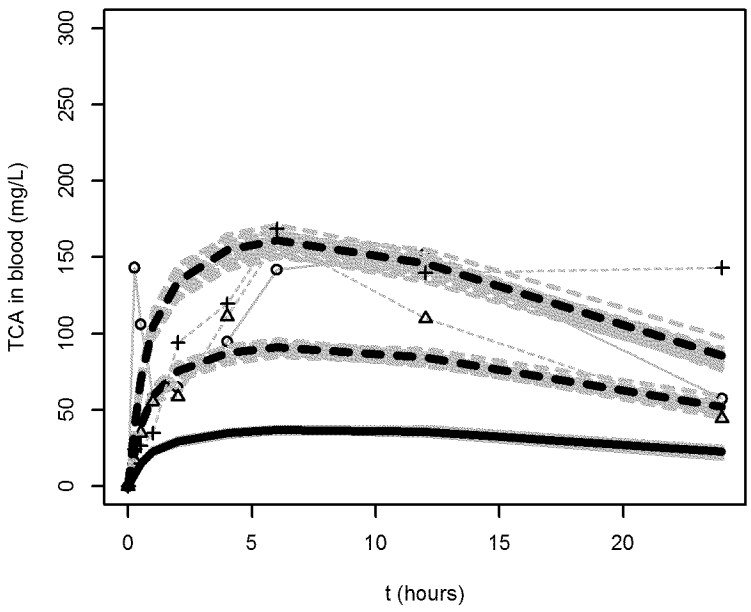

Philip et al. (2007) [Mouse]

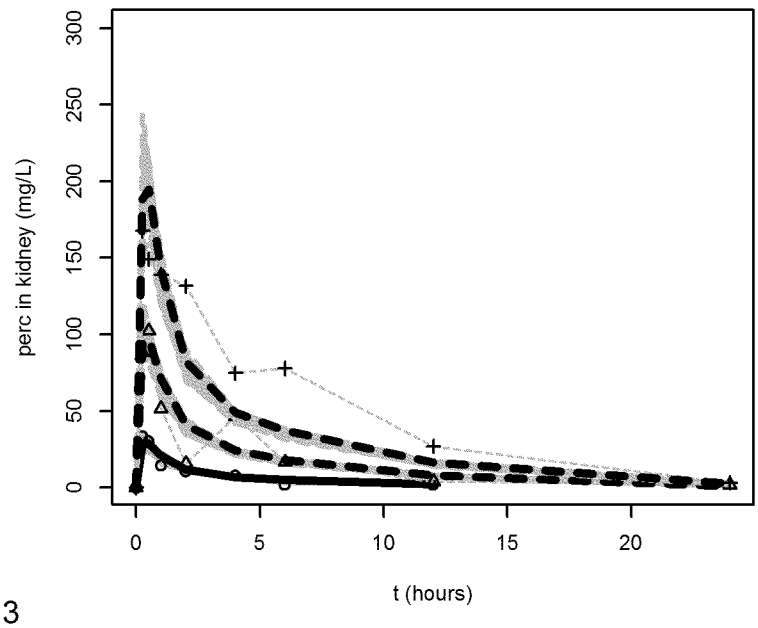

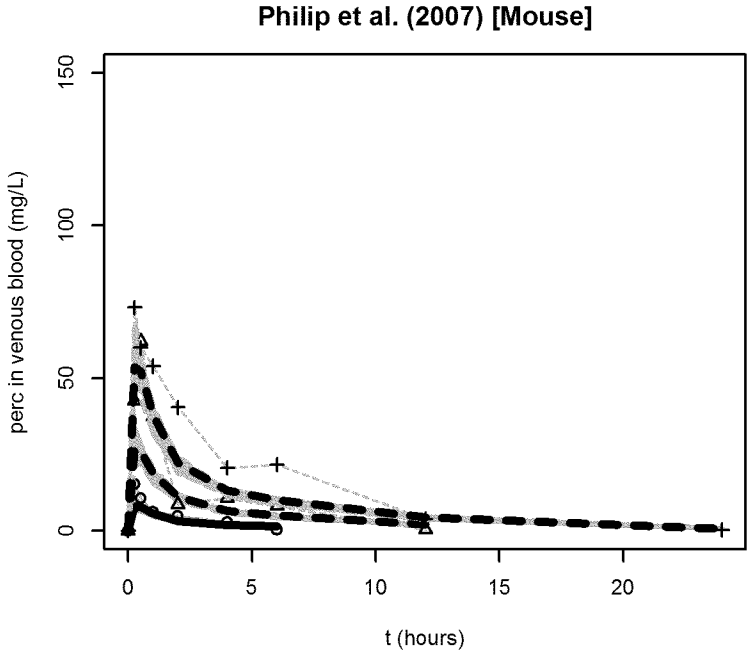
Philip et al. (2007) [Mouse]
perc in venous blood (mg/L)
0
50
100
150
0
5
10
15
20
t (hours)

Buben and O'Flaherty (1985) [Mouse]

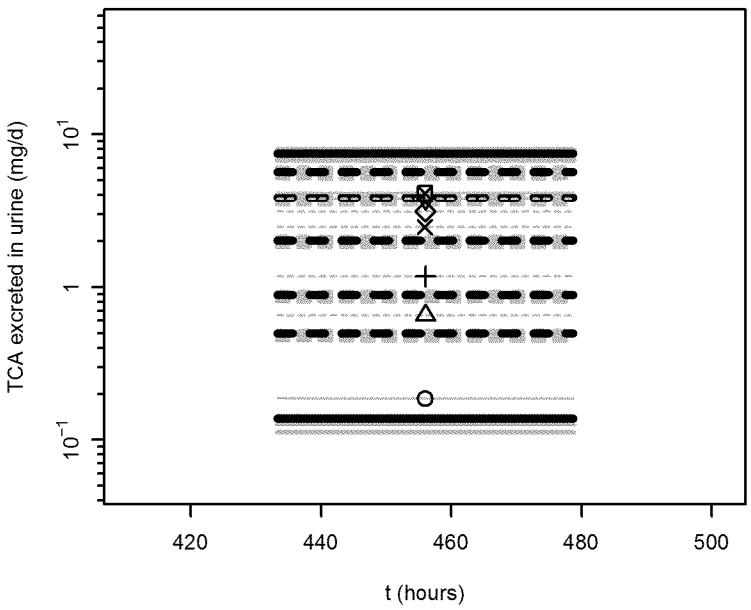

Ikeda and Ohtsuji (1972) [Mouse]

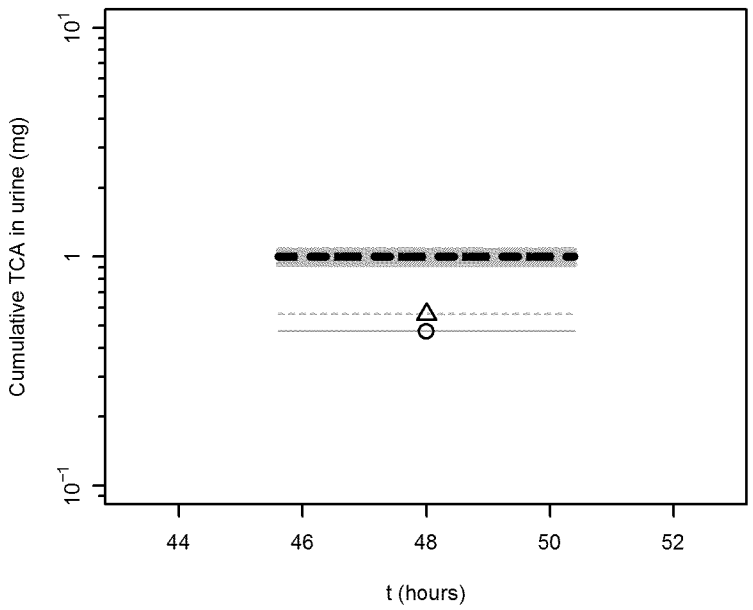

Green (2003c) males [Mouse]

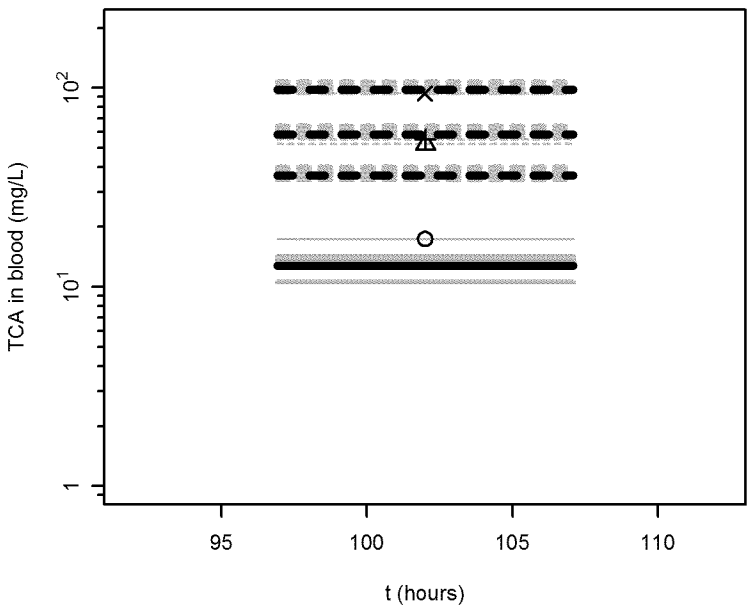

Philip et al. (2007) [Mouse]

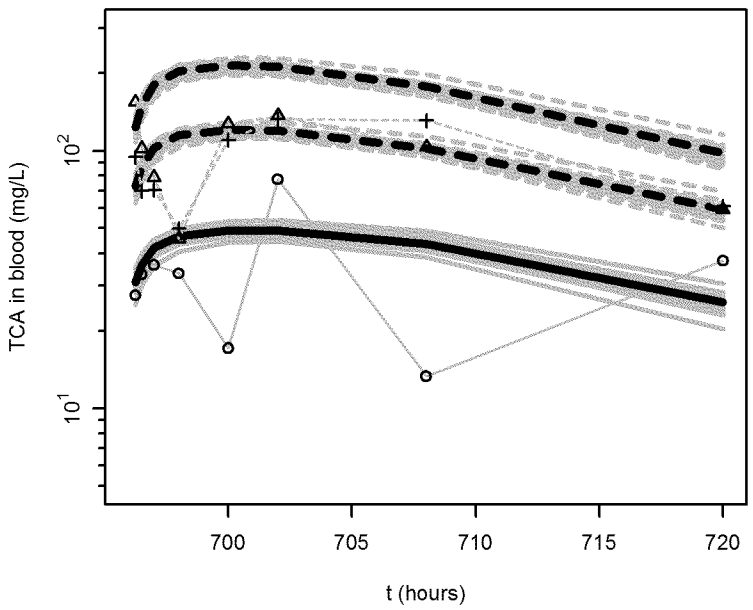

Green (2003c) females [Mouse]

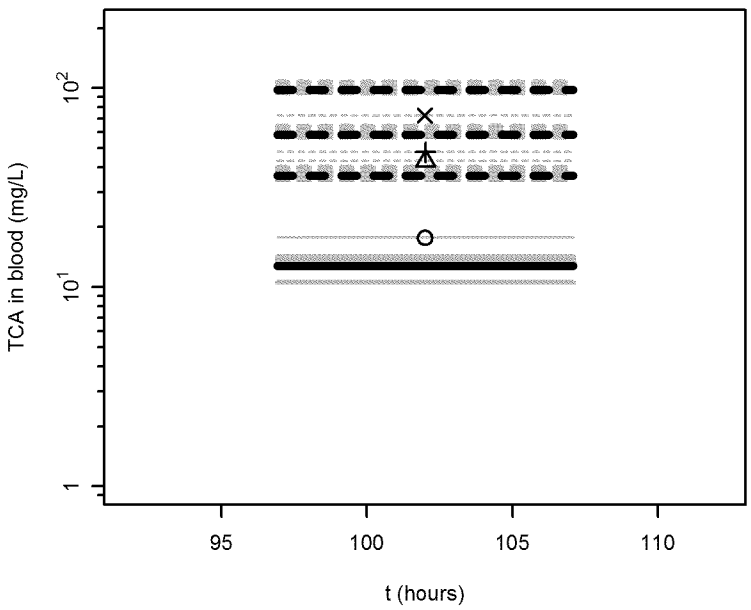

Philip et al. (2007) [Mouse]

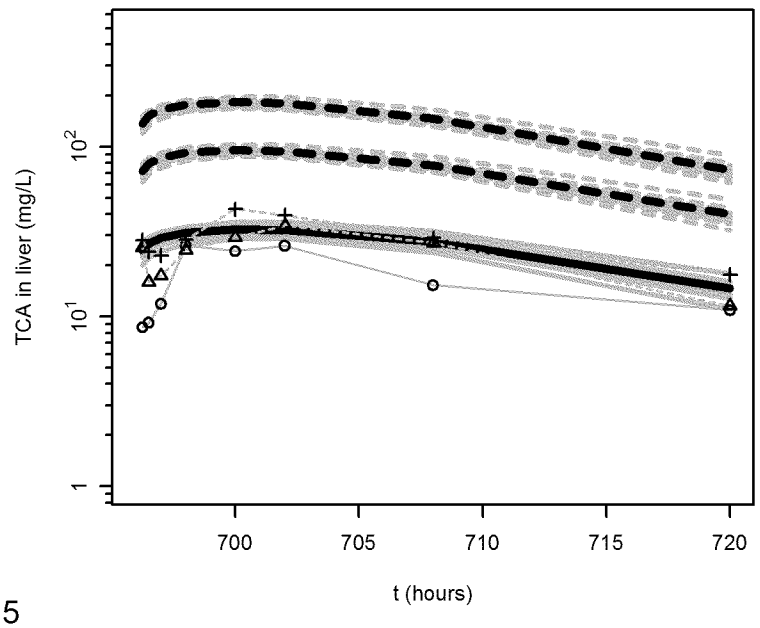

Philip et al. (2007) [Mouse]

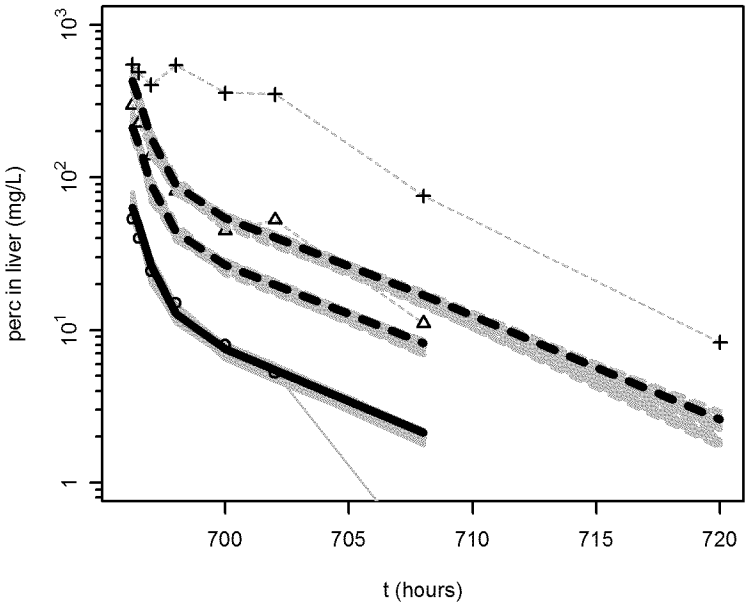

Schumann et al. (1980) inhalation [Mouse]

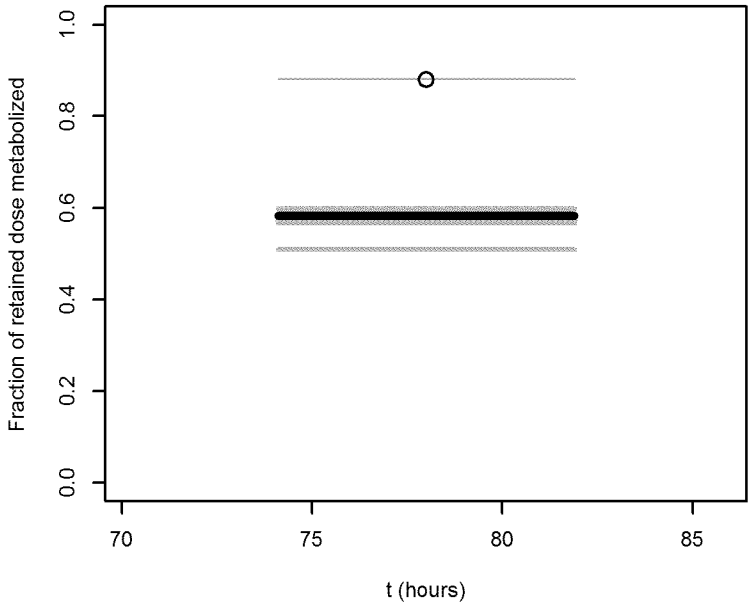

Philip et al. (2007) [Mouse]

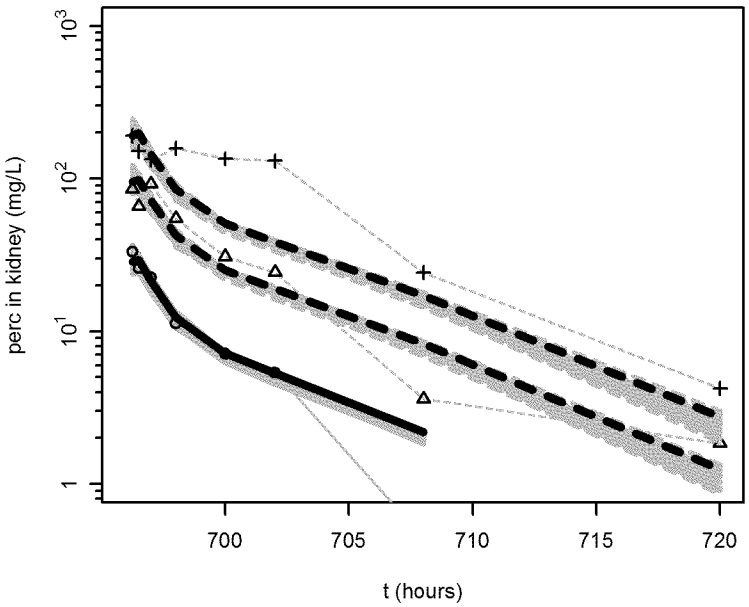

Schumann et al. (1980) inhalation [Mouse]

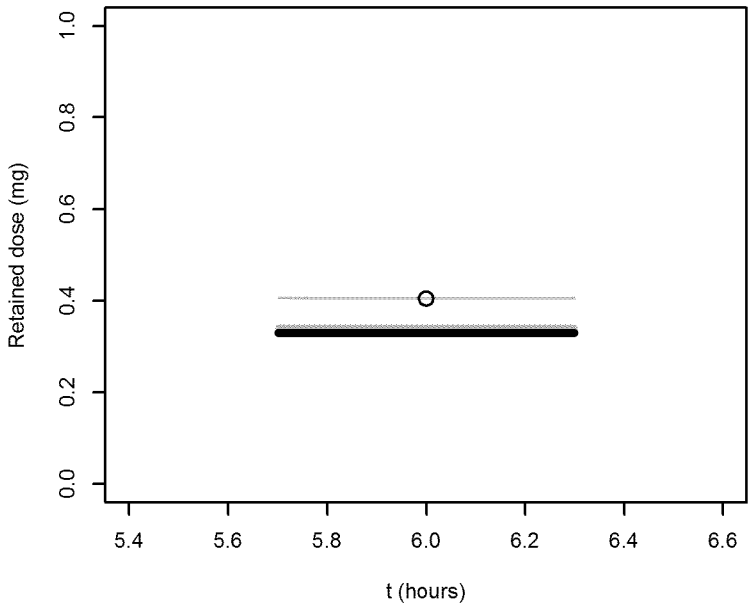

Philip et al. (2007) [Mouse]

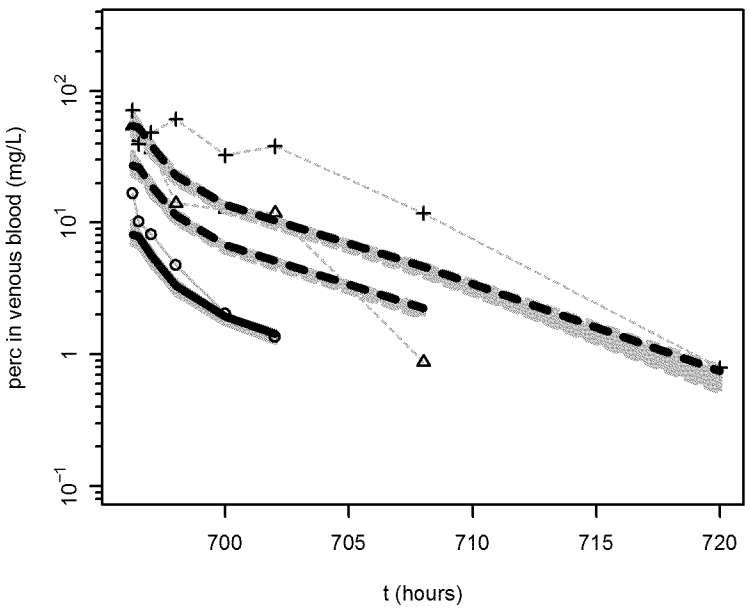

Schumann et al. (1980) oral [Mouse]

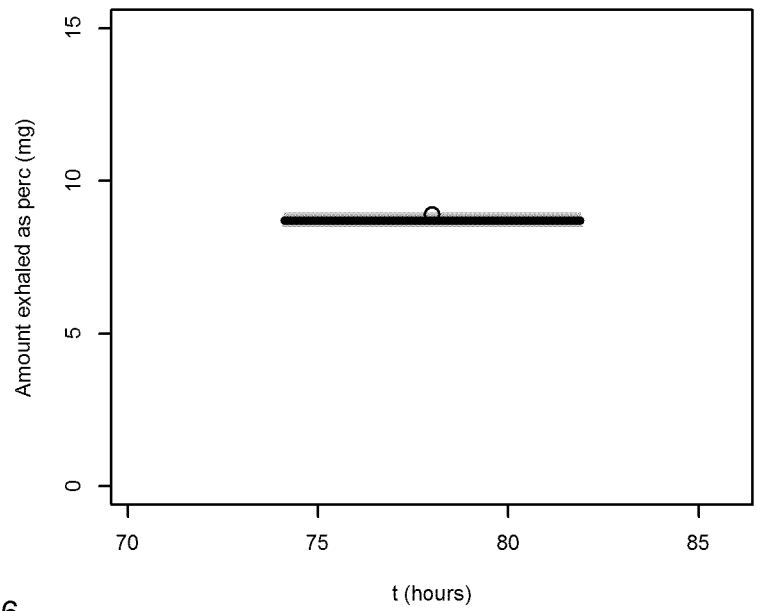

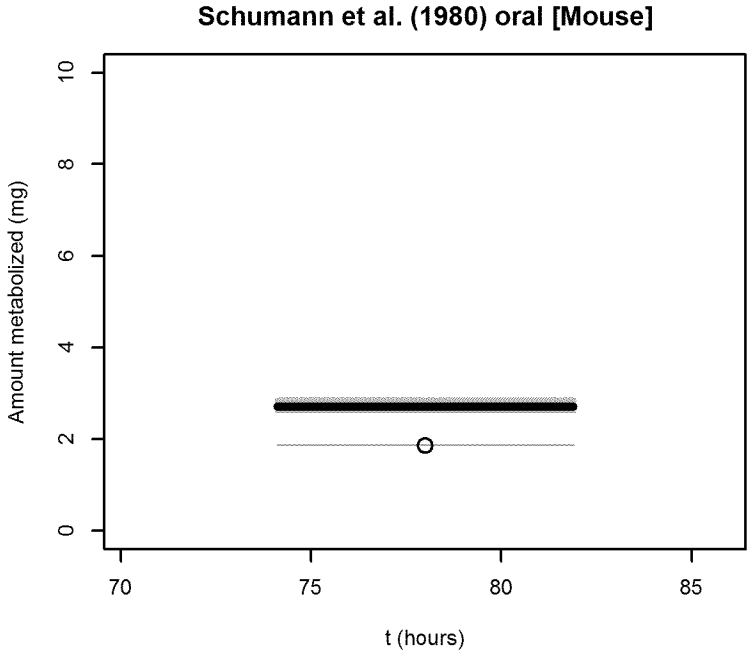
Schumann et al. (1980) oral [Mouse]
Amount metabolized (mg)
0
2
4
6
8
10
70
75
80
85
t (hours)

Boyes et al. (2009) [Rat]

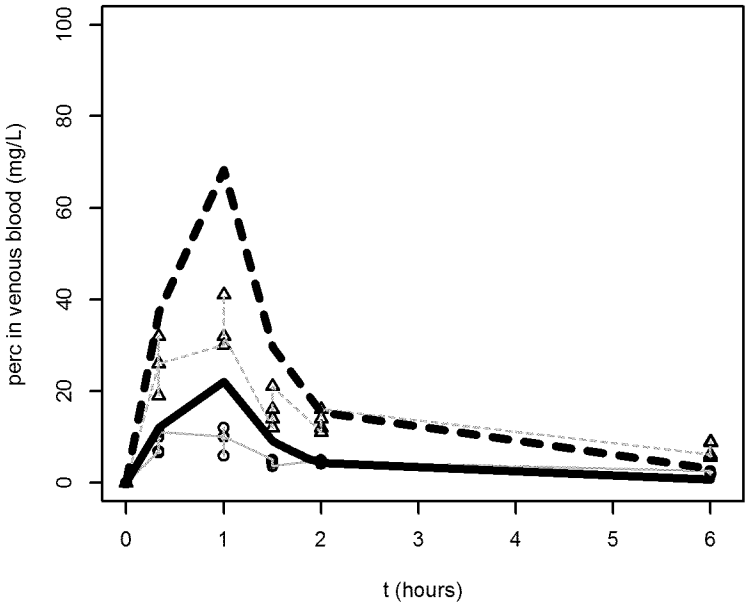

Dallas et al. (1994a) inh [Rat]

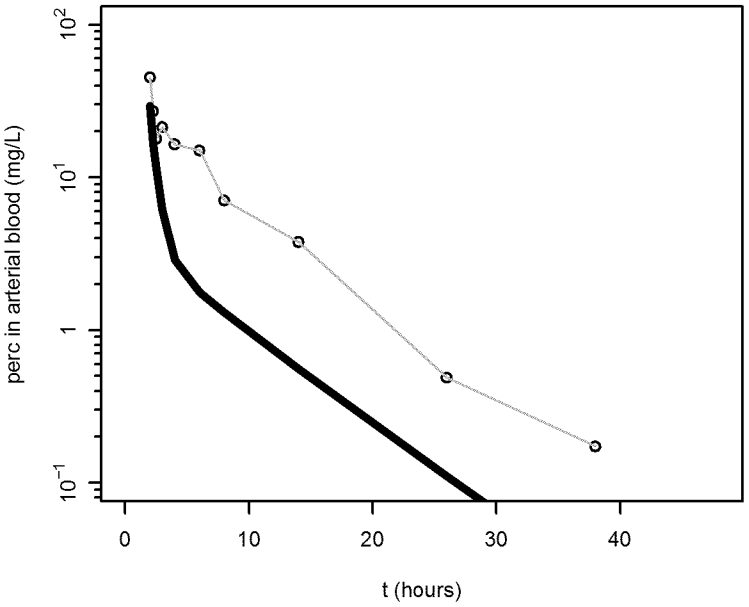

Boyes et al. (2009) [Rat]

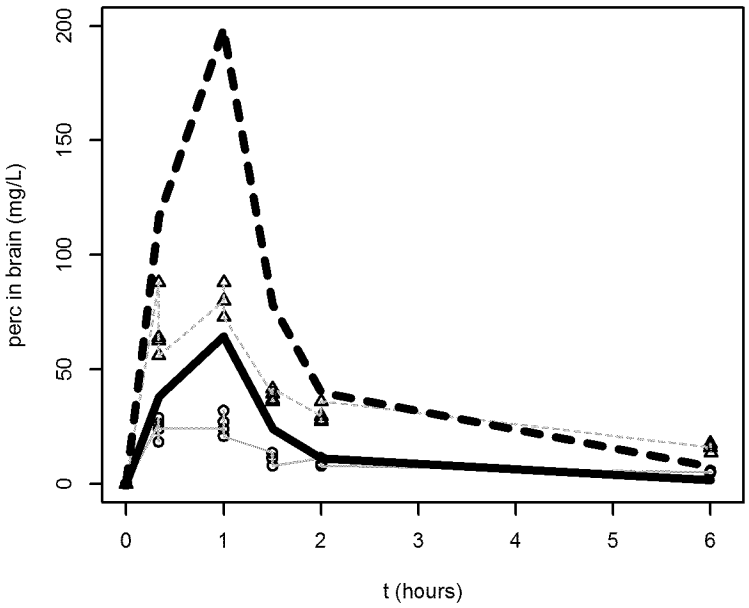

Dallas et al. (1994a) ia [Rat]

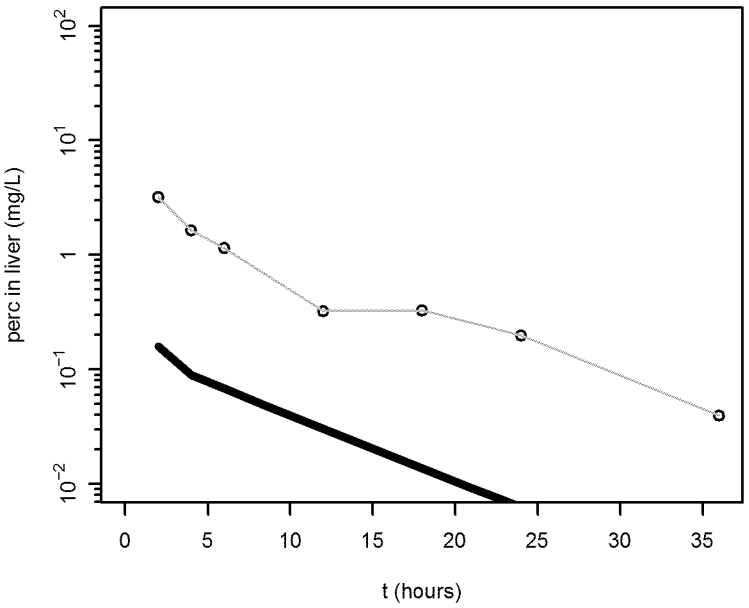

Dallas et al. (1994a) ia [Rat]

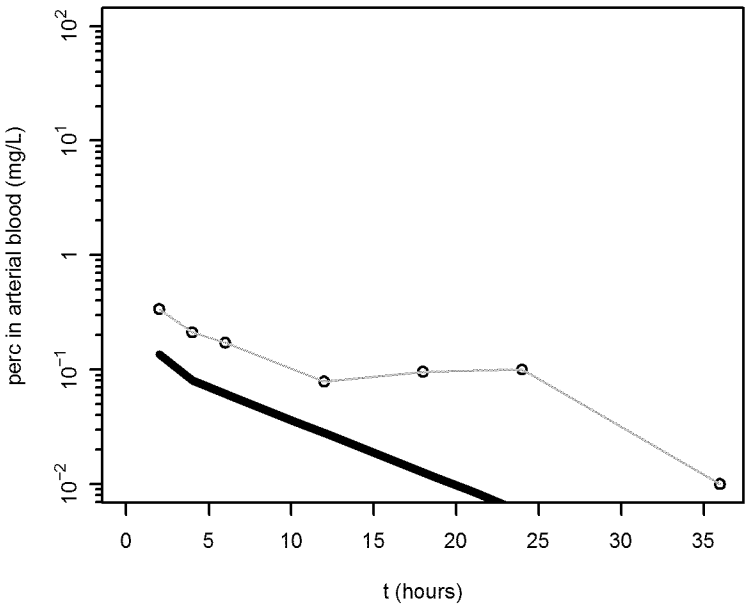

Dallas et al. (1994a) inh [Rat]

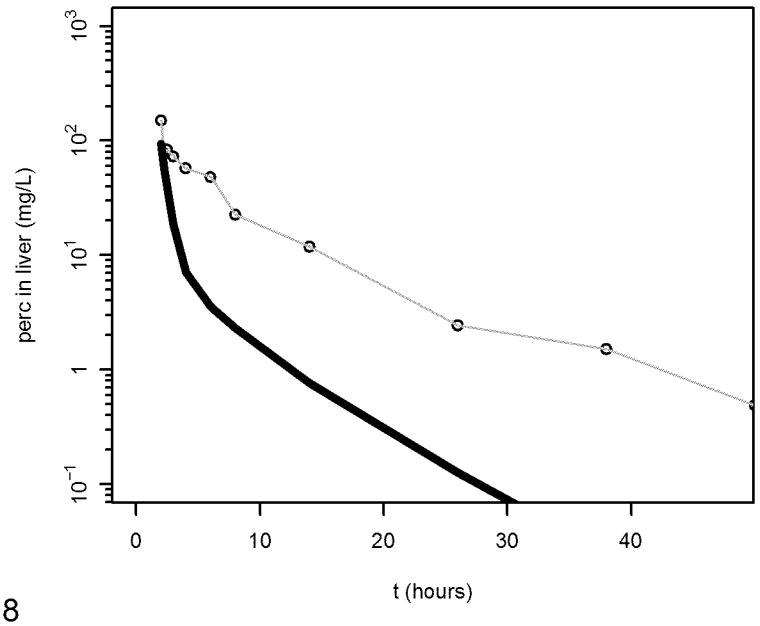

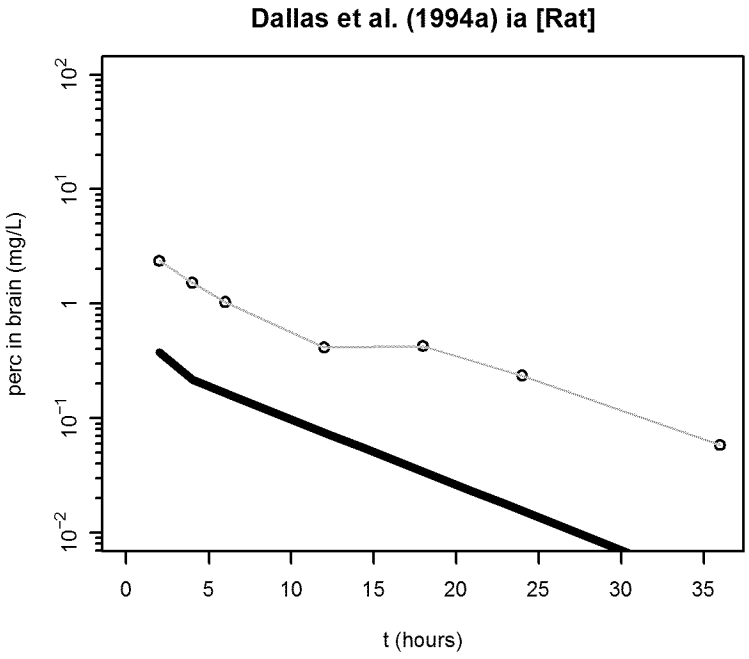
Dallas et al. (1994a) ia [Rat]
perc in brain (mg/L)
t (hours)

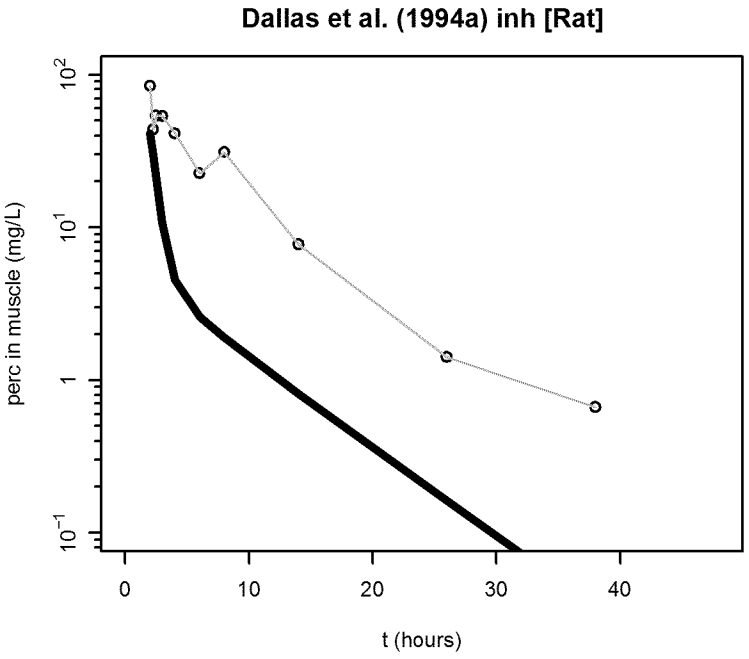
Dallas et al. (1994a) inh [Rat]
perc in muscle (mg/L)
t (hours)

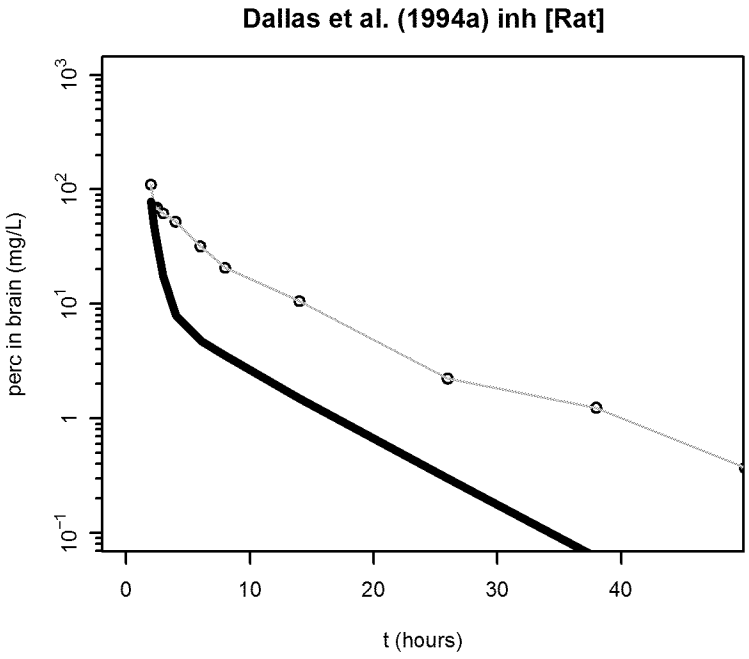
Dallas et al. (1994a) inh [Rat]
perc in brain (mg/L)
t (hours)

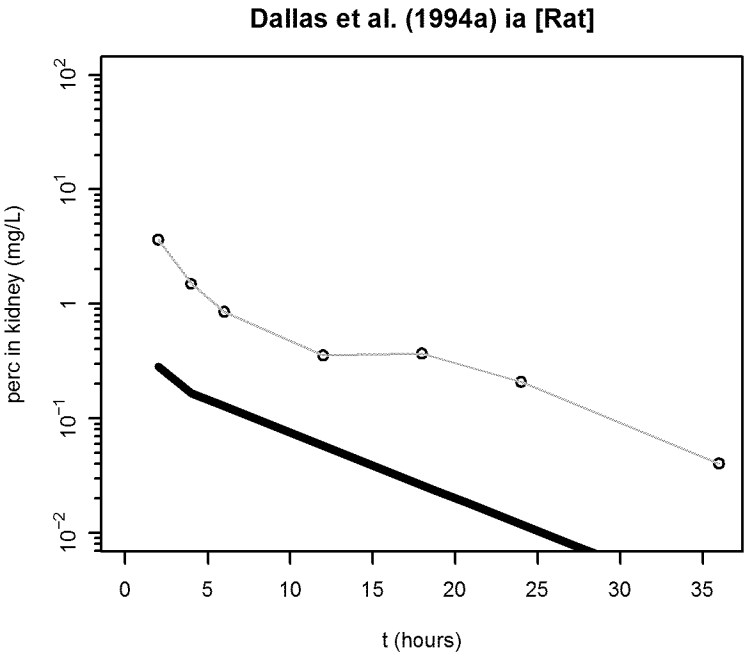
Dallas et al. (1994a) ia [Rat]
perc in kidney (mg/L)
t (hours)

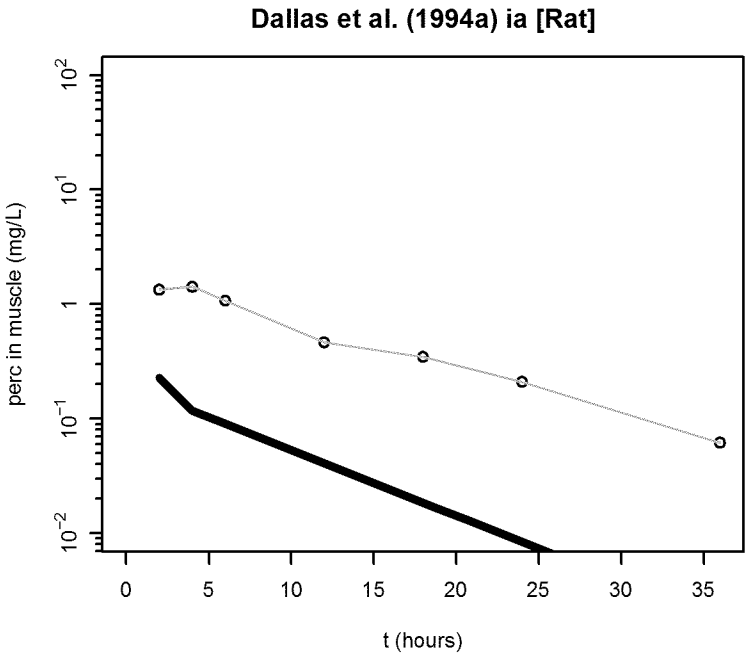
Dallas et al. (1994a) ia [Rat]
perc in muscle (mg/L)
t (hours)

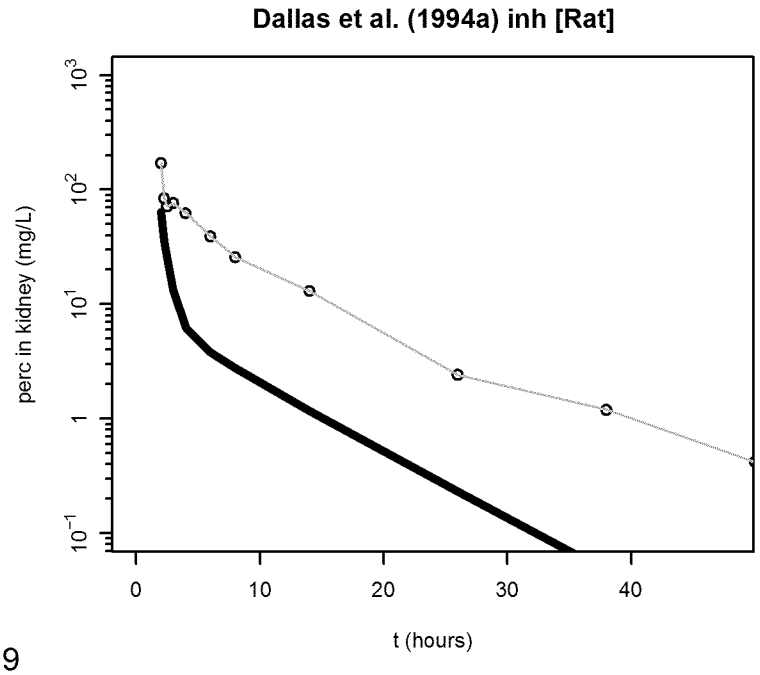
Dallas et al. (1994a) inh [Rat]
perc in kidney (mg/L)
t (hours)

Dallas et al. (1994a) ia [Rat]

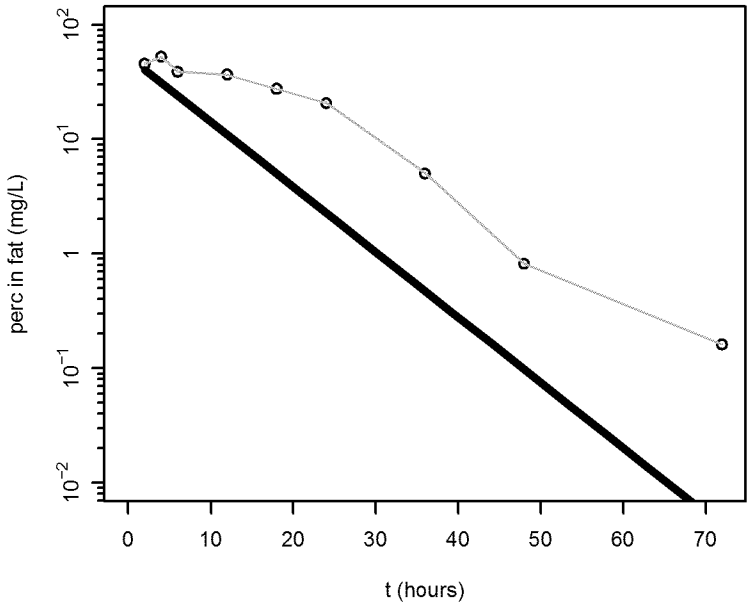

Pegg et al. (1979) [Rat]

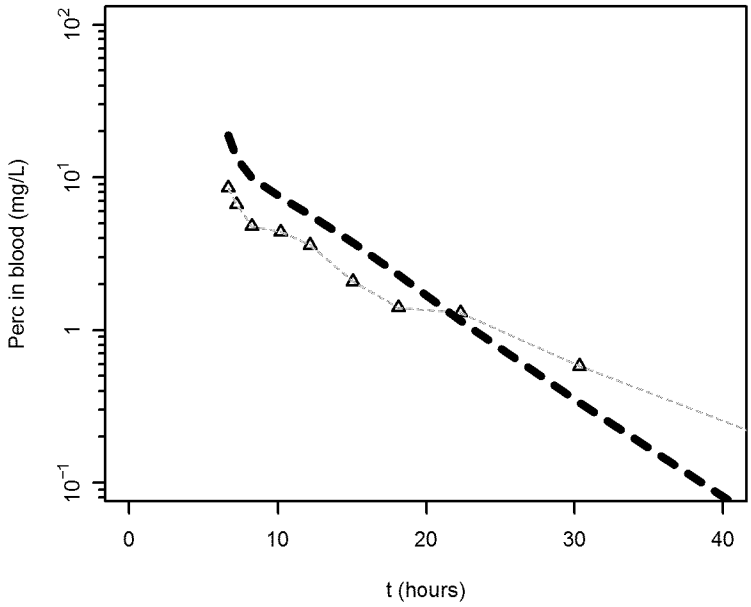

Dallas et al. (1994a) inh [Rat]

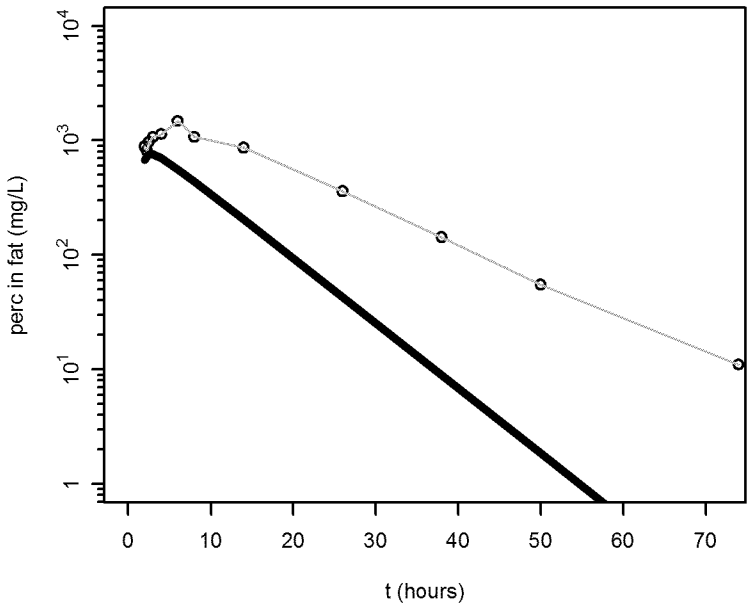

Pegg et al. (1979) [Rat]

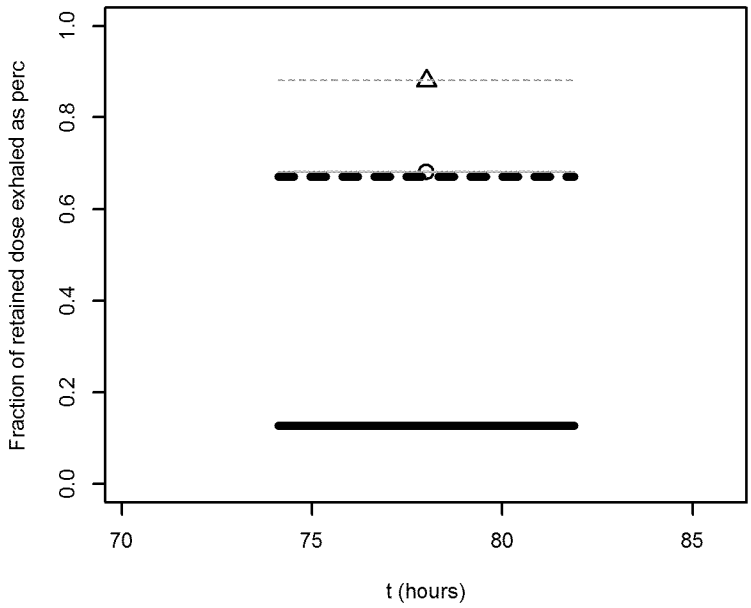

Odum et al. (1998) [Rat]

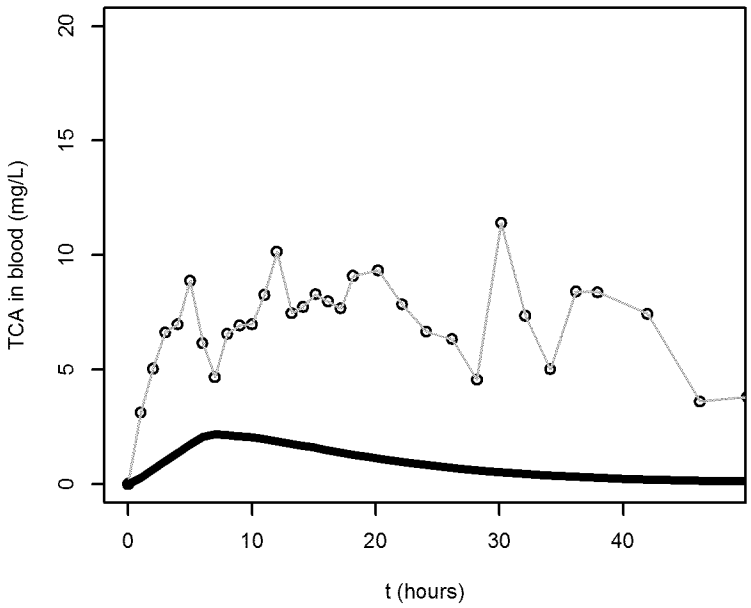

Pegg et al. (1979) [Rat]

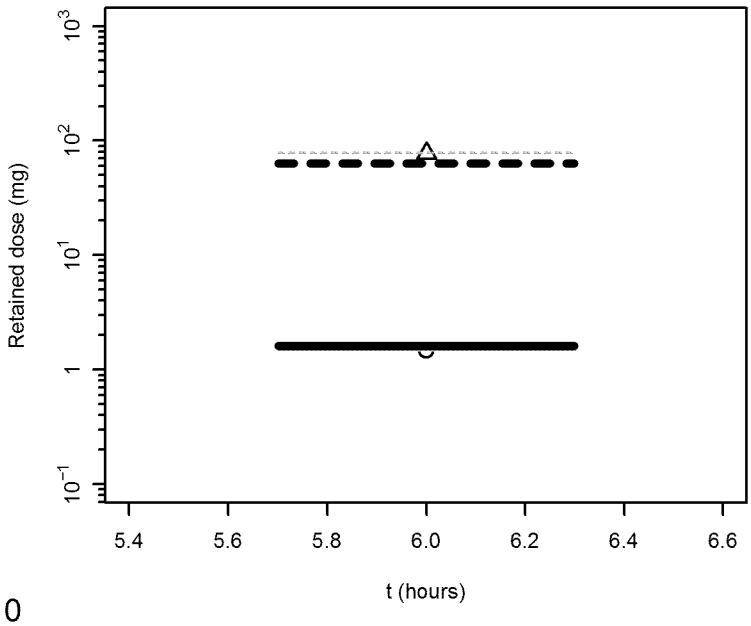

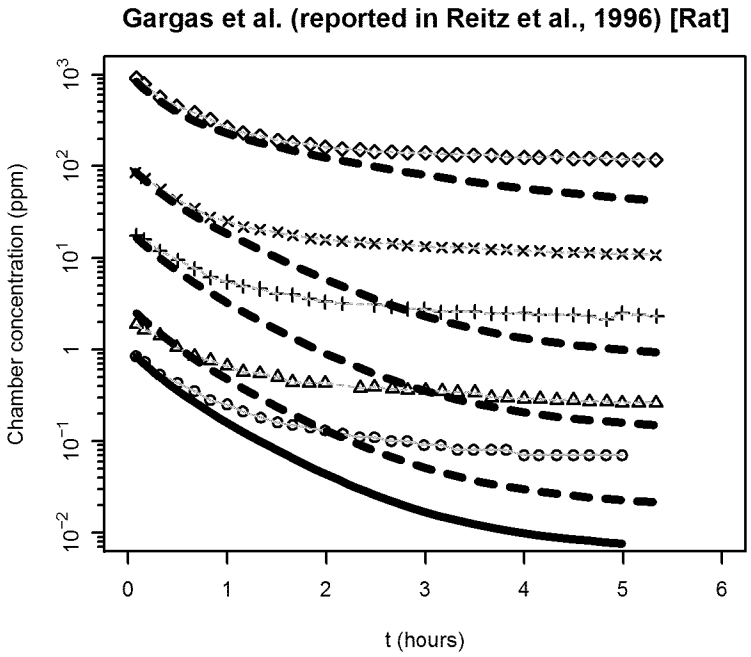
Gargas et al. (reported in Reitz et al., 1996) [Rat]
Chamber concentration (ppm)
t (hours)

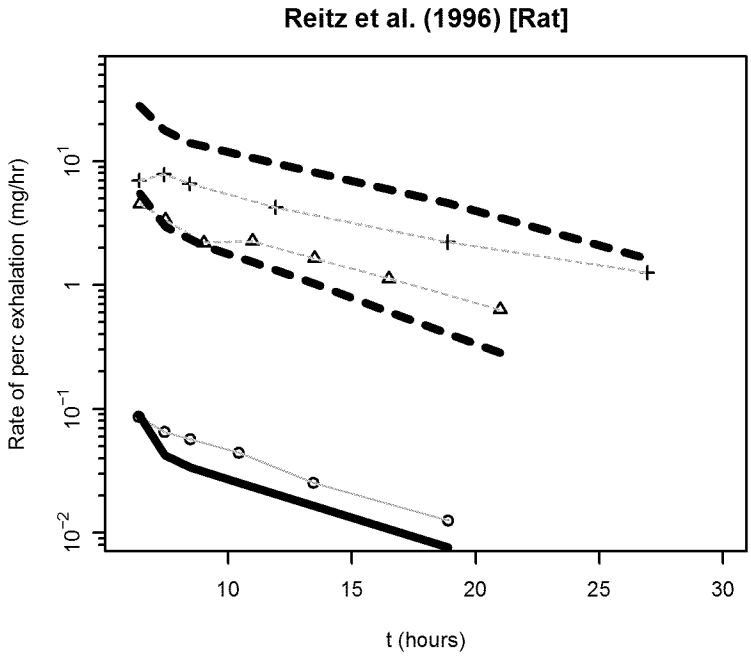
Reitz et al. (1996) [Rat]
Rate of perc exhalation (mg/hr)
t (hours)

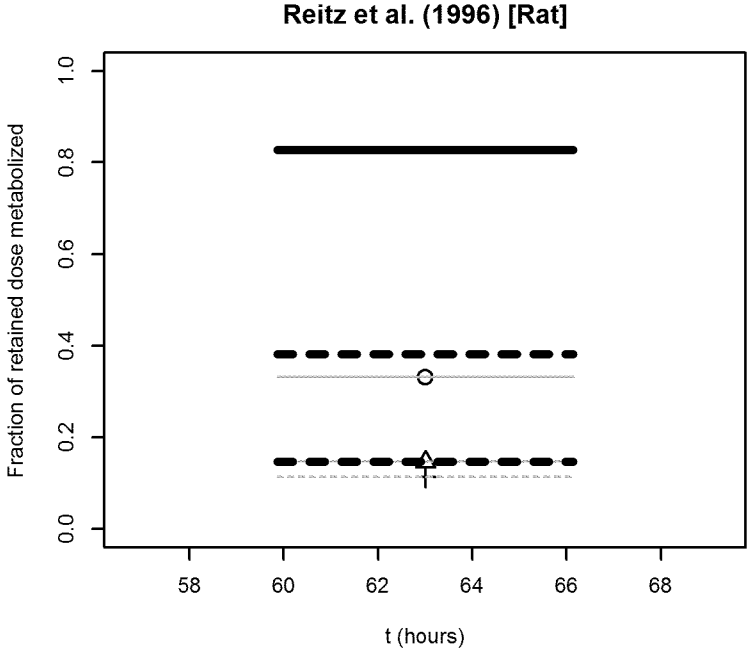
Reitz et al. (1996) [Rat]
Fraction of retained dose metabolized
t (hours)

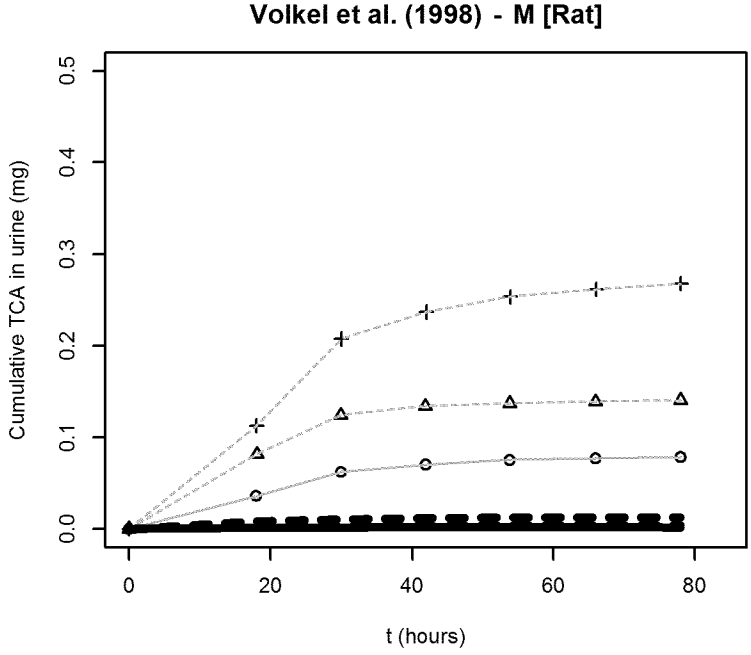
Volkel et al. (1998) - M [Rat]
Cumulative TCA in urine (mg)
t (hours)

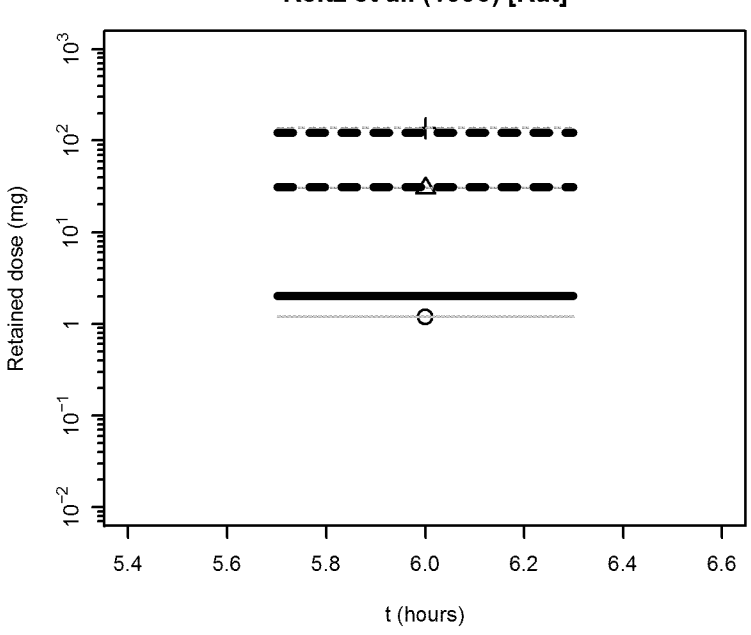
Reitz et al. (1996) [Rat]
Retained dose (mg)
t (hours)

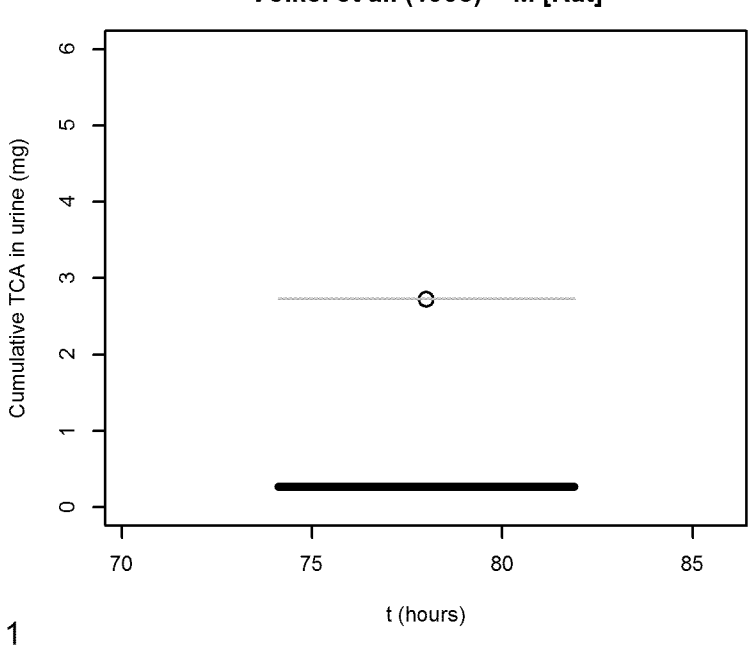
Volkel et al. (1998) - M [Rat]
Cumulative TCA in urine (mg)
t (hours)

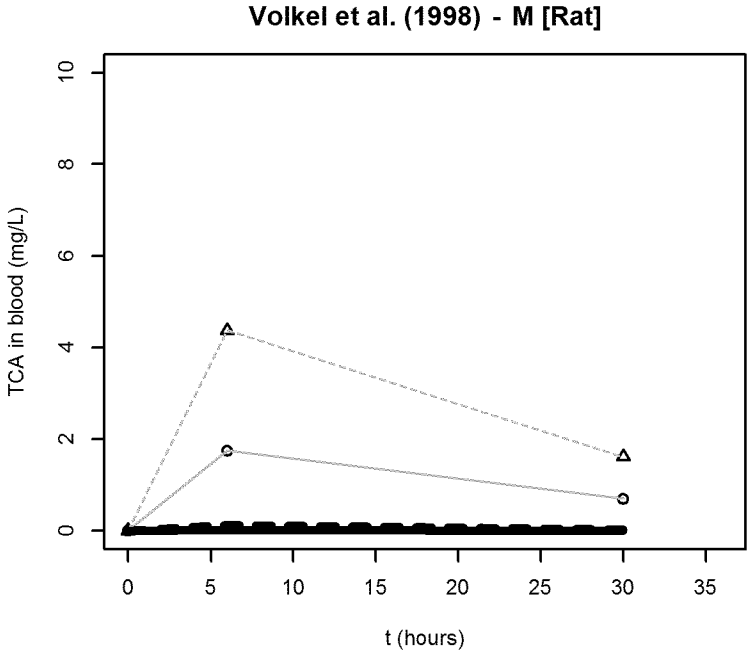
Volkel et al. (1998) - M [Rat]
TCA in blood (mg/L)
0
2
4
6
8
10
0
5
10
15
20
25
30
35
t (hours)

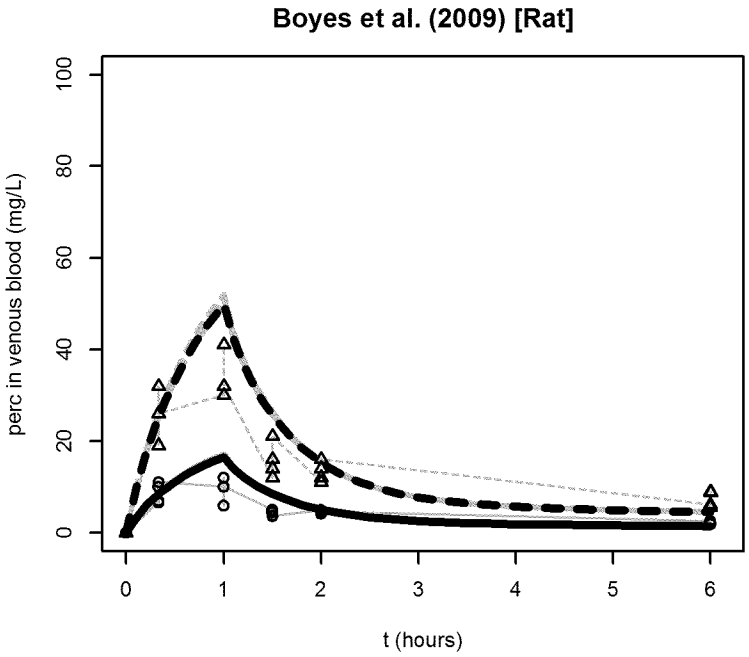
Boyes et al. (2009) [Rat]
perc in venous blood (mg/L)
t (hours)

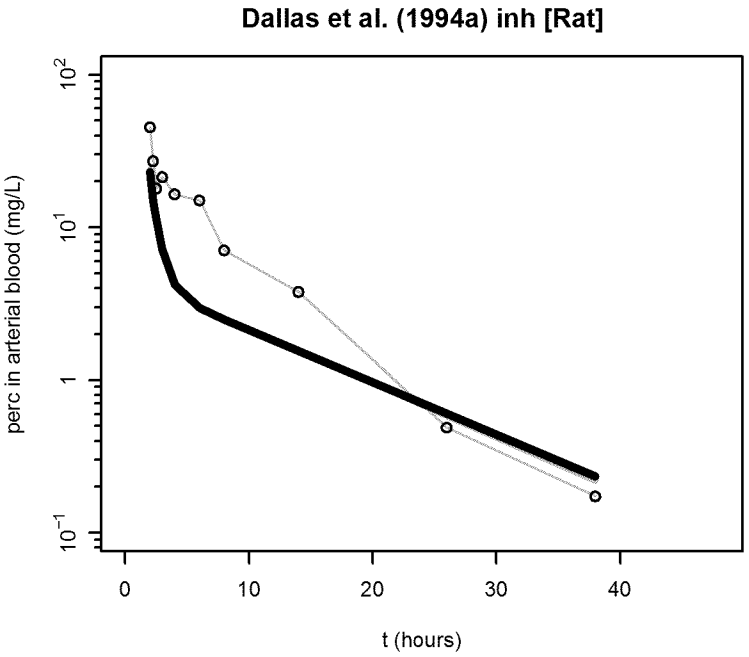
Dallas et al. (1994a) inh [Rat]
perc in arterial blood (mg/L)
t (hours)

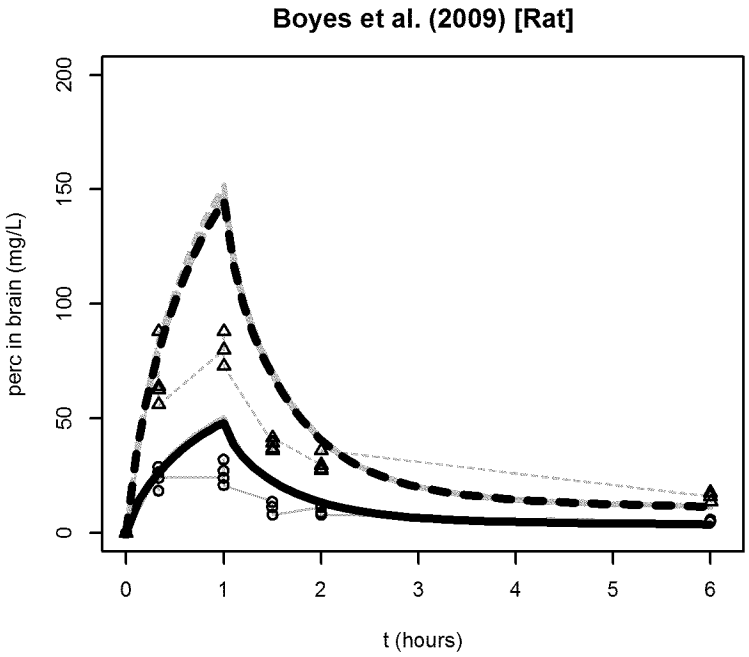
Boyes et al. (2009) [Rat]
perc in brain (mg/L)
t (hours)

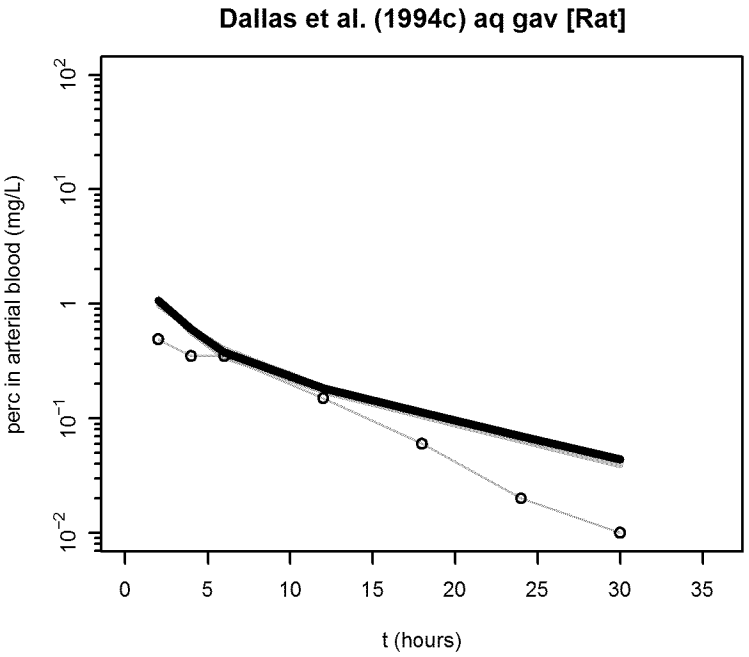
Dallas et al. (1994c) aq gav [Rat]
perc in arterial blood (mg/L)
t (hours)

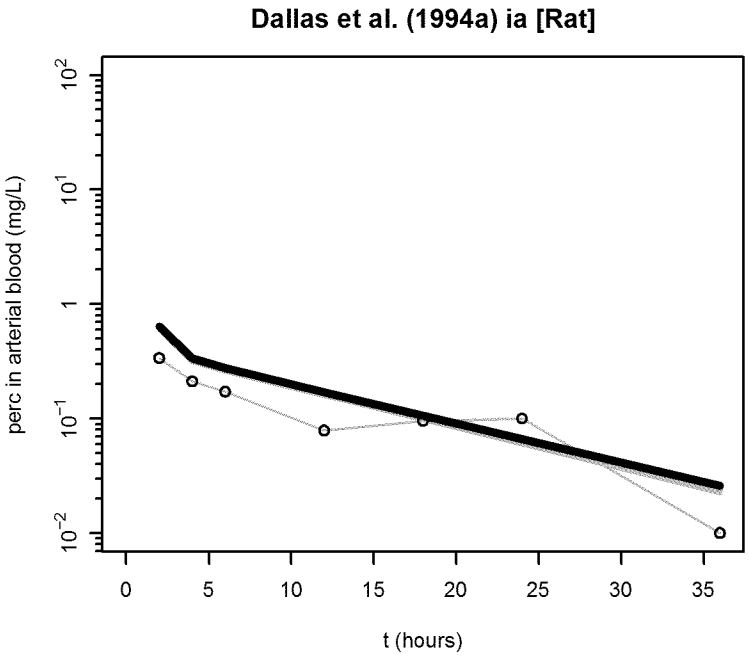
Dallas et al. (1994a) ia [Rat]
perc in arterial blood (mg/L)
t (hours)

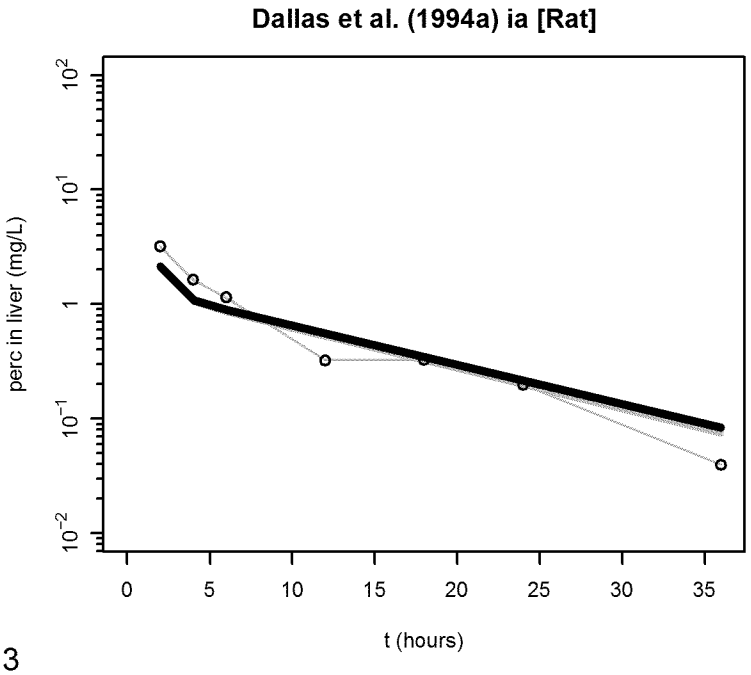
Dallas et al. (1994a) ia [Rat]
perc in liver (mg/L)
t (hours)

Dallas et al. (1994a) inh [Rat]

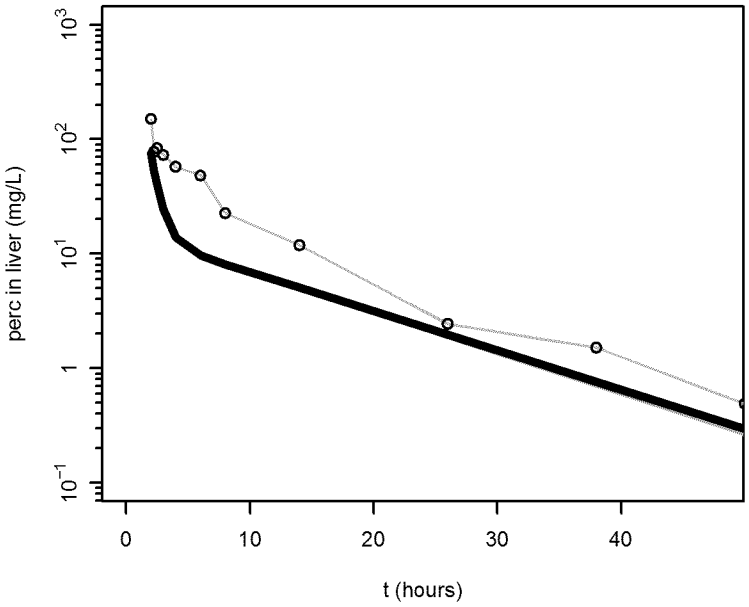

Dallas et al. (1994a) inh [Rat]

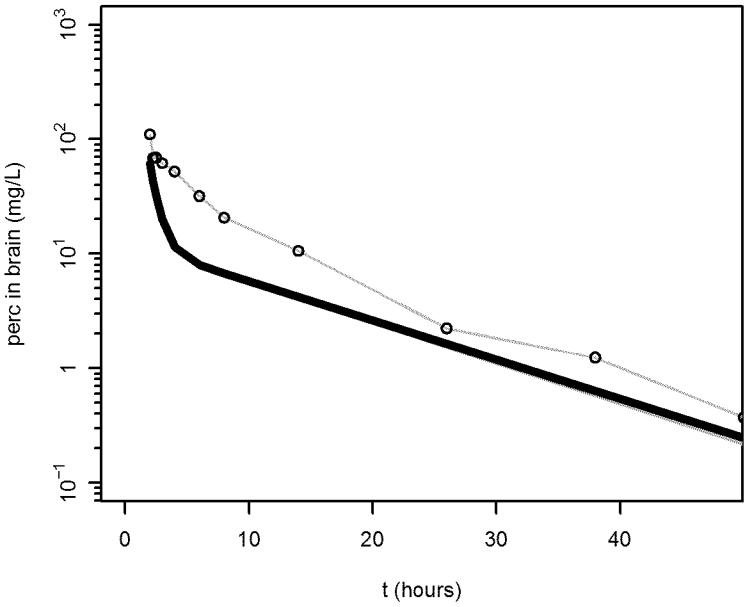

Dallas et al. (1994c) aq gav [Rat]

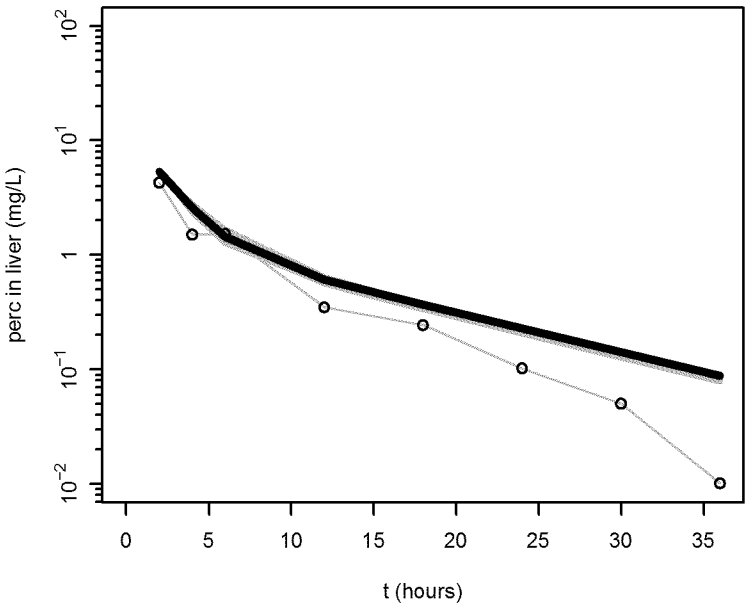

Dallas et al. (1994c) aq gav [Rat]

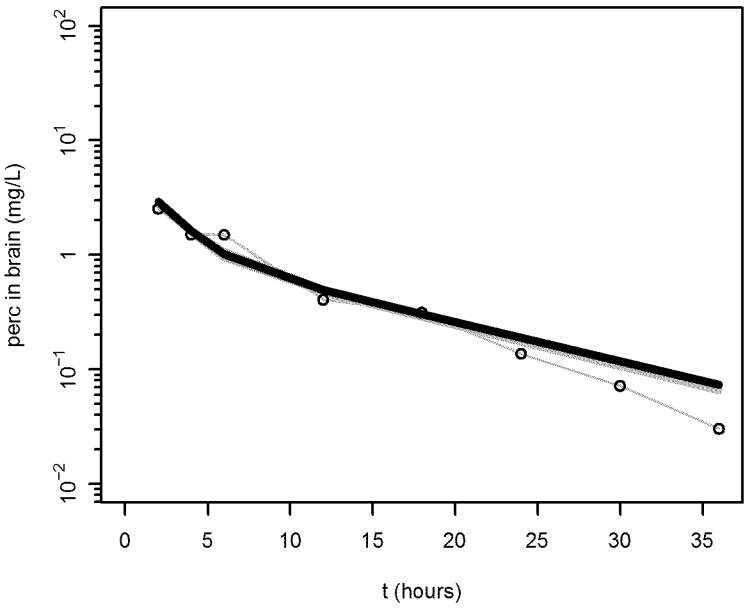

Dallas et al. (1994a) ia [Rat]

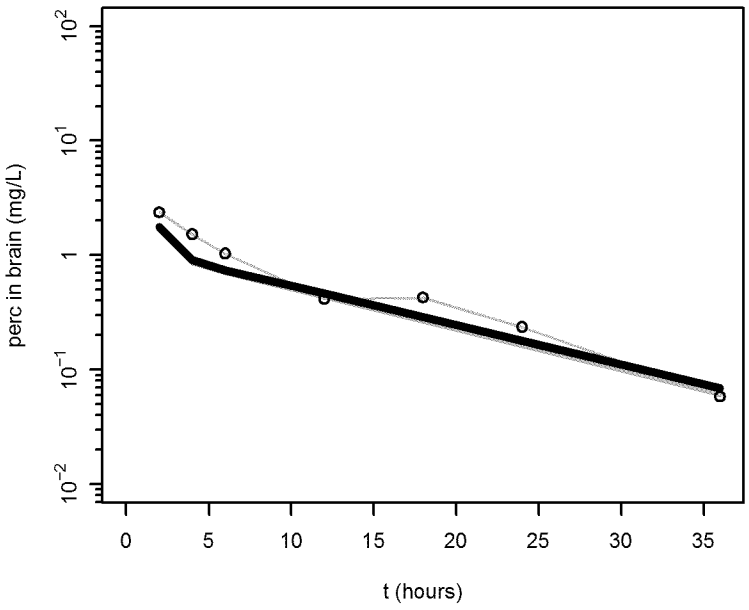

Dallas et al. (1994a) ia [Rat]

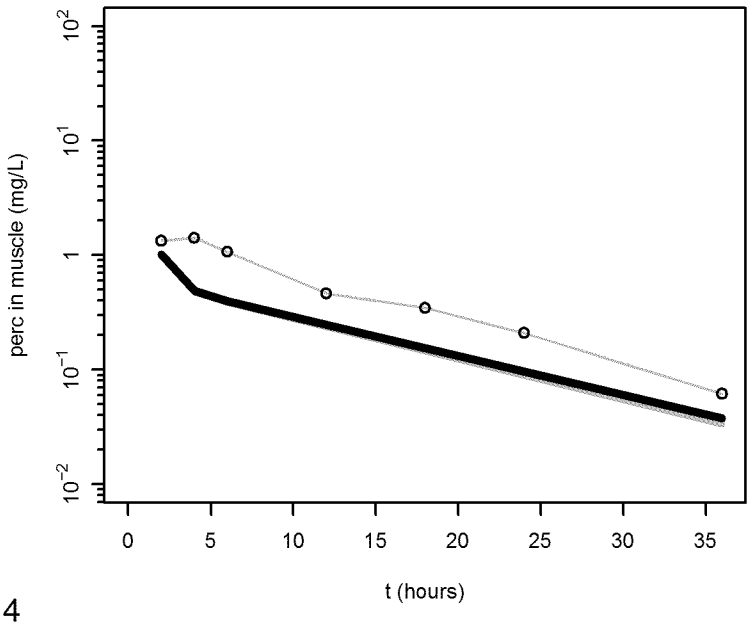

Dallas et al. (1994a) inh [Rat]

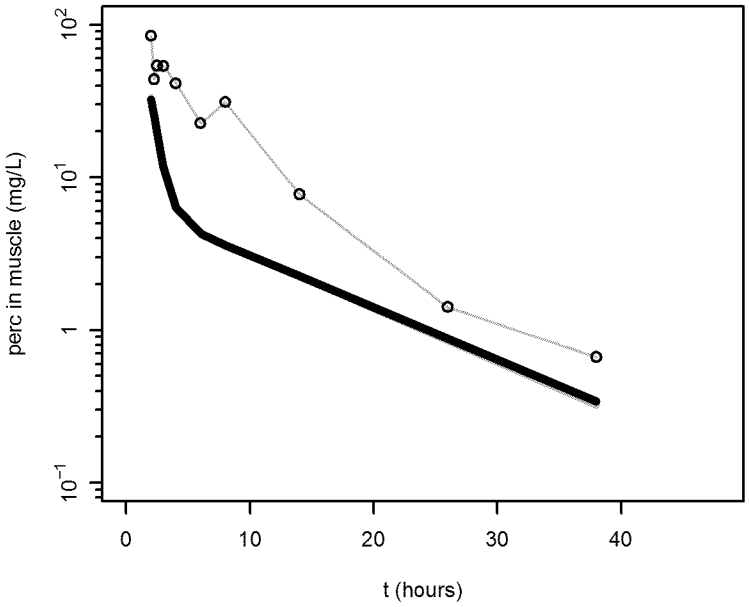

Dallas et al. (1994a) inh [Rat]

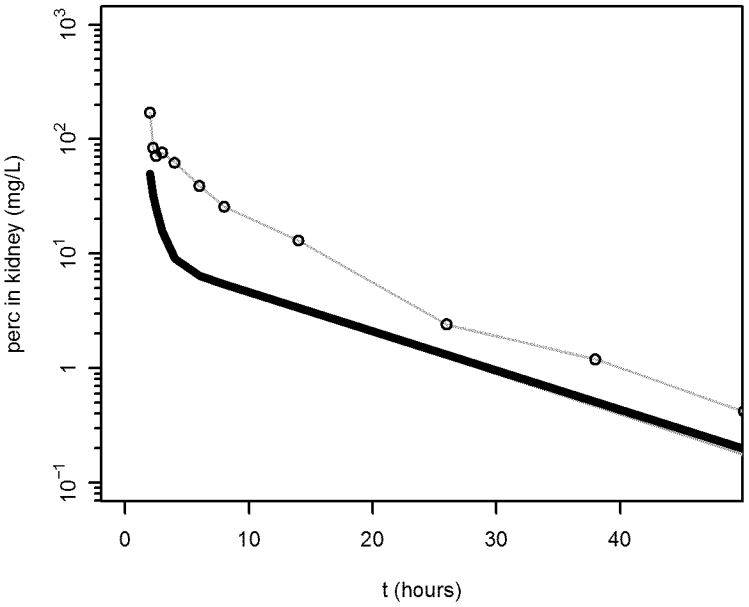

Dallas et al. (1994c) aq gav [Rat]

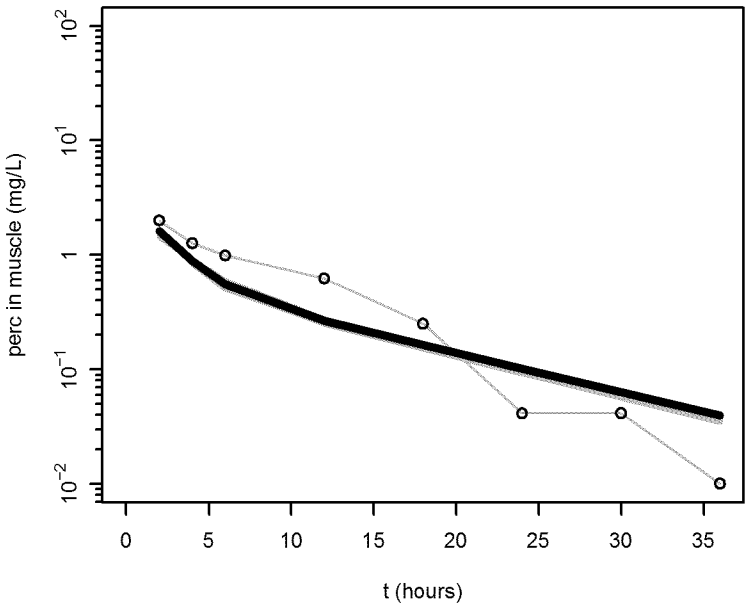

Dallas et al. (1994c) aq gav [Rat]

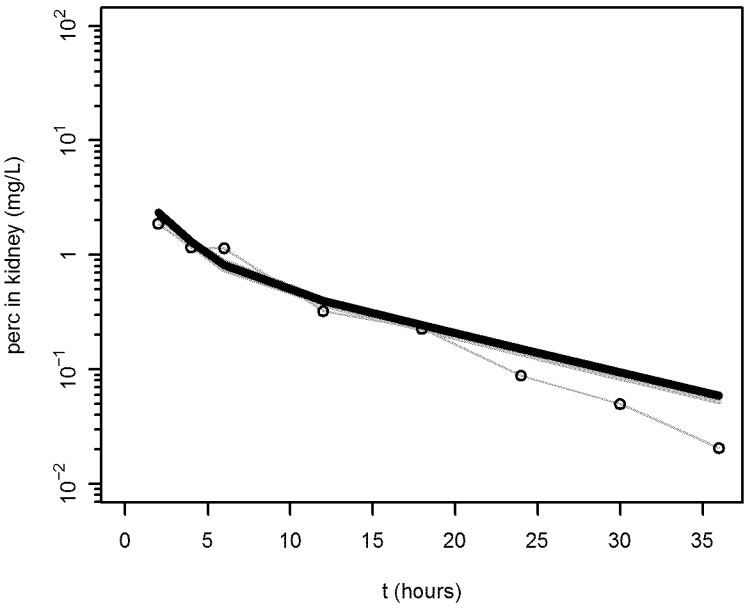

Dallas et al. (1994a) ia [Rat]

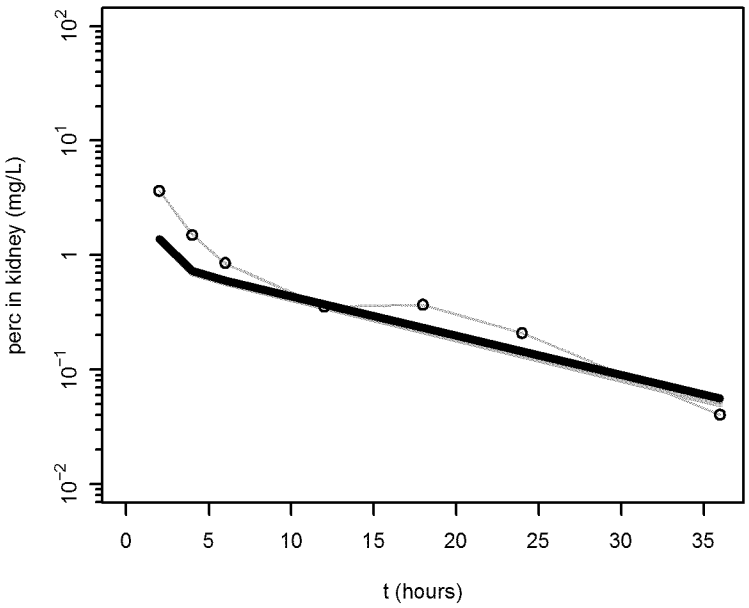

Dallas et al. (1994a) ia [Rat]

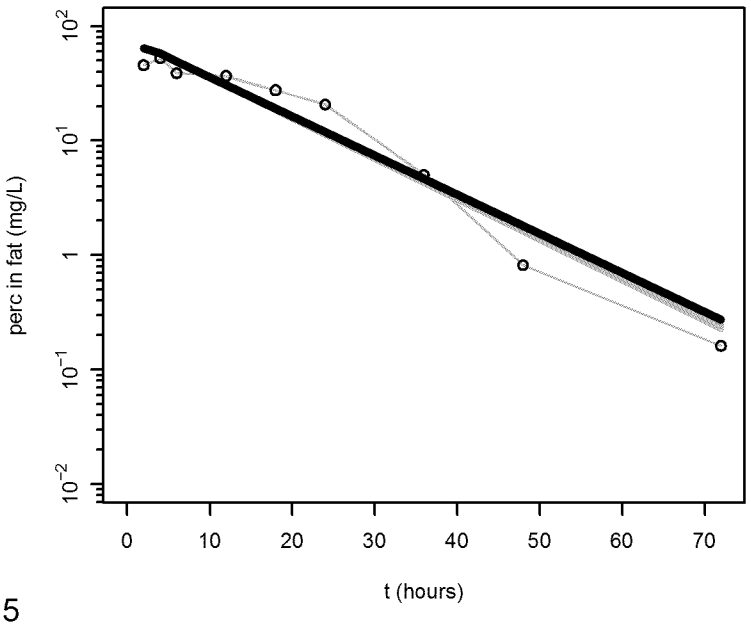

Dallas et al. (1994a) inh [Rat]

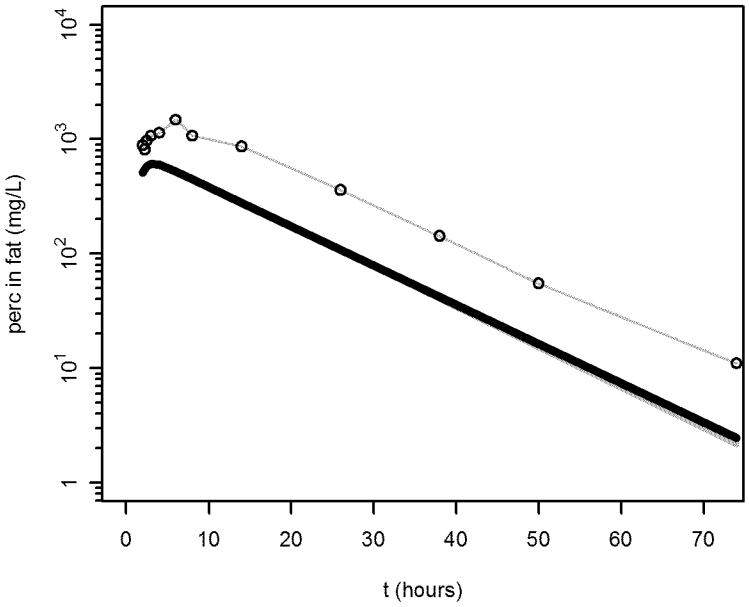

Pegg et al. (1979) [Rat]

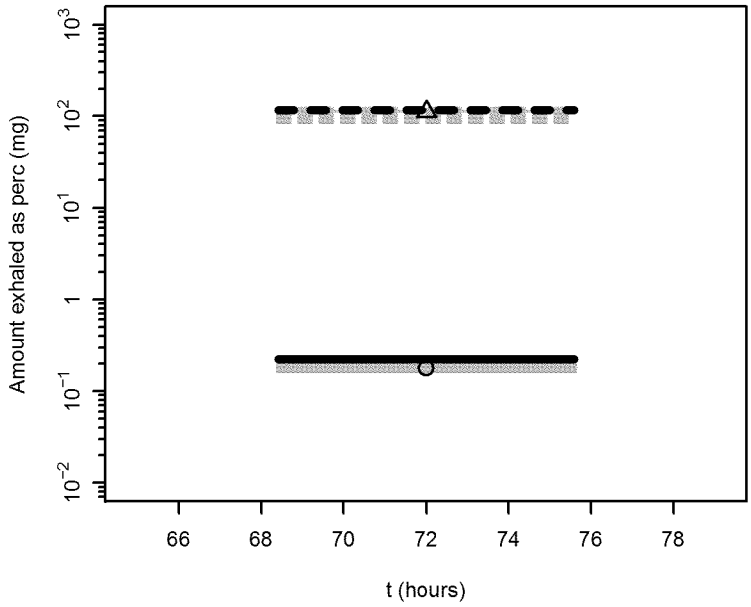

Dallas et al. (1994c) aq gav [Rat]

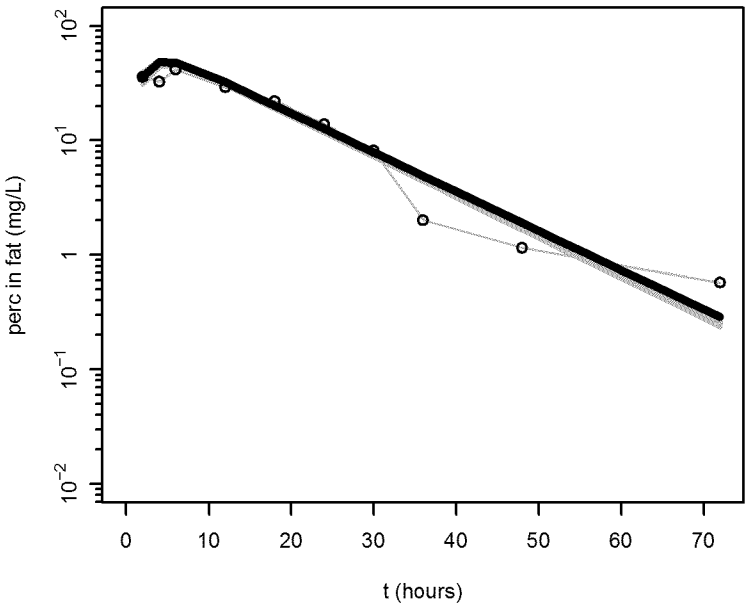

Pegg et al. (1979) [Rat]

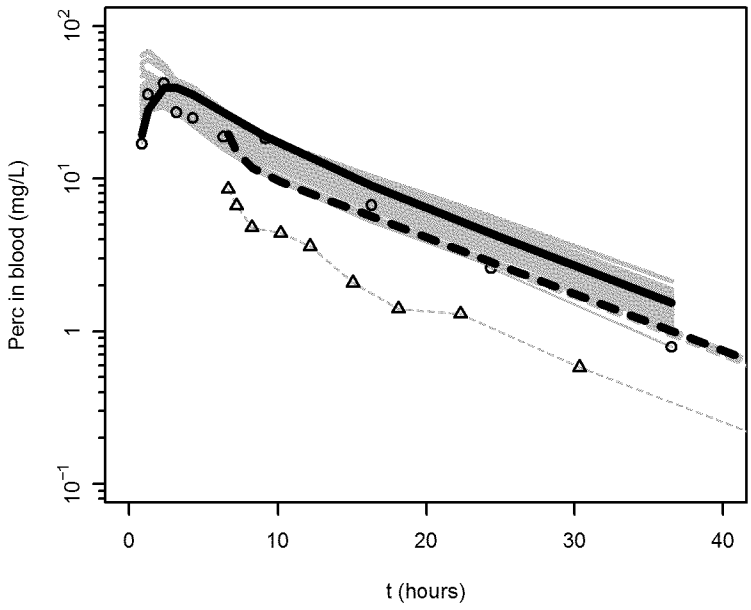

Odum et al. (1998) [Rat]

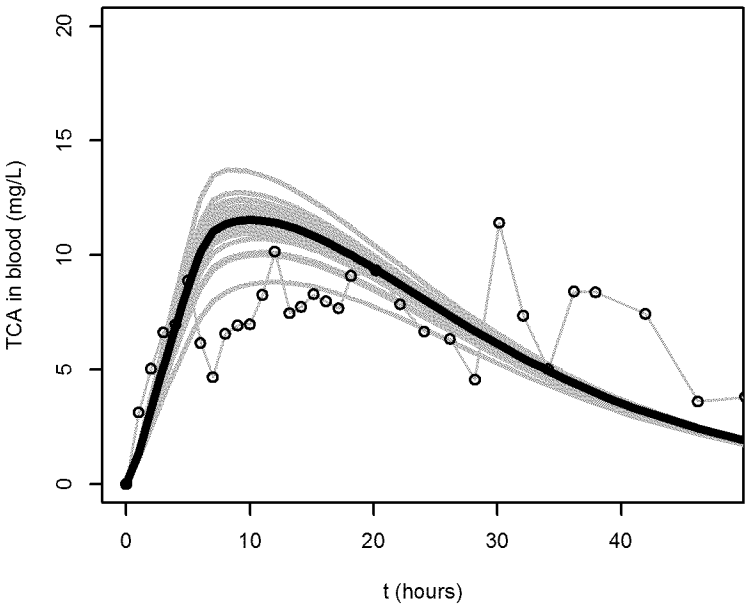

Pegg et al. (1979) [Rat]

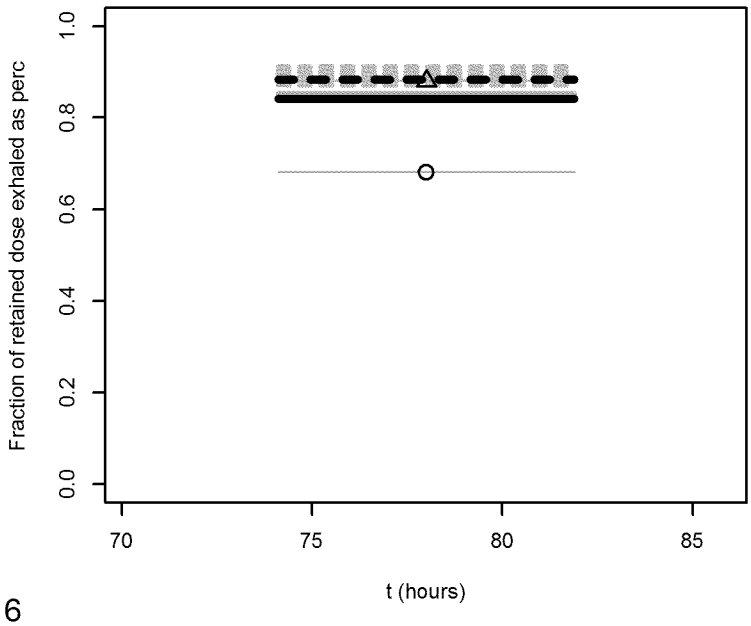

Pegg et al. (1979) [Rat]

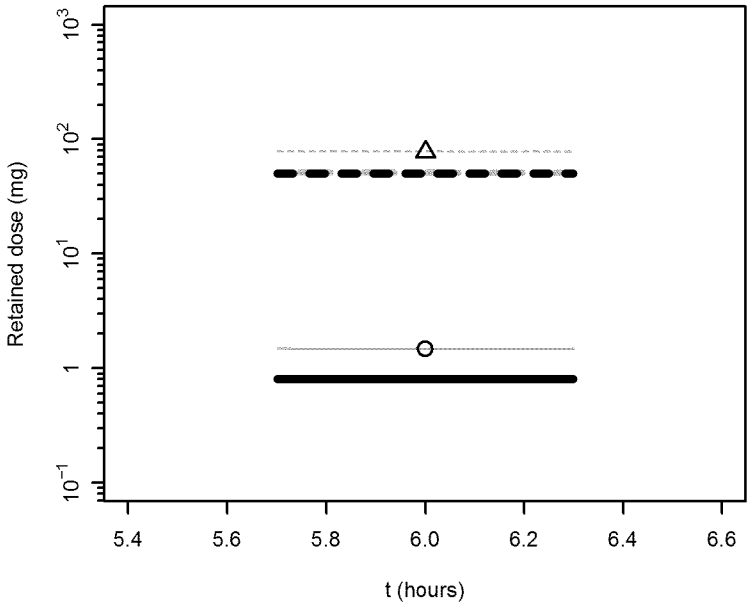

Reitz et al. (1996) [Rat]

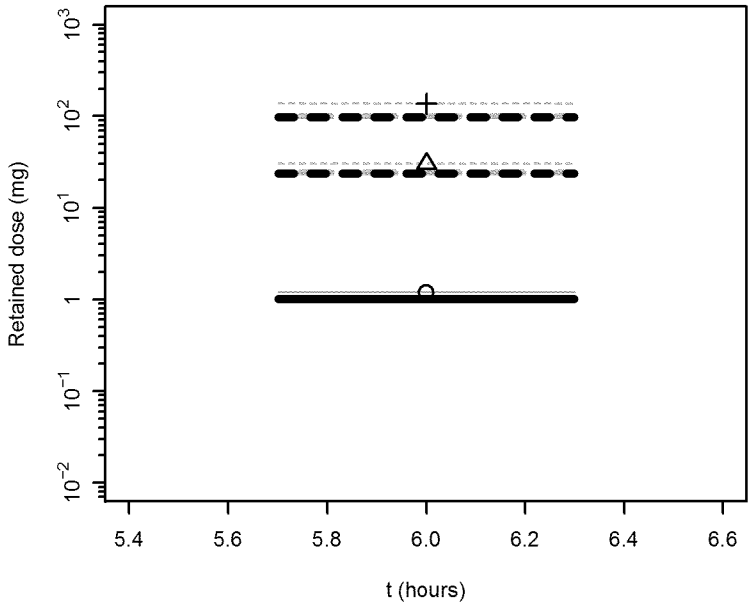

Gargas et al. (reported in Reitz et al., 1996) [Rat]

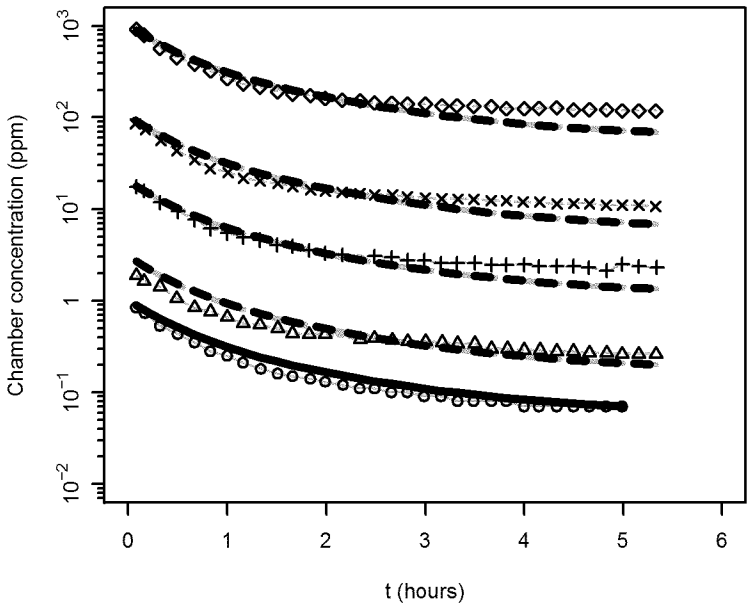

Reitz et al. (1996) [Rat]

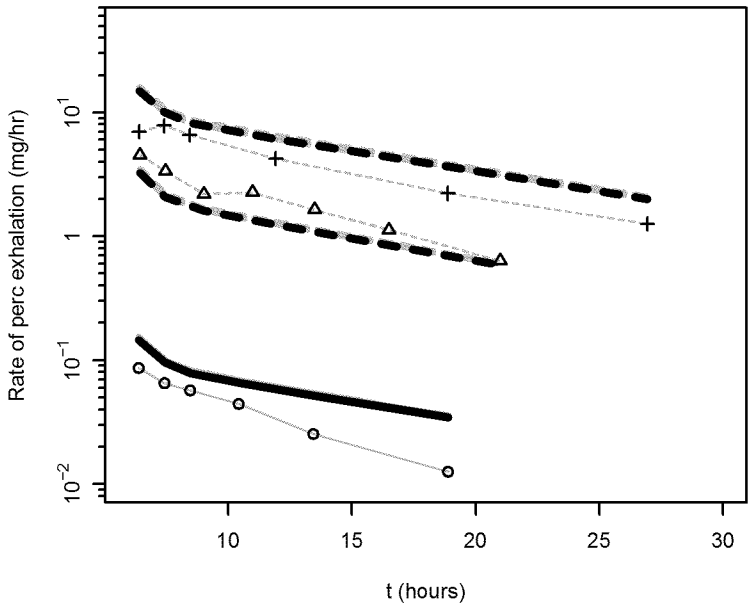

Reitz et al. (1996) [Rat]

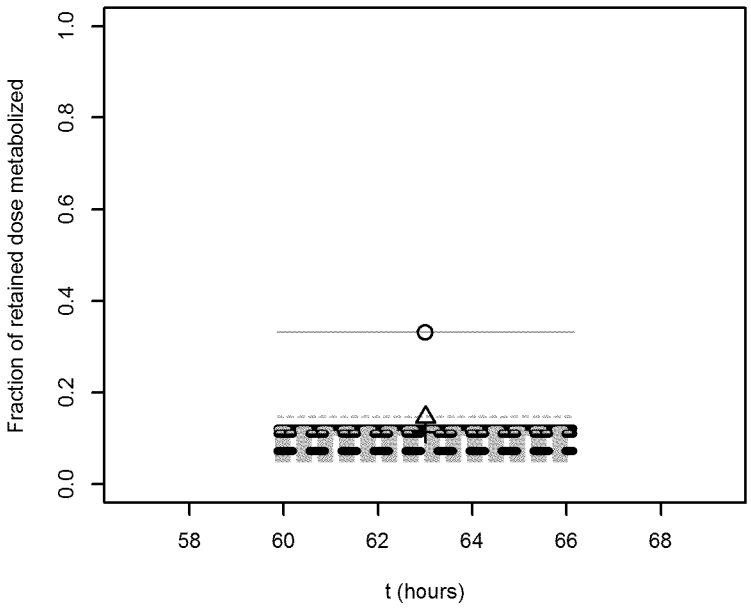

Volkel et al. (1998) - M [Rat]

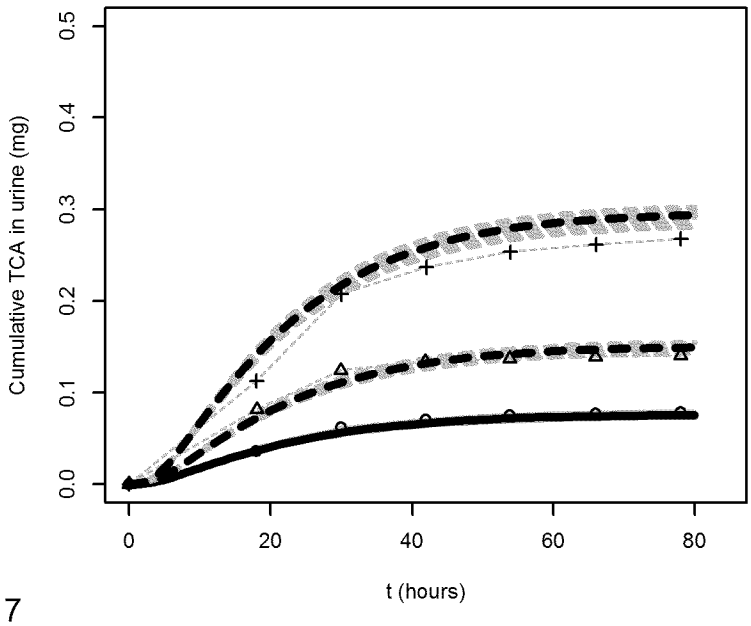

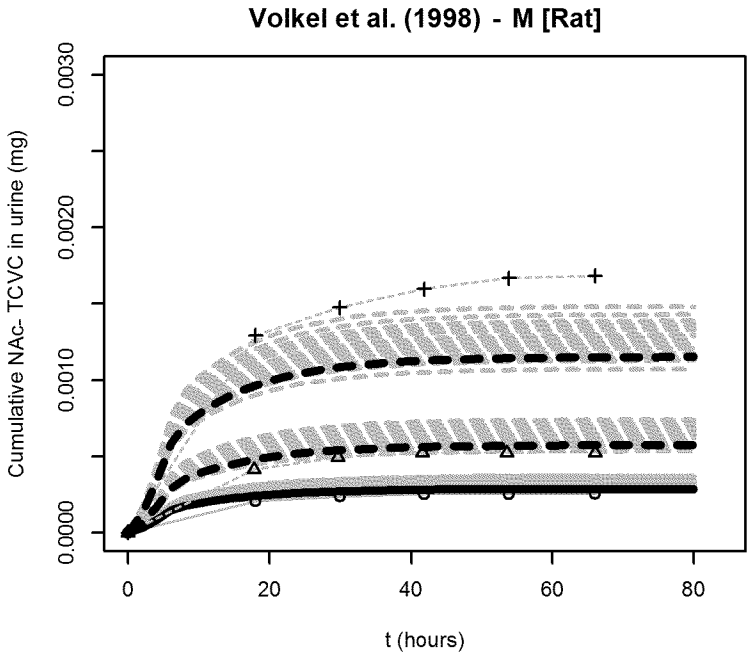
Volkel et al. (1998) - M [Rat]
Cumulative NAc- TCVC in urine (mg)
0.0000
0.0010
0.0020
0.0030
0
20
40
60
80
t (hours)

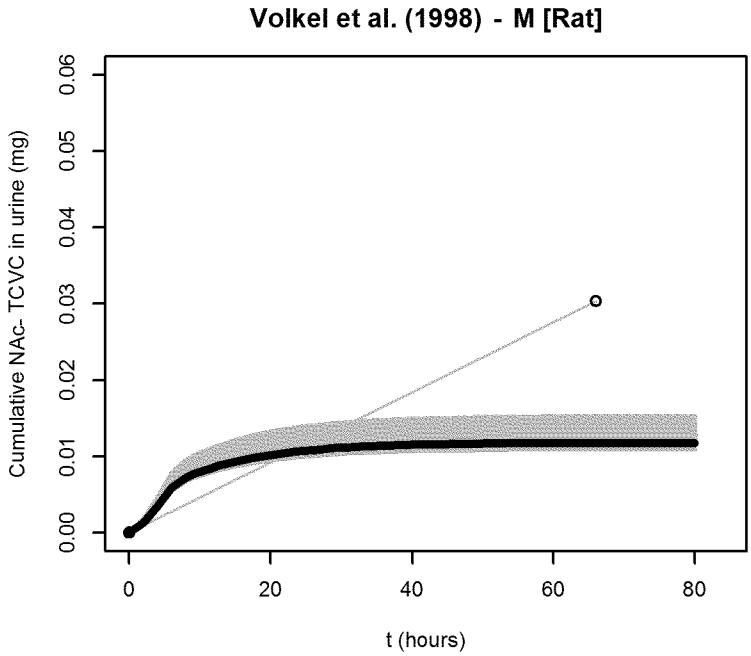
Volkel et al. (1998) - M [Rat]
Cumulative NAc- TCVC in urine (mg)
0.00
0.01
0.02
0.03
0.04
0.05
0.06
0
20
40
60
80
t (hours)

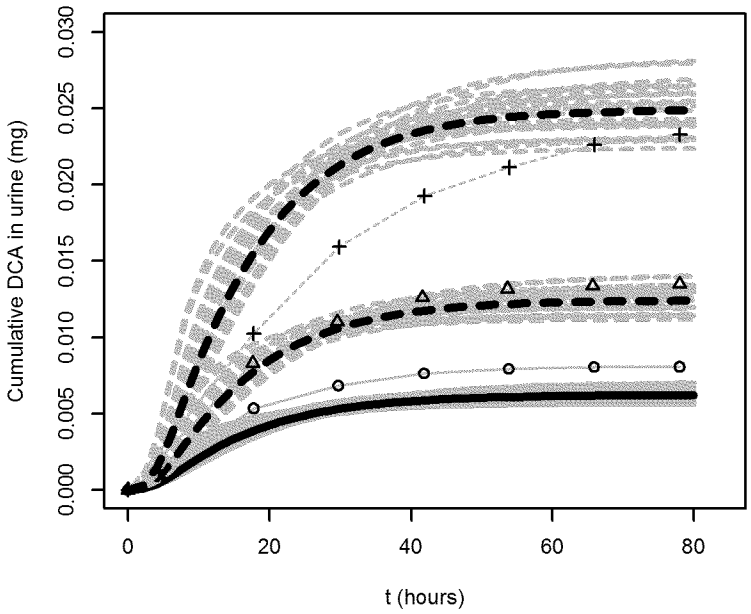
Volkel et al. (1998) - M [Rat]
Cumulative DCA in urine (mg)
0.000
0.005
0.010
0.015
0.020
0.025
0.030
0
20
40
60
80
t (hours)

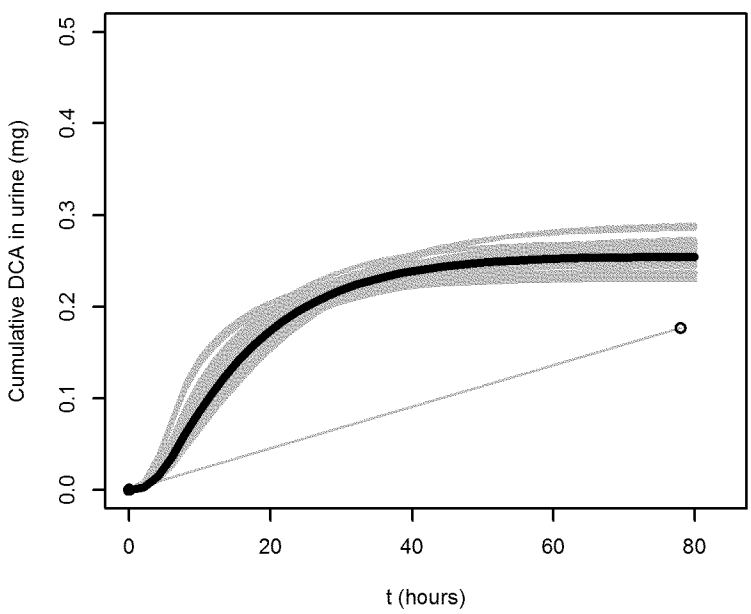
Volkel et al. (1998) - M [Rat]
Cumulative DCA in urine (mg)
0.0
0.1
0.2
0.3
0.4
0.5
0
20
40
60
80
t (hours)

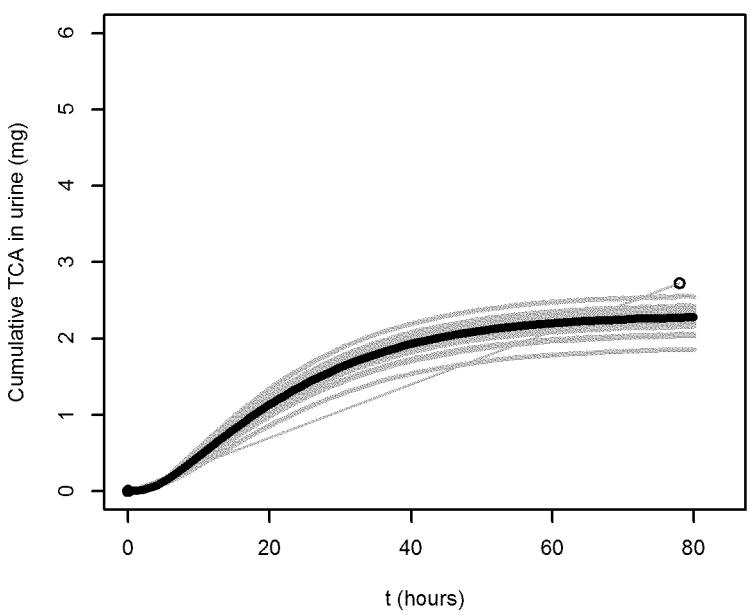
Volkel et al. (1998) - M [Rat]
Cumulative TCA in urine (mg)
0
1
2
3
4
5
6
0
20
40
60
80
t (hours)

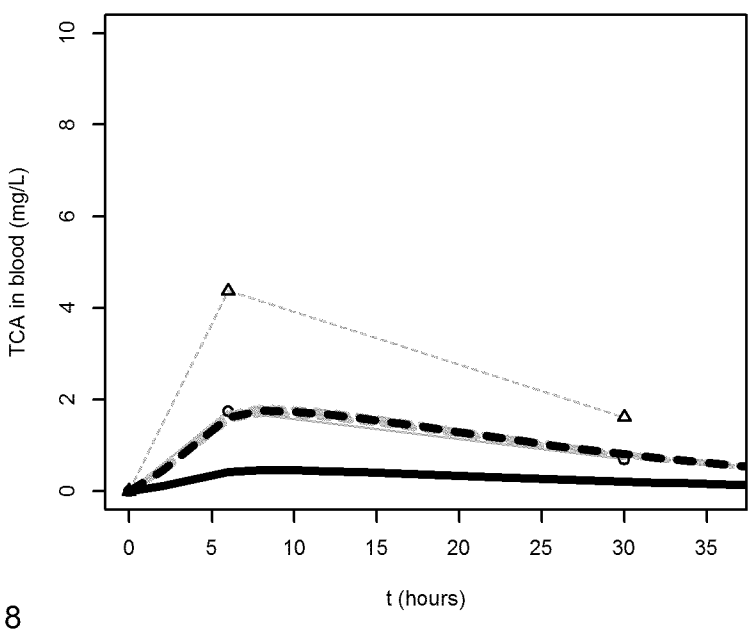
Volkel et al. (1998) - M [Rat]
TCA in blood (mg/L)
0
2
4
6
8
10
0
5
10
15
20
25
30
35
t (hours)

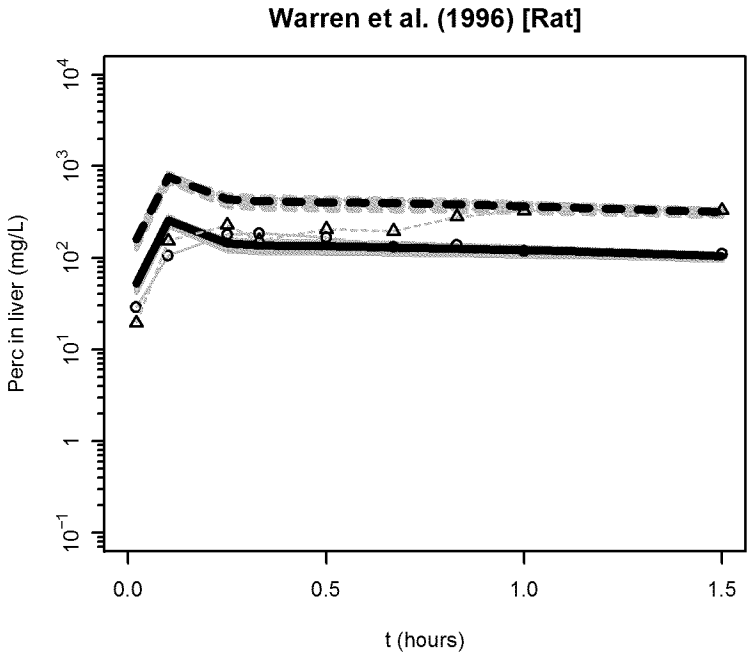
Warren et al. (1996) [Rat]
Perc in liver (mg/L)
t (hours)

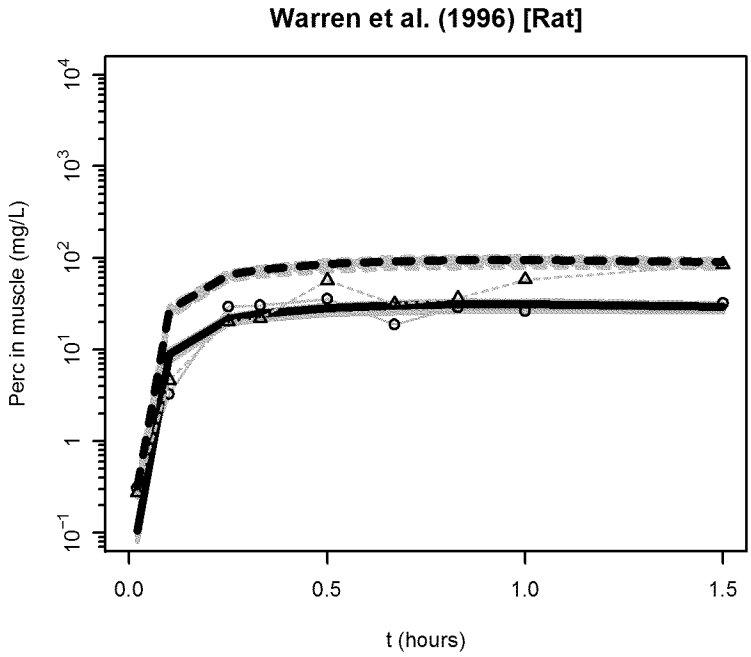
Warren et al. (1996) [Rat]
Perc in muscle (mg/L)
t (hours)

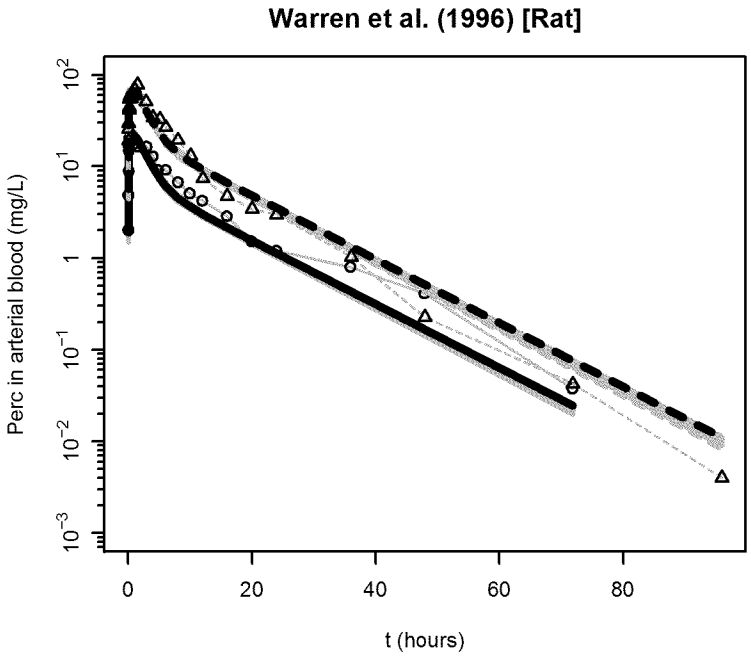
Warren et al. (1996) [Rat]
Perc in arterial blood (mg/L)
t (hours)

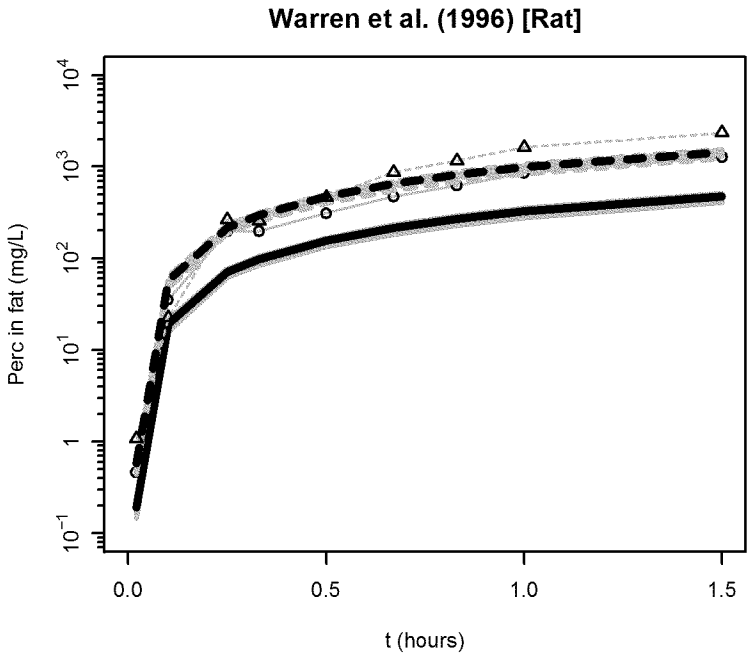
Warren et al. (1996) [Rat]
Perc in fat (mg/L)
t (hours)

Dallas et al. (1994b) [Rat]

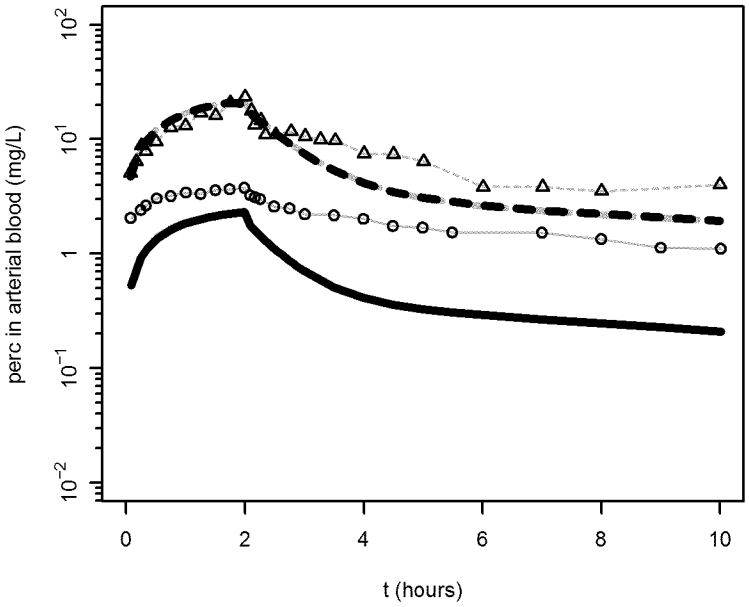

Dallas et al. (1995) po [Rat]

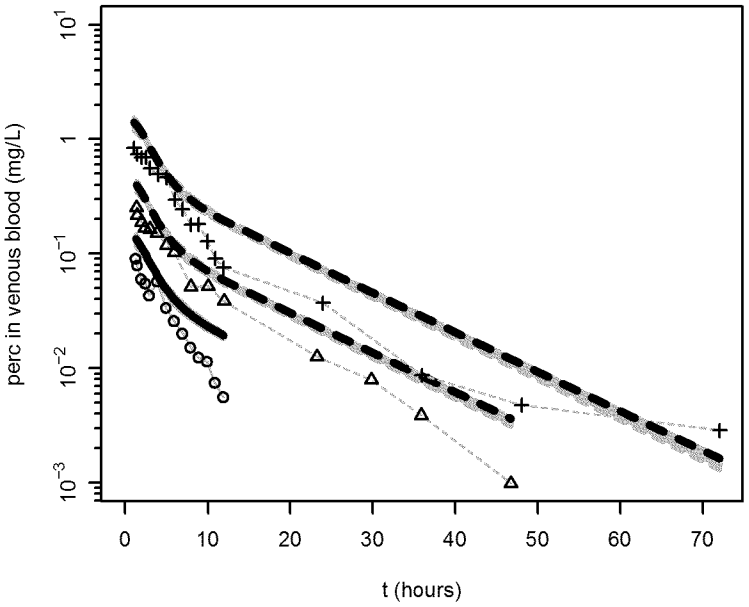

Dallas et al. (1994b) [Rat]

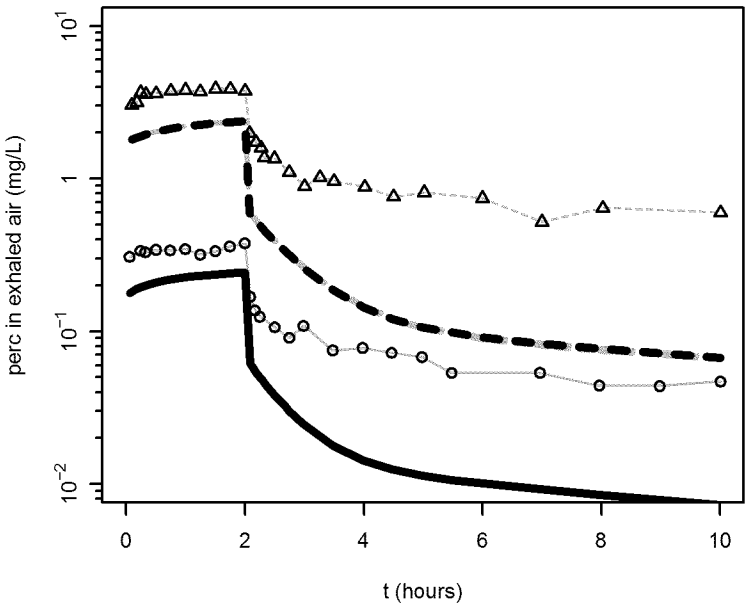

Franz and Watanabe (1983) [Rat]

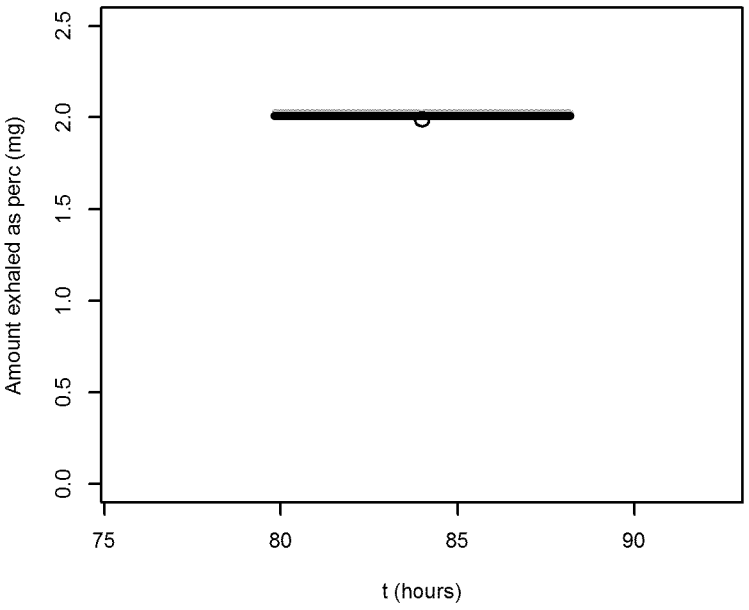

Dallas et al. (1995) ia [Rat]

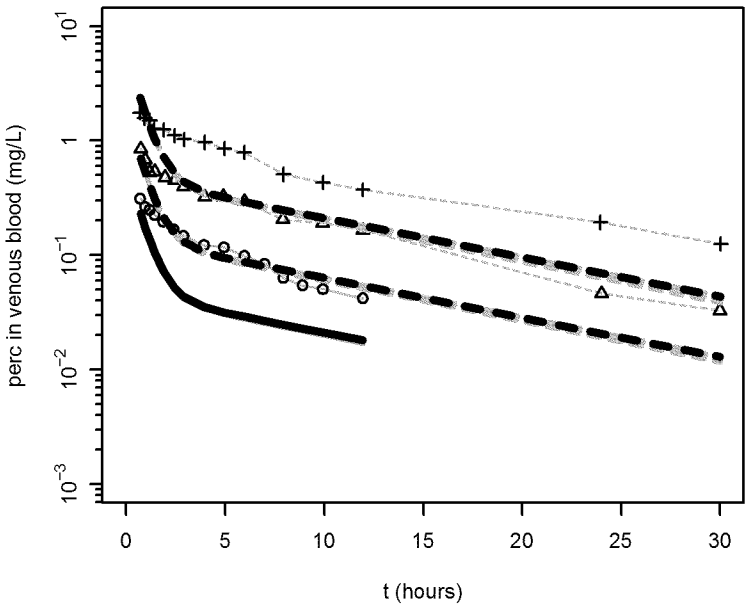

Ikeda and Ohtsuji (1972) [Rat]

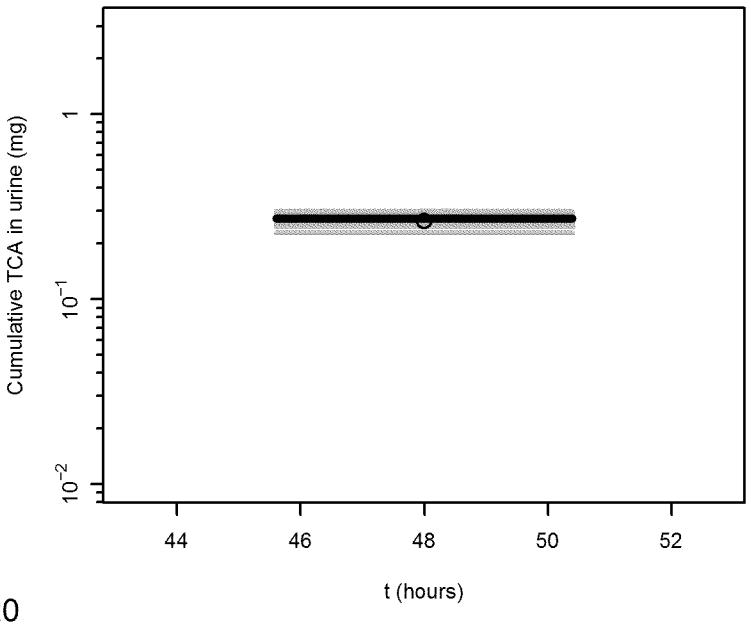

Ikeda et al. (1972) [Rat]

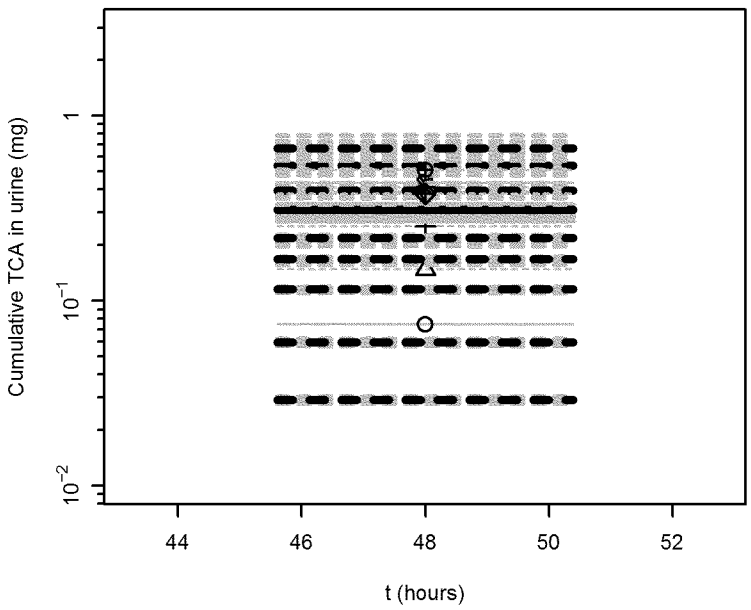

Savolainen et al. (1977) [Rat]

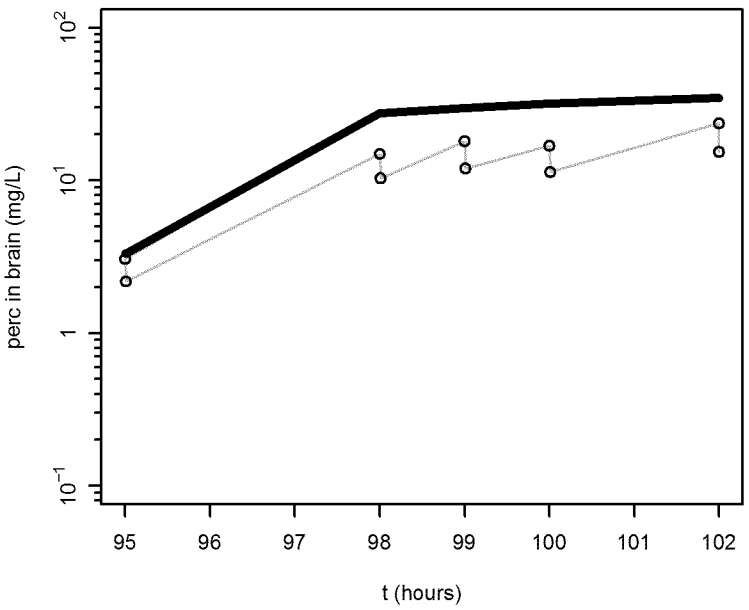

Savolainen et al. (1977) [Rat]

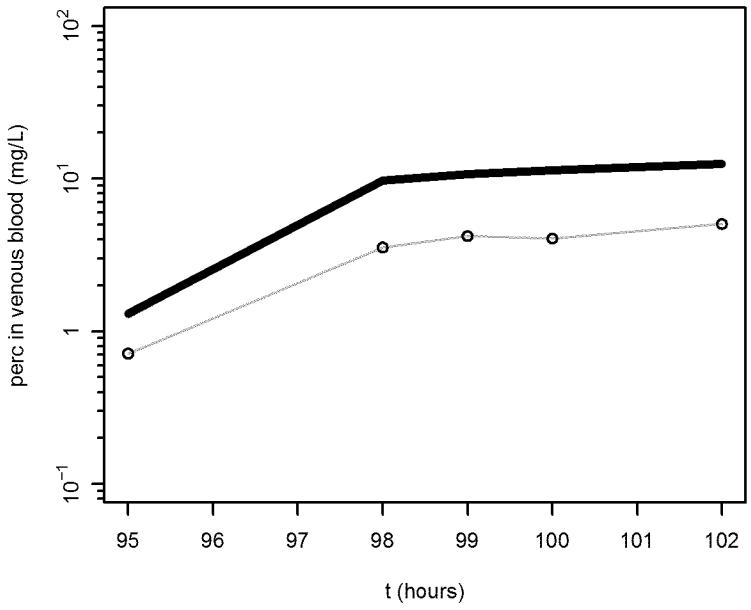

Savolainen et al. (1977) [Rat]

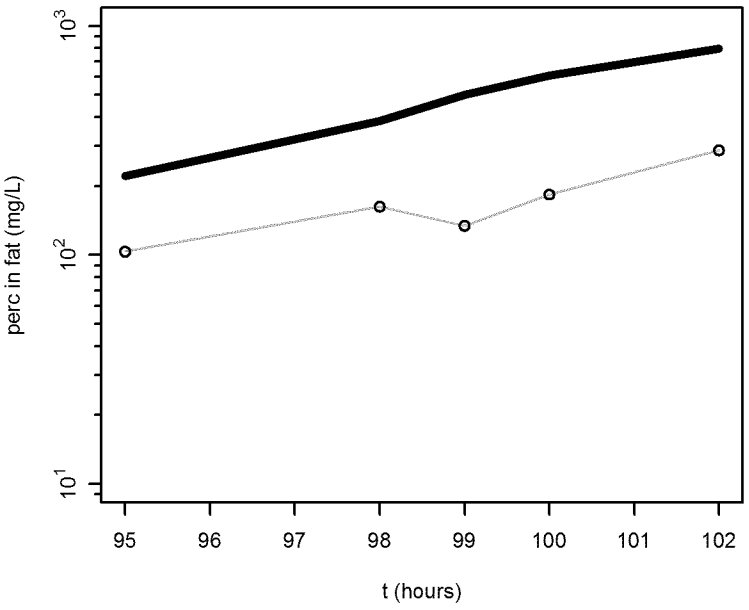

Savolainen et al. (1977) [Rat]

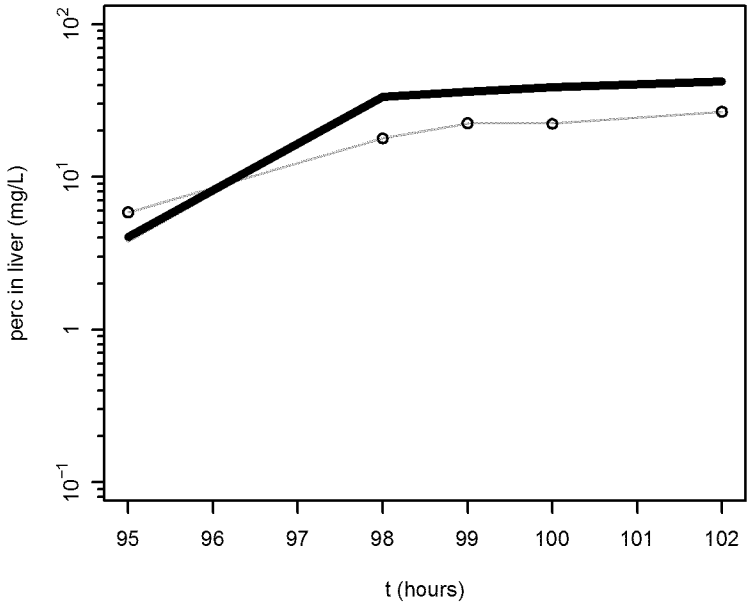

Chiu et al. (2007) A [Human]

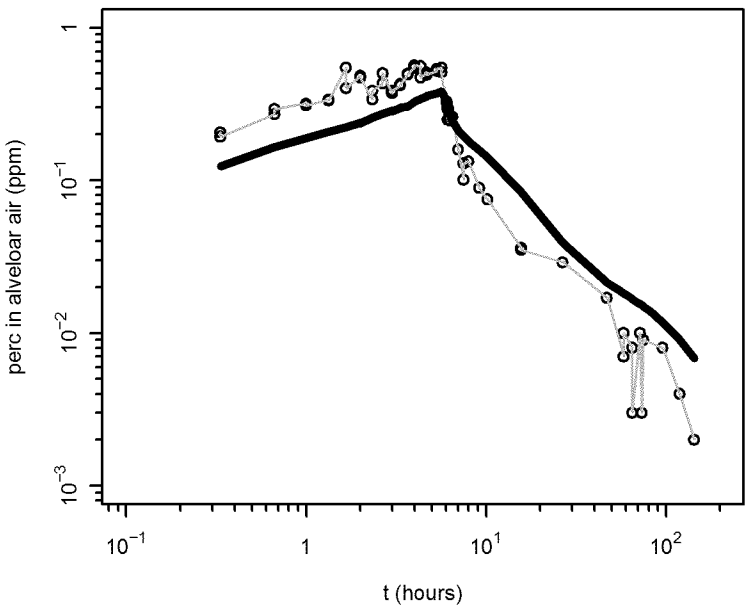

Chiu et al. (2007) D [Human]

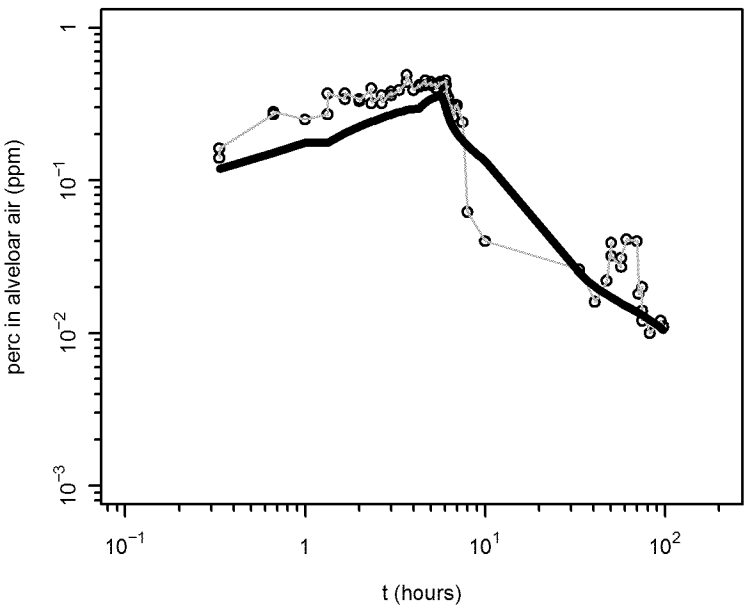

Chiu et al. (2007) B [Human]

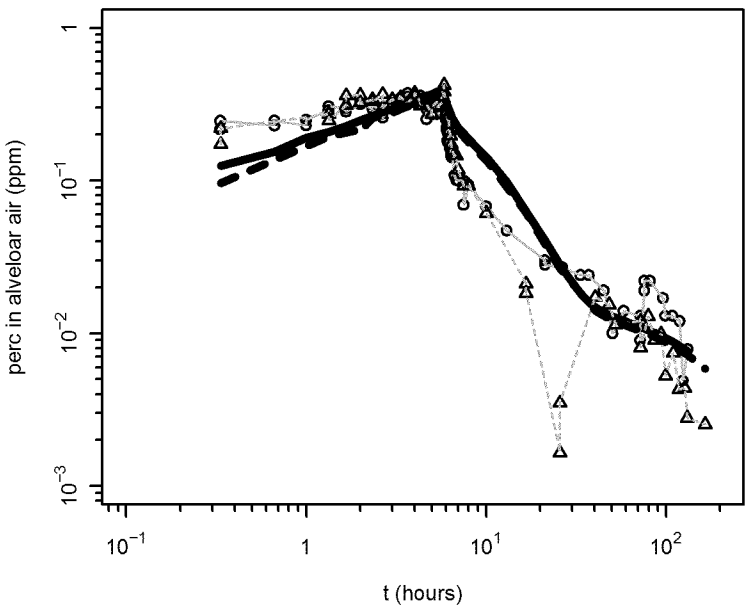

Chiu et al. (2007) E [Human]

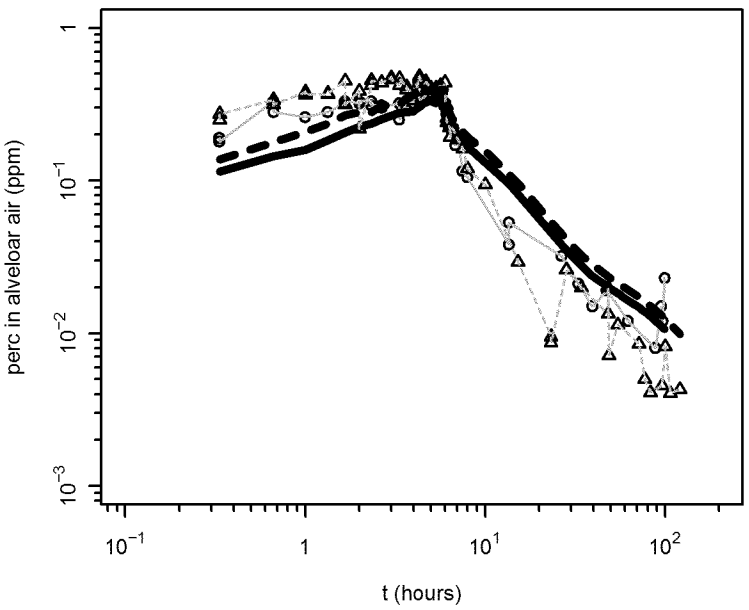

Chiu et al. (2007) C [Human]

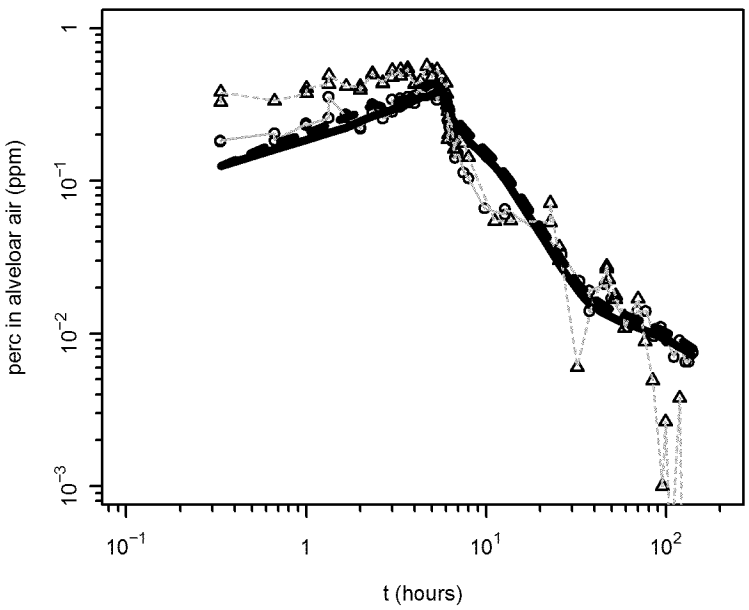

Chiu et al. (2007) F [Human]

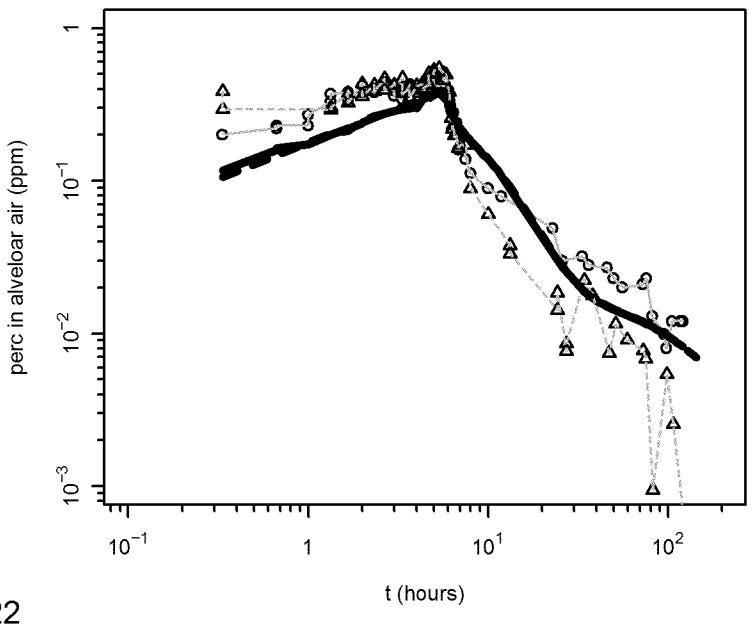

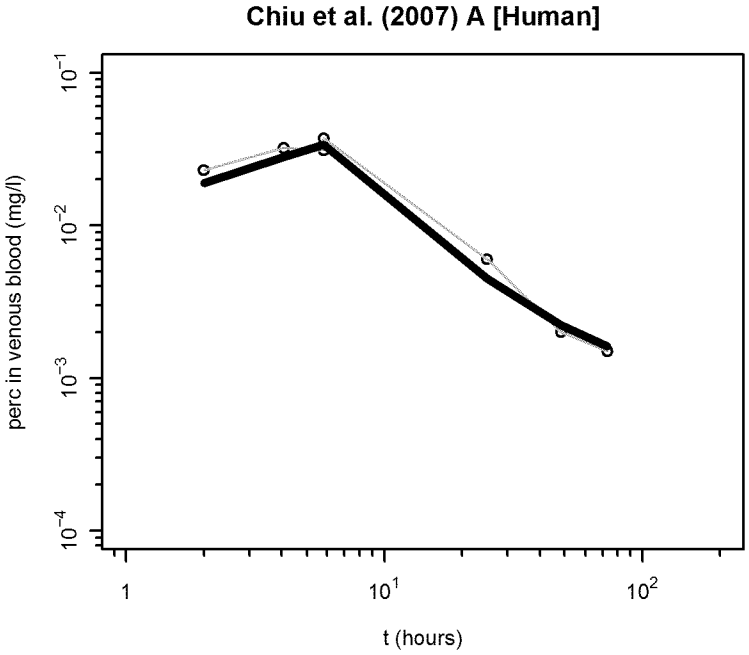
Chiu et al. (2007) A [Human]
perc in venous blood (mg/l)
t (hours)

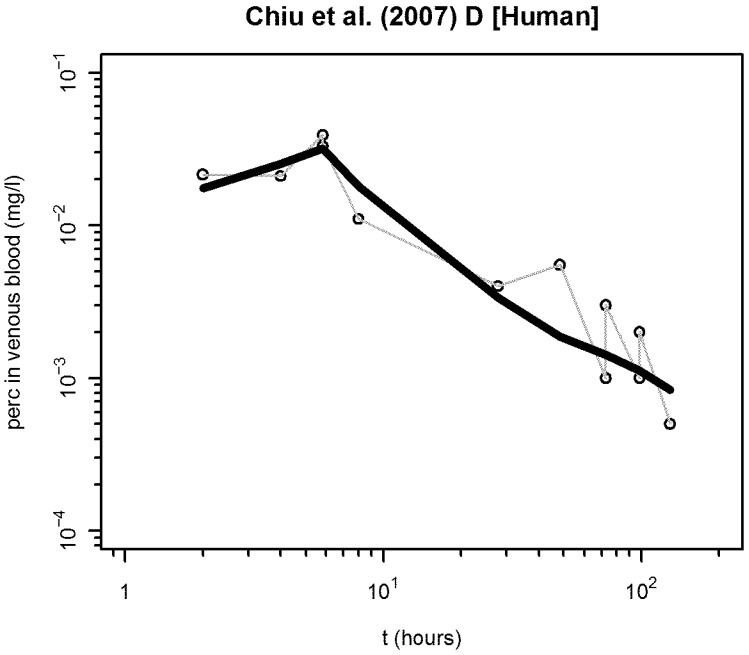
Chiu et al. (2007) D [Human]
perc in venous blood (mg/l)
t (hours)

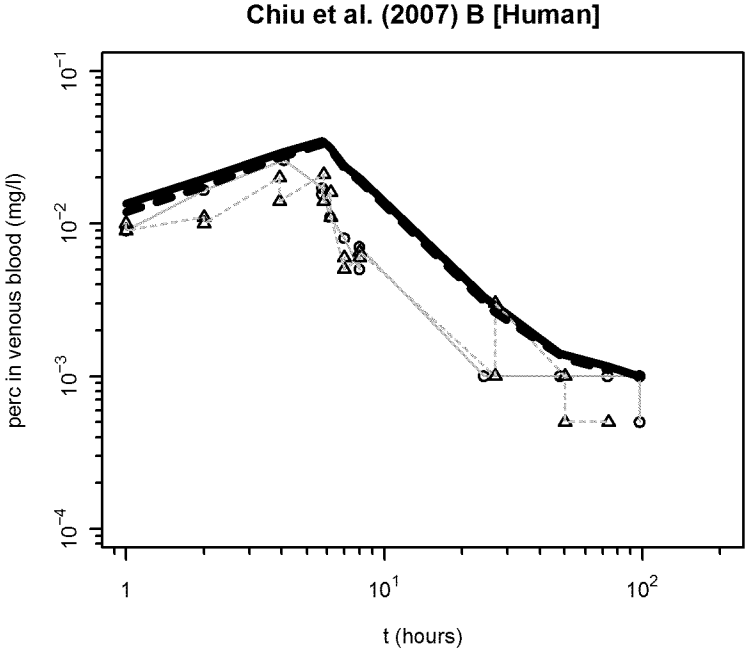
Chiu et al. (2007) B [Human]
perc in venous blood (mg/l)
t (hours)

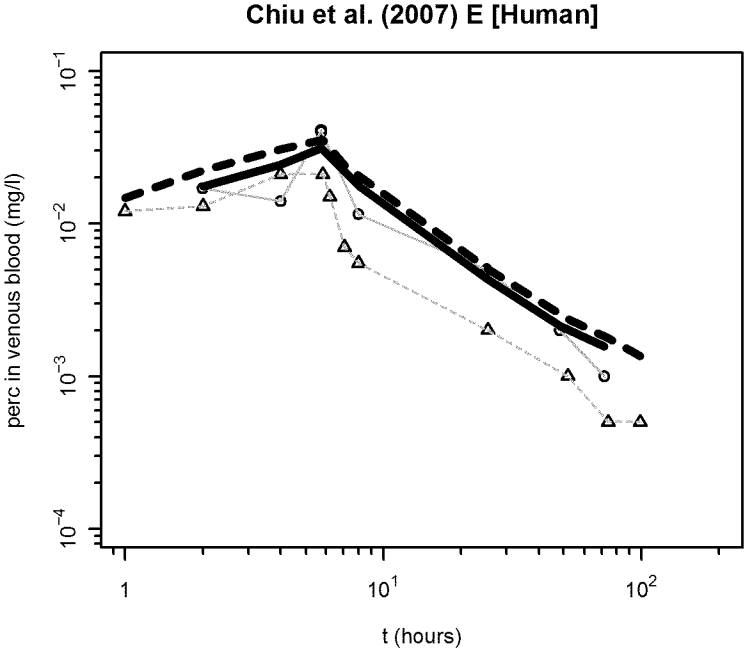
Chiu et al. (2007) E [Human]
perc in venous blood (mg/l)
t (hours)

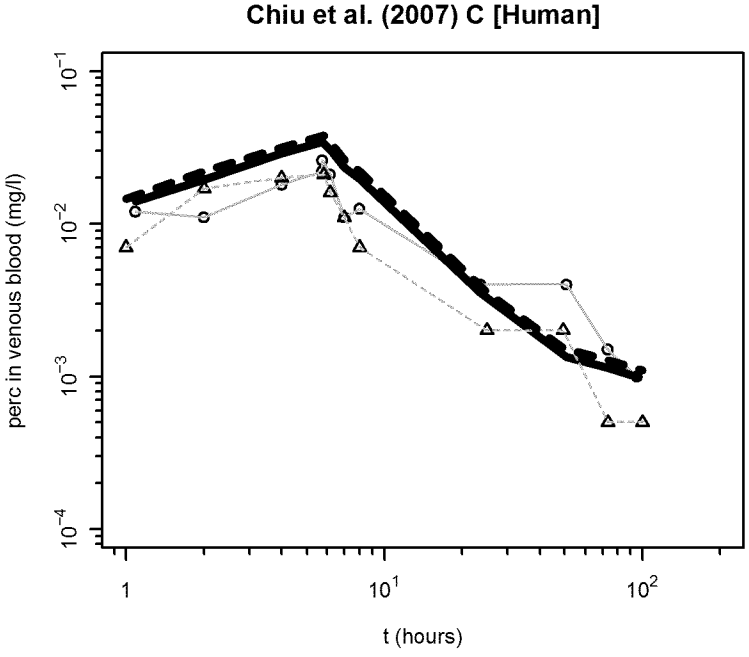
Chiu et al. (2007) C [Human]
perc in venous blood (mg/l)
t (hours)

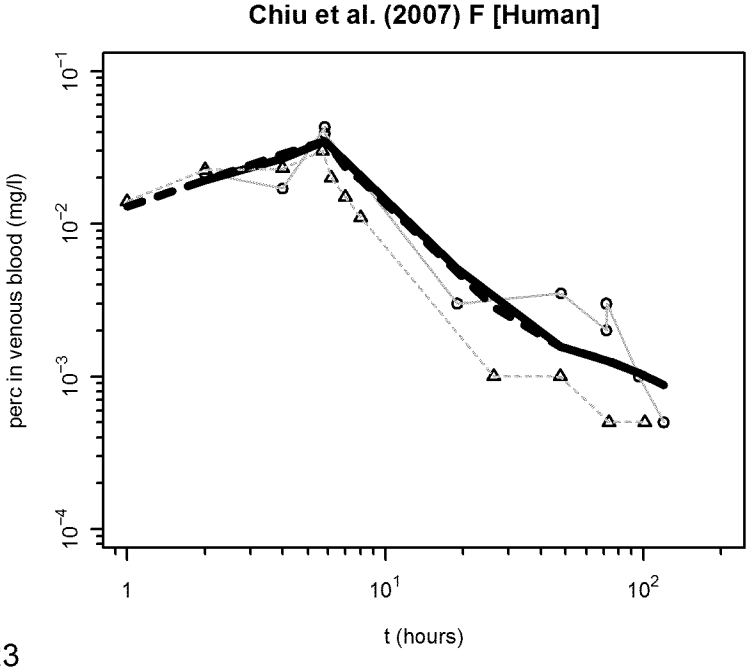
Chiu et al. (2007) F [Human]
perc in venous blood (mg/l)
t (hours)

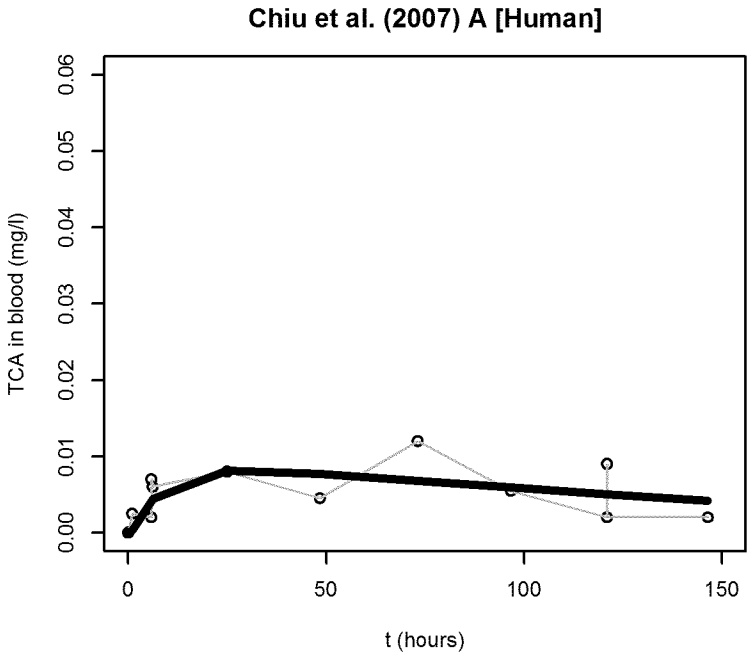
Chiu et al. (2007) A [Human]
TCA in blood (mg/l)
0.00
0.01
0.02
0.03
0.04
0.05
0.06
0
50
100
150
t (hours)

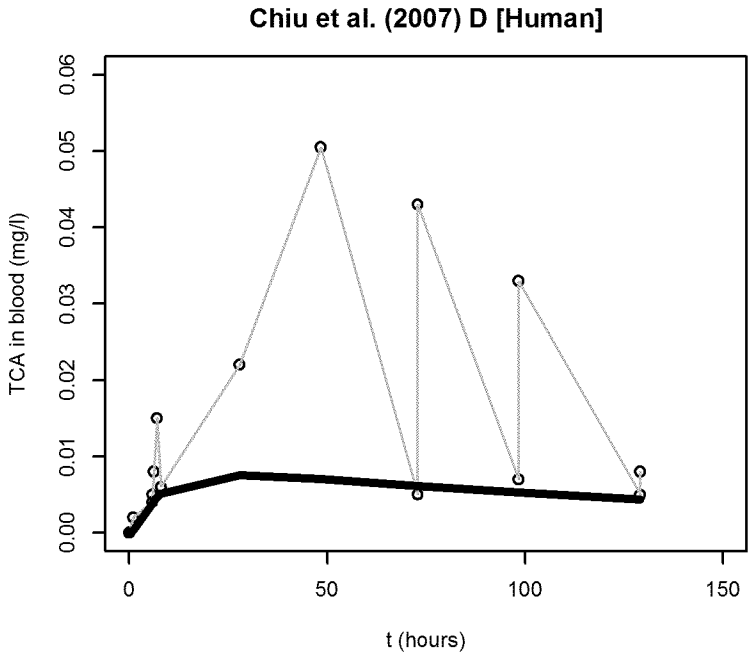
Chiu et al. (2007) D [Human]
TCA in blood (mg/l)
0.00
0.01
0.02
0.03
0.04
0.05
0.06
0
50
100
150
t (hours)

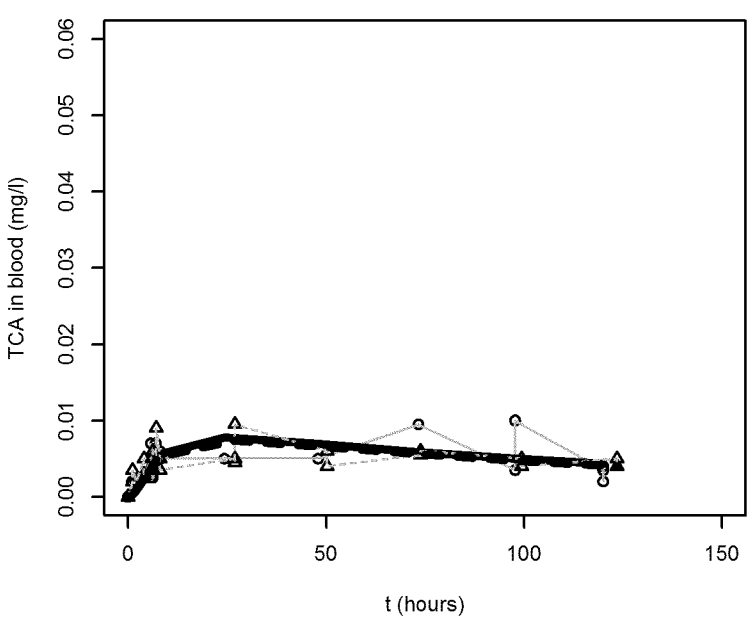
Chiu et al. (2007) B [Human]
TCA in blood (mg/l)
0.00
0.01
0.02
0.03
0.04
0.05
0.06
0
50
100
150
t (hours)

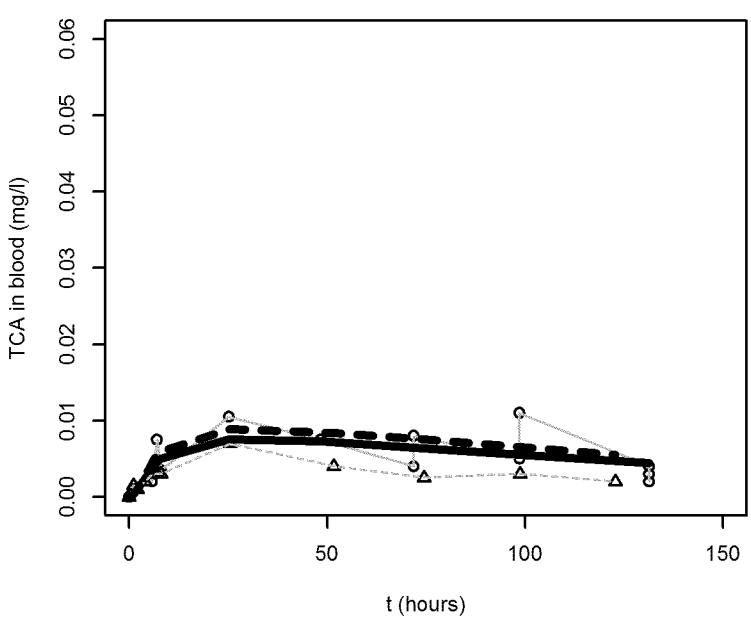
Chiu et al. (2007) E [Human]
TCA in blood (mg/l)
0.00
0.01
0.02
0.03
0.04
0.05
0.06
0
50
100
150
t (hours)

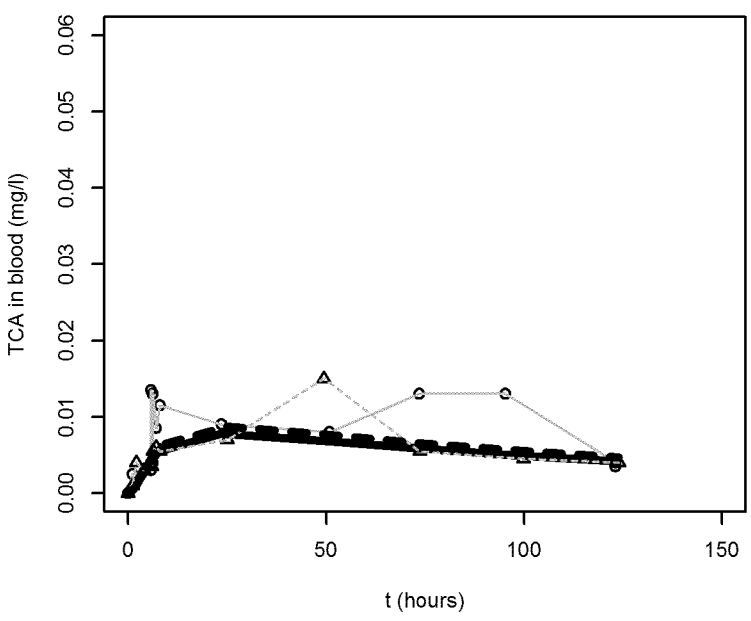
Chiu et al. (2007) C [Human]
TCA in blood (mg/l)
0.00
0.01
0.02
0.03
0.04
0.05
0.06
0
50
100
150
t (hours)

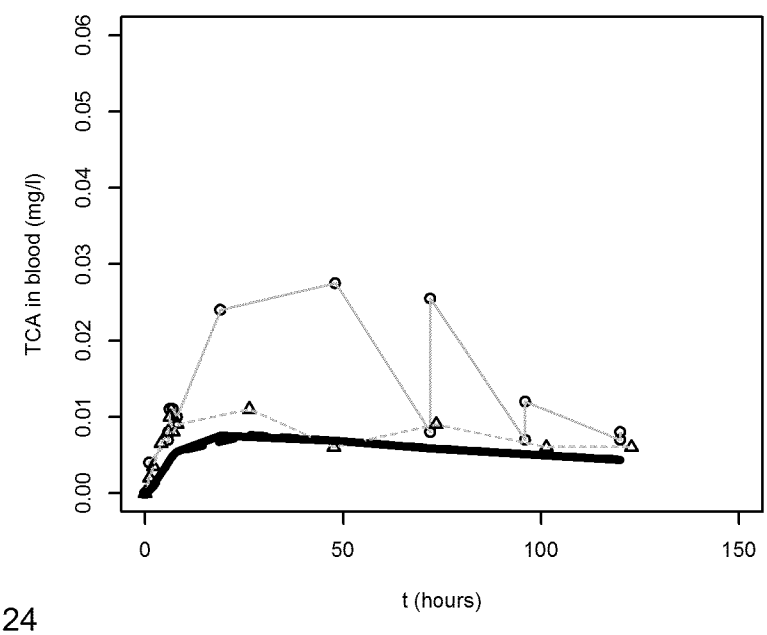
Chiu et al. (2007) F [Human]
TCA in blood (mg/l)
0.00
0.01
0.02
0.03
0.04
0.05
0.06
0
50
100
150
t (hours)

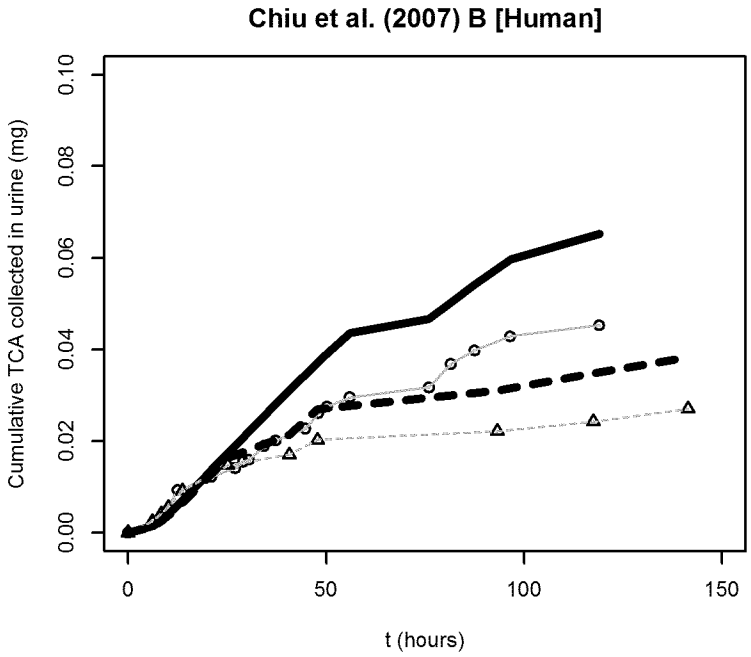
Chiu et al. (2007) B [Human]
Cumulative TCA collected in urine (mg)
0.00
0.02
0.04
0.06
0.08
0.10
0
50
100
150
t (hours)

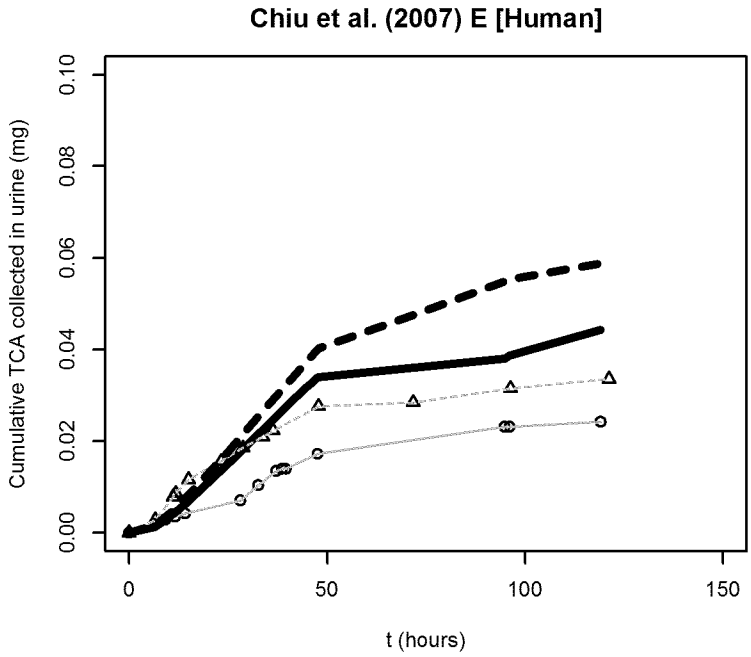
Chiu et al. (2007) E [Human]
Cumulative TCA collected in urine (mg)
0.00
0.02
0.04
0.06
0.08
0.10
0
50
100
150
t (hours)

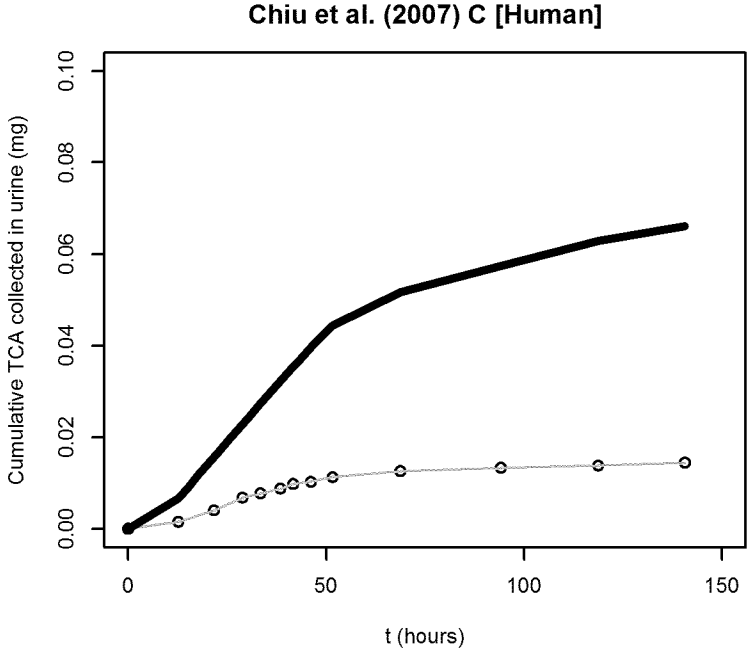
Chiu et al. (2007) C [Human]
Cumulative TCA collected in urine (mg)
0.00
0.02
0.04
0.06
0.08
0.10
0
50
100
150
t (hours)

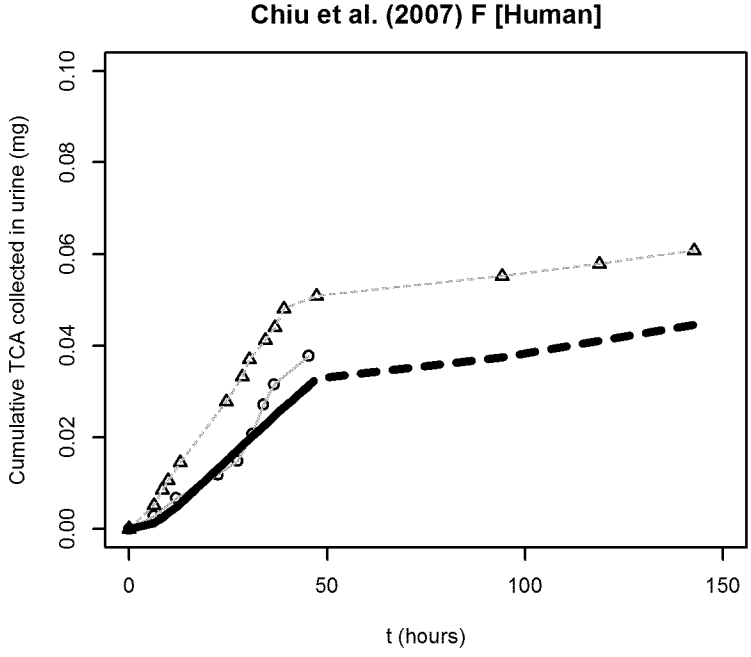
Chiu et al. (2007) F [Human]
Cumulative TCA collected in urine (mg)
0.00
0.02
0.04
0.06
0.08
0.10
0
50
100
150
t (hours)

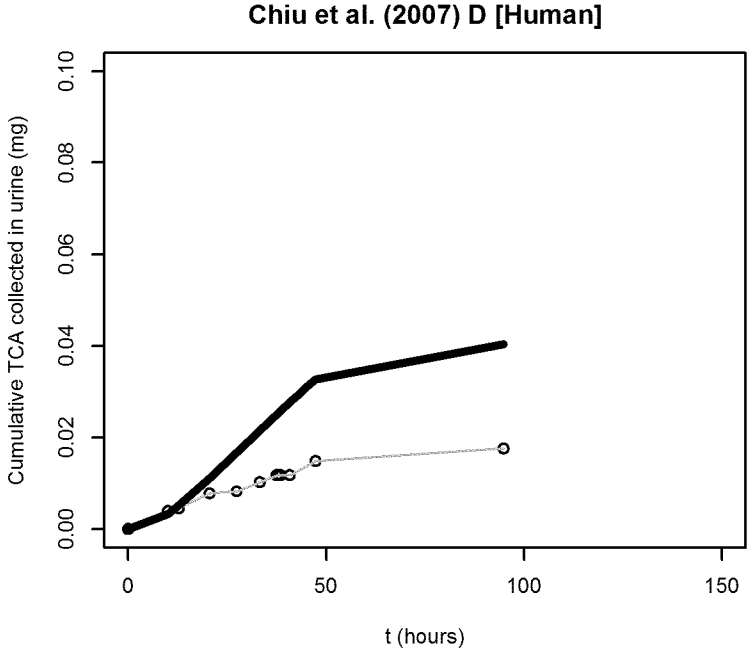
Chiu et al. (2007) D [Human]
Cumulative TCA collected in urine (mg)
0.00
0.02
0.04
0.06
0.08
0.10
0
50
100
150
t (hours)

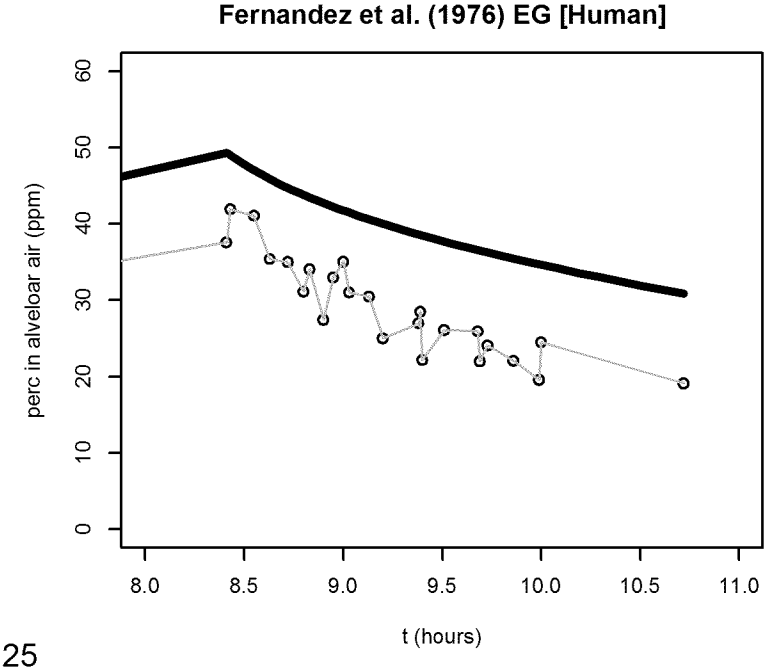
Fernandez et al. (1976) EG [Human]
perc in alveloar air (ppm)
0
10
20
30
40
50
60
8.0
8.5
9.0
9.5
10.0
10.5
11.0
t (hours)

Fernandez et al. (1976) EG [Human]

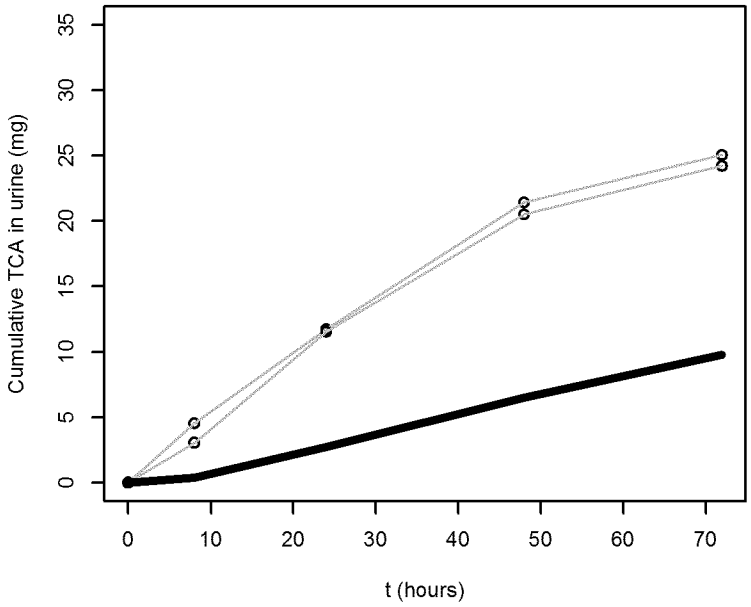

Monster et al. (1979) C [Human]

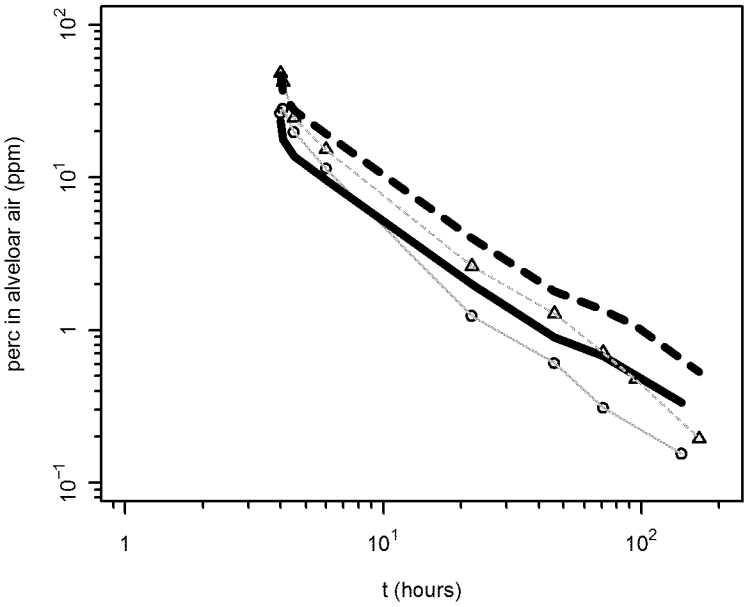

Monster et al. (1979) A [Human]

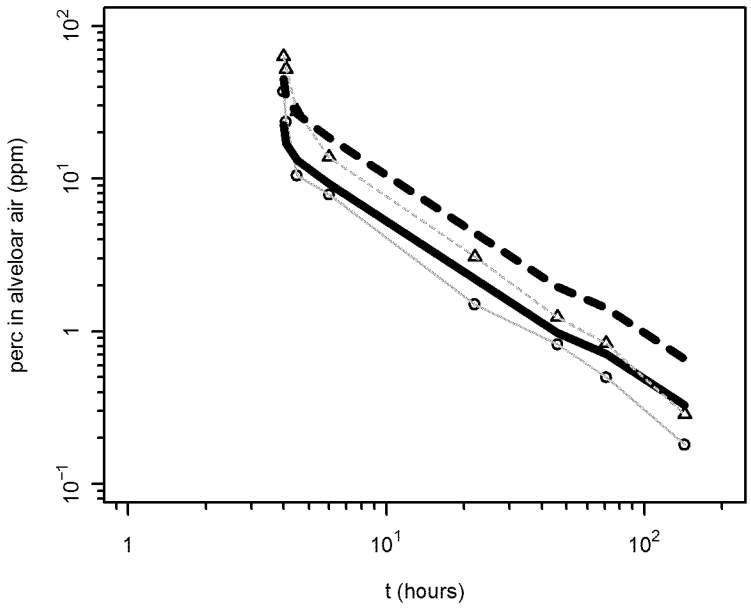

Monster et al. (1979) D [Human]

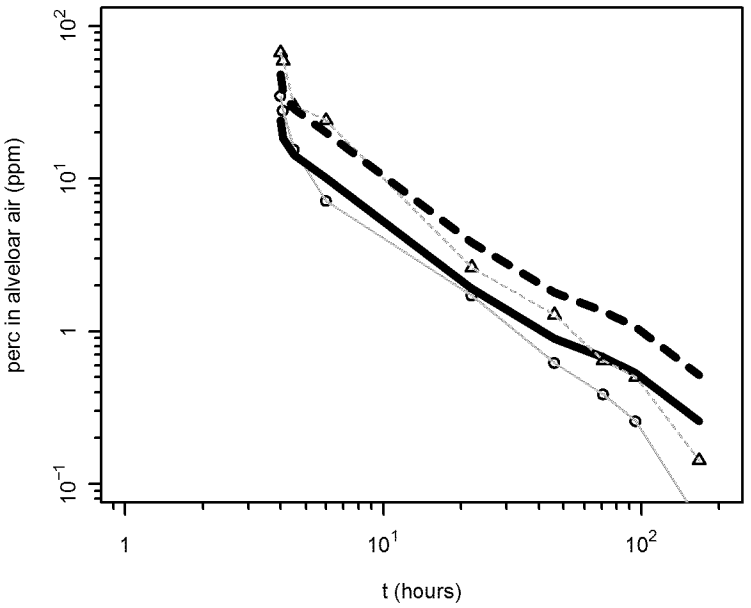

Monster et al. (1979) B [Human]

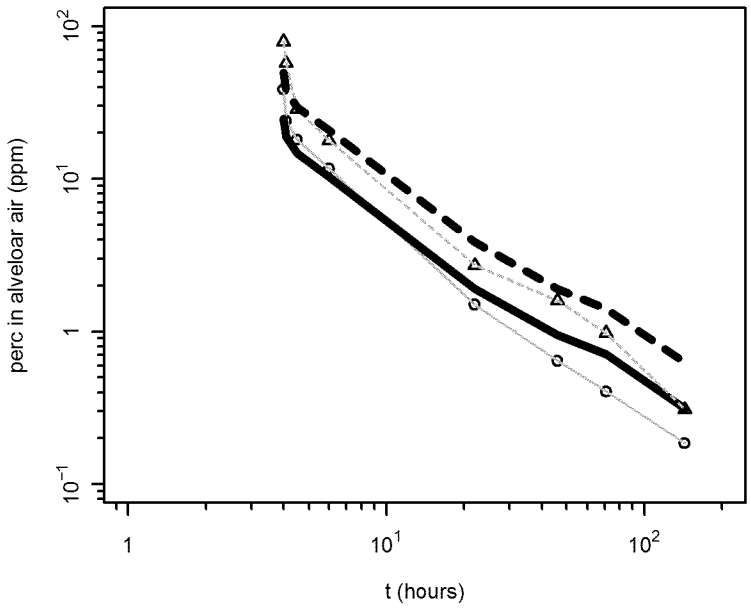

Monster et al. (1979) E [Human]

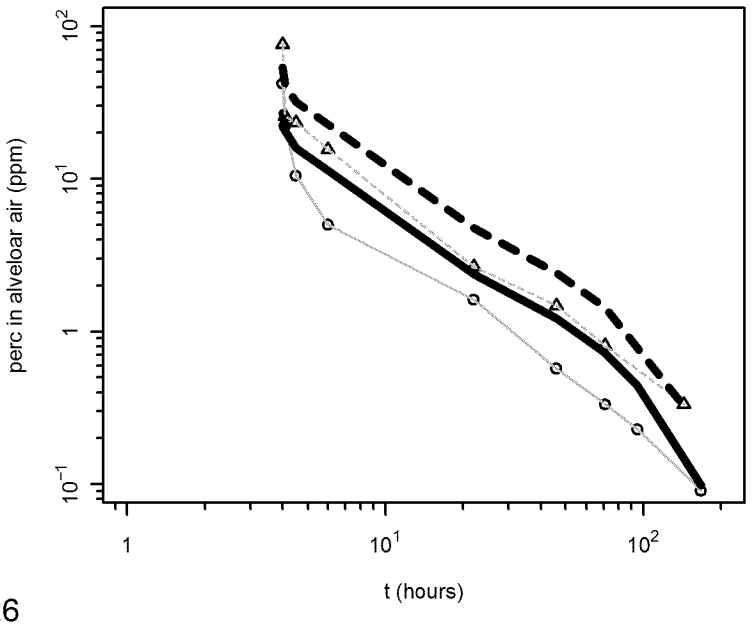

Monster et al. (1979) F [Human]

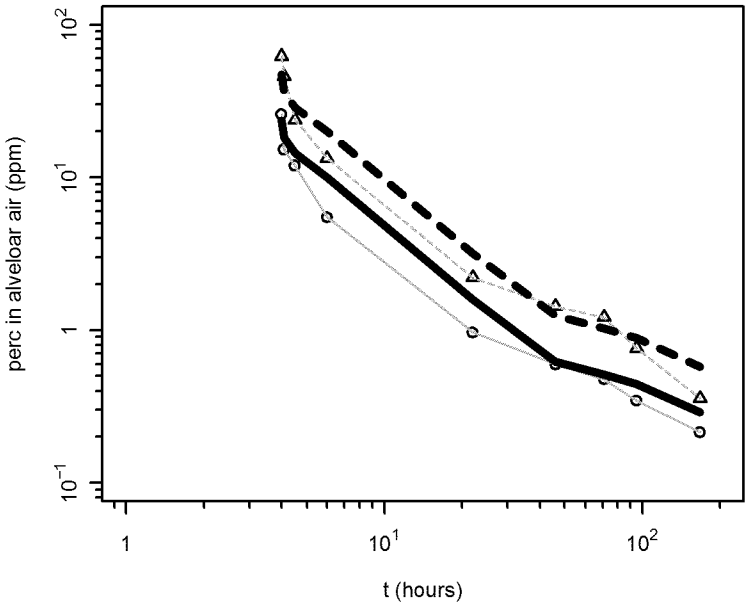

Monster et al. (1979) C [Human]

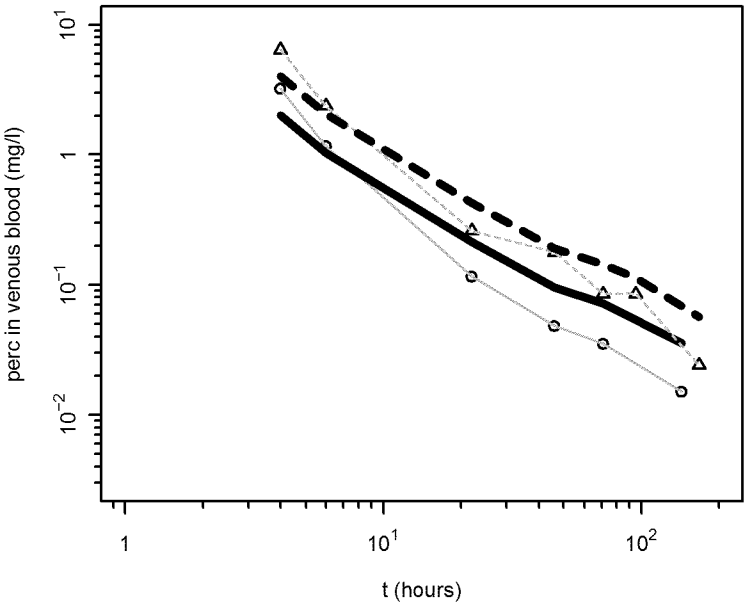

Monster et al. (1979) A [Human]

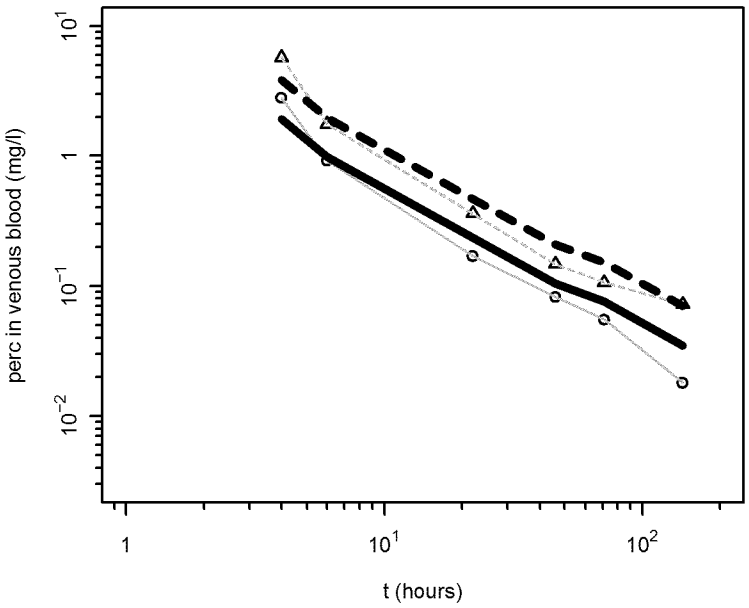

Monster et al. (1979) D [Human]

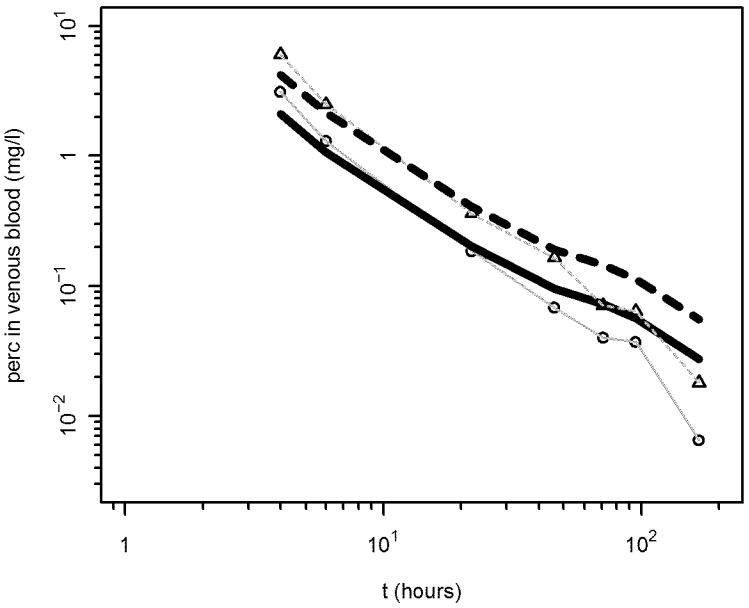

Monster et al. (1979) B [Human]

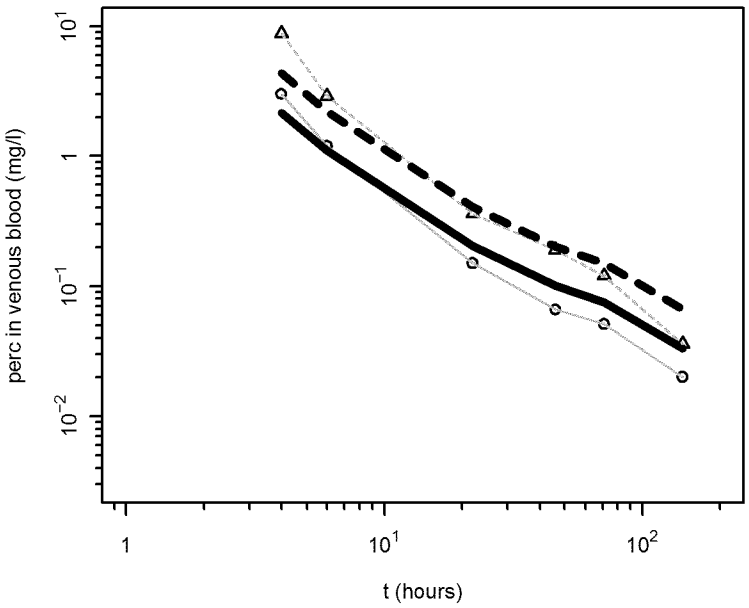

Monster et al. (1979) E [Human]

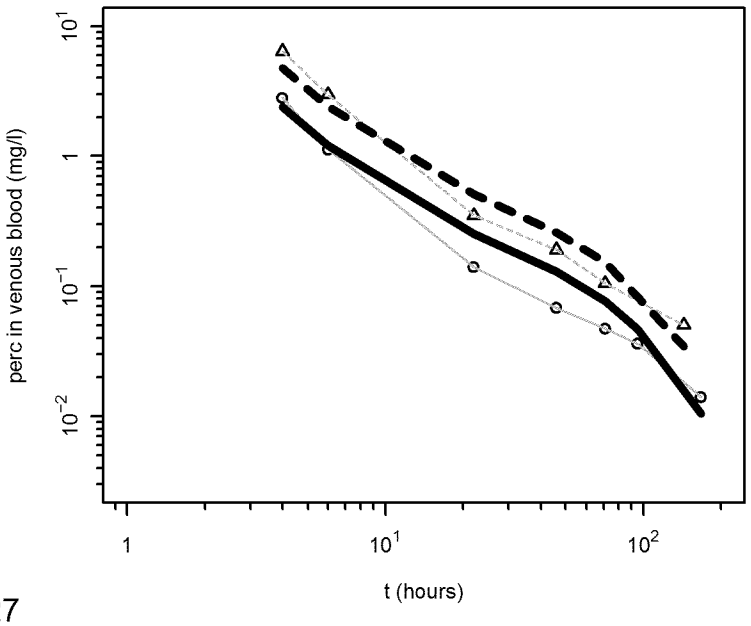

Monster et al. (1979) F [Human]

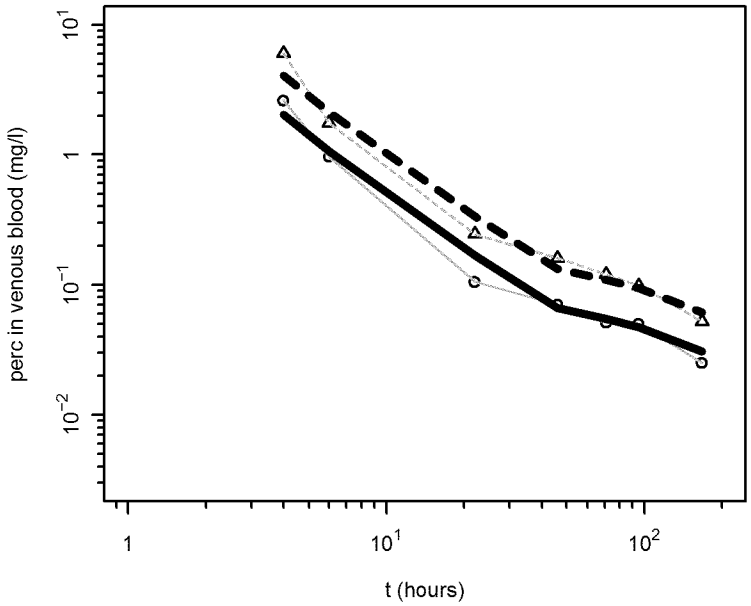

Monster et al. (1979) C [Human]

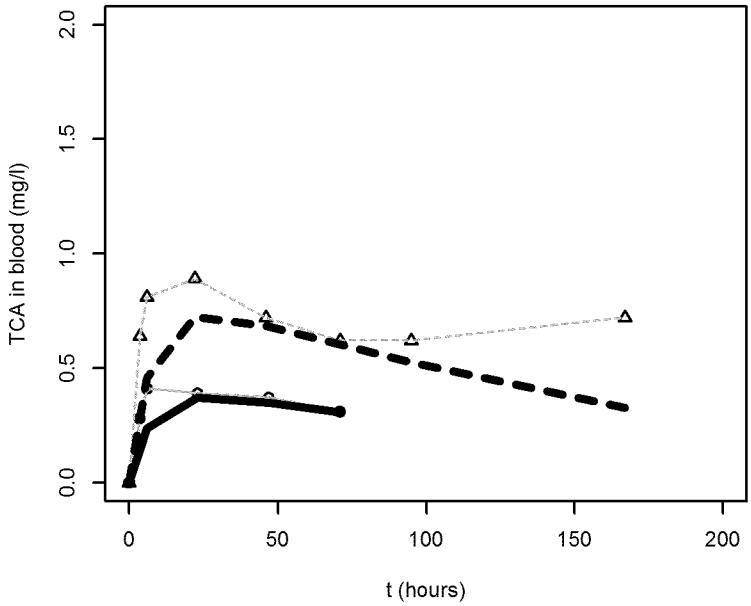

Monster et al. (1979) A [Human]

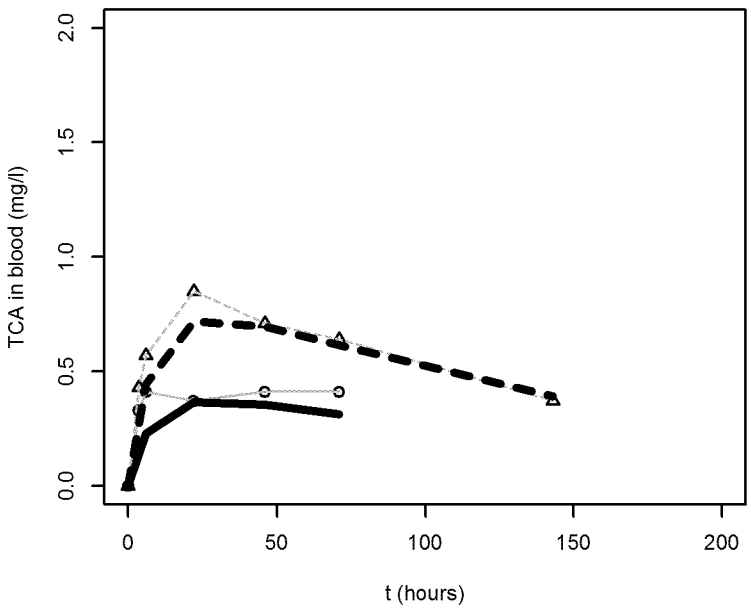

Monster et al. (1979) D [Human]

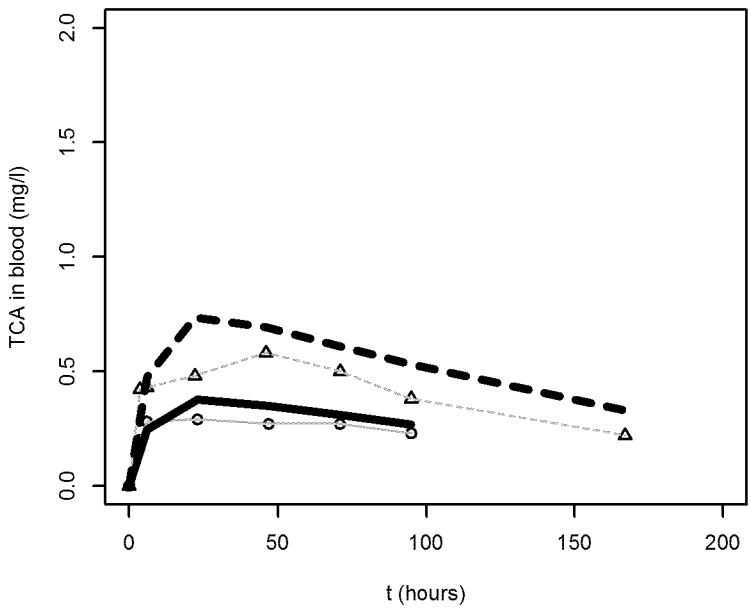

Monster et al. (1979) B [Human]

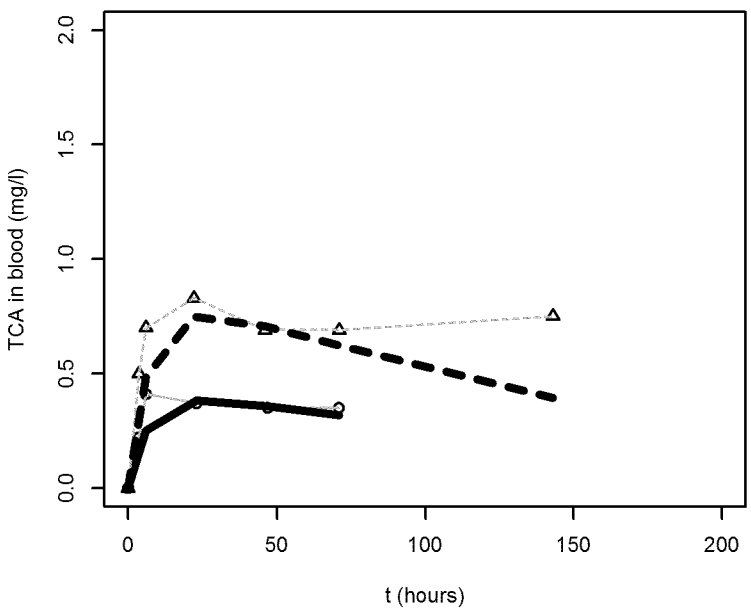

Monster et al. (1979) E [Human]

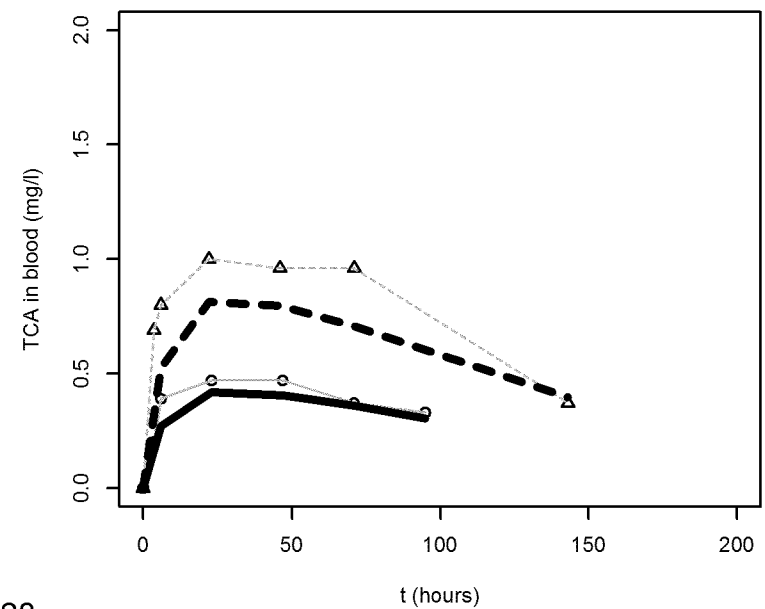

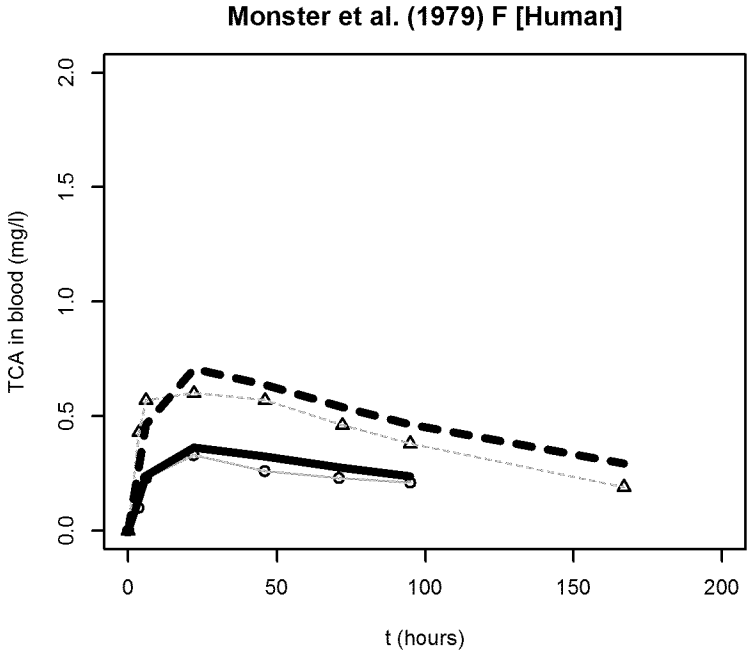
Monster et al. (1979) F [Human]
TCA in blood (mg/l)
t (hours)

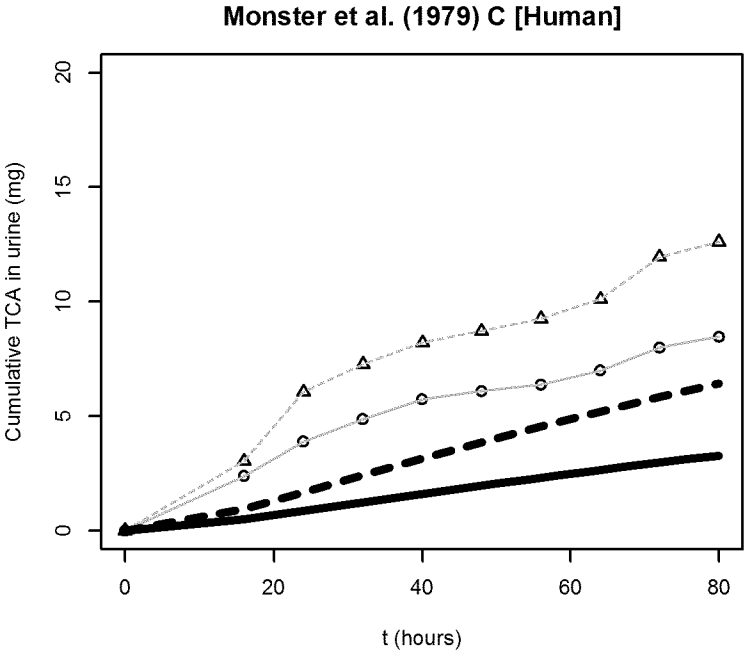
Monster et al. (1979) C [Human]
Cumulative TCA in urine (mg)
t (hours)

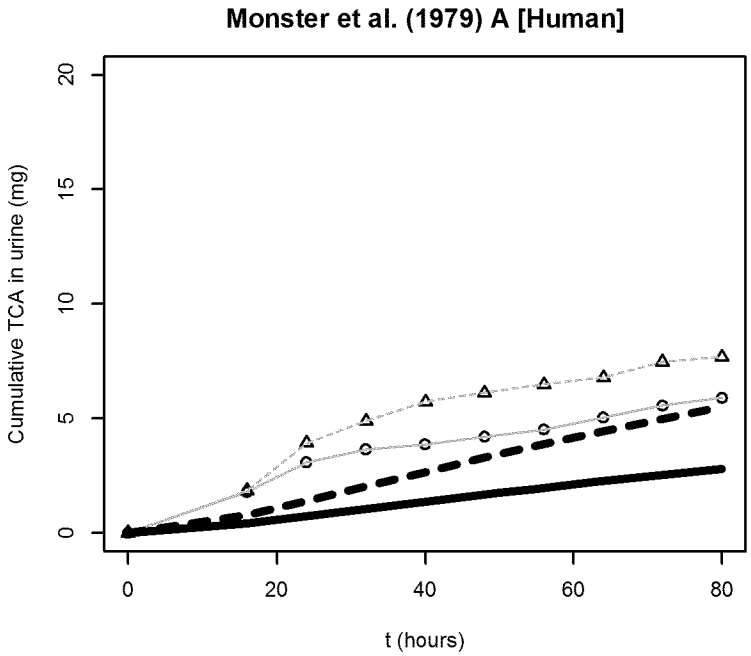
Monster et al. (1979) A [Human]
Cumulative TCA in urine (mg)
t (hours)

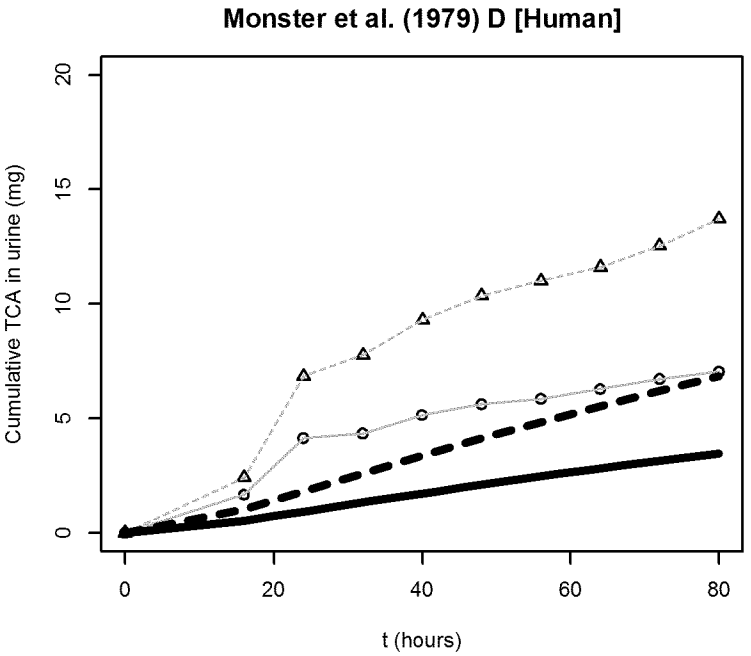
Monster et al. (1979) D [Human]
Cumulative TCA in urine (mg)
t (hours)

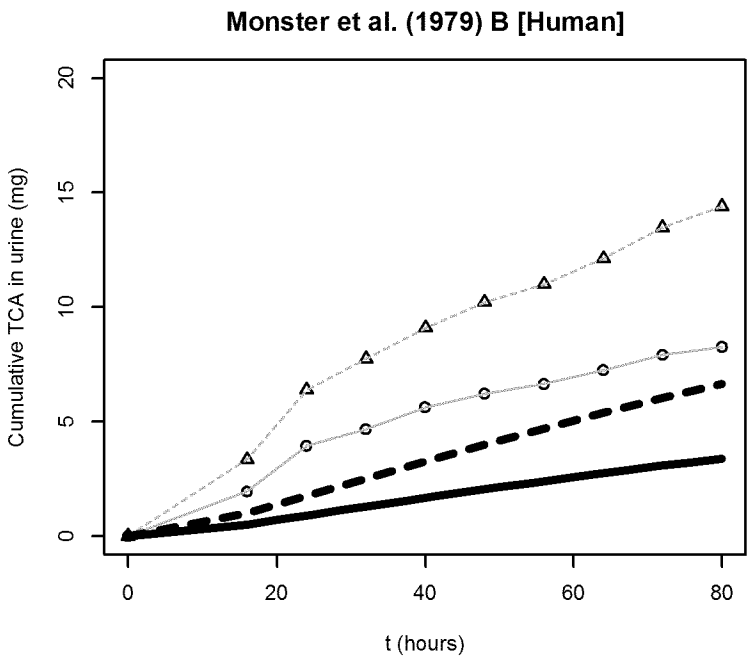
Monster et al. (1979) B [Human]
Cumulative TCA in urine (mg)
t (hours)

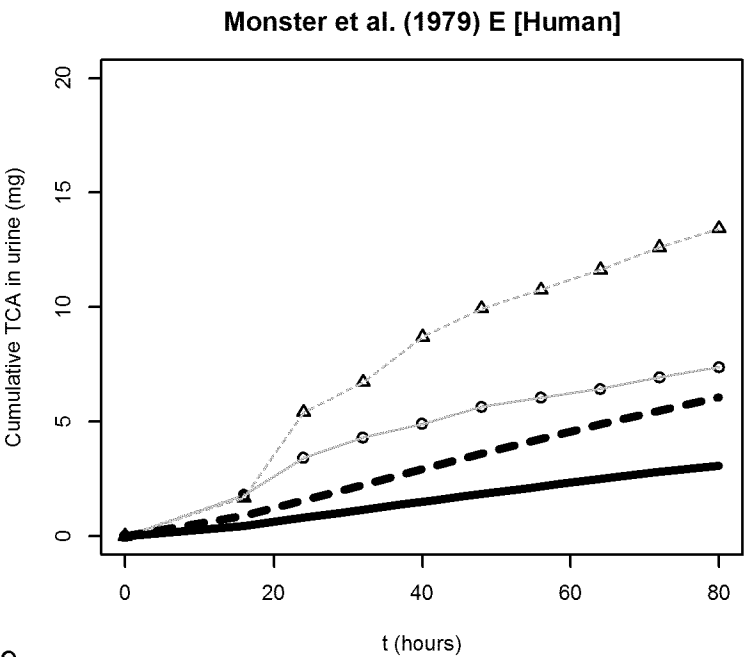
Monster et al. (1979) E [Human]
Cumulative TCA in urine (mg)
t (hours)

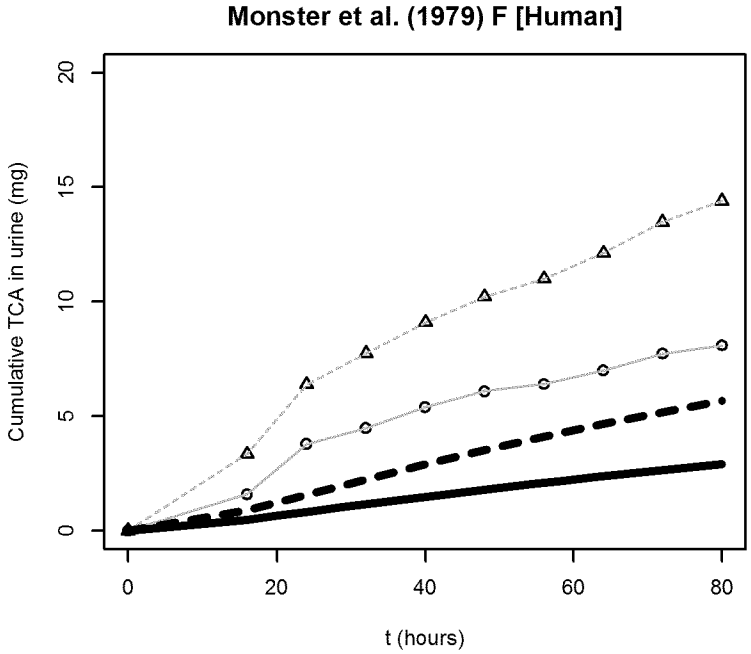
Monster et al. (1979) F [Human]
Cumulative TCA in urine (mg)
t (hours)

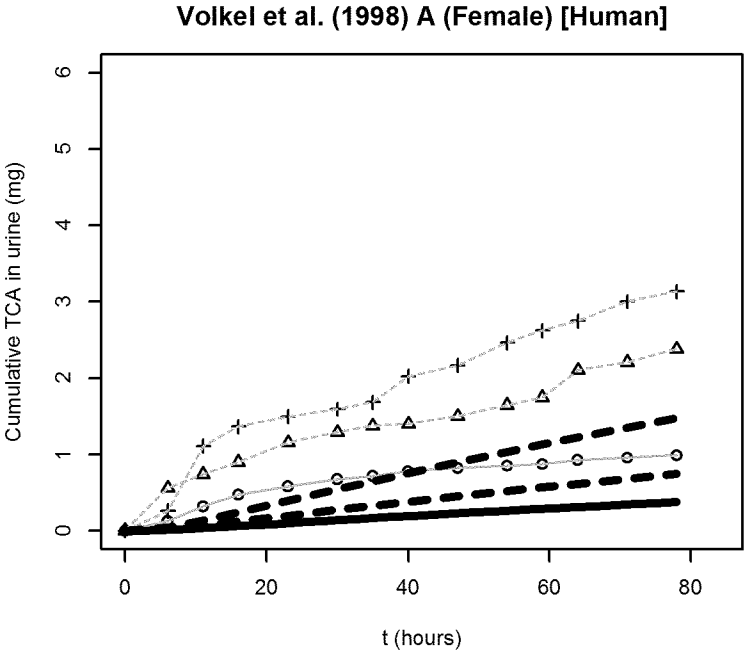
Volkel et al. (1998) A (Female) [Human]
Cumulative TCA in urine (mg)
t (hours)

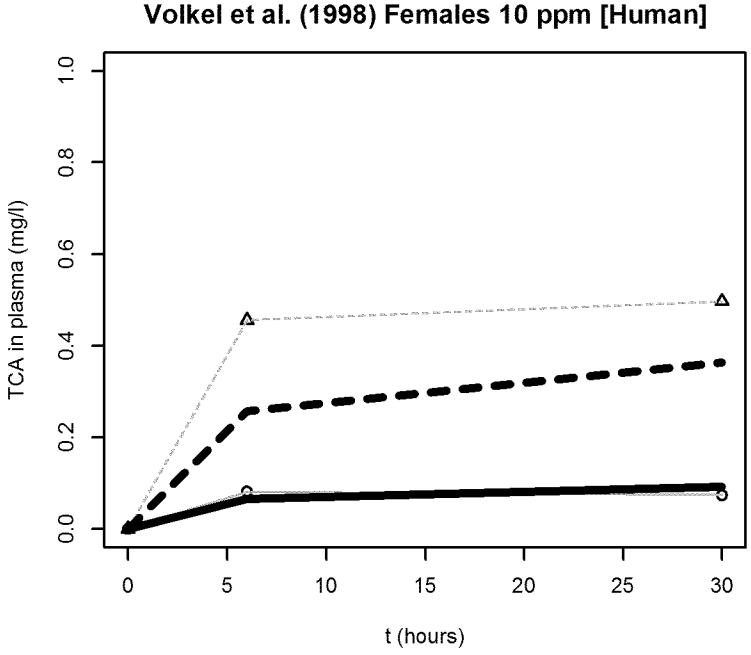
Volkel et al. (1998) Females 10 ppm [Human]
TCA in plasma (mg/l)
t (hours)

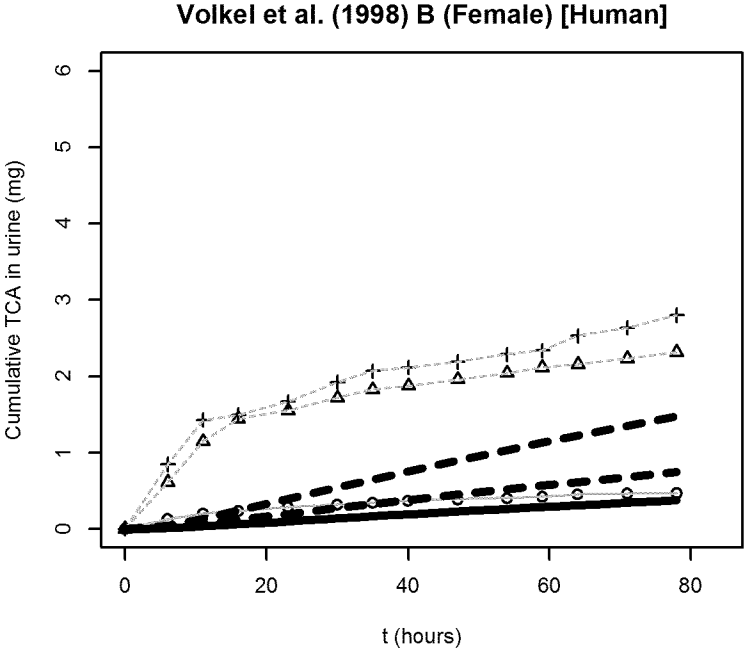
Volkel et al. (1998) B (Female) [Human]
Cumulative TCA in urine (mg)
t (hours)

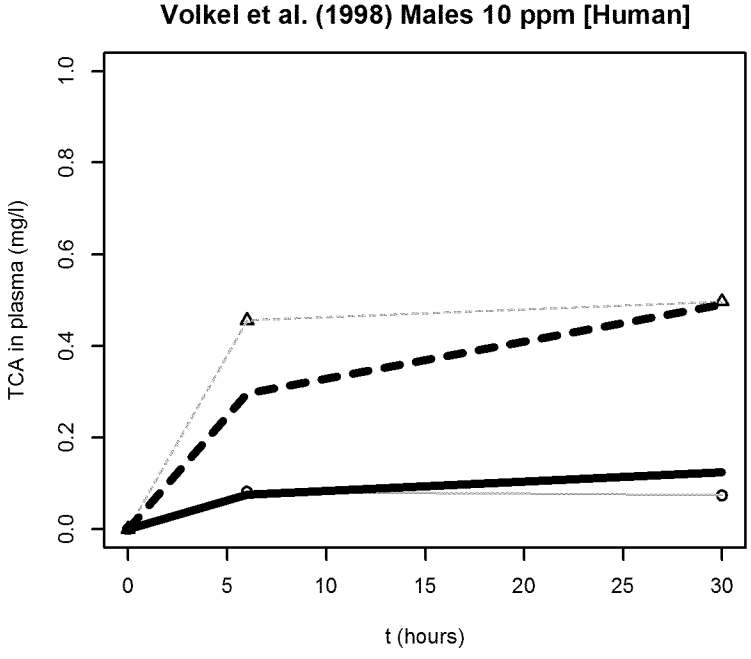
Volkel et al. (1998) Males 10 ppm [Human]
TCA in plasma (mg/l)
t (hours)

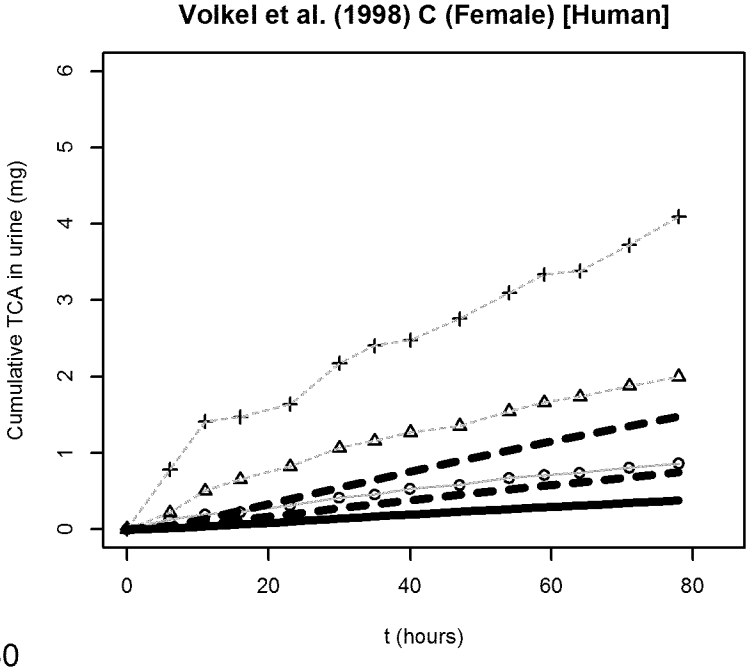
Volkel et al. (1998) C (Female) [Human]
Cumulative TCA in urine (mg)
t (hours)

Volkel et al. (1998) D (Male) [Human]

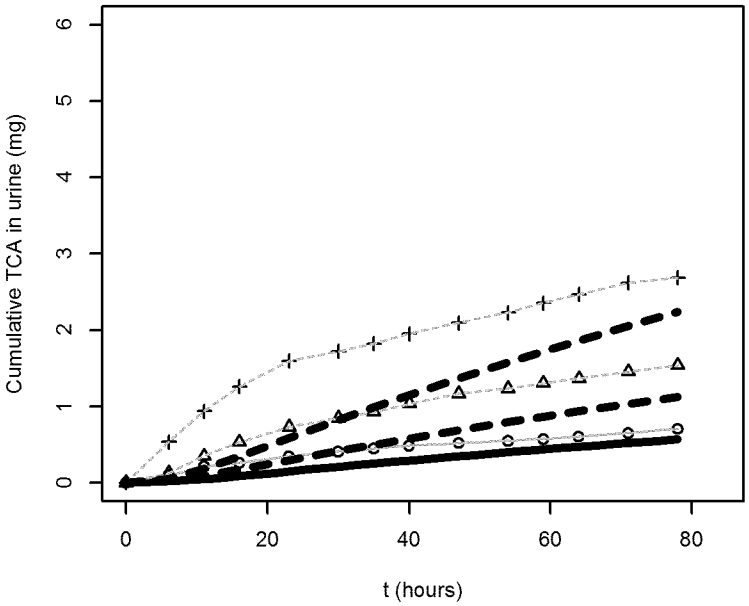

Volkel et al. (1998) E (Male) [Human]

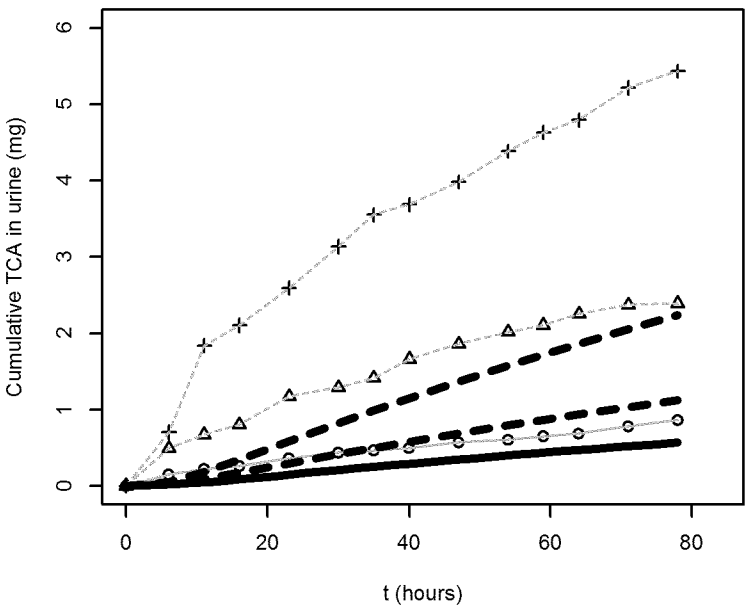

Volkel et al. (1998) F (Male) [Human]

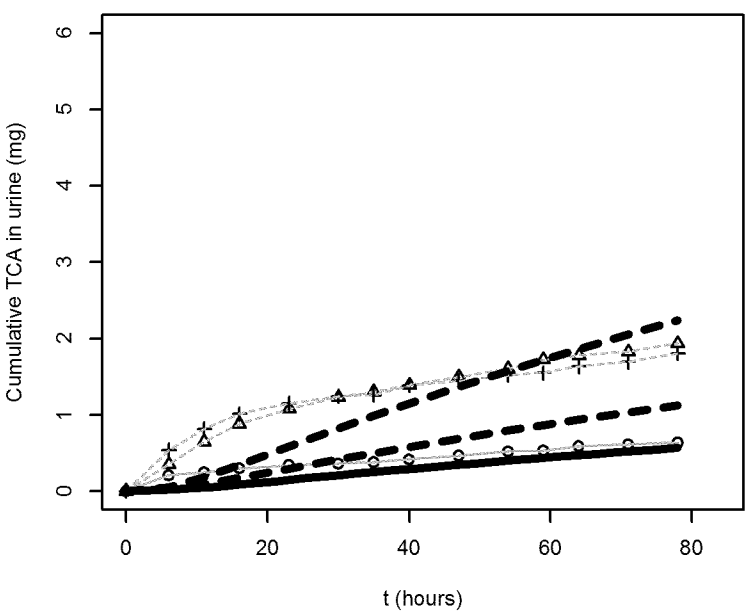

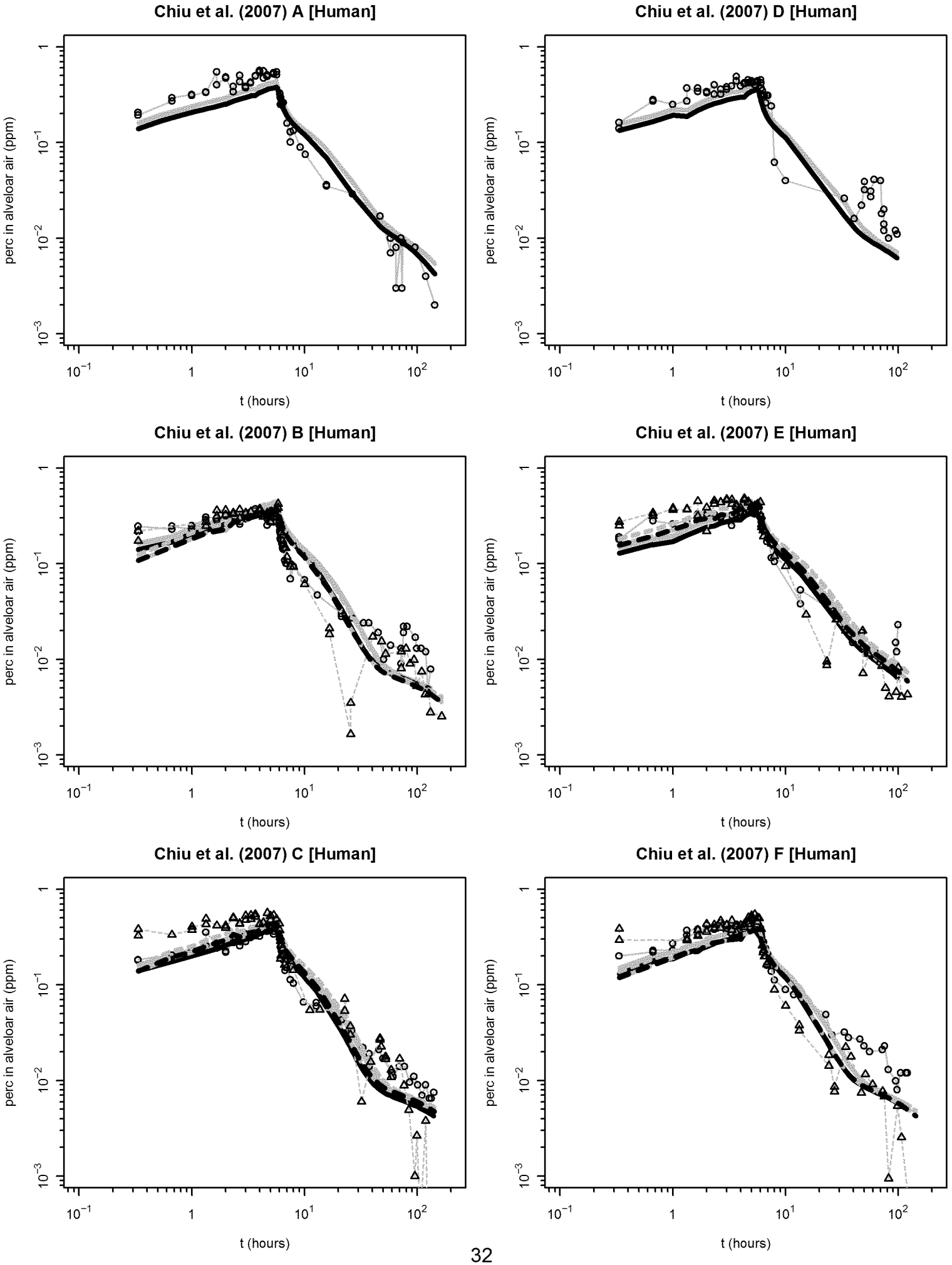
Chiu et al. (2007) A [Human]
Chiu et al. (2007) D [Human]
Chiu et al. (2007) B [Human]
Chiu et al. (2007) E [Human]
Chiu et al. (2007) C [Human]
Chiu et al. (2007) F [Human]
perc in alveloar air (ppm)
t (hours)

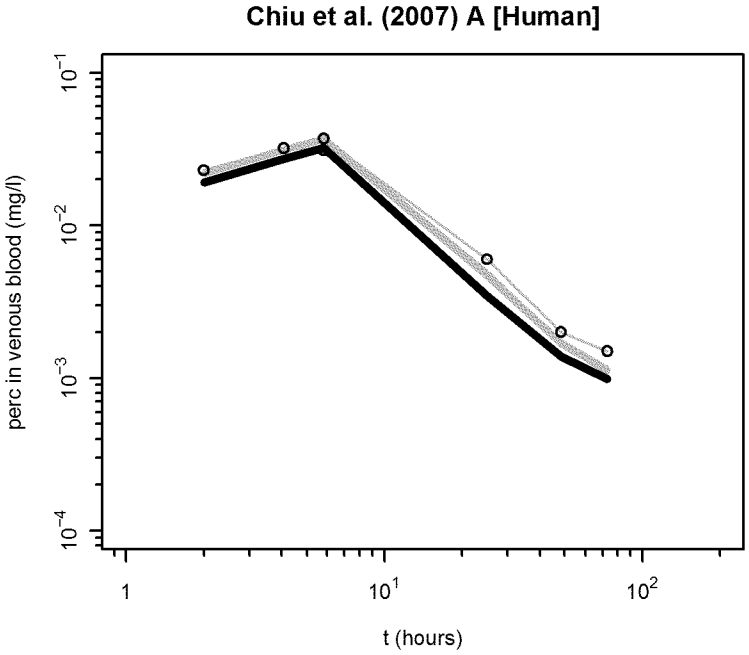
Chiu et al. (2007) A [Human]
perc in venous blood (mg/l)
t (hours)

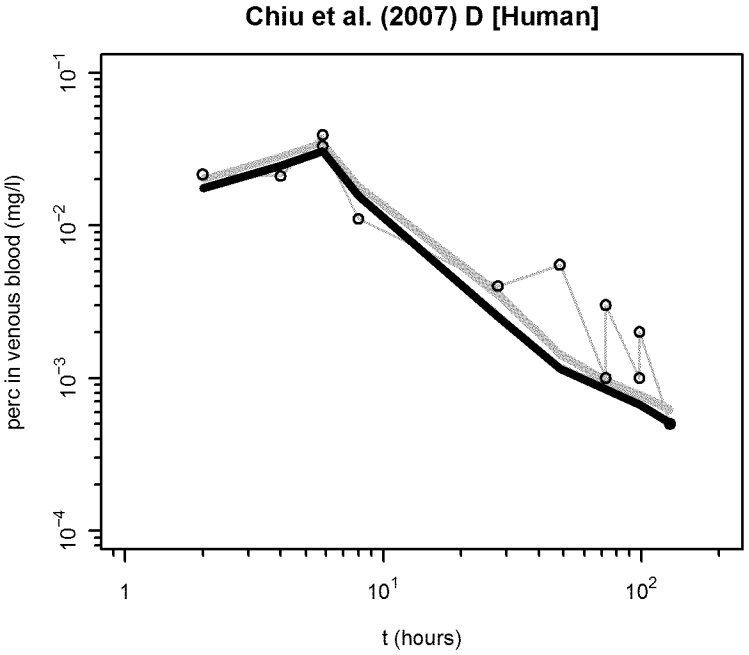
Chiu et al. (2007) D [Human]
perc in venous blood (mg/l)
t (hours)

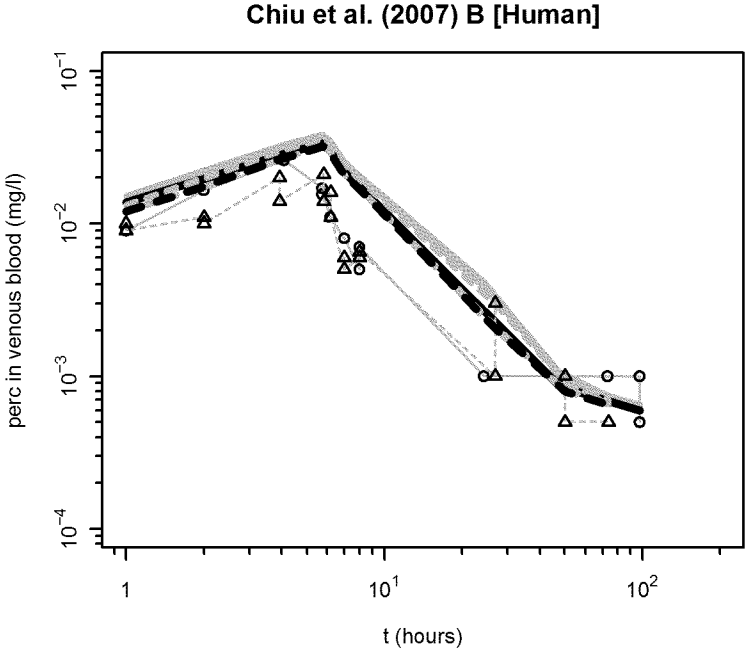
Chiu et al. (2007) B [Human]
perc in venous blood (mg/l)
t (hours)

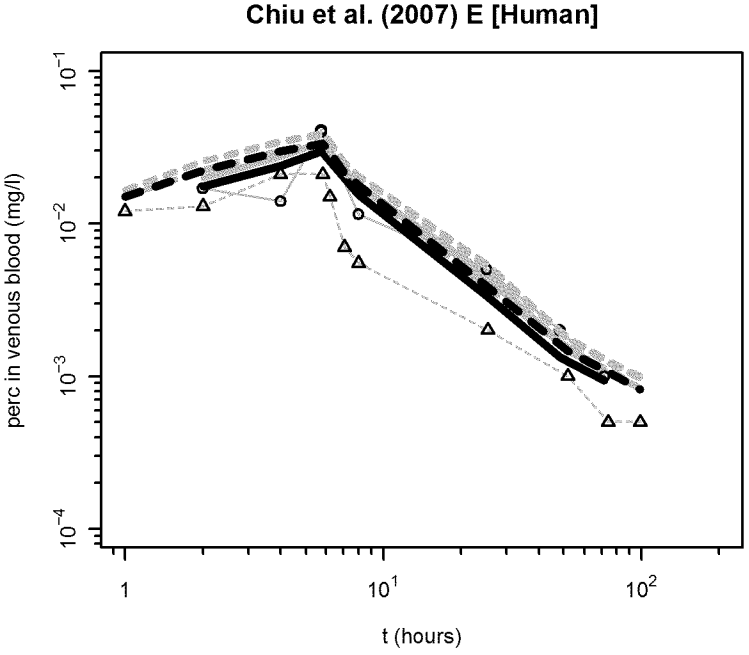
Chiu et al. (2007) E [Human]
perc in venous blood (mg/l)
t (hours)

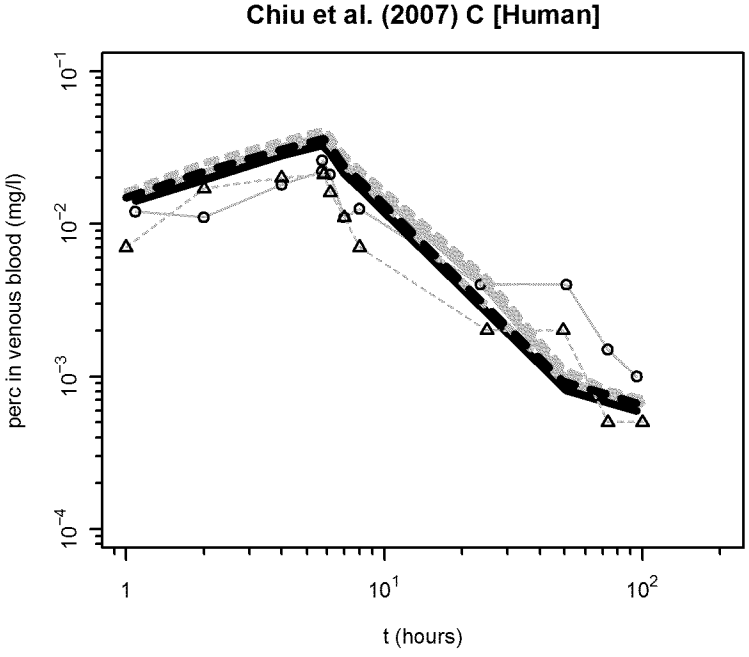
Chiu et al. (2007) C [Human]
perc in venous blood (mg/l)
t (hours)

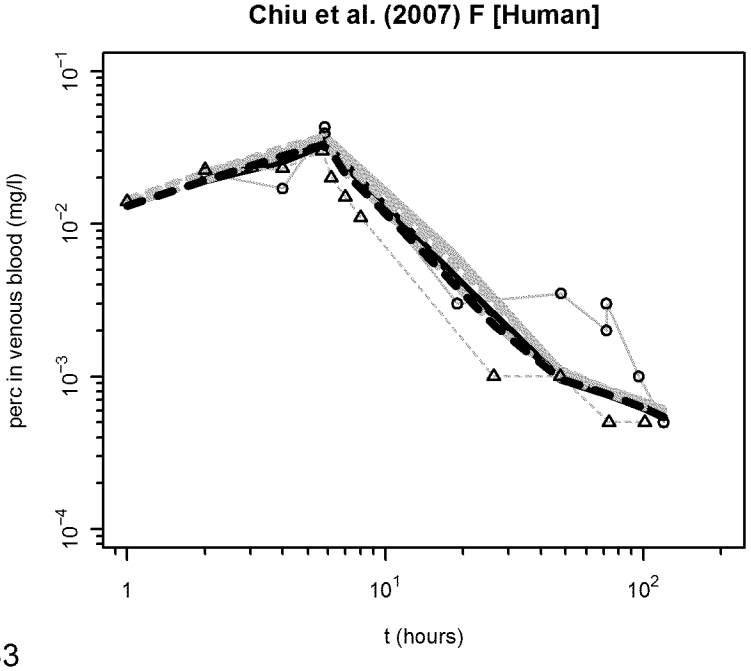
Chiu et al. (2007) F [Human]
perc in venous blood (mg/l)
t (hours)

Human calibration

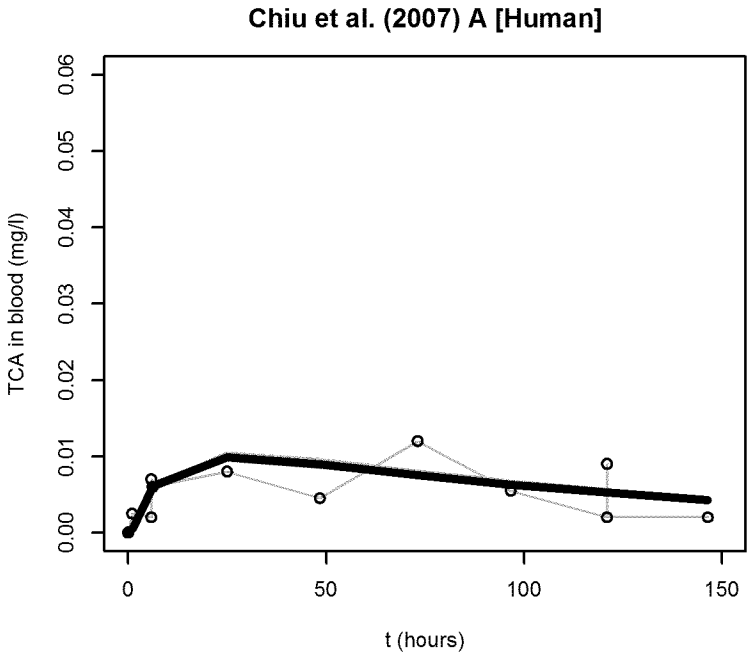

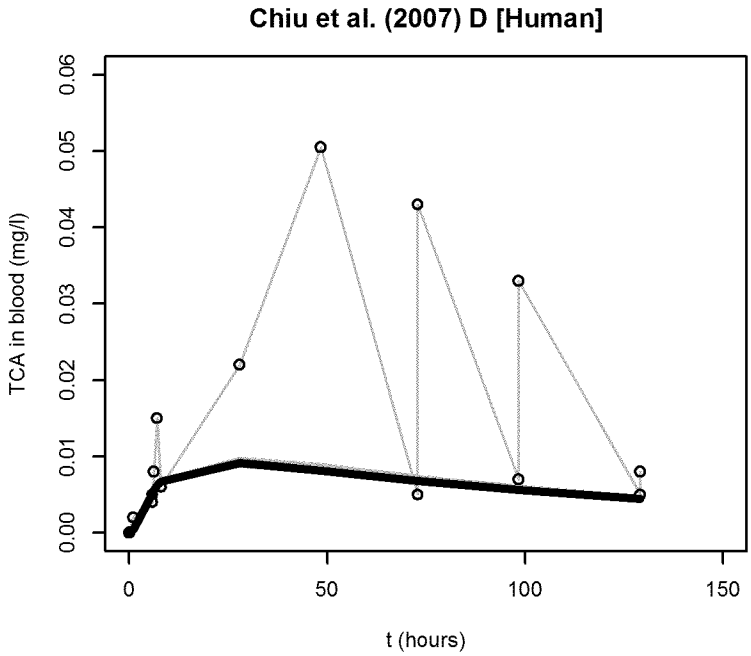

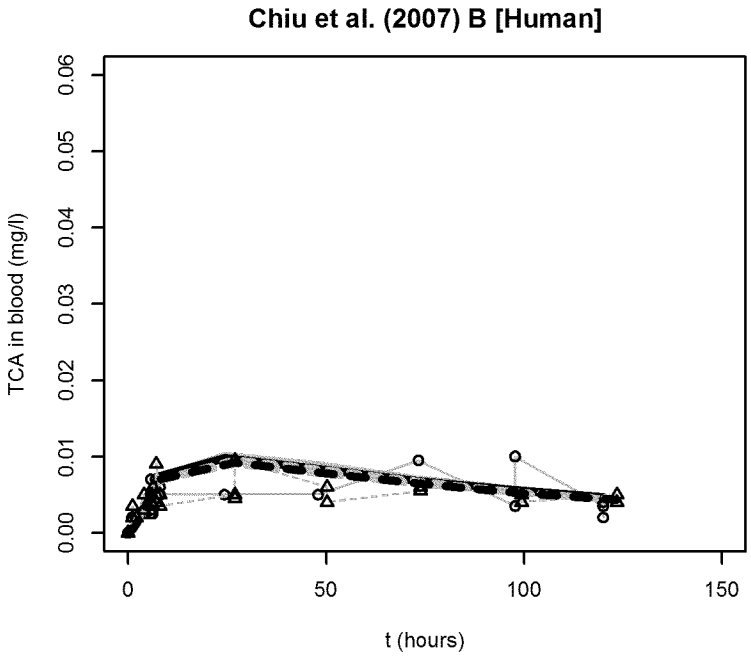

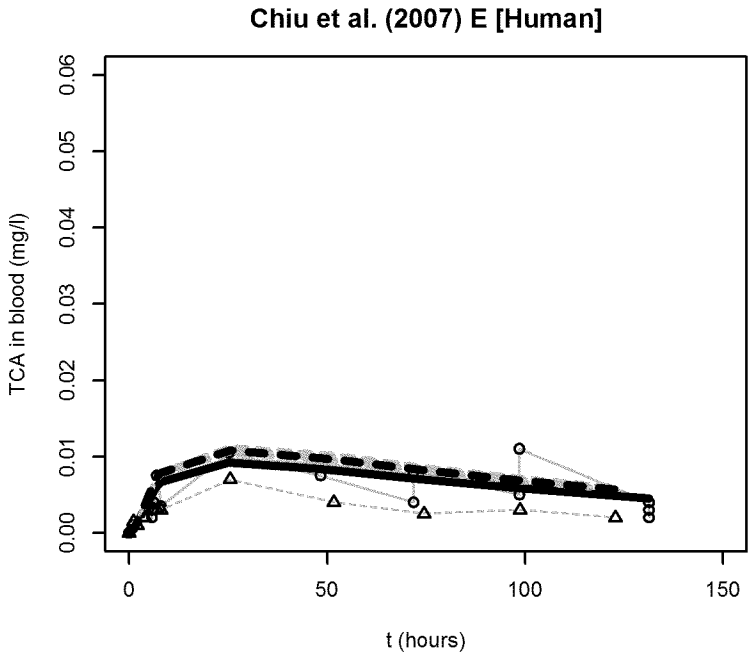

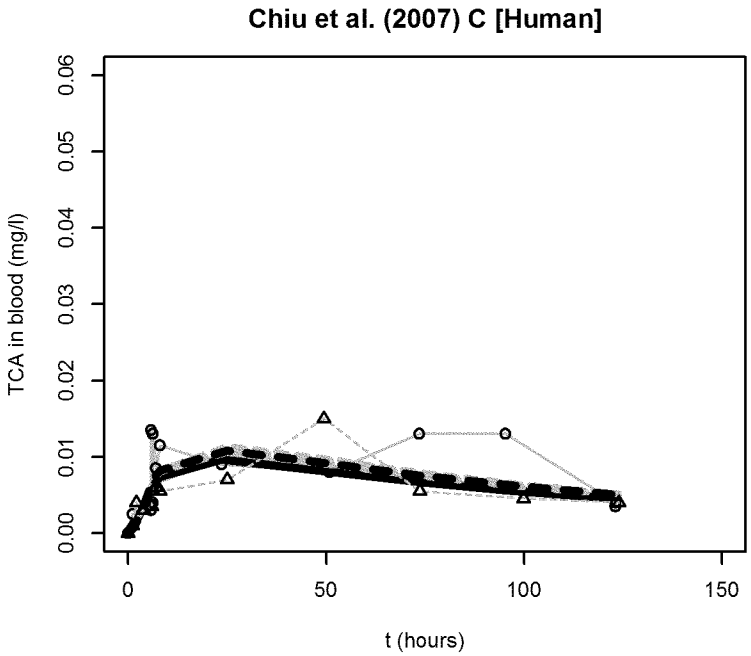

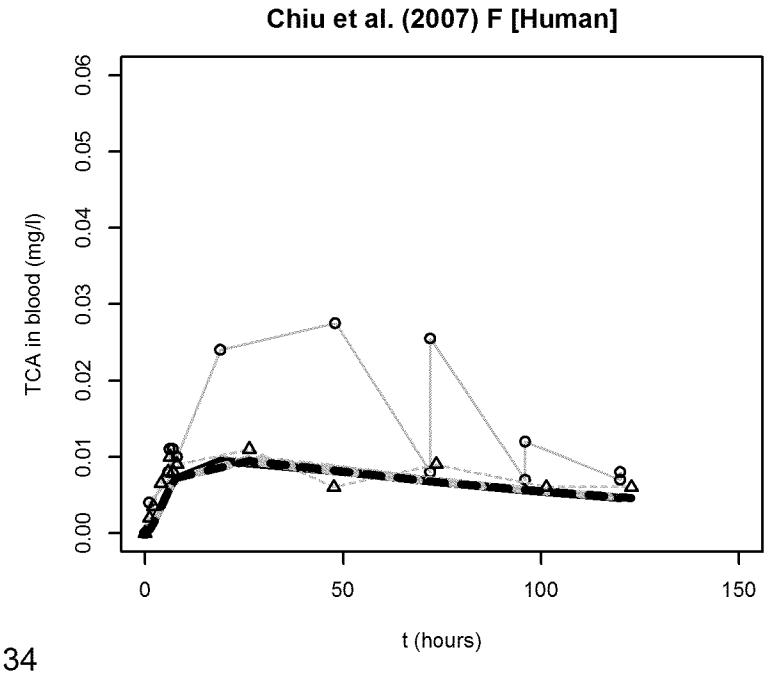

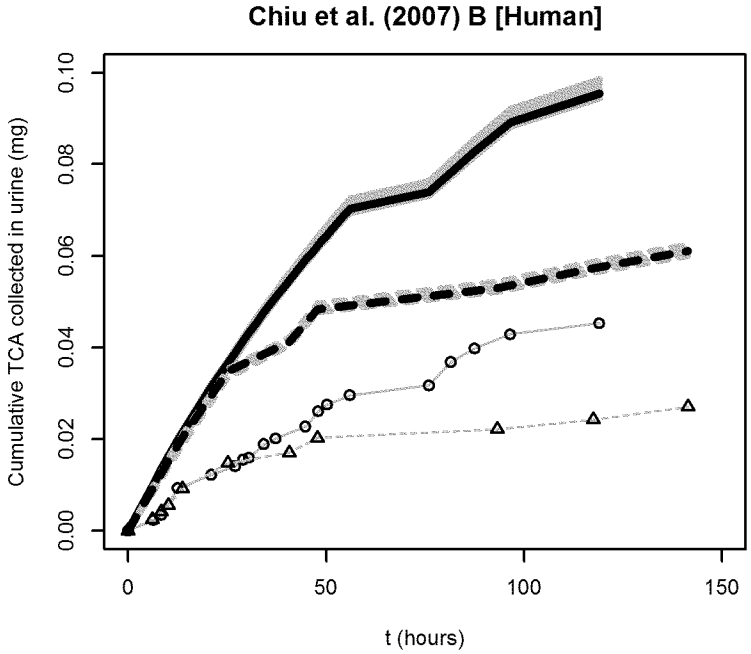
Chiu et al. (2007) B [Human]
Cumulative TCA collected in urine (mg)
0.00
0.02
0.04
0.06
0.08
0.10
0
50
100
150
t (hours)

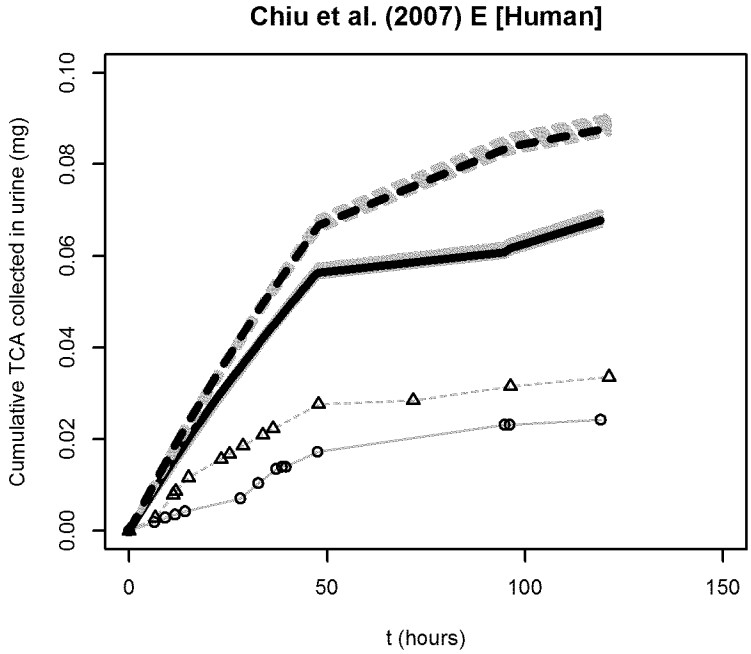
Chiu et al. (2007) E [Human]
Cumulative TCA collected in urine (mg)
0.00
0.02
0.04
0.06
0.08
0.10
0
50
100
150
t (hours)

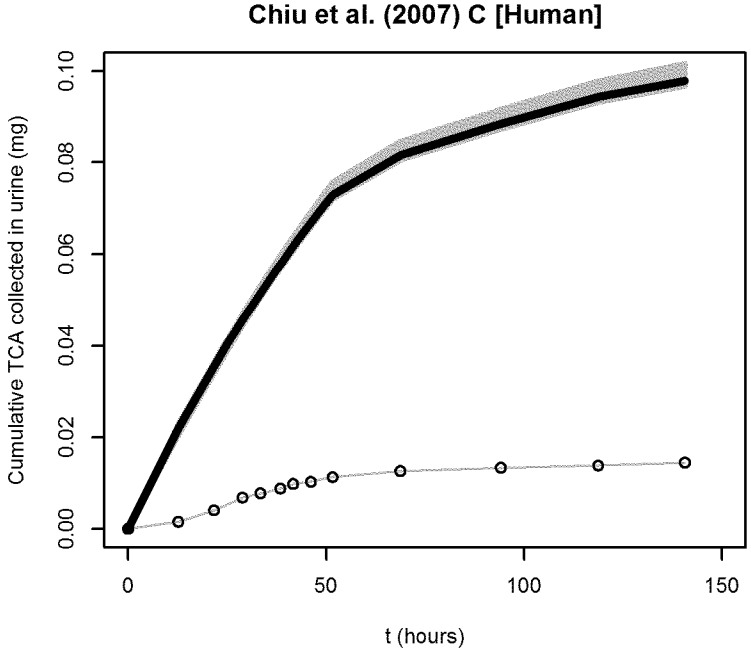
Chiu et al. (2007) C [Human]
Cumulative TCA collected in urine (mg)
0.00
0.02
0.04
0.06
0.08
0.10
0
50
100
150
t (hours)

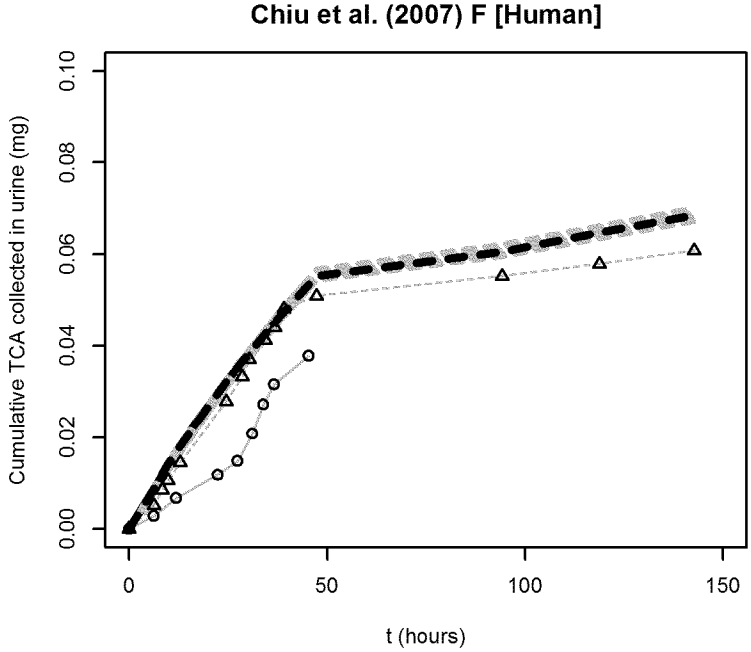
Chiu et al. (2007) F [Human]
Cumulative TCA collected in urine (mg)
0.00
0.02
0.04
0.06
0.08
0.10
0
50
100
150
t (hours)

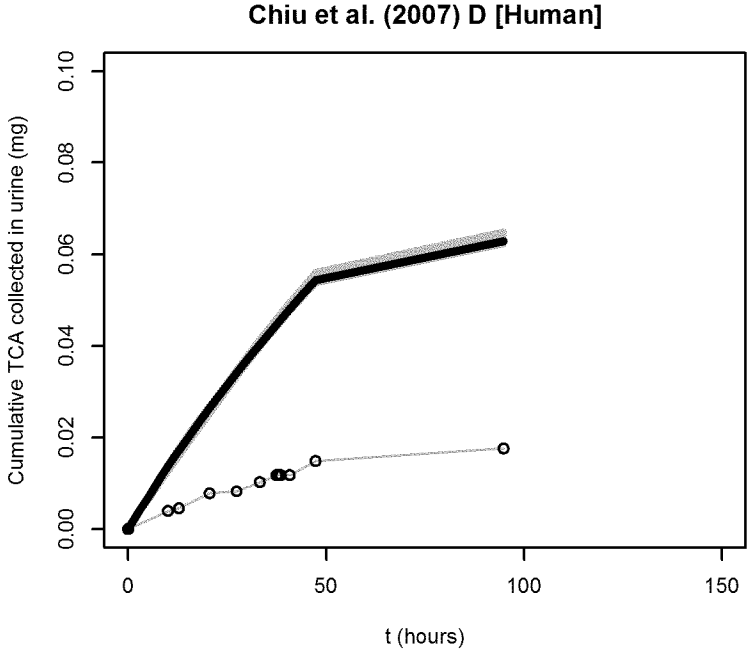
Chiu et al. (2007) D [Human]
Cumulative TCA collected in urine (mg)
0.00
0.02
0.04
0.06
0.08
0.10
0
50
100
150
t (hours)

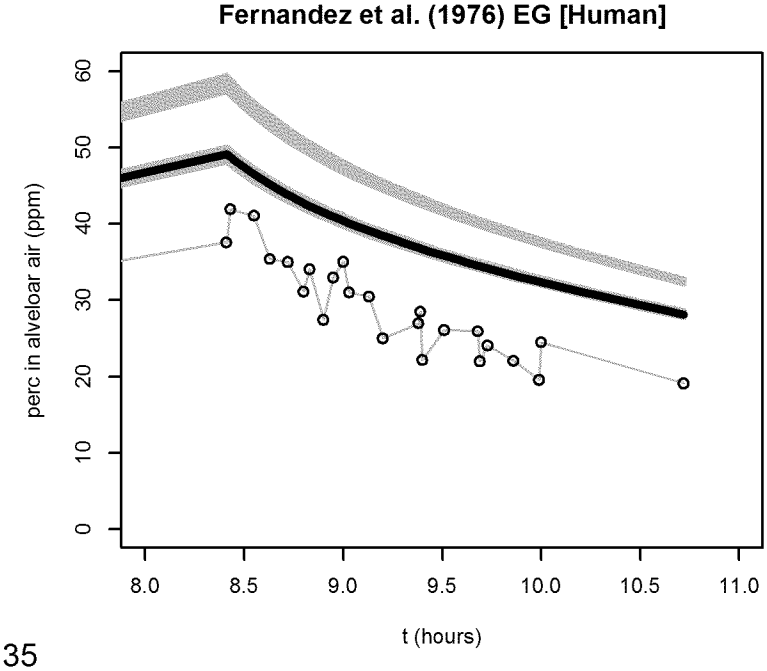
Fernandez et al. (1976) EG [Human]
perc in alveloar air (ppm)
0
10
20
30
40
50
60
8.0
8.5
9.0
9.5
10.0
10.5
11.0
t (hours)

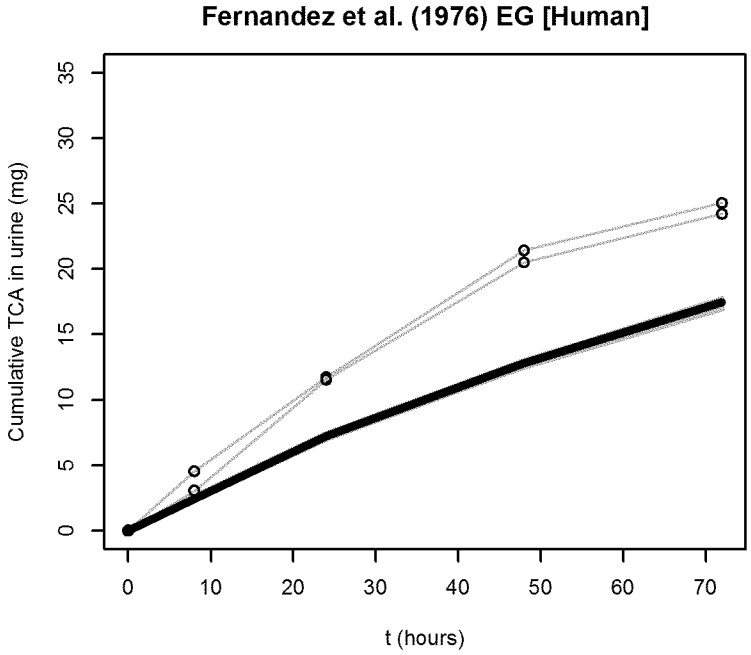
Fernandez et al. (1976) EG [Human]
Cumulative TCA in urine (mg)
0
5
10
15
20
25
30
35
0
10
20
30
40
50
60
70
t (hours)

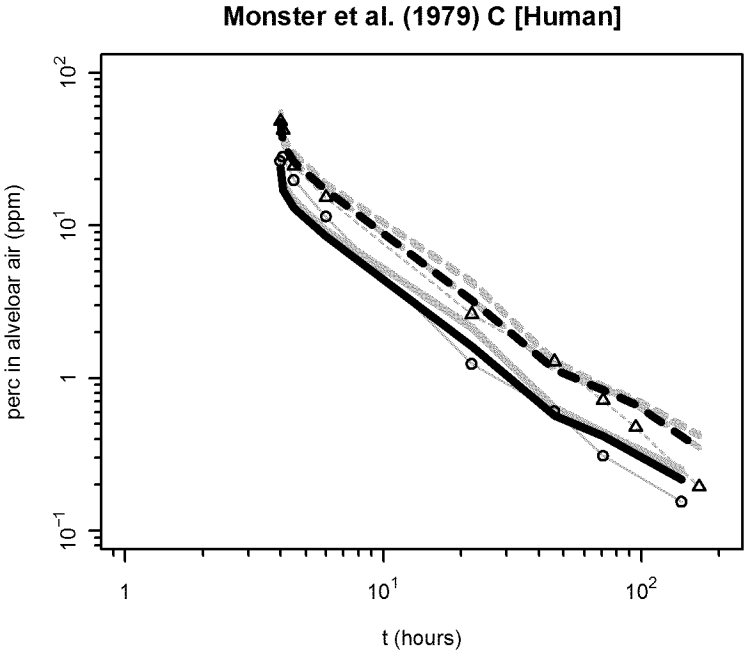
Monster et al. (1979) C [Human]
perc in alveloar air (ppm)
10^{-1}
1
10^{1}
10^{2}
1
10^{1}
10^{2}
t (hours)

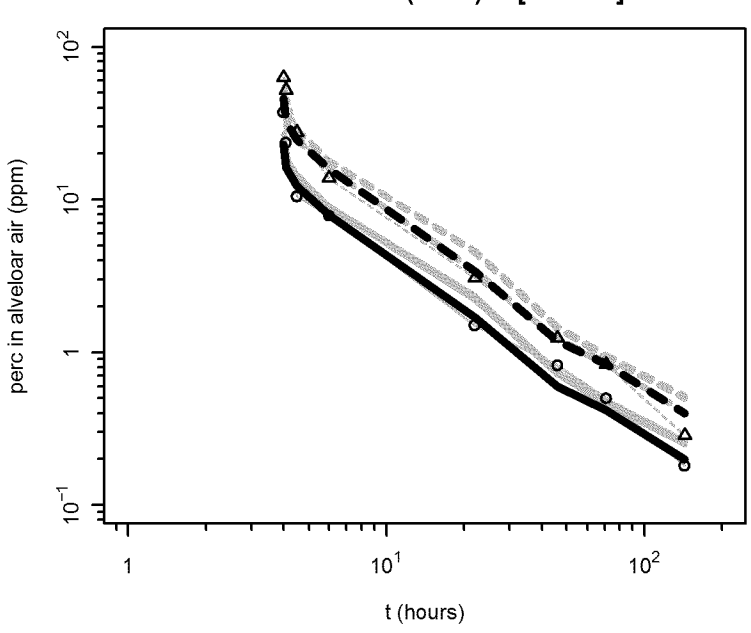
Monster et al. (1979) A [Human]
perc in alveloar air (ppm)
10^{-1}
1
10^{1}
10^{2}
1
10^{1}
10^{2}
t (hours)

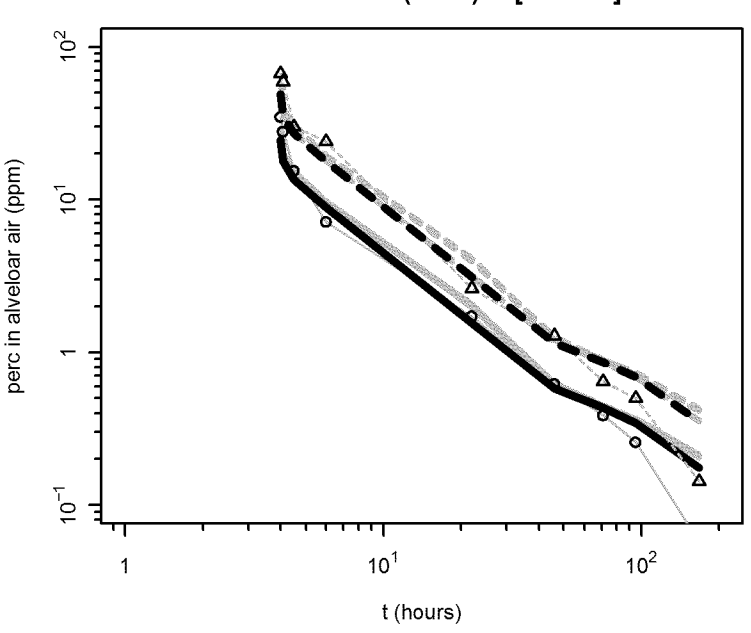
Monster et al. (1979) D [Human]
perc in alveloar air (ppm)
10^{-1}
1
10^{1}
10^{2}
1
10^{1}
10^{2}
t (hours)

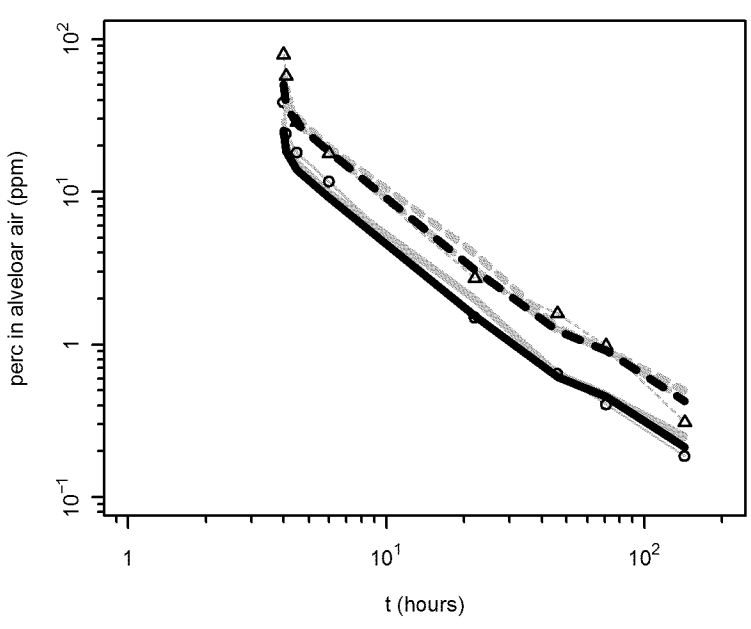
Monster et al. (1979) B [Human]
perc in alveloar air (ppm)
10^{-1}
1
10^{1}
10^{2}
1
10^{1}
10^{2}
t (hours)

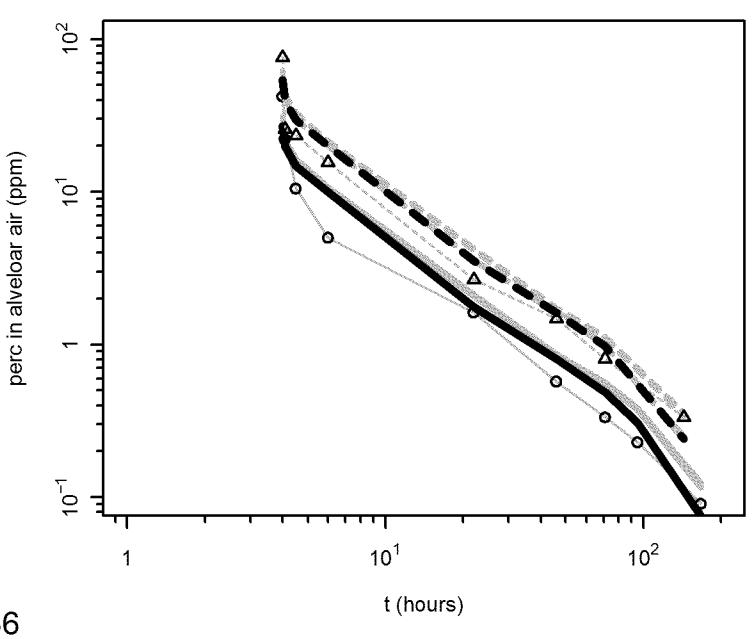
Monster et al. (1979) E [Human]
perc in alveloar air (ppm)
10^{-1}
1
10^{1}
10^{2}
1
10^{1}
10^{2}
t (hours)

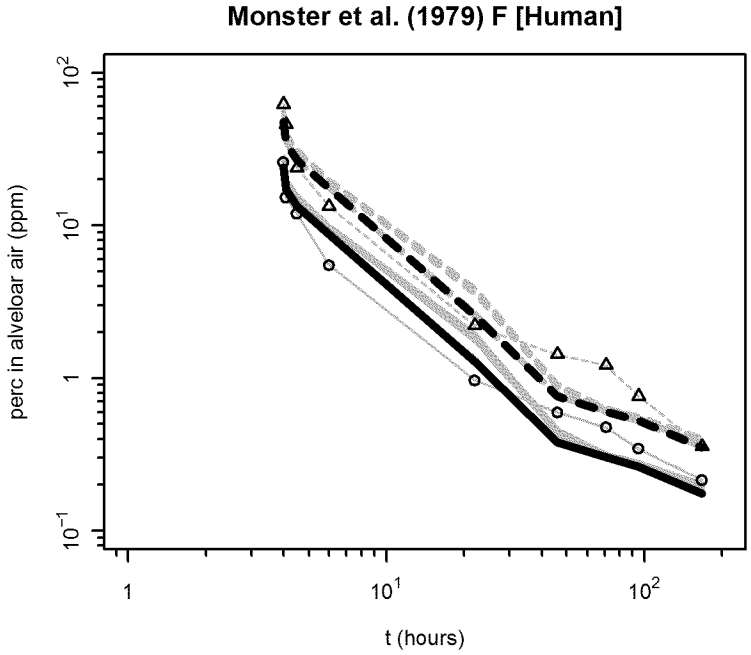
Monster et al. (1979) F [Human]
perc in alveloar air (ppm)
t (hours)

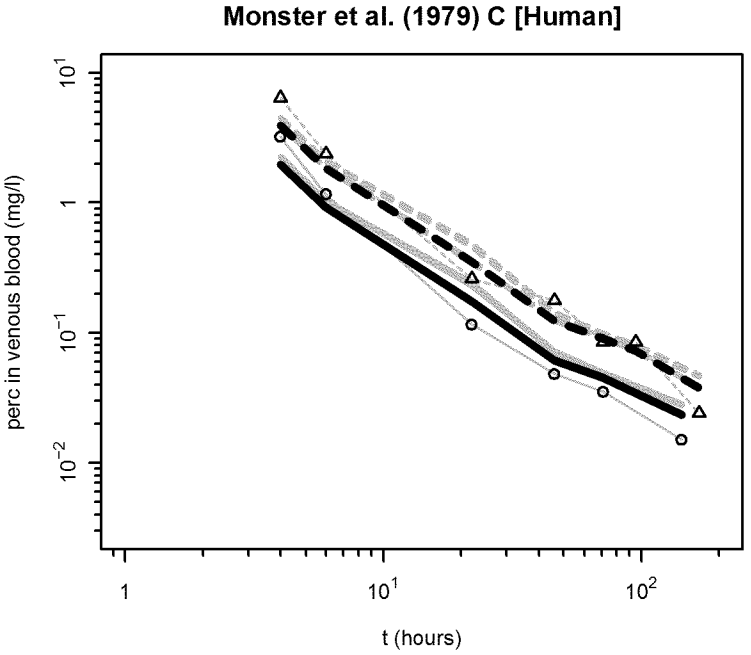
Monster et al. (1979) C [Human]
perc in venous blood (mg/l)
t (hours)

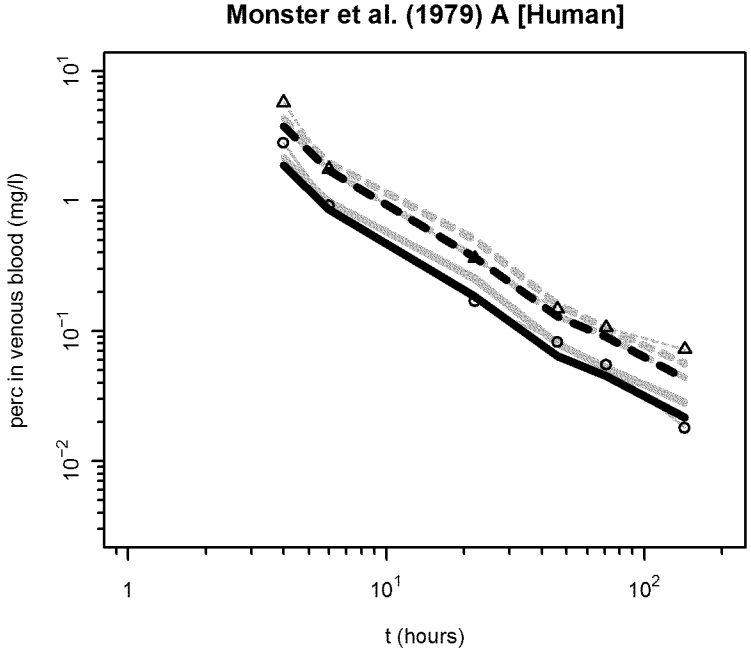
Monster et al. (1979) A [Human]
perc in venous blood (mg/l)
t (hours)

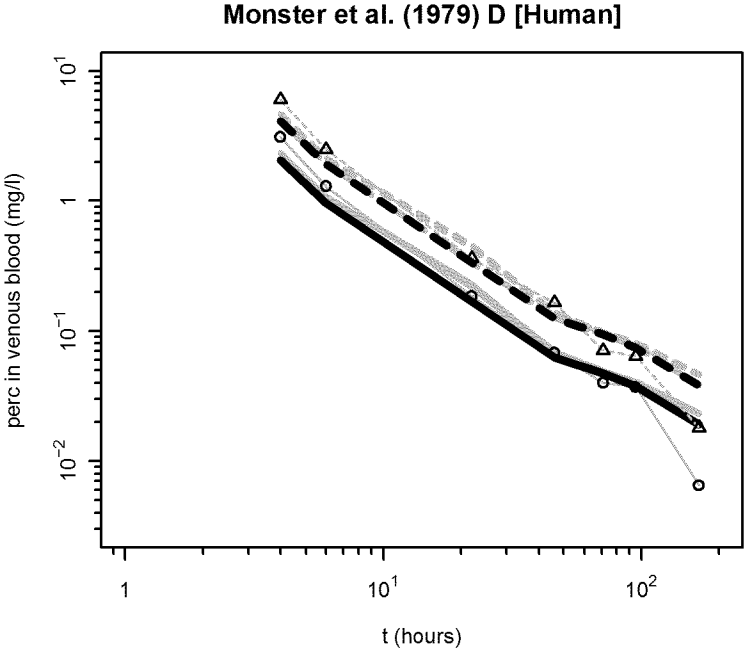
Monster et al. (1979) D [Human]
perc in venous blood (mg/l)
t (hours)

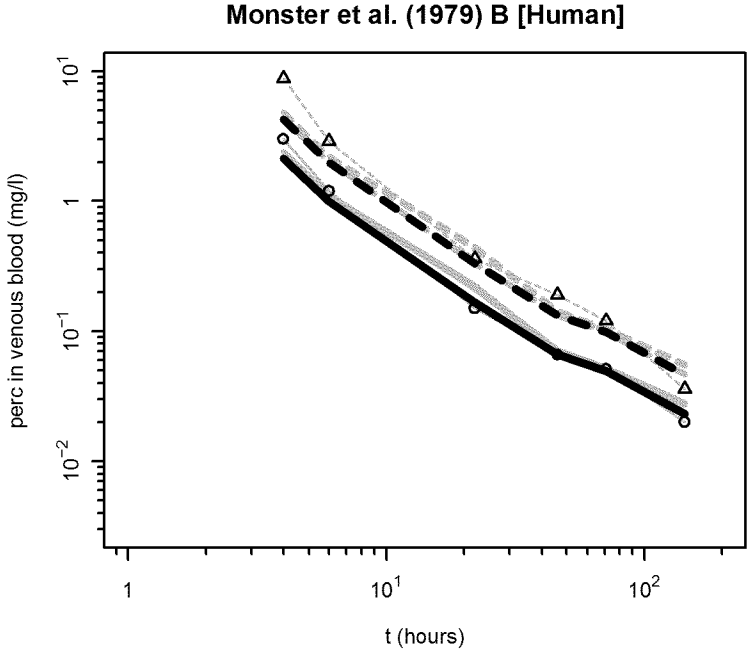
Monster et al. (1979) B [Human]
perc in venous blood (mg/l)
t (hours)

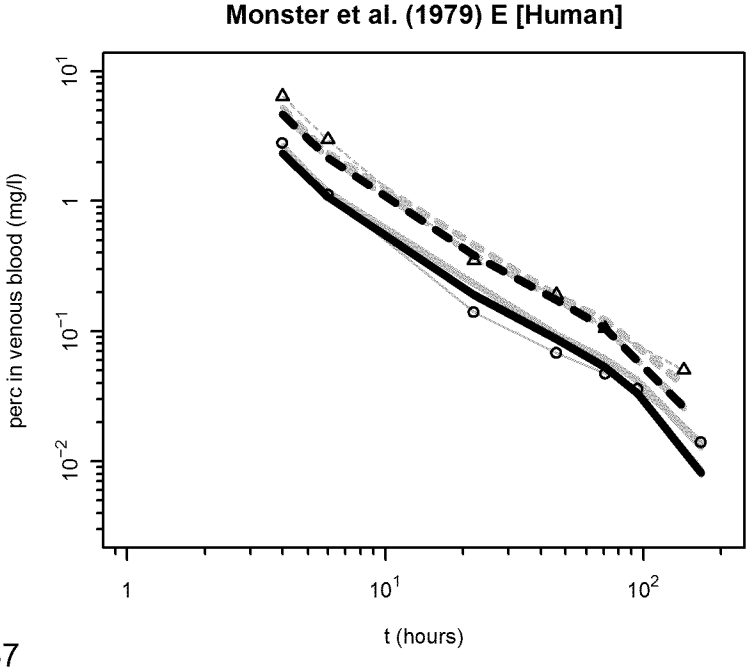
Monster et al. (1979) E [Human]
perc in venous blood (mg/l)
t (hours)

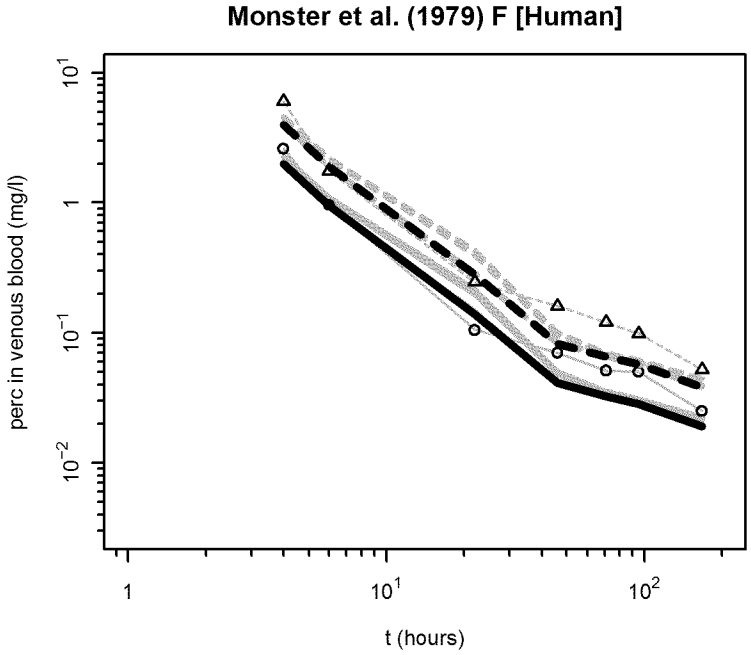
Monster et al. (1979) F [Human]
perc in venous blood (mg/l)
t (hours)

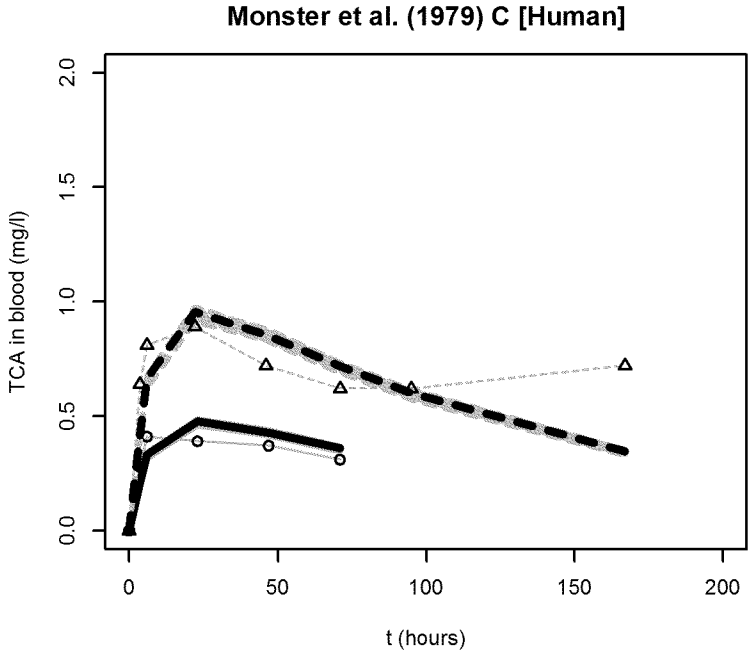
Monster et al. (1979) C [Human]
TCA in blood (mg/l)
t (hours)

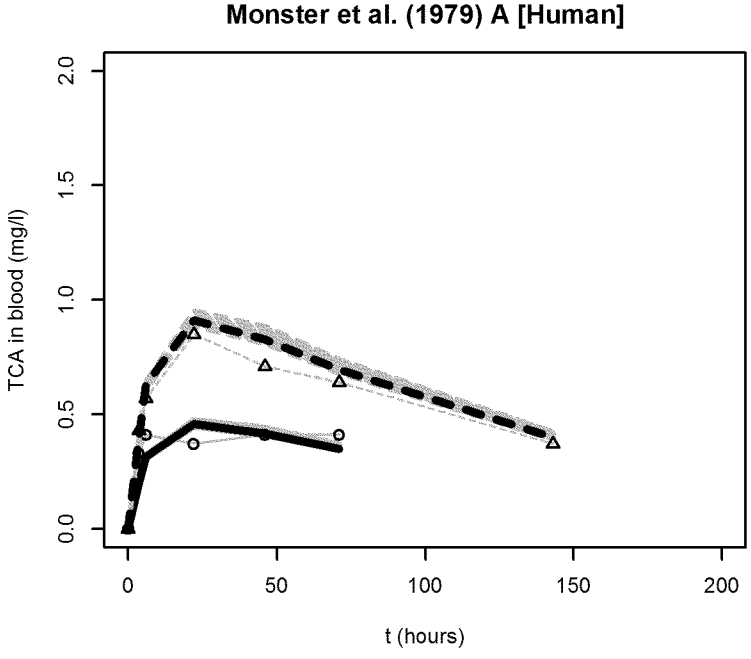
Monster et al. (1979) A [Human]
TCA in blood (mg/l)
t (hours)

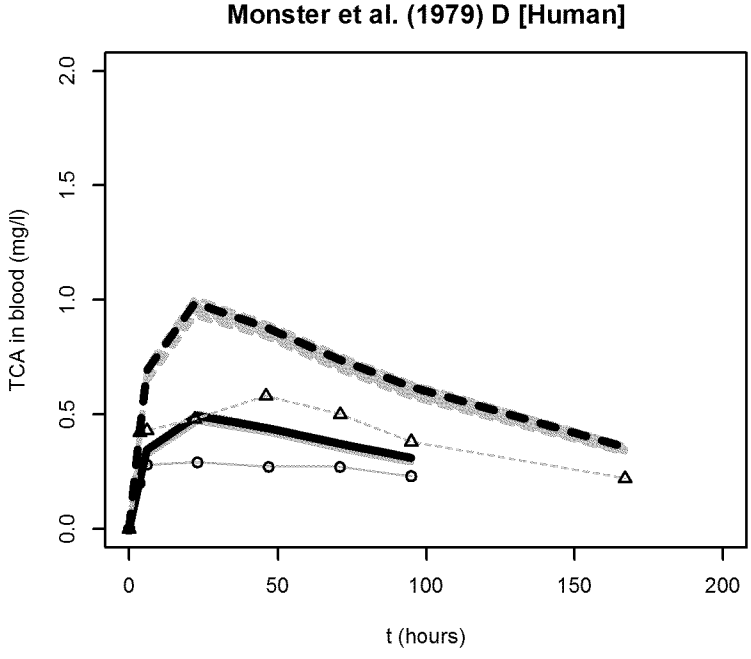
Monster et al. (1979) D [Human]
TCA in blood (mg/l)
t (hours)

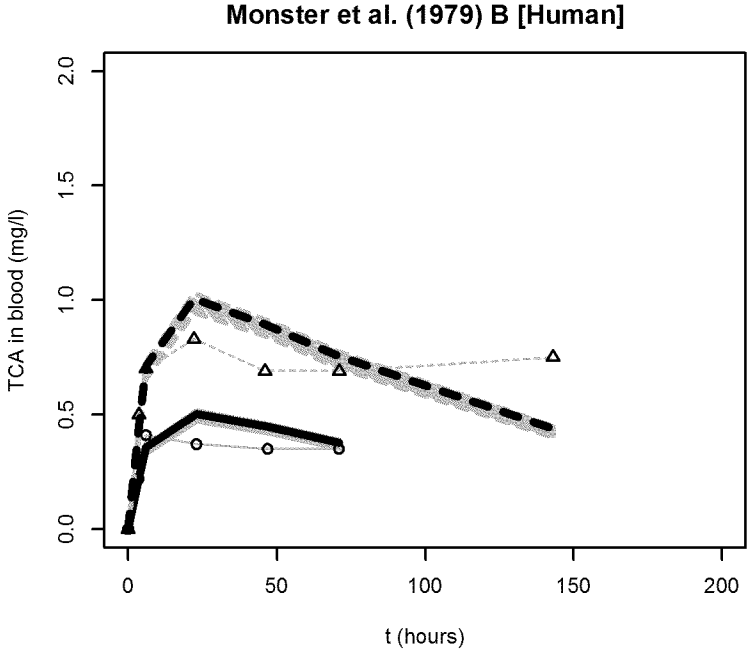
Monster et al. (1979) B [Human]
TCA in blood (mg/l)
t (hours)

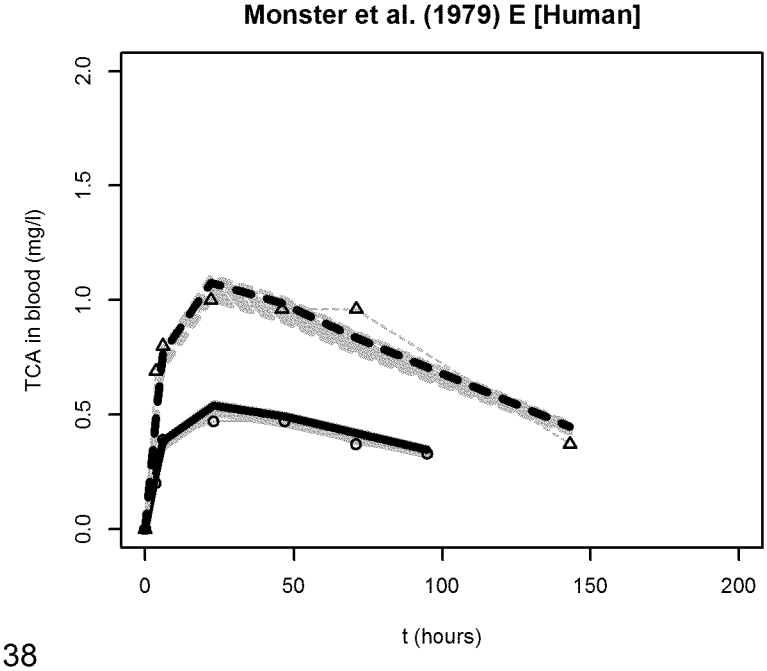
Monster et al. (1979) E [Human]
TCA in blood (mg/l)
t (hours)

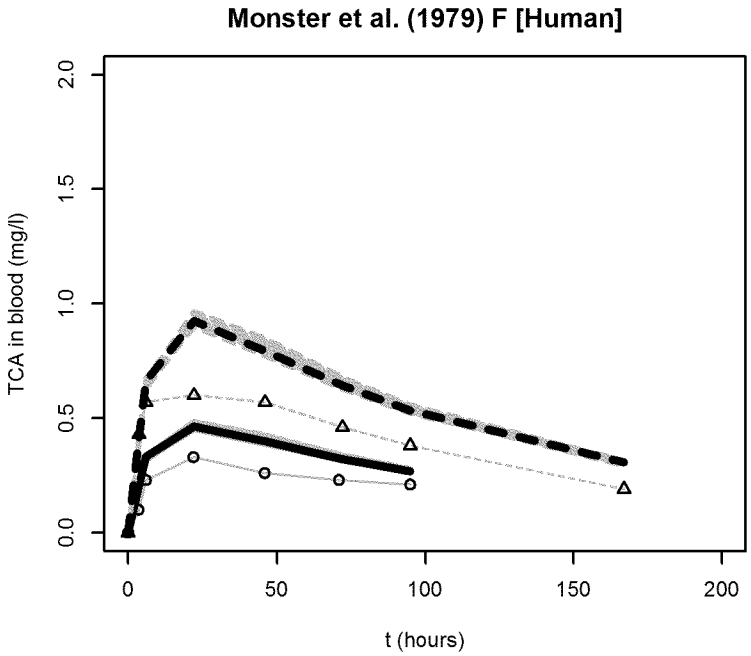
Monster et al. (1979) F [Human]
TCA in blood (mg/l)
t (hours)

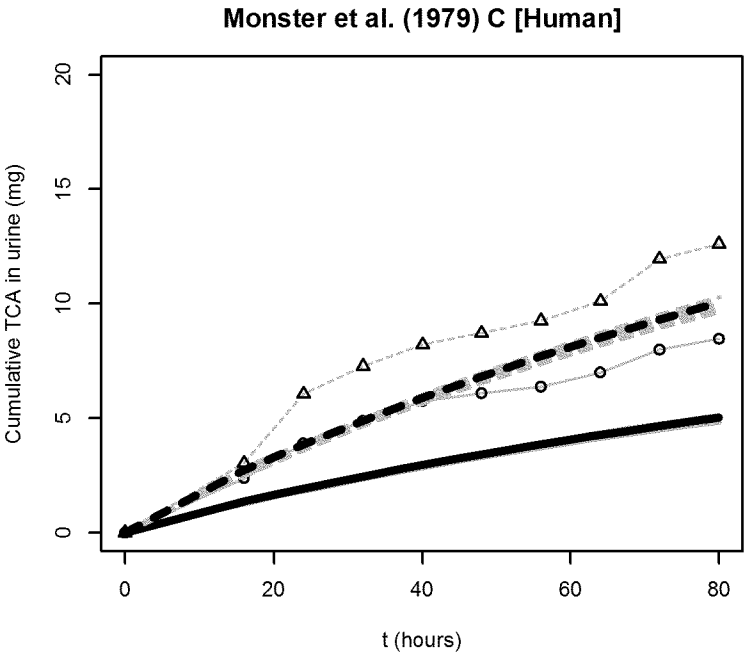
Monster et al. (1979) C [Human]
Cumulative TCA in urine (mg)
t (hours)

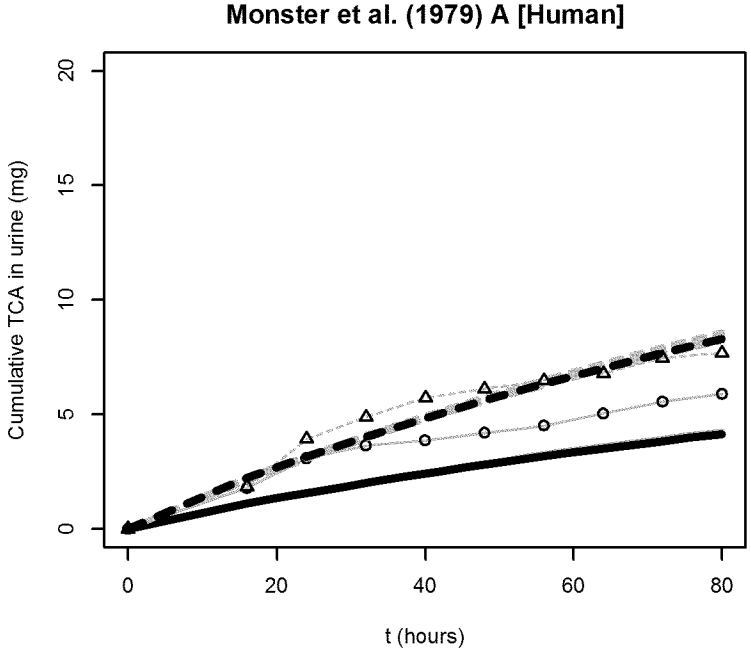
Monster et al. (1979) A [Human]
Cumulative TCA in urine (mg)
t (hours)

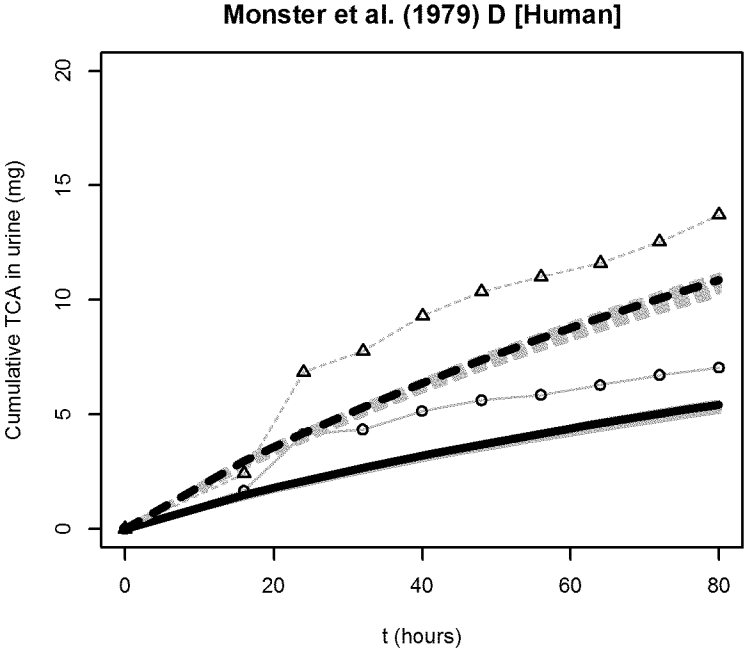
Monster et al. (1979) D [Human]
Cumulative TCA in urine (mg)
t (hours)

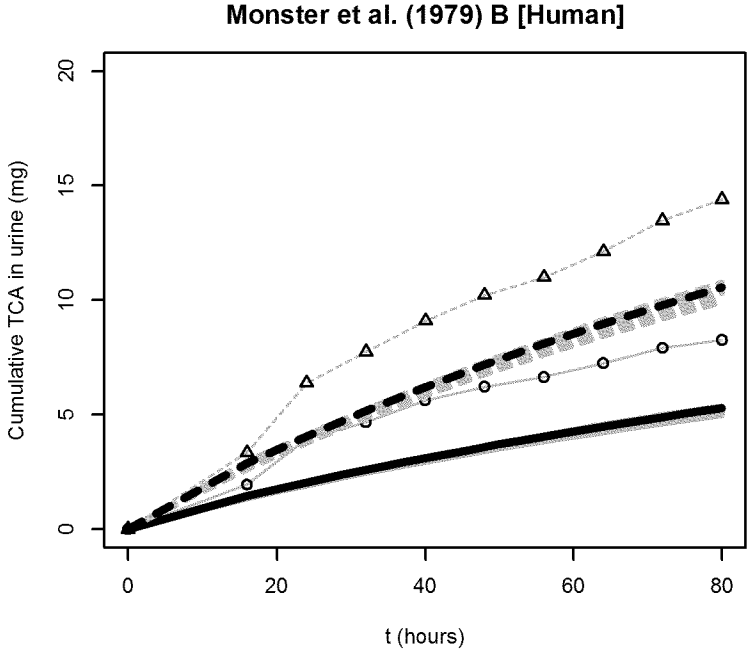
Monster et al. (1979) B [Human]
Cumulative TCA in urine (mg)
t (hours)

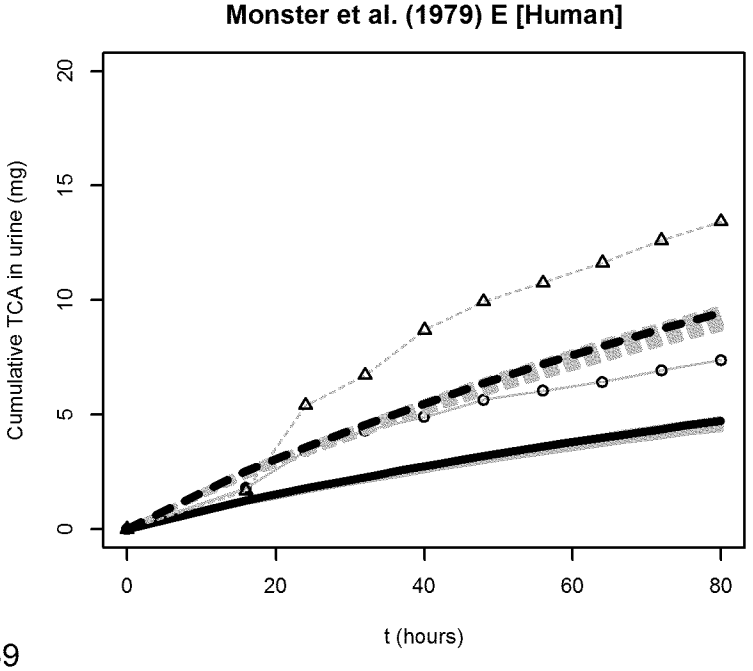
Monster et al. (1979) E [Human]
Cumulative TCA in urine (mg)
t (hours)

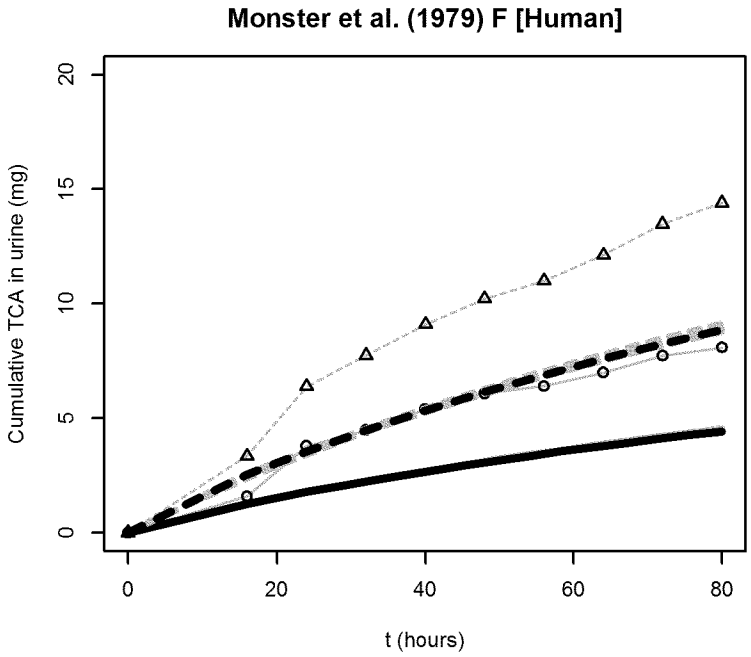
Monster et al. (1979) F [Human]
Cumulative TCA in urine (mg)
t (hours)

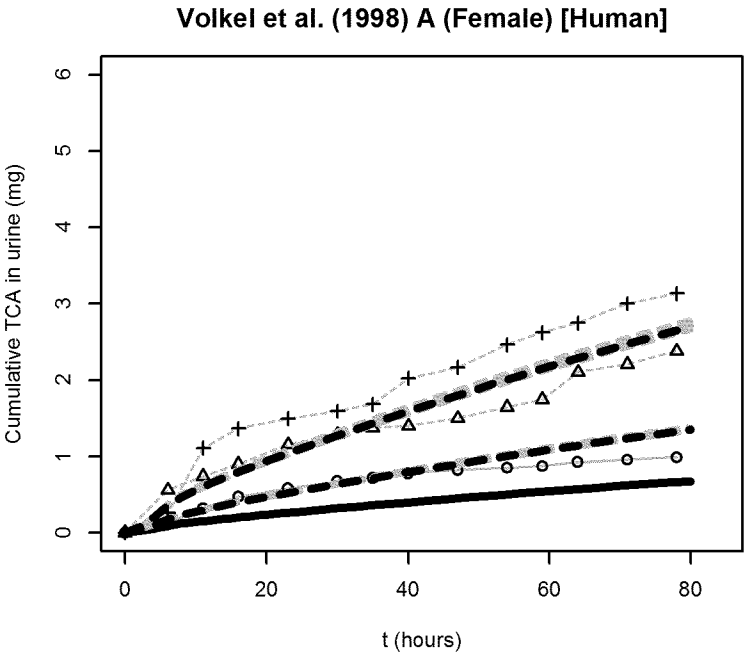
Volkel et al. (1998) A (Female) [Human]
Cumulative TCA in urine (mg)
t (hours)

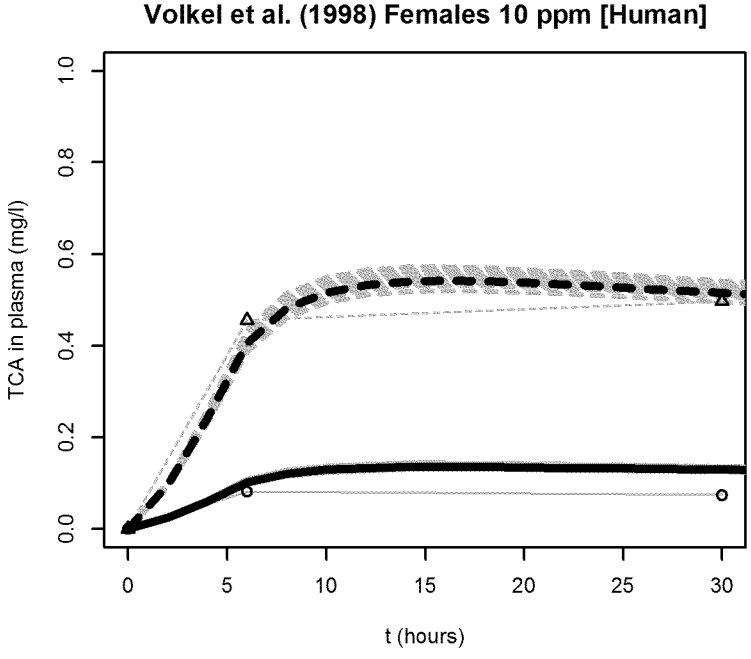
Volkel et al. (1998) Females 10 ppm [Human]
TCA in plasma (mg/l)
t (hours)

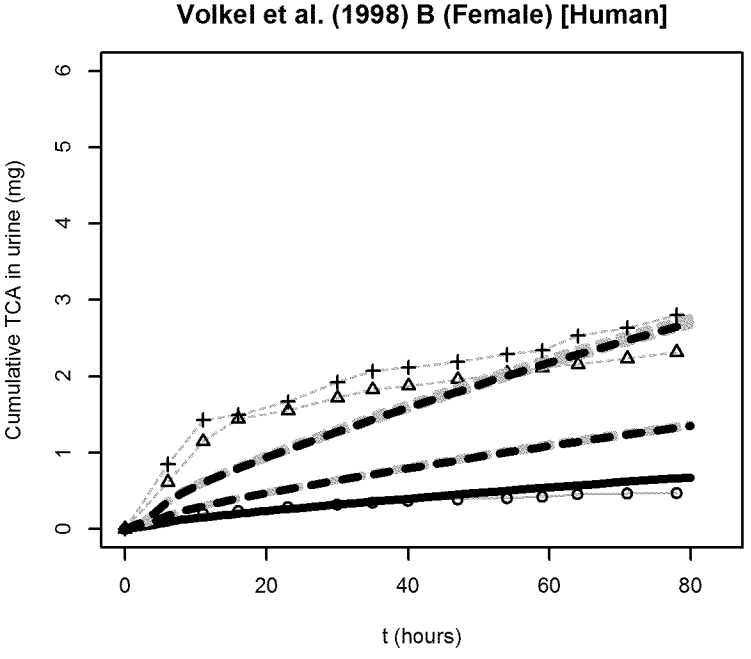
Volkel et al. (1998) B (Female) [Human]
Cumulative TCA in urine (mg)
t (hours)

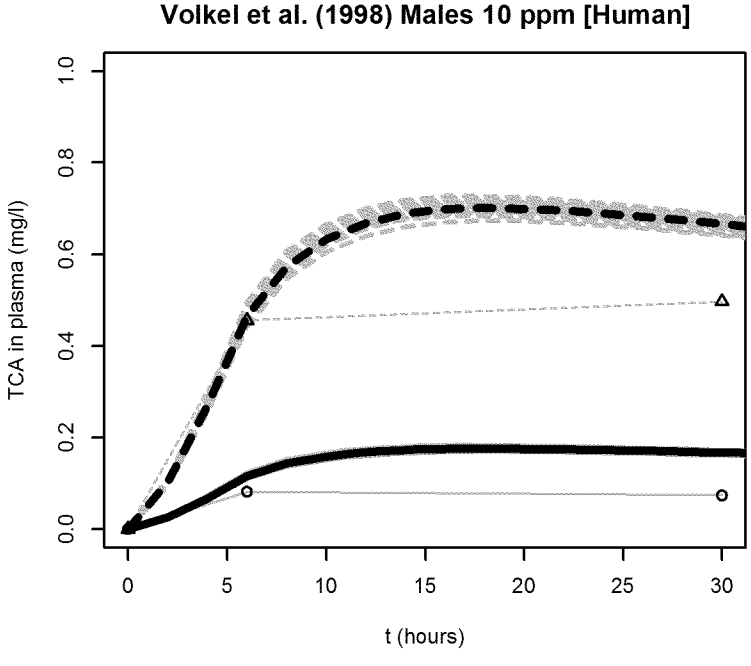
Volkel et al. (1998) Males 10 ppm [Human]
TCA in plasma (mg/l)
t (hours)

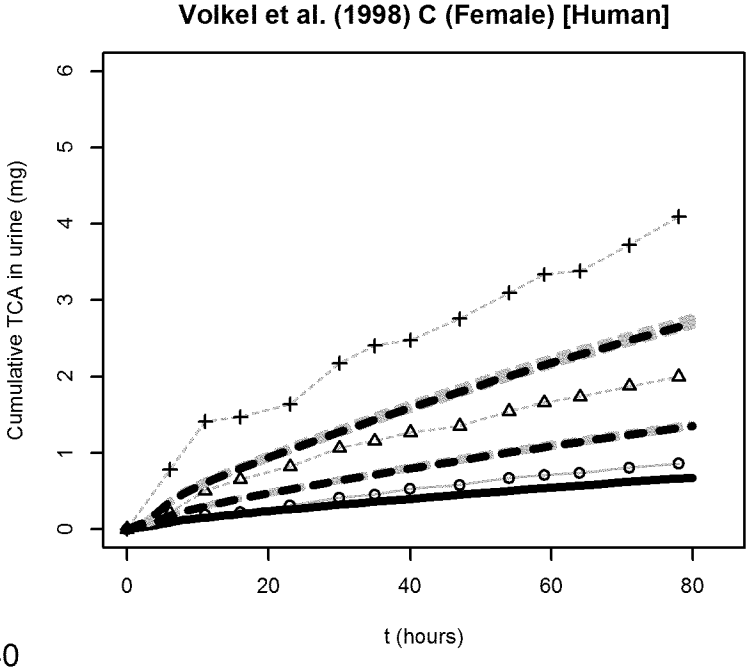
Volkel et al. (1998) C (Female) [Human]
Cumulative TCA in urine (mg)
t (hours)

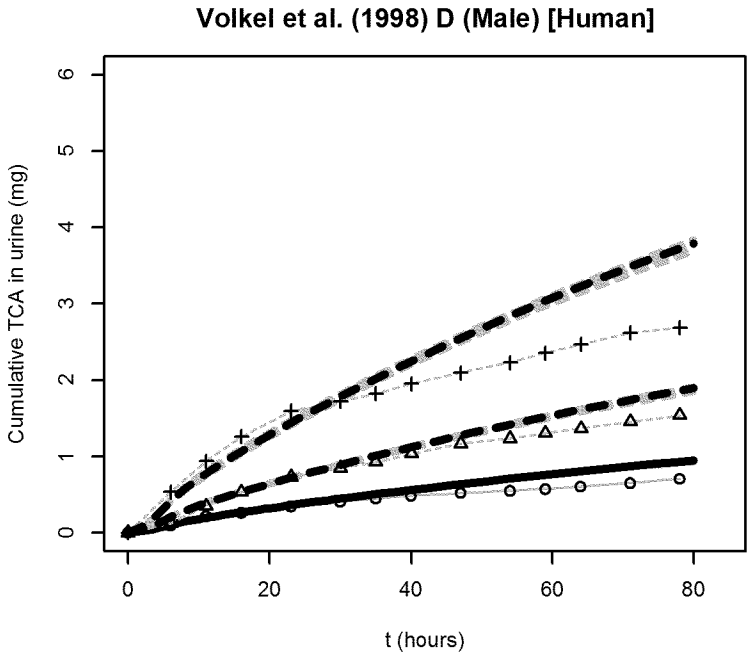
Volkel et al. (1998) D (Male) [Human]
Cumulative TCA in urine (mg)
t (hours)

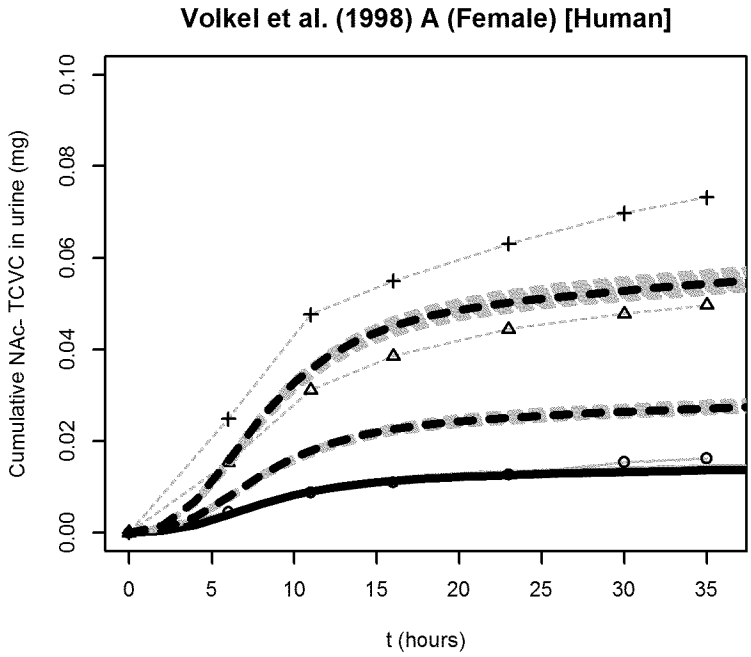
Volkel et al. (1998) A (Female) [Human]
Cumulative NAc- TCVC in urine (mg)
t (hours)

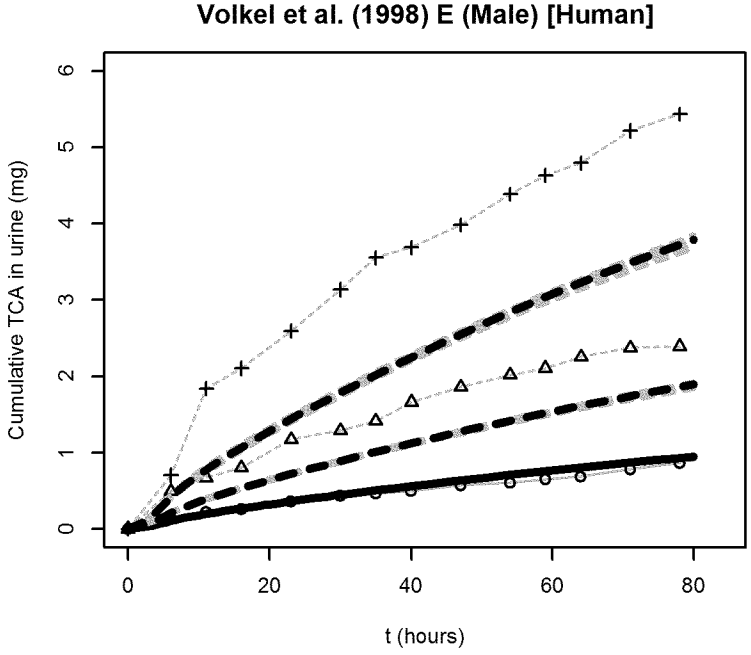
Volkel et al. (1998) E (Male) [Human]
Cumulative TCA in urine (mg)
t (hours)

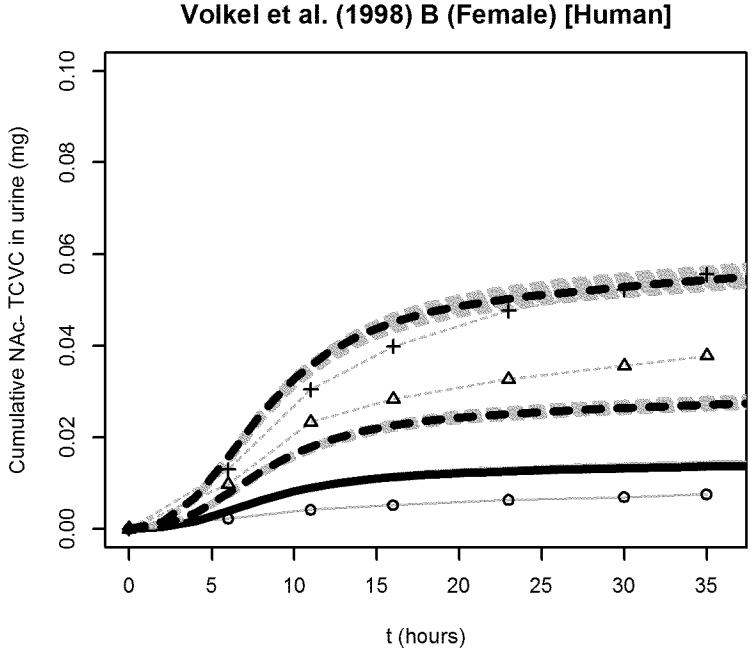
Volkel et al. (1998) B (Female) [Human]
Cumulative NAc- TCVC in urine (mg)
t (hours)

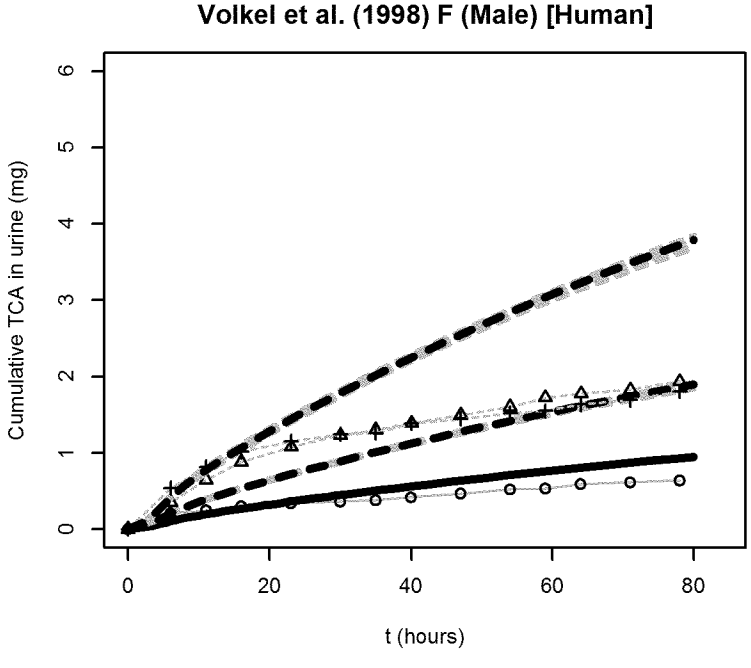
Volkel et al. (1998) F (Male) [Human]
Cumulative TCA in urine (mg)
t (hours)

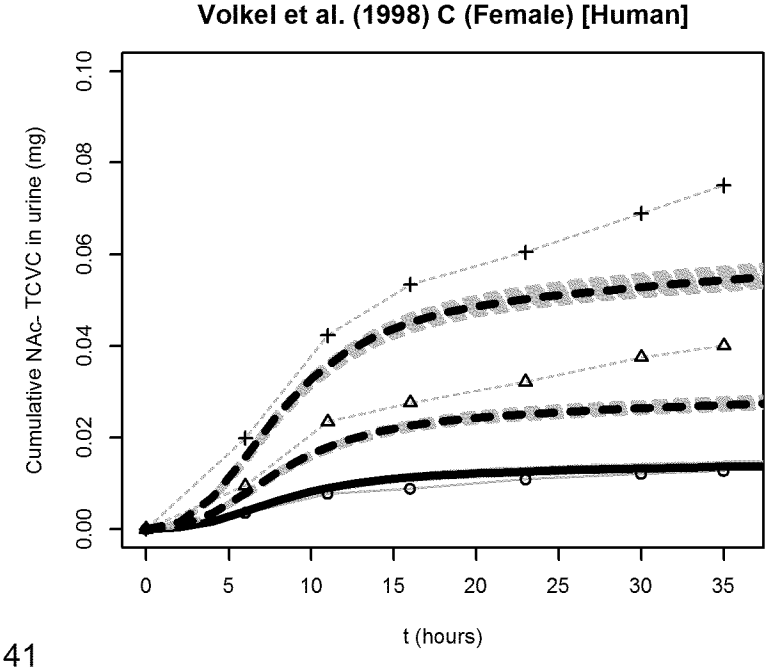
Volkel et al. (1998) C (Female) [Human]
Cumulative NAc- TCVC in urine (mg)
t (hours)

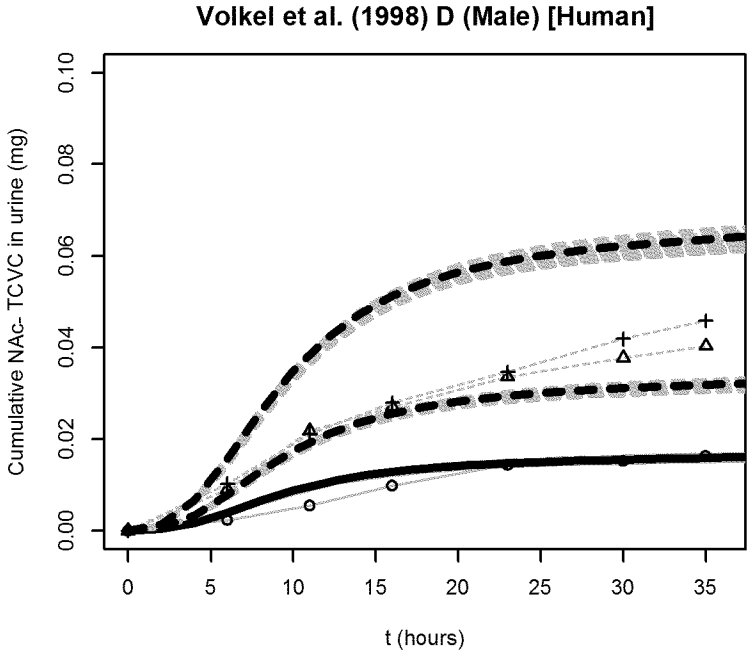
Volkel et al. (1998) D (Male) [Human]
Cumulative NAc- TCVC in urine (mg)
t (hours)

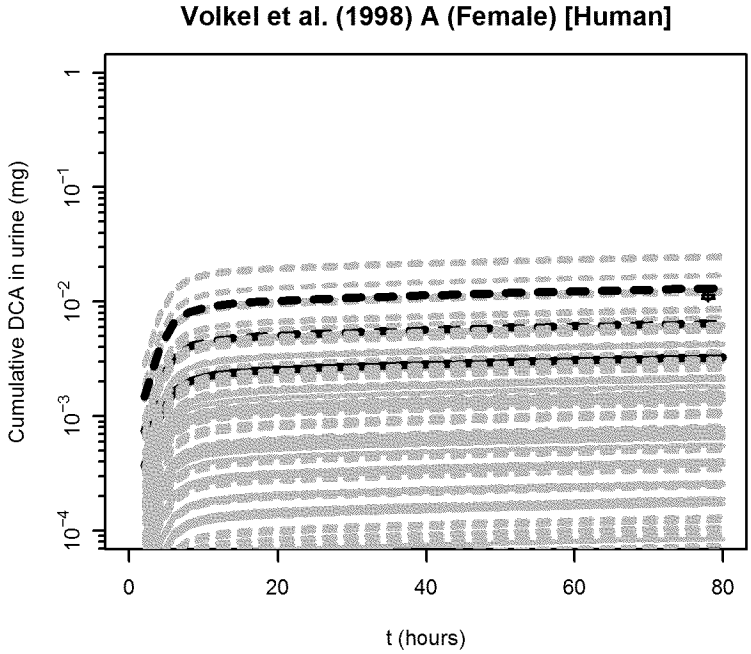
Volkel et al. (1998) A (Female) [Human]
Cumulative DCA in urine (mg)
t (hours)

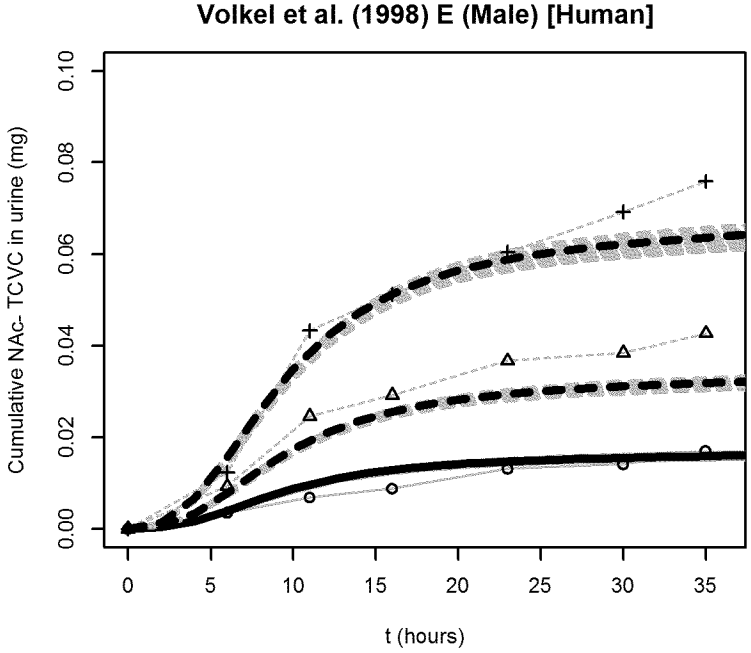
Volkel et al. (1998) E (Male) [Human]
Cumulative NAc- TCVC in urine (mg)
t (hours)

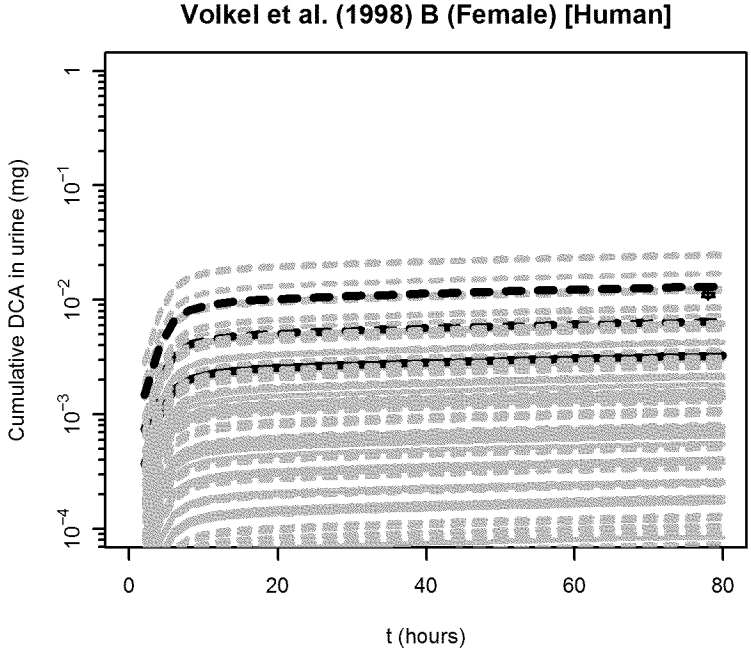
Volkel et al. (1998) B (Female) [Human]
Cumulative DCA in urine (mg)
t (hours)

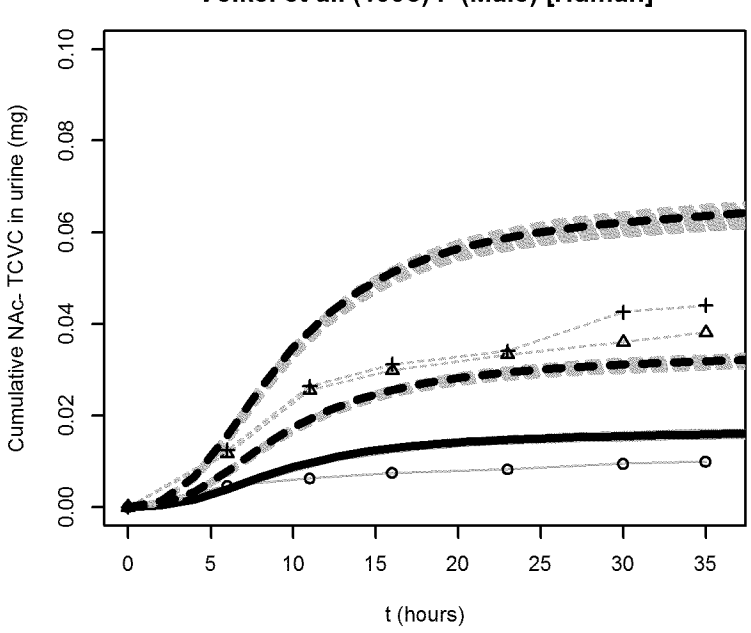
Volkel et al. (1998) F (Male) [Human]
Cumulative NAc- TCVC in urine (mg)
t (hours)

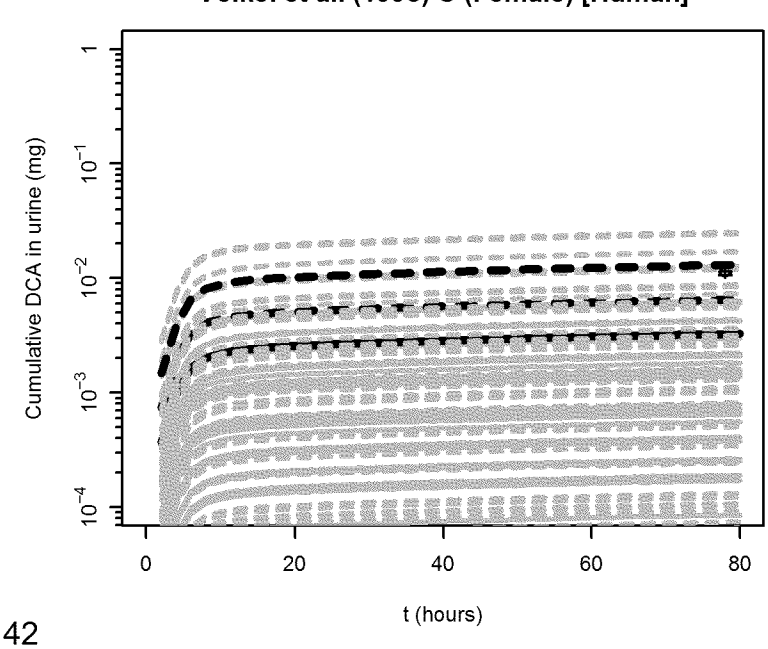
Volkel et al. (1998) C (Female) [Human]
Cumulative DCA in urine (mg)
t (hours)

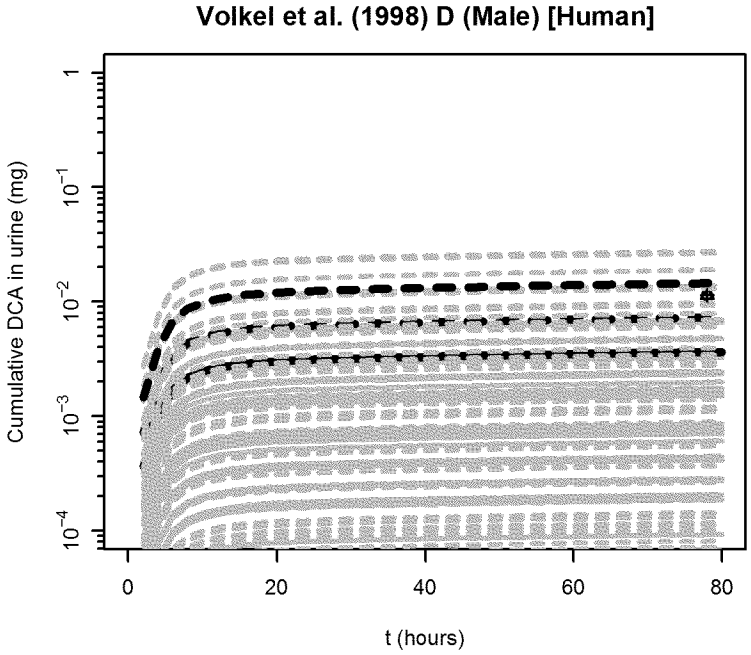
Volkel et al. (1998) D (Male) [Human]
Cumulative DCA in urine (mg)
t (hours)

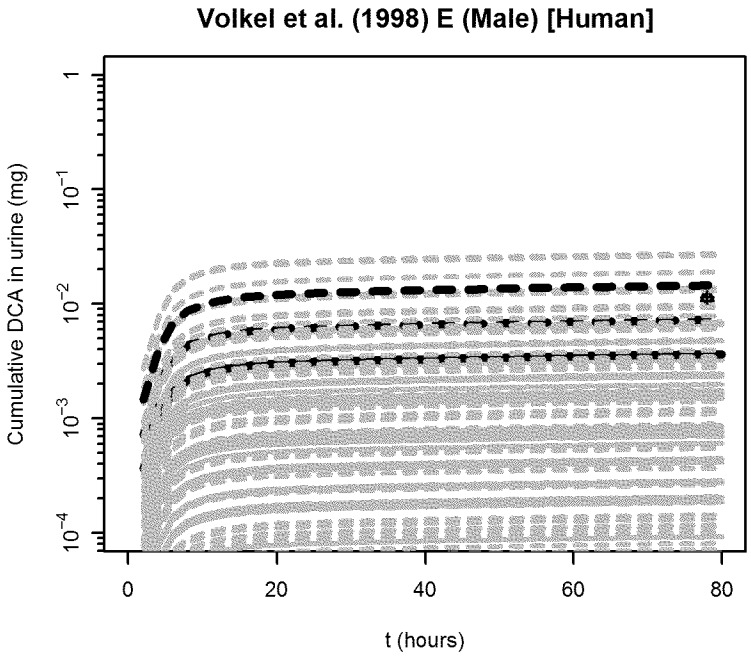
Volkel et al. (1998) E (Male) [Human]
Cumulative DCA in urine (mg)
t (hours)

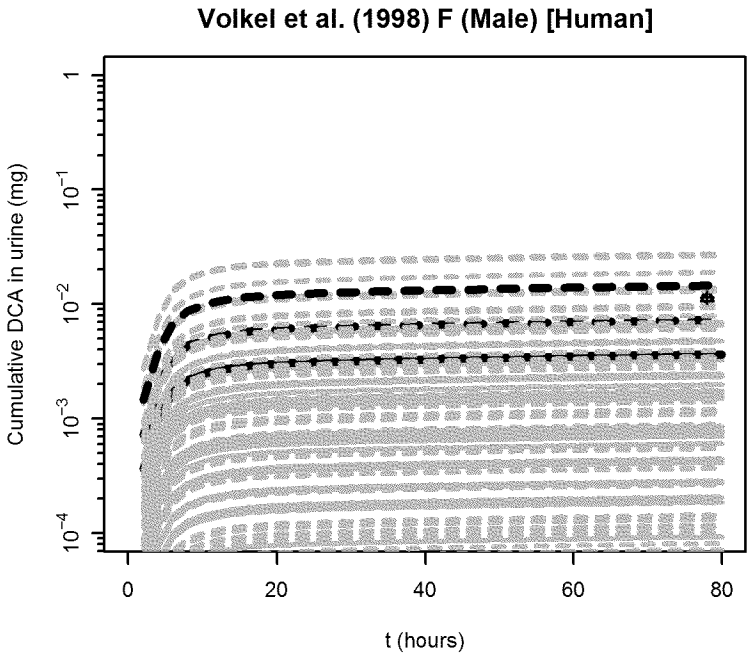
Volkel et al. (1998) F (Male) [Human]
Cumulative DCA in urine (mg)
t (hours)

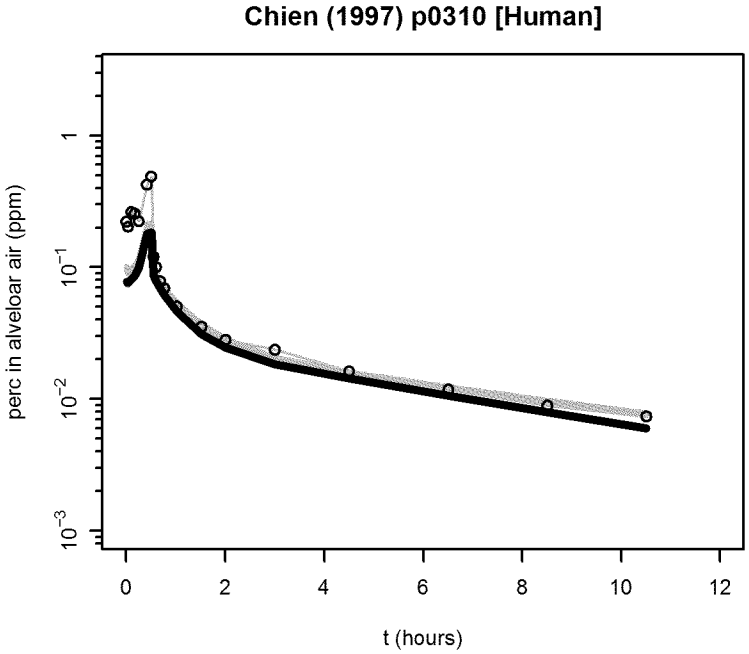
Chien (1997) p0310 [Human]
perc in alveloar air (ppm)
t (hours)

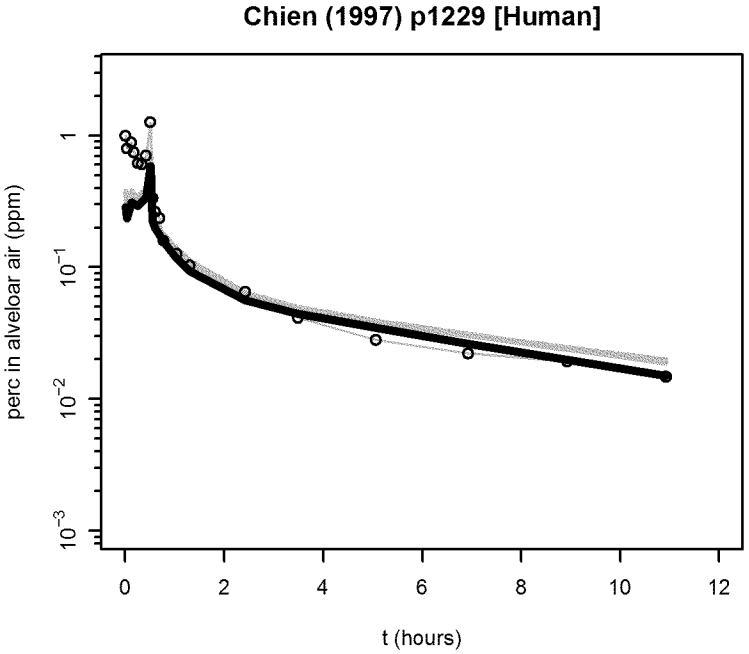
Chien (1997) p1229 [Human]
perc in alveloar air (ppm)
t (hours)

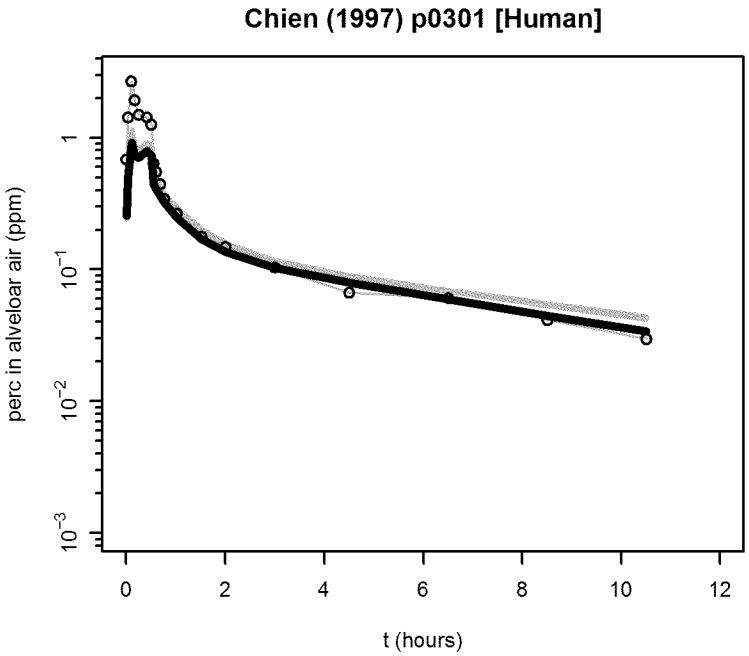
Chien (1997) p0301 [Human]
perc in alveloar air (ppm)
t (hours)

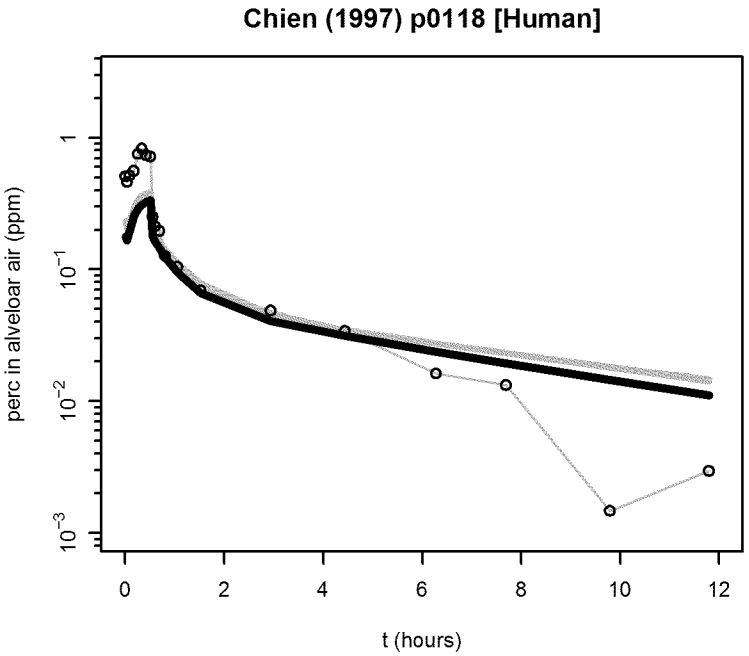
Chien (1997) p0118 [Human]
perc in alveloar air (ppm)
t (hours)

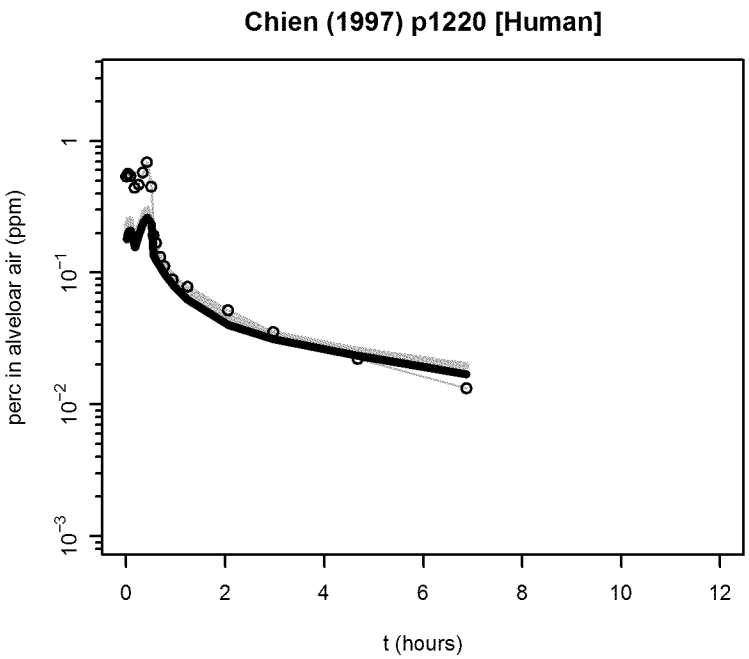
Chien (1997) p1220 [Human]
perc in alveloar air (ppm)
t (hours)

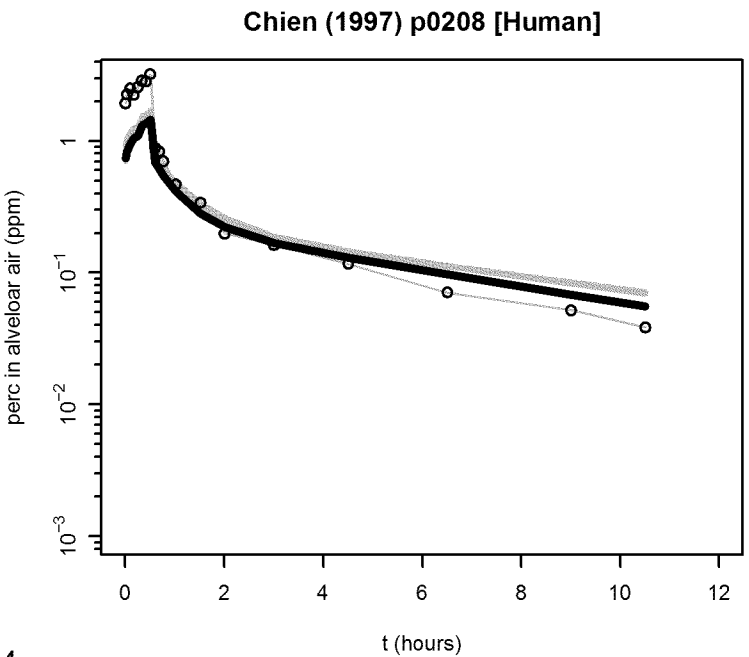
Chien (1997) p0208 [Human]
perc in alveloar air (ppm)
t (hours)

Chien (1997) p0830 [Human]

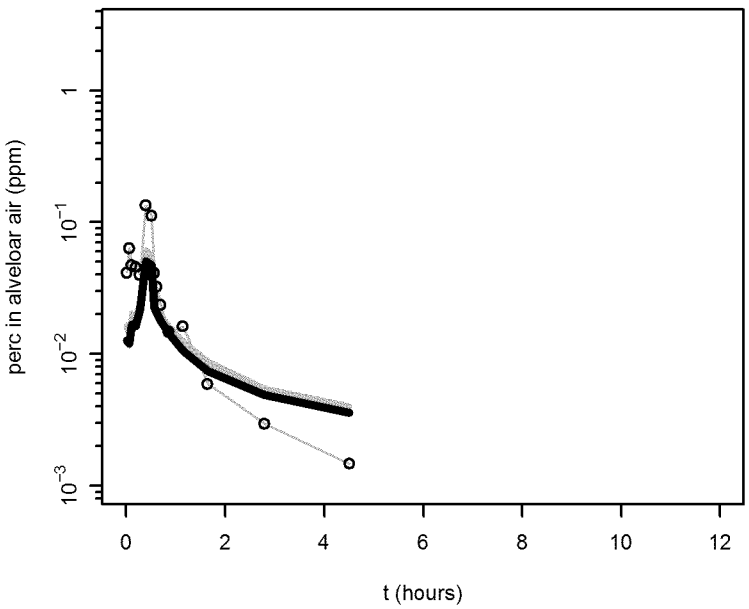

Chien (1997) p1214 [Human]

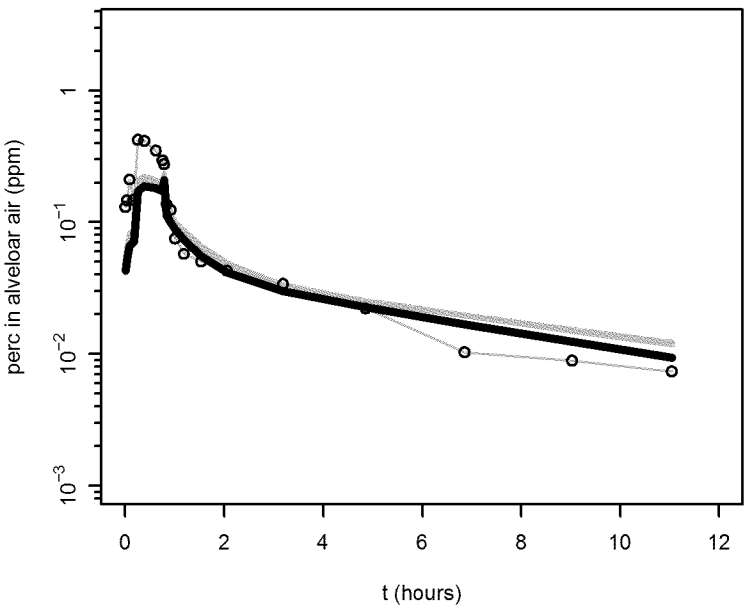

Chien (1997) p1202 [Human]

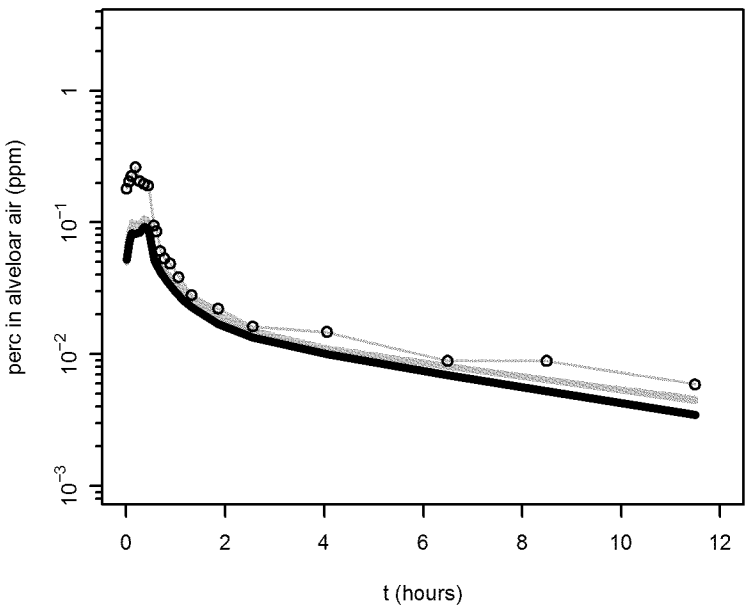

Chien (1997) p0124 [Human]

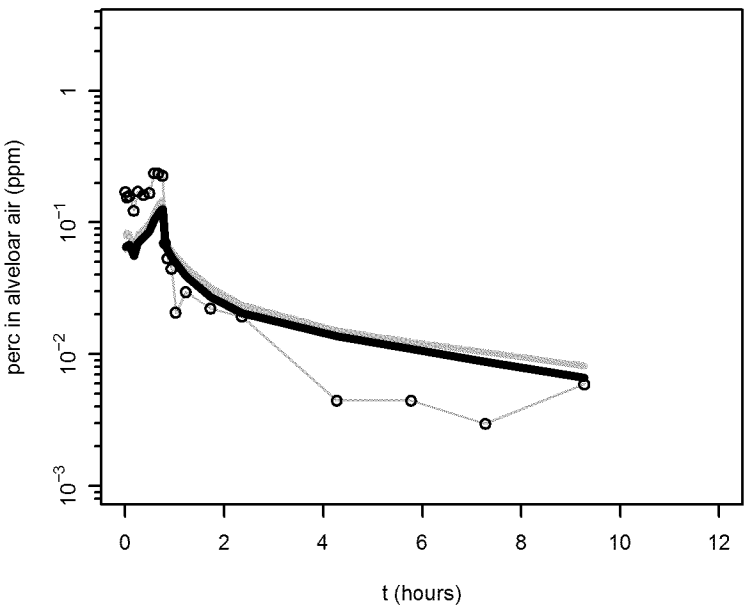

Chien (1997) p1208 [Human]

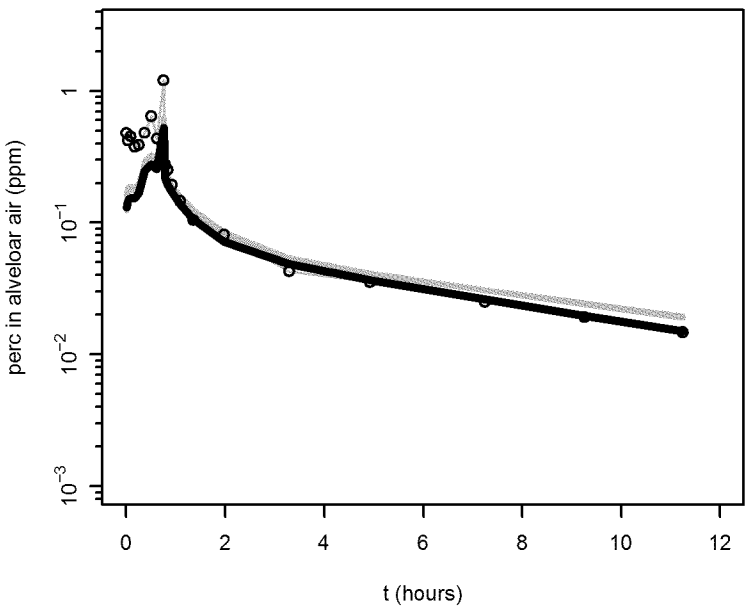

Chien (1997) p1103 [Human]

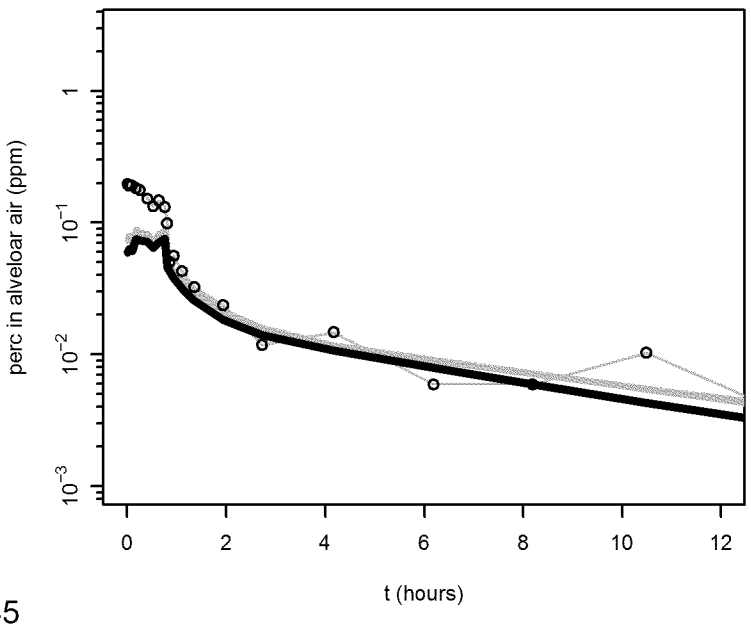

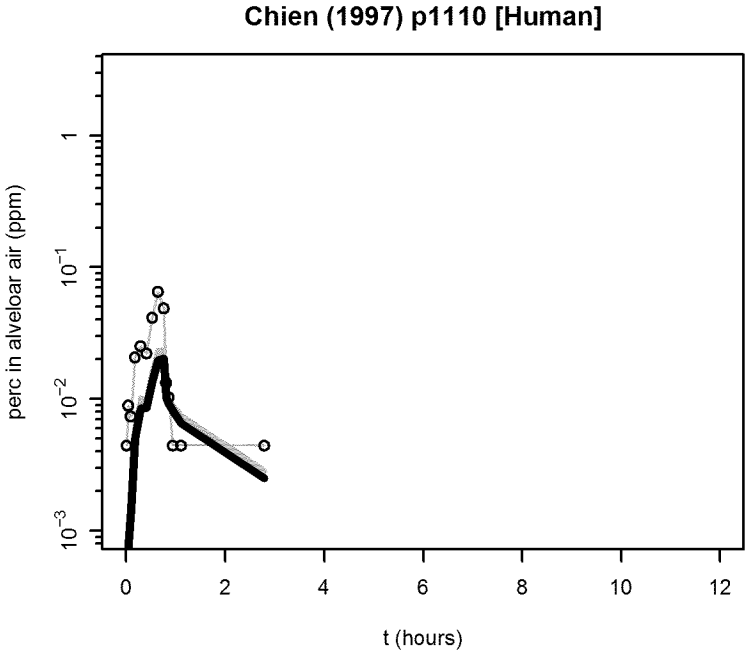
Chien (1997) p1110 [Human]
perc in alveloar air (ppm)
t (hours)

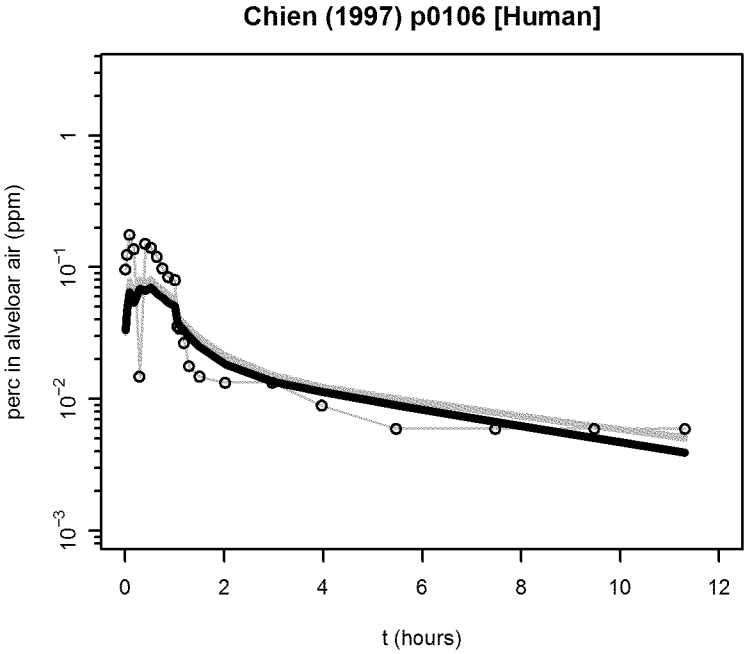
Chien (1997) p0106 [Human]
perc in alveloar air (ppm)
t (hours)

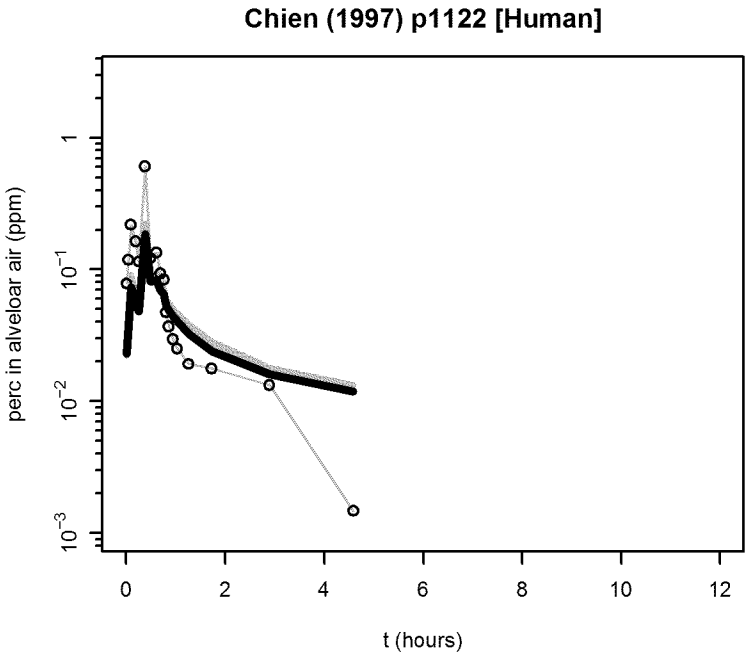
Chien (1997) p1122 [Human]
perc in alveloar air (ppm)
t (hours)

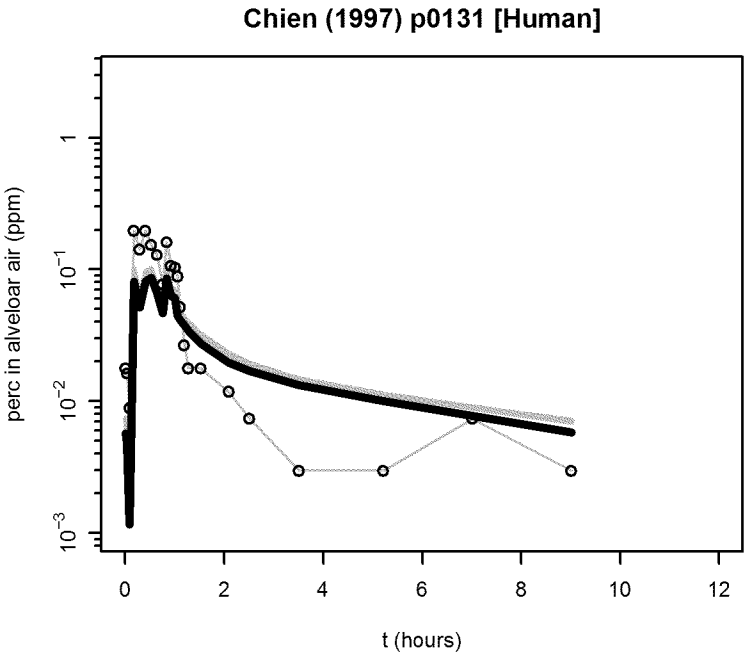
Chien (1997) p0131 [Human]
perc in alveloar air (ppm)
t (hours)

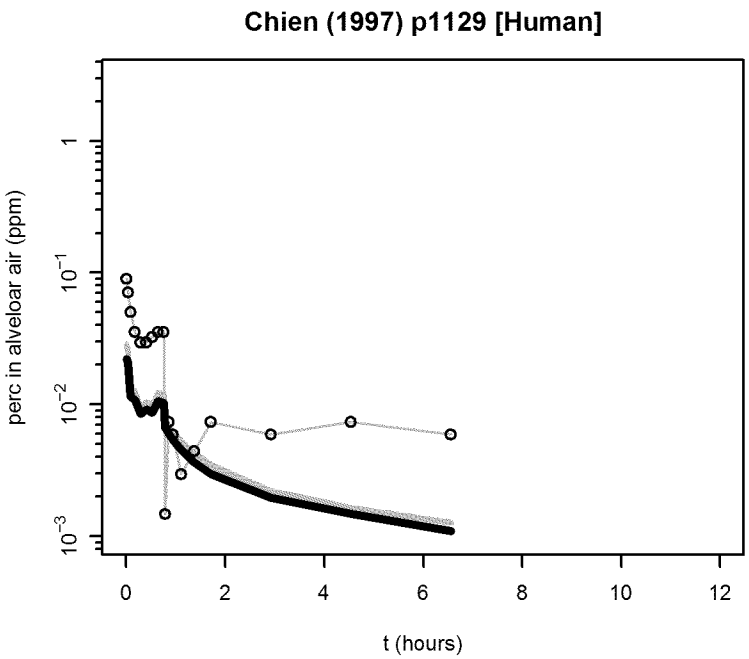
Chien (1997) p1129 [Human]
perc in alveloar air (ppm)
t (hours)

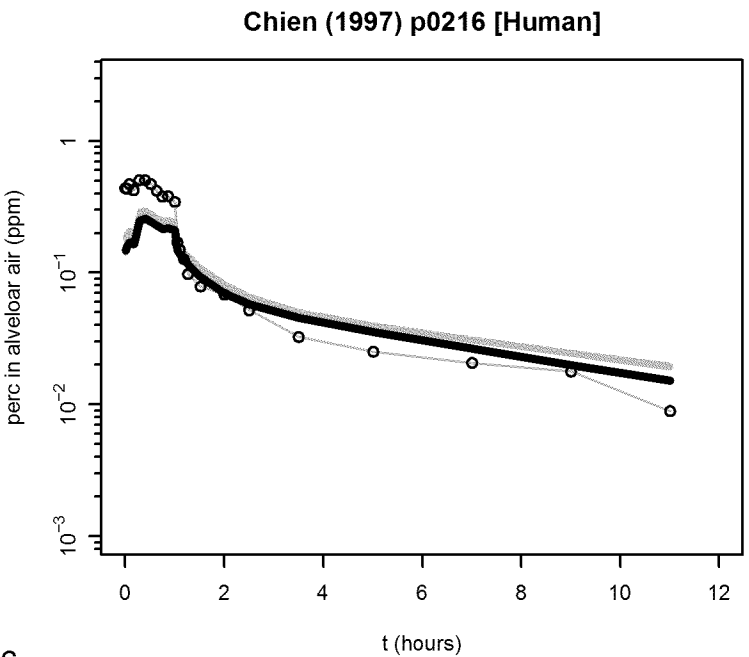
Chien (1997) p0216 [Human]
perc in alveloar air (ppm)
t (hours)

Chien (1997) p0322 [Human]

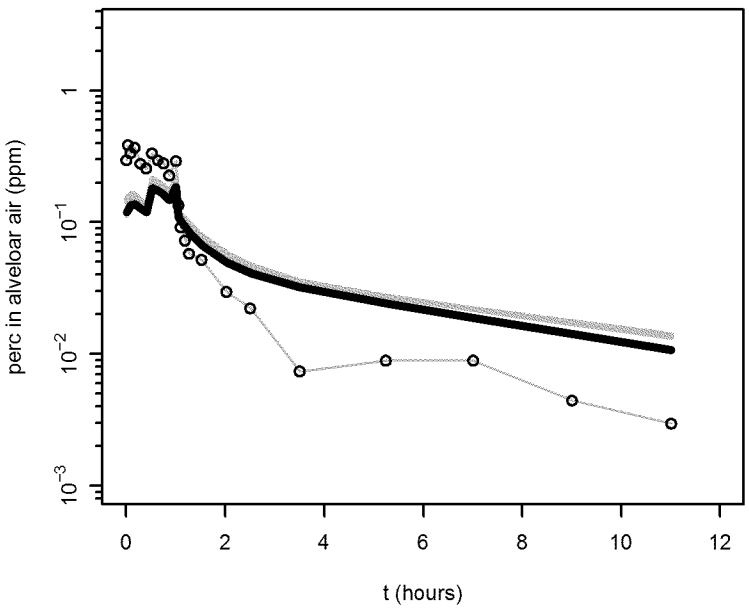

Chien (1997) p0329 [Human]

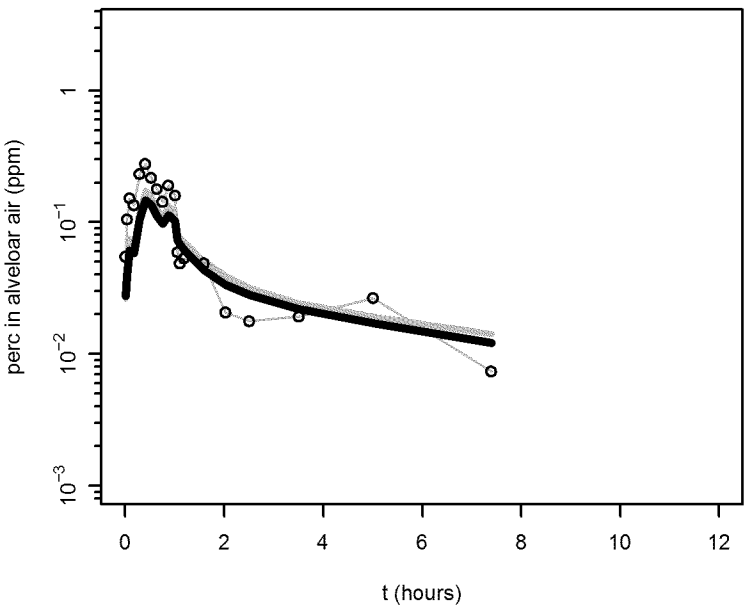

Chien (1997) p1020 [Human]

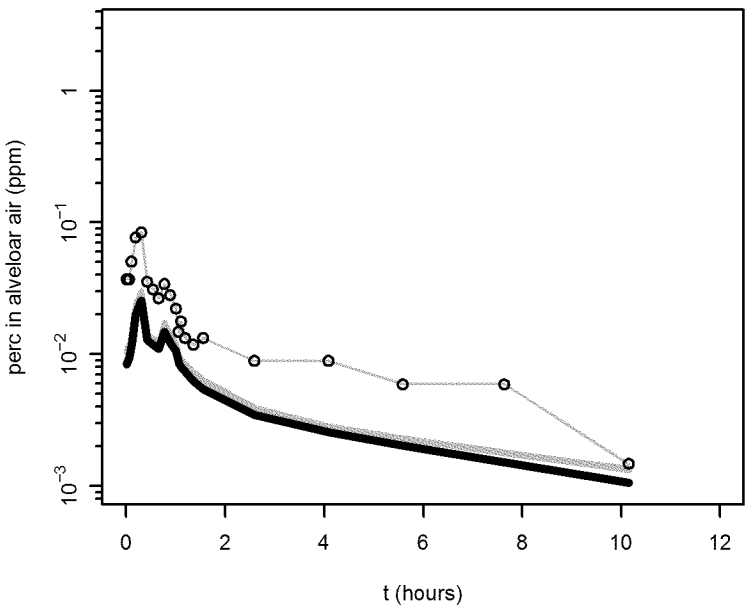

Chien (1997) p12195,01046,02146 [Human]

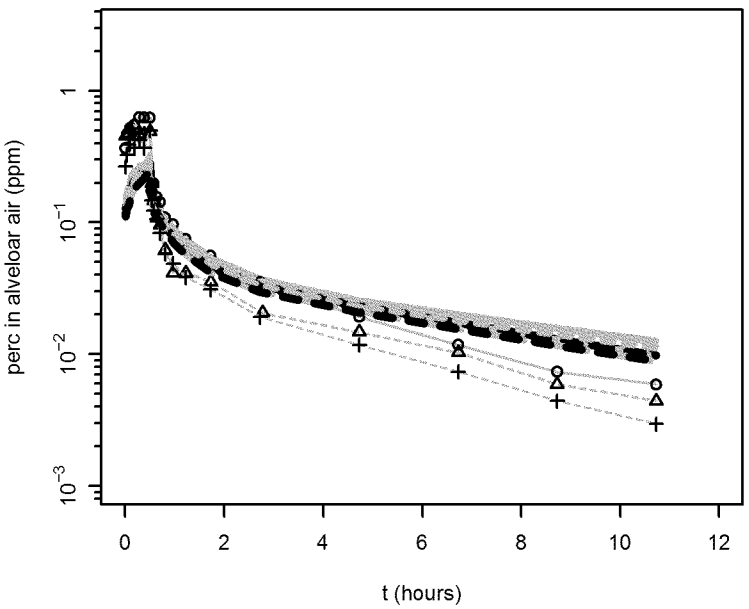

Chien (1997) p1117 [Human]

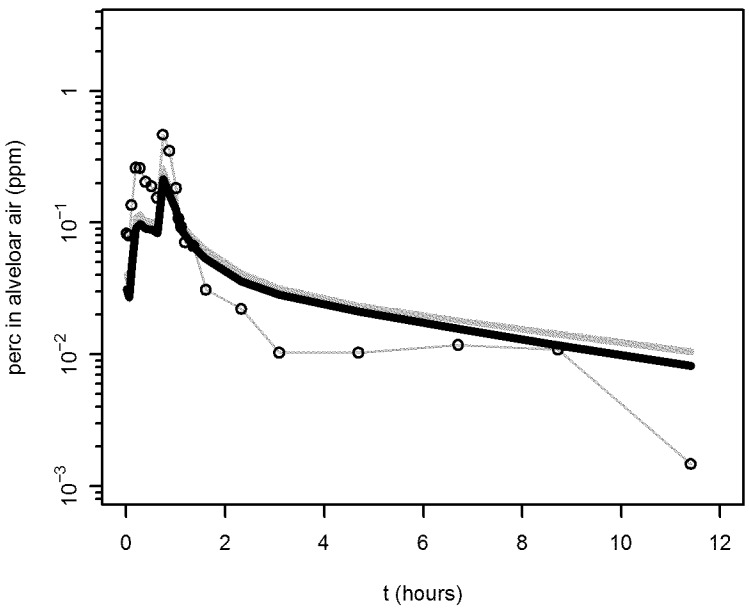

Chien (1997) p01166 [Human]

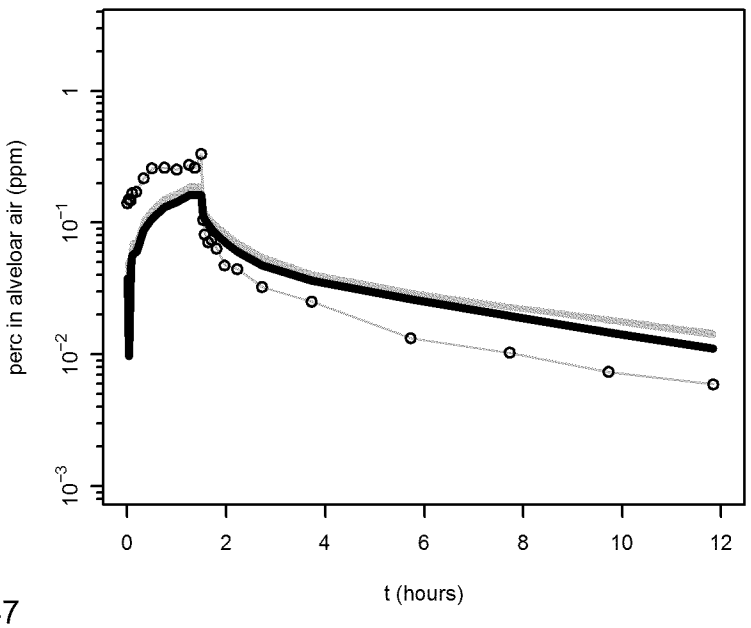

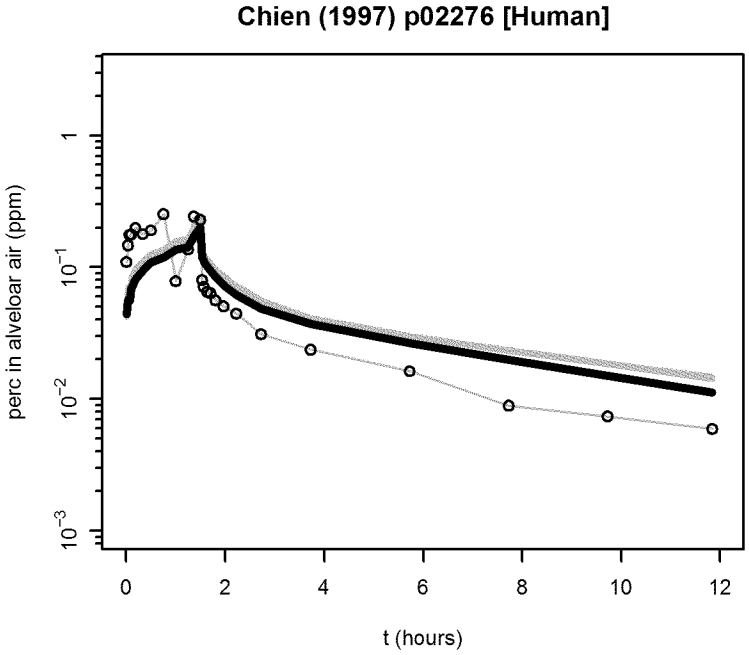
Chien (1997) p02276 [Human]
perc in alveloar air (ppm)
t (hours)

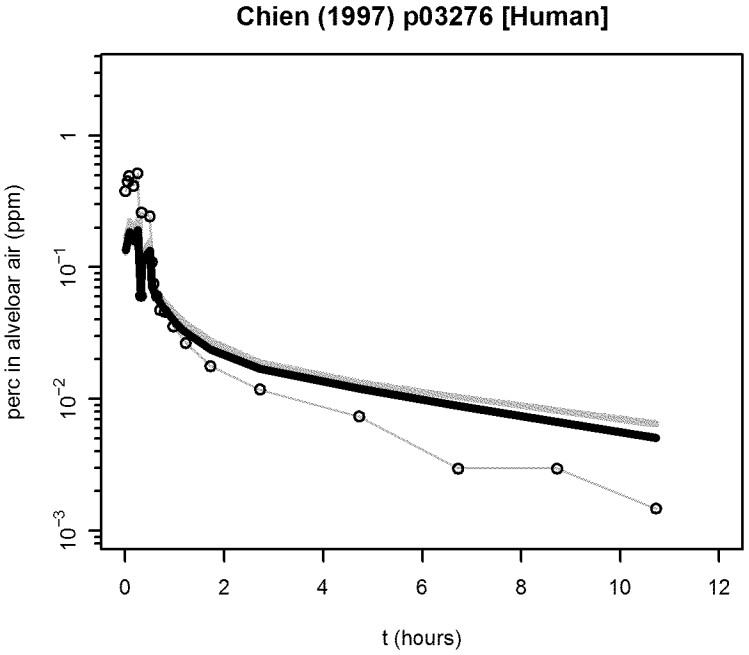
Chien (1997) p03276 [Human]
perc in alveloar air (ppm)
t (hours)

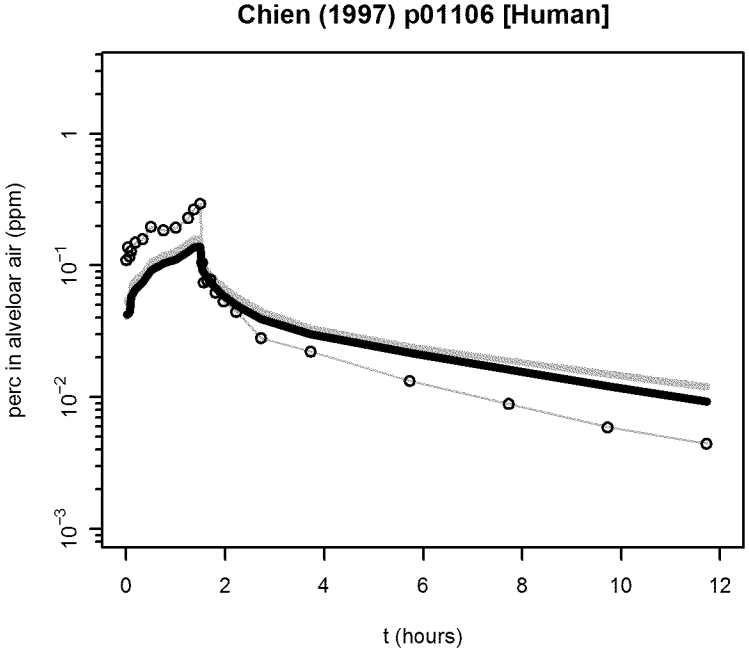
Chien (1997) p01106 [Human]
perc in alveloar air (ppm)
t (hours)

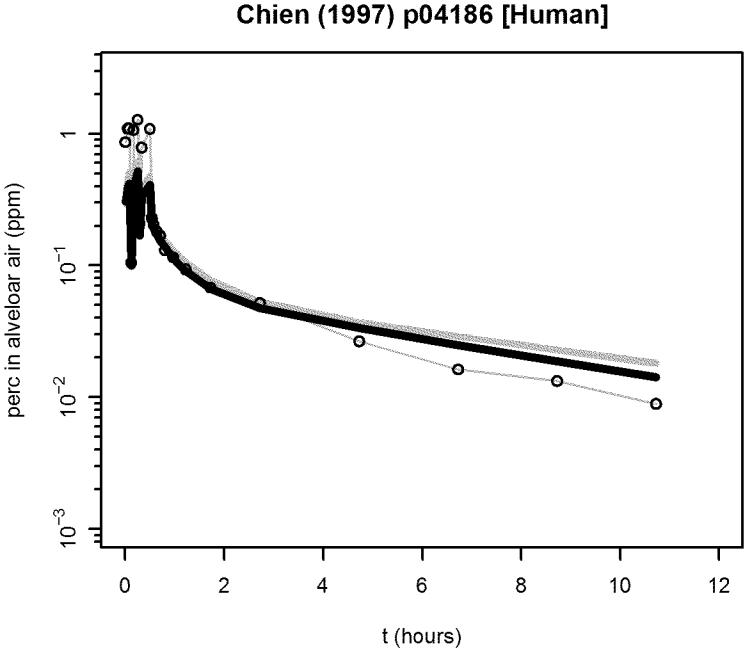
Chien (1997) p04186 [Human]
perc in alveloar air (ppm)
t (hours)

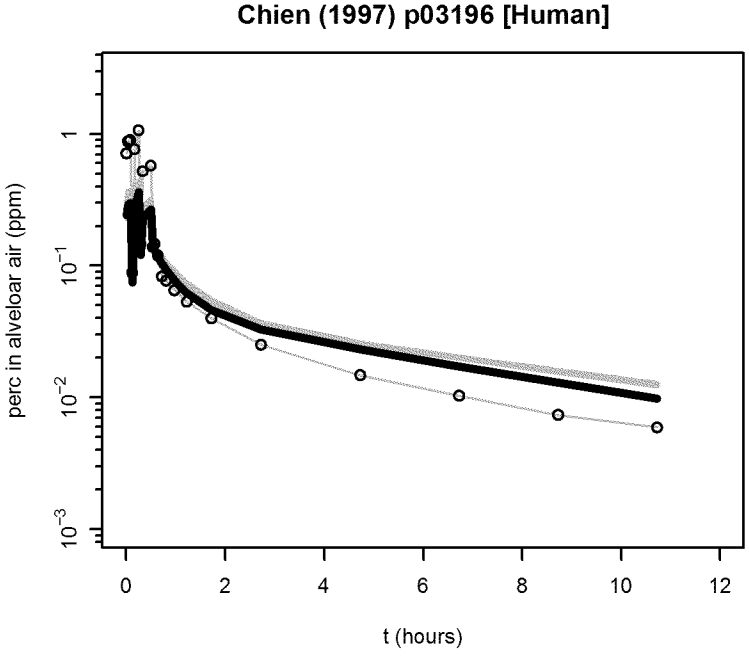
Chien (1997) p03196 [Human]
perc in alveloar air (ppm)
t (hours)

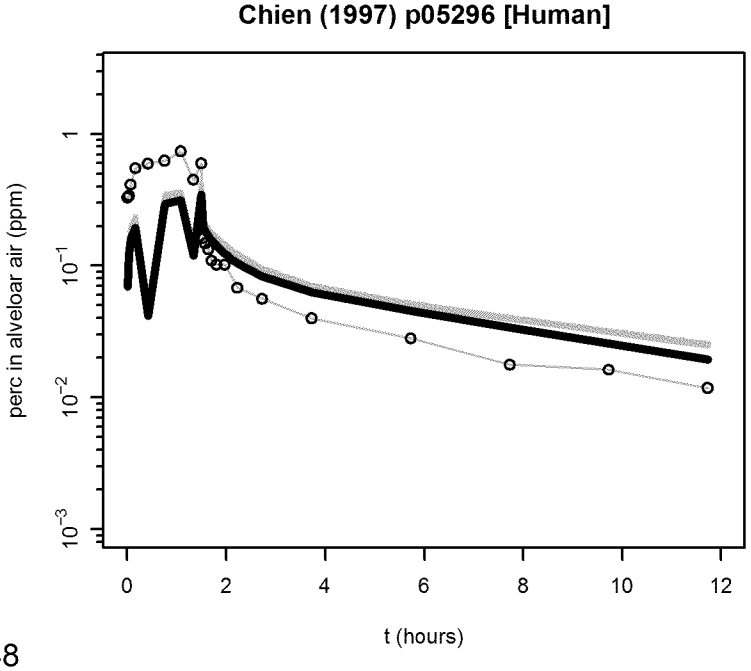
Chien (1997) p05296 [Human]
perc in alveloar air (ppm)
t (hours)

Chien (1997) p06206 [Human]

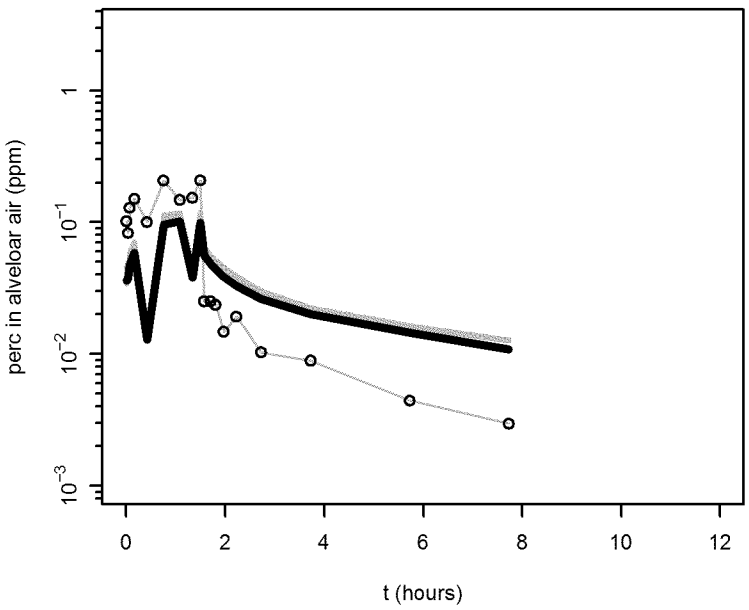

Fernandez et al. (1976) [Human]

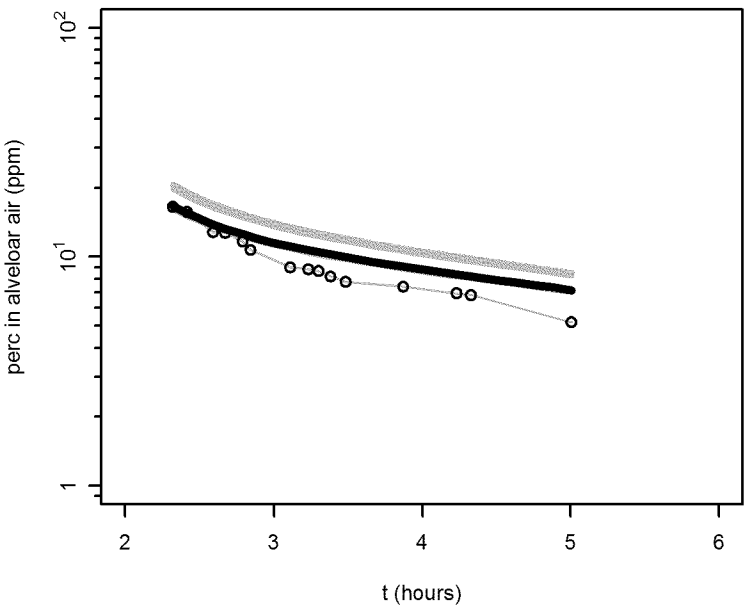

Chien (1997) p07036 [Human]

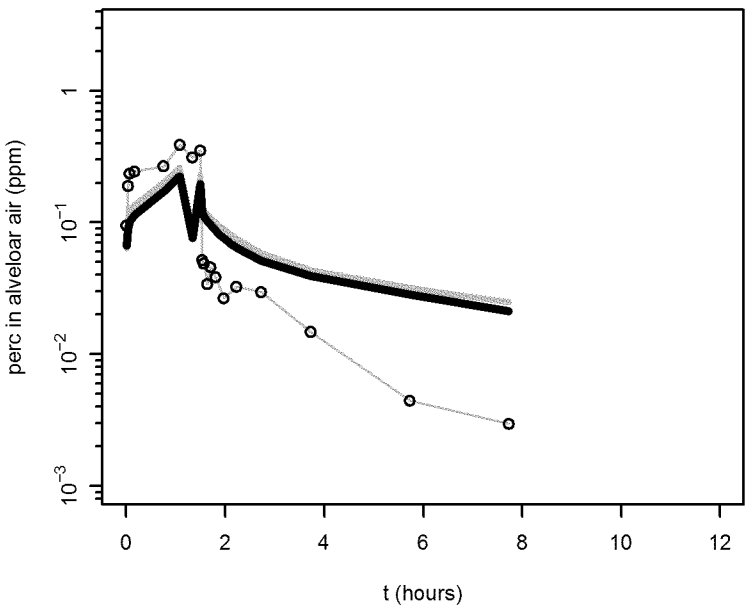

Fernandez et al. (1976) [Human]

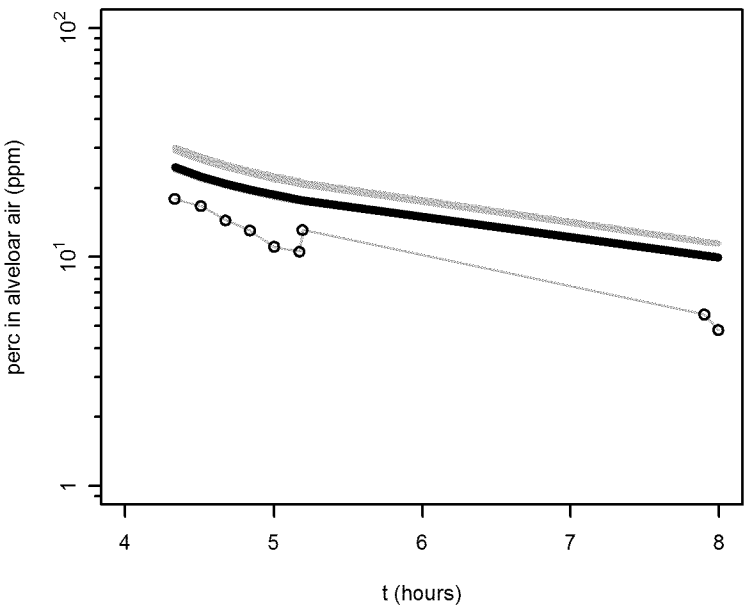

Fernandez et al. (1976) [Human]

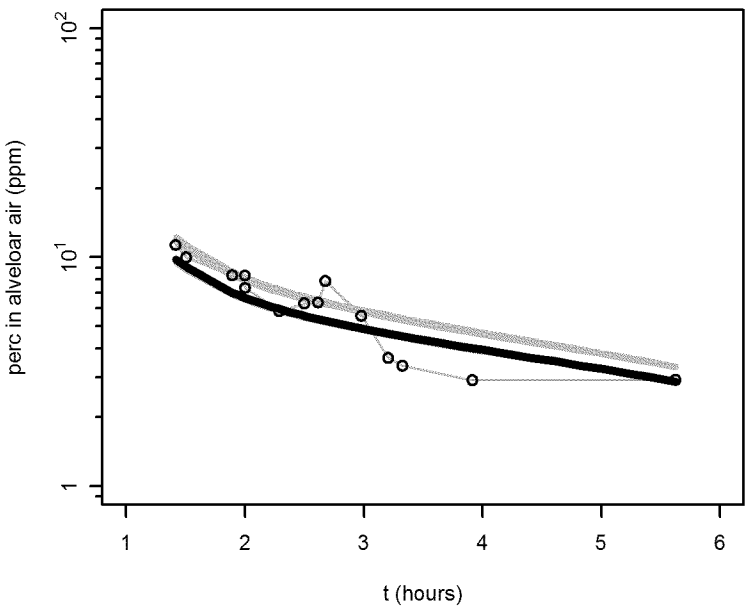

Fernandez et al. (1976) [Human]

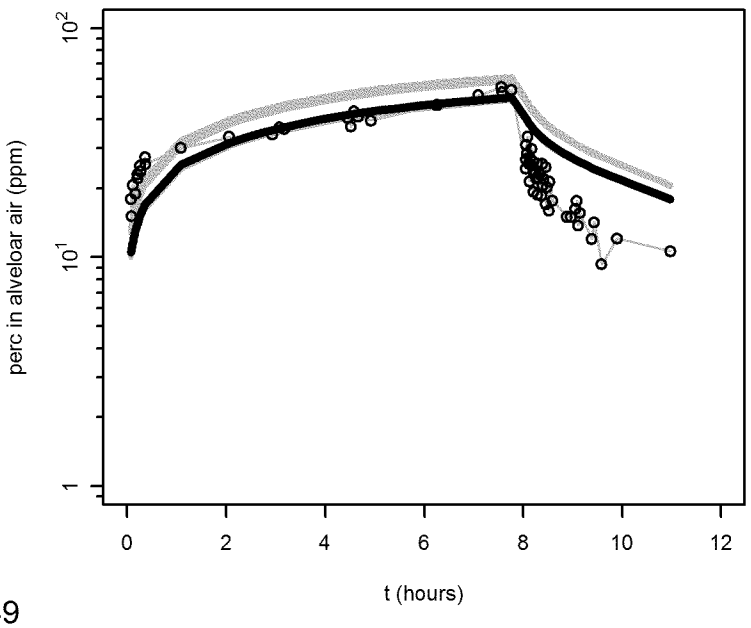

Human validation

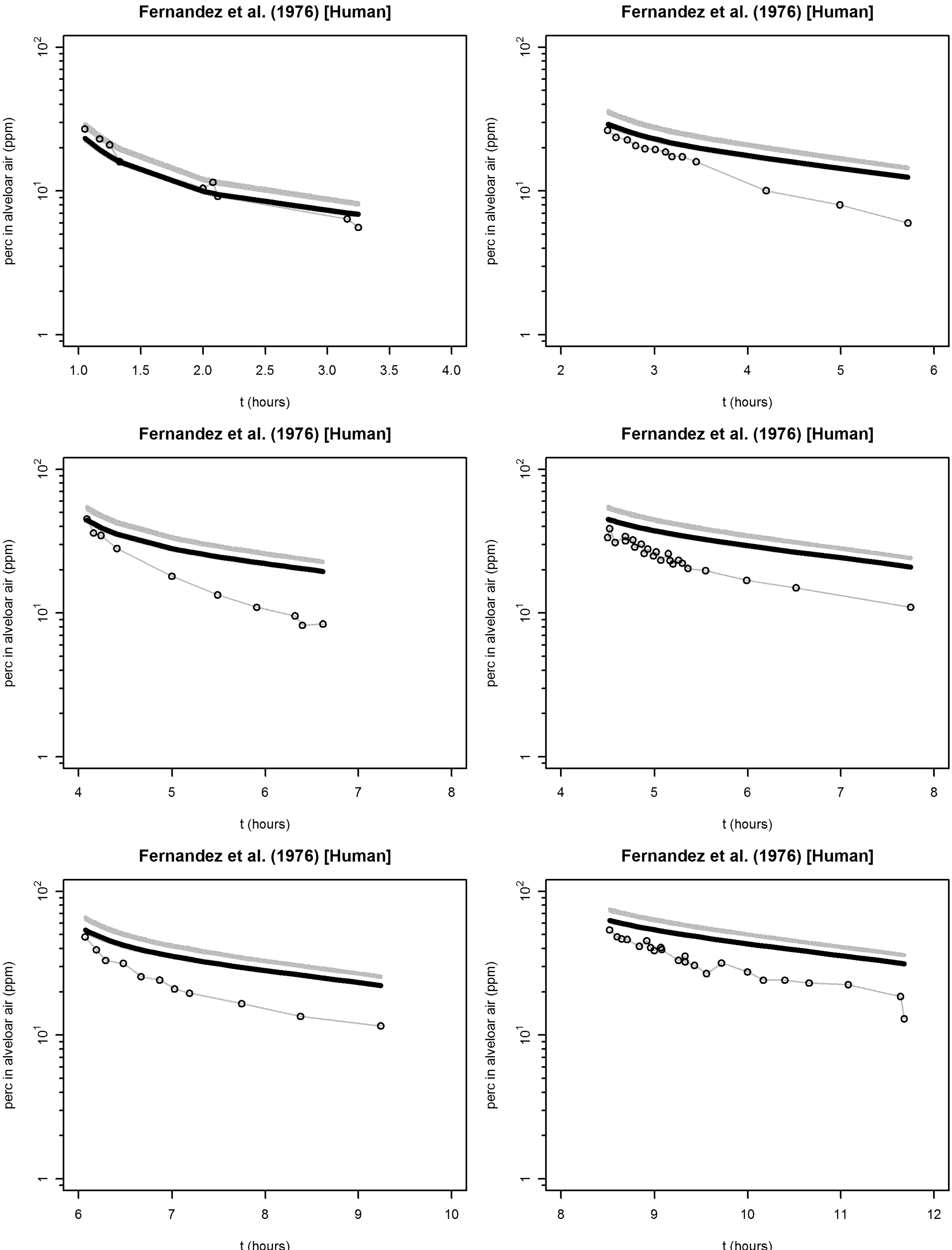

Hake and Stewart (1977) [Human]

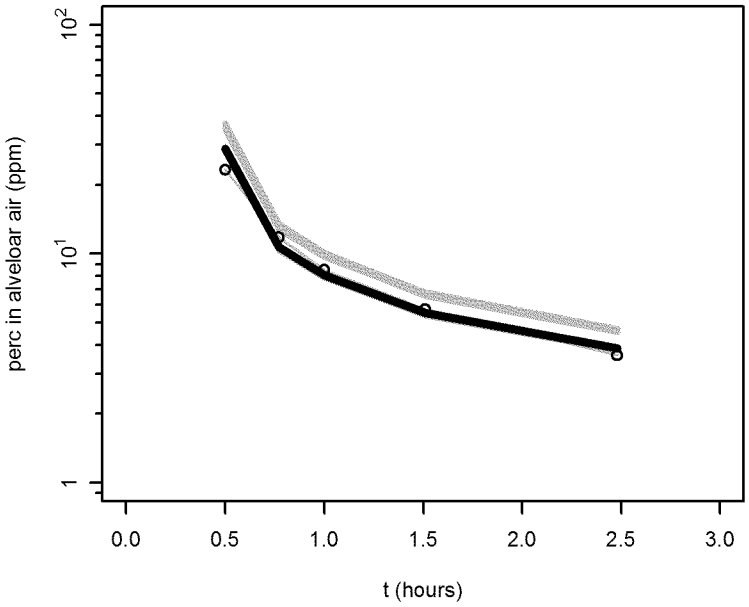

Stewart et al. (1961) 101 ppm [Human]

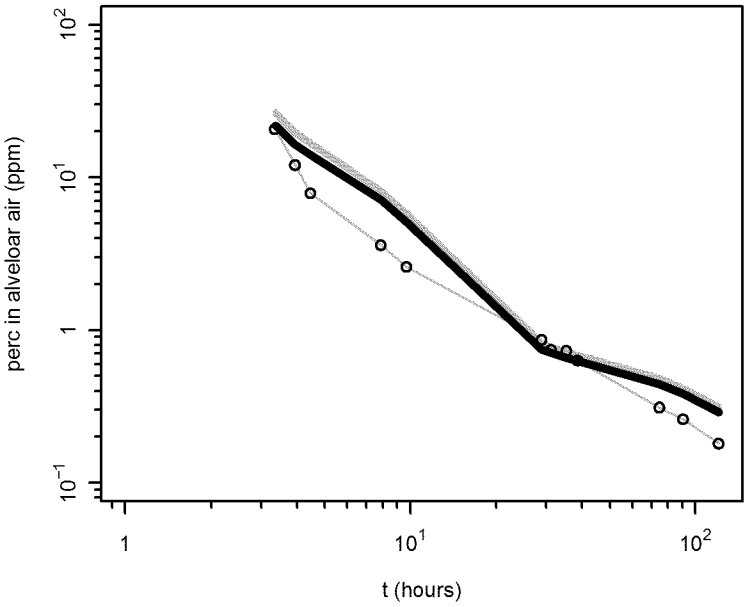

Stewart et al. (1961) 194 ppm [Human]

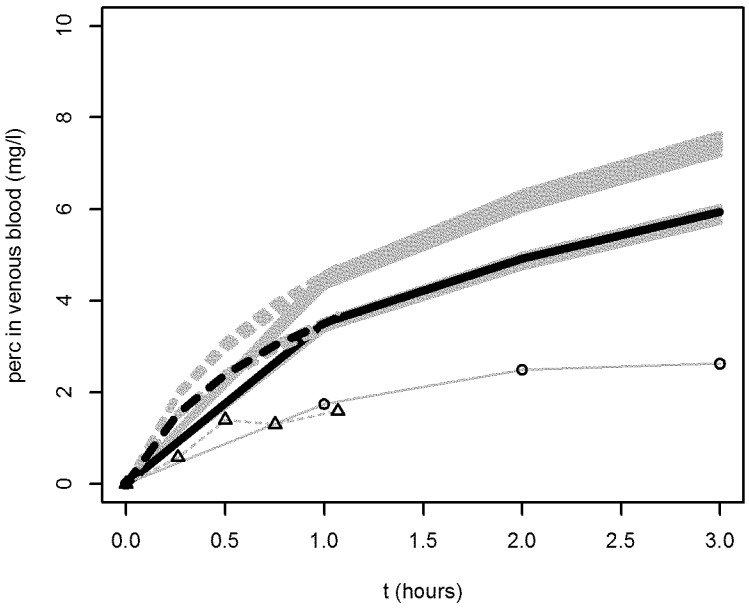

Stewart et al. (1970) [Human]

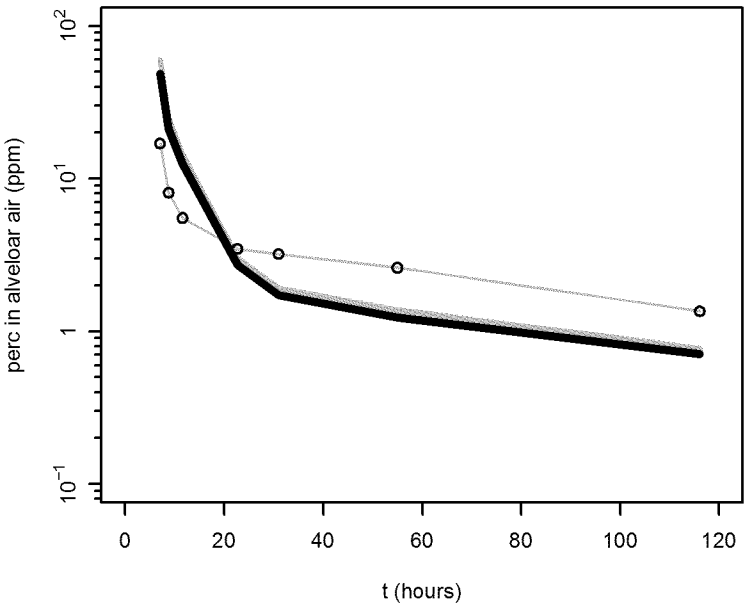

Stewart et al. (1961) 194 ppm [Human]

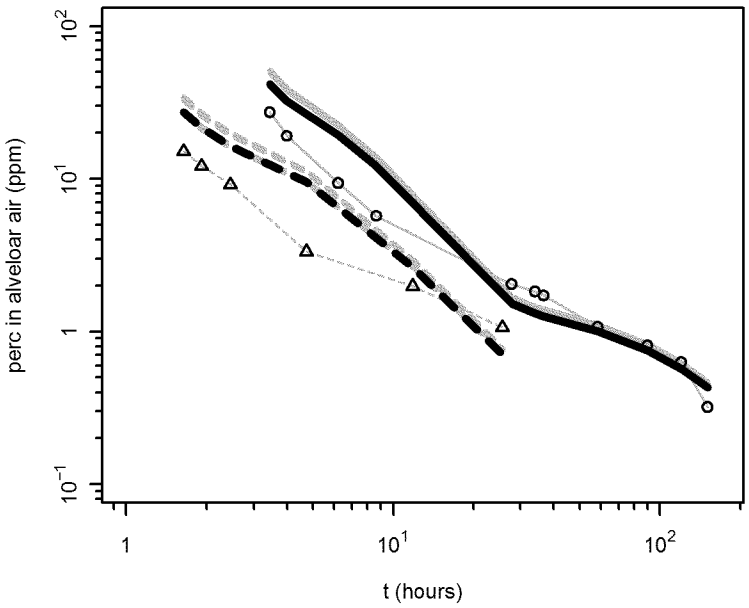

Stewart et al. (1970) [Human]

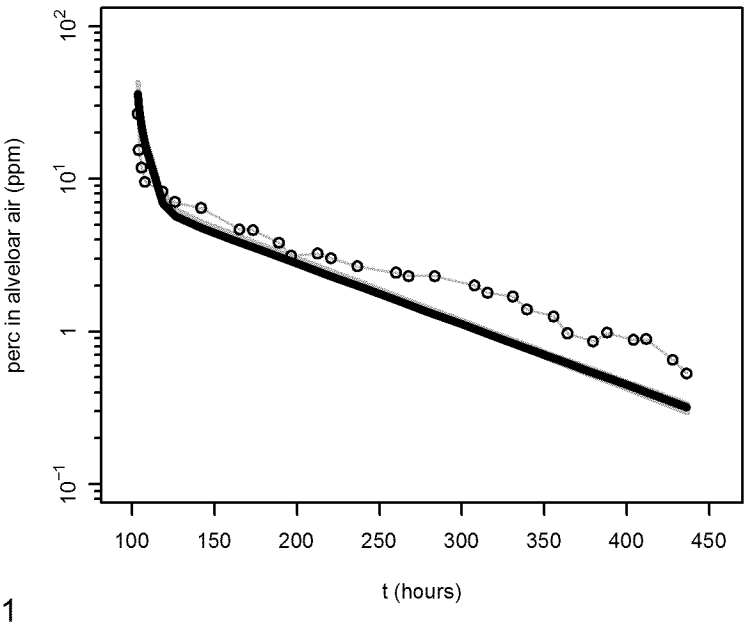

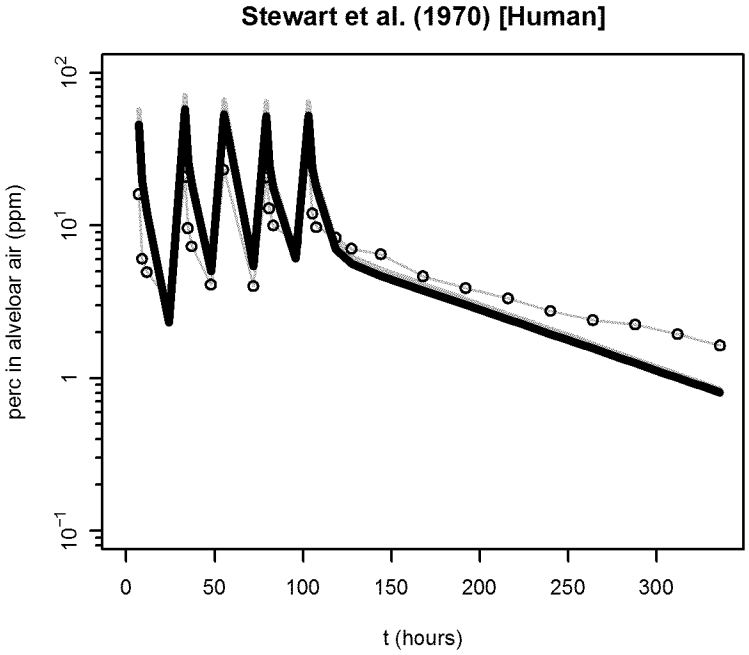
Stewart et al. (1970) [Human]
perc in alveloar air (ppm)
10^{-1}
1
10^{1}
10^{2}
0
50
100
150
200
250
300
t (hours)